DETERMINATION OF WATER BALANCE COMPONENTS OF A MICRO WATERSHED FOR IMPROVED WATER MANAGEMENT PRACTICES

by

BOWLEKAR ADWAIT PRAKASH

2019-28-002

THESIS

Submitted in the partial fulfilment of the
requirements for the degree of

DOCTOR OF PHILOSOPHY

IN

AGRICULTURAL ENGINEERING
(Soil and Water Conservation Engineering)

Faculty of Agricultural Engineering and Technology
Kerala Agricultural University

DEPARTMENT OF SOIL AND WATER CONSERVATION ENGINEERING

**KELAPPAJI COLLEGE OF AGRICULTURAL ENGINEERING
AND TECHNOLOGY, TAVANUR - 679 573**

KERALA, INDIA
2023

CANDIDATE'S DECLARATION

I, hereby declare that this thesis entitled **"DETERMINATION OF WATER BALANCE COMPONENTS OF A MICRO WATERSHED FOR IMPROVED WATER MANAGEMENT PRACTICES"** is a bonafide record of research work done by me during the course of research and the thesis has not previously formed the basis for the award of any degree, diploma, associateship, fellowship or other similar title, of any other University or Society.

Place **:** Tavanur

Date **:** 23/11/2023

Bowlekar Adwait Prakash

(2019-28-002)

CERTIFICATE

Certified that this thesis entitled **"DETERMINATION OF WATER BALANCE COMPONENTS OF A MICRO WATERSHED FOR IMPROVED WATER MANAGEMENT PRACTICES"** is a record of research work done independently by **Er. Bowlekar Adwait Prakash** under my guidance and supervision and that it has not previously formed the basis for the award of any degree, diploma, fellowship or associateship to him.

Place : Tavanur

Date : 23/11/2023

Dr. Sathian K. K.

(Major Advisor, Advisory Committee)
Professor and Head
Dept. of SWCE
KCAET, Tavanur

CERTIFICATE

We, the undersigned members of advisory committee of **Er. Bowlekar Adwait Prakash (2019-28-002)**, a candidate for degree of **Doctor of Philosophy in Agricultural Engineering** with major in Soil and Water Engineering, agree that the thesis entitled **"DETERMINATION OF WATER BALANCE COMPONENTS OF A MICRO WATERSHED FOR IMPROVED WATER MANAGEMENT PRACTICES"** may be submitted by **Er. Bowlekar Adwait Prakash (2019-28-002)** in partial fulfilment of the requirement for the degree.

Dr. Sathian K. K.

(Chairman, Advisory Committee)
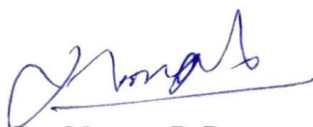Professor and Head
Dept. of SWCE
KCAET, Tavanur

Dr. Anu Varughese

(Member, Advisory Committee)
Assistant Professor
Dept. of IDE
KCAET, Tavanur

Dr. Jinu A.

(Member, Advisory Committee)
Assistant Professor
Dept. of SWCE
KCAET, Tavanur

Dr. Moossa P. P.

(Member, Advisory Committee)
Professor
(Soil Science)
RARS, Pattambi

Er. Sanchu Sukumaran

(Member, Advisory Committee)
Assistant Professor
Dept. of FMPE
KCAET, Tavanur

Dr. K. Nagarajan

Professor and Head,
Dept. of SWCE,
AEC & RI, TNAU

ACKNOWLEDGEMENT

I am thankful to all my teachers, **Dr. Abdul Hakkim V.M.**, **Dr. Shyla Joseph**, **Dr. Asha Joseph**, **Dr. Sajeena S.**, **Dr. Priya G. Nair**, *and all other teachers for their suggestions and cooperation throughout my degree programme.*

I extend my sincere thanks to **Dr. Sarathjith M.C.**, **Er. Sreeja K.**, **Er. Adarsh S.S.**, **Dr. Anjaly C. Sunny**, **Er. Namitha M.R.**, **Er. Ardra Wilson**, **Er. Praveena K.K.**, *and* **Dr. Sheeja P.S.** *for their constant and invaluable support rendered during the conduct of this research work.*

I am very fortunate to have seniors like **Dr. Dipak Khatawkar, Dr. Md. Majeed Pasha,** *and* **Dr. Jyothy Narayanan** *for constructive suggestions and emotional support throughout the study.*

I recall, with utmost pleasure, the precious support of my classmates **Chethan**, **Venkata Sai,** *and* **Aiswarya.**

I fall short of words in expressing my thanks to my juniors **Yesubabu**, **Siddharam**, **Aravind**, **Sambha**, **Rajesh**, **Mrunalini**, **Abhishek**, **Shubham**, **Rahul**, *and all others for their constant support and timely help during this research work.*

The words are not enough to express my sincere, deep respect for my beloved parents. My **Aai (Mrs. Pratiksha Bowlekar)** *and* **Baba (Adv. Prakash Bowlekar),** *who have nurtured and cultured me by putting there all possible efforts to put me on right track and for my betterment. With their blessing and support, I could complete this study.*

I am extremely obliged to acknowledge the love and affection of my best friend, **Ranju.** *No words are enough to describe her efforts in building up my educational career and my all-round development.*

Finally, I thank the eternal love of **The Almighty** *for gracing the peaceful atmosphere during the course of my study.*

I express my sincere thanks to those who directly and indirectly extended help during this research work. Any omission in this brief acknowledgement does not mean lack of gratitude!!!

Place : Tavanur
Date : 23/11/2023 **(Bowlekar Adwait Prakash)**

TABLE OF CONTENTS

LIST OF TABLES

LIST OF FIGURES

LIST OF SYMBOLS

Symbol	Description
&	And
^{0}	Degree
^0C	Degree Celsius
Δ	Delta
=	Equal to
>	Greater Than
<	Less Than
-	Minus
'	Minutes
×	Multiplication
ω	Omega
/	Or
%	Per cent
+	Plus
±	Plus or minus
®	Registered Trademark
"	Seconds
σ	Sigma
√	Square Root
∑	Summation
θ	Theta

LIST OF ABBREVIATIONS

Abbreviation	Meaning
95PPU	95 Per cent Prediction Uncertainty
3D	Three Dimensional
AEC & RI	Agricultural Engineering College and Research Institute
Ah	Ampere Hour
ALPHA_BNK	Base flow alpha factor for bank storage
AMC	Antecedent Moisture Content
ANN	Artificial Neural Networks
ANOVA	Analysis of Variance
API	Application Programming Interface
ARS	Agricultural Research Service
BMPs	Best Management Practices
CGWB	Central Ground Water Board
CH_K2	Effective hydraulic conductivity in main channel alluvium
CH_N2	Manning's n value for the main channel
cm	Centimetre
CN	Curve Number
CN2	Initial SCS curve number for moisture condition II
CROPWAT	Crop Water and Irrigation Requirements Program
CSA	Cubic Spline Algorithm
CSV	Comma Separated Values
CV	Coefficient of Variation
CWB	Climatic Water Balance
D	Per cent Difference
D_RCH	Deep Recharge

Abbreviation	Meaning
DEM	Digital Elevation Model
Dept.	Department
EC	Electrical Conductivity
EEWU	Economic Efficiency of Water Use
EMCON	Environmental Measurements and Control
EPCO	Plant uptake compensation factor
Eq.	Equation
ESCO	Soil evaporation compensation factor
ESRI	Environmental Systems Research Institute
ET	Evapotranspiration
ET_0	Reference Evapotranspiration
ET_a	Actual Evapotranspiration
ET_c	Crop evapotranspiration under standard conditions
FAO-PM	Food and Agriculture Organization Penman-Monteith
Fig.	Figure
FMPE	Farm Machinery and Power Engineering
g	Gram
GEE	Google Earth Engine
GIS	Geographic Information System
GLDAS	Global Land Data Assimilation System
GLUE	Generalised Likelihood Uncertainty Estimation
GPRS	General Packet Radio Service
GPS	Global Positioning System
GR	Groundwater Recharge
GRACE	Gravity Recovery and Climate Experiment
GW	Groundwater

Abbreviation	Meaning
GW_DELAY	Groundwater Delay Time
GW_Q	Groundwater Flow
GW_REVAP	Groundwater revap coefficient
GWQMN	The threshold depth of water in the shallow aquifer required for return flow to occur
H_2O	Water
h	Hour
Ha	Hectare
HRUs	Hydrologic Response Units
HSG	Hydrologic Soil Groups
Hz	Hertz
IDE	Irrigation and Drainage Engineering
IDF	Intensity-Duration-Frequency
IDW	Inverse Distance Weighted
IMD	India Meteorological Department
IMSD	Integrated Mission for Sustainable Development
IWMI	International Water Management Institute
K_a	Apparent Dielectric Constant
K_c	Crop Coefficients
KCAET	Kelappaji College of Agricultural Engineering and Technology
kg	Kilogram
km	Kilometre
km^2	Square Kilometre
kPa	Kilopascal
l	Litre
LAT_Q	Lateral Flow
LULC	Land Use/Land Cover

Abbreviation	Meaning
m	Metre
m^2	Square Metre
m^3	Cubic Metre
MAE	Mean Absolute Error
MAME	Maximum Absolute Measurement Error
MAPD	Mean Absolute Percentage Discrepancy
MB	Megabyte
MCM	Million Cubic Meters
MCMC	Markov Chain Monte Carlo
MHz	Mega Hertz
MJ	Mega Joule
MLR	Multiple Linear Regression
mm	Millimetre
MODFLOW	Modular three-dimensional finite-difference ground-water flow
MODIS	Moderate Resolution Imaging Spectroradiometer
MR	Measurement Report
MS	Microsoft
ms	Milliseconds
MSL	Mean Sea Level
NASA	National Aeronautics and Space Administration
NDVI	Normalised Difference Vegetation Index
No.	Number
NRCS	Natural Resources Conservation Service
NSE	Nash-Sutcliffe Efficiency
NWP	National Water Policy
OV_N	Manning's 'n' value for overland flow

Abbreviation	Meaning
P	Precipitation
PARASOL	Parameter Solution
PBIAS	Per cent Bias
PE	Potential Evaporation
PET	Potential Evapotranspiration
PSO	Particle Swarm Optimization
Q-Q	Quantile-Quantile
Qt	Quasar Technologies
r	Regression Coefficient
R	Runoff
R^2	Coefficient of Determination
RARS	Regional Agricultural Research Station
REVAPMN	Threshold depth of water in the shallow aquifer for revap or percolation to the deep aquifer to occur
RMSE	Root Mean Square Error
RRKHS	Regression in the Reproducing Kernel Hilbert Space
RSR	RMSE-observations Standard deviation Ratio
RVM	Relevance Vector Machine
RWH	Rainwater Harvesting
s	Seconds
SCS-CN	Soil Conservation Service Curve Number
SD	Standard Deviation
SDI	Serial Digital Interface
SEBAL	Surface Energy Balance Algorithm
SHAW	Simultaneous Heat and Water
Sl.	Serial

Abbreviation	Meaning
SM	Soil Moisture
SMODERP	Simulation model of overland flow and erosion processes
SOL_AWC	Available water holding capacity of soil
SOL_BD	Moist Bulk Density
SOL_K	Saturated hydraulic conductivity
SPAW	Soil-Plant-Atmosphere-Water
SR	Surface Runoff
SRTM	Shuttle Radar Topography Mission
SSR	Subsurface Runoff
SUFI-2	Sequential Uncertainty Fitting
SUR_Q	Surface Flow
SWAT	Soil and Water Assessment Tool
SWAT-CF	SWAT-Crack Flow
SWAT-CUP	SWAT-Calibration and Uncertainty Programs
SWAT-ML	SWAT-Maharlu Lake
SWC	Soil and Water Conservation
TBR	Tipping Bucket Rain gauges
TDR	Time Domain Reflectometry
TIN	Triangular Irregular Network
TNAU	Tamil Nadu Agricultural University
TW	Treated Watershed
TWSA	Terrestrial Water Storage Anomalies
TWSC	Terrestrial Water Storage Change
US	United States
USA	United States of America
USB	Universal Serial Bus

Abbreviation	Meaning
USDA	United States Department of Agriculture
USGS	United States Geological Survey
UTM	Universal Transverse Mercator
UV	Ultraviolet
UW	Untreated Watersheds
V	Volts
VCB	Vented Cross Bars
VCC	Voltage Common Collector
VDC	Volts Direct Current
VWC	Volumetric Water Content
WB	Water Balance
WGS	World Geodetic System
WiFi	Wireless Fidelity
WYLD	Water Yield
ZRW	Zarqa River Watershed

CHAPTER - I
INTRODUCTION

Water is the most essential natural resource of the earth and has been considered critical for human survival. It is a resource with very high spatial and temporal variation in its availability. Though water is fundamental to life, livelihood, food security, and sustainable development; water scarcity is widely experienced. It is considered one of the basic environmental problems of the 21st century in most parts of the developing World (National Water Policy [NWP], 2012).

Water shortage could lead to economic, social, and political volatility besides the most apparent environmental disasters. As the water demand is growing faster, the severity of water scarcity will be more serious worldwide, particularly in developing countries. There are further constraints on the utilisable quantities of water owing to uneven distribution over time and space. Water woes are rising at an alarming level in all parts of the World, and India is no exception. It is to be viewed seriously that India has more than 17% of the global population but has only 2.5% of the World's freshwater resources. Therefore, better and more efficient water use is a real challenge for Indian agriculture and industry (NWP, 2012).

The rise in water demands and a decline in water availability in surface and groundwater is a significant problem today. The increase in water consumption per capita has significantly increased the demand for available water resources due to abnormal increase in population, rapid urbanisation, industrialisation, surface water contamination, and recent climate change trends (NWP, 2012). Therefore, the availability of utilisable water needs to be augmented in time and space to meet the increasing water demands. Hence, it is evident that both land and water resources need to be managed comprehensively and used effectively.

Agriculture consumes 70-90% of the planet's freshwater resources globally. Numerous research studies have highlighted that the extensive utilisation of both surface water and groundwater for irrigation has significantly altered the hydrological processes within river basins. This has given rise to various

environmental issues, including the shrinking of lakes, declining groundwater levels, decreased natural vegetation, and soil salinisation (Lu *et al*., 2015; Zhang *et al*., 2015; Huang *et al*., 2017). A study conducted by the International Water Management Institute (IWMI) in 2007 reveals that the total water demand in India will increase by 32% by 2050. Therefore, the researchers, planners, and managers must examine these issues at the regional and watershed/catchment scale to develop policies and plans for ensuring a sustainable future. To make agriculture more profitable and improve the prosperity of farming communities, the Government of India and different states have introduced many new initiatives to meet the challenges of the overall water scarcity scenario in the country. These initiatives include the construction of water storage structures, large-scale awareness of water conservation among the citizens, revitalisation of existing water bodies, inter-connecting of rivers and many other such things (Kumar, 2018). However, all these measures have yet to yield the desired results.

Since all land areas on the earth's surface are part of some watershed or river basin, the watershed plan can cover the entire geographical area. Water availability within watersheds is primarily determined by how rainfall is distributed and allocated among different components, including evapotranspiration, surface runoff, and infiltration. The specific distribution of rainfall into these components is influenced by the land use characteristics and soil type within the watershed (Sajikumar and Remya, 2015; Kundu *et al*., 2017). Significant reasons for regional water scarcity are low magnitudes of precipitation and its inter-seasonal variability (Menzel *et al*., 2009; Maliva and Missimer, 2012; Oroud, 2015). Also, improper attention to scientific water conservation leads to only a small amount of water being recharged as groundwater, leading to more and more water-scarce situations. One of the major impediments to economic growth and development in many areas, including semi-humid tropics, is the scarcity of water resources.

The future availability of water for human consumption depends on how water resources are managed in terms of their conservation and effective utilisation. Water resource planners must quantify how much water flows into and out of a

hydrological unit (watershed) to ensure enough water is available for human consumption. It is also essential to achieve optimum utilisation of available water resources. At the same time, management of water resources in watersheds requires quantitative knowledge of them in time and space. Land use/land cover (LULC) influences water availability in watersheds. Quantifying the elements of hydrologic processes at the micro watershed scale with a monthly/weekly temporal scale is the prerequisite for water resources development of a locality since all the hydrologic processes take place within the individual micro watersheds (Tejaswini and Sathian, 2018). For effective water resource management, first of all, various hydrological components and the water cycle must be studied and considered, including evapotranspiration, transpiration, precipitation, and runoff. The availability of fresh water for food production and other primary uses depends on effective water management.

The study of water balance in watersheds is a crucial aspect of understanding the underlying hydrology on which water resources in a watershed are dependent. The water balance is defined as considering all the water that enters and exits a hydrological system, including any alterations in water storage. This method is helpful in identifying the specific times during the year when an area experiences either a shortage or excess moisture. Similarly, groundwater depletion and replenishment can also be quantified through water balance. The long-term average monthly rainfall, long-term average evapotranspiration, and soil-vegetation characteristics are required to compute the water balance (Kumar and Srinivasan, 2016; Gophen, 2020). It is also reported that quantifying the components of the water balance for a watershed is crucial to the understanding of the dominant hydrologic processes occurring in a basin (Gebru and Tesfahunegn, 2020; Mestry *et al*., 2020; Nasiri *et al*., 2020). Although several water balance studies have been conducted for a variety of watersheds throughout the world, such studies are less in the Indian peninsular context.

Many researchers have also stated that a better understanding of the impact of hydrological properties on water balance components at the basin scale is of great

importance for the planning and development of sustainable water management strategies (Abbaspour *et al*., 2015; Lee *et al*., 2020; Ouallali *et al*., 2020; Juma *et al*., 2022). Many authors further state that accurately estimating hydrologic cycle variables is significant for catchment water security, water resource management, irrigation management, and ecological and environmental protection (Liu *et al*., 2020; Serur and Adi, 2022). To better utilise water resources, the assessment of water quality and quantity has become increasingly important, and to adequately assess these components, an understanding of hydrologic processes is critical (Harmel and Smith, 2007). To use water resources sustainably, it is vital to understand the spatial and temporal variations of the water balance. Human activities are changing watershed characteristics, such as land cover, which affects water inflow from the watershed into the streams (Ayivi and Jha, 2018).

The deficiency of hydrologic measurements precludes adequate assessment of the actual water resources of an area. Poor measurements and a lack of knowledge of the hydrological processes that control stormwater runoff dynamics have resulted in severe misjudgments regarding the capacity of dams, bridges, and culverts. There needs to be more research on water balance components generated over these watersheds; hence, there is a pressing need to assess them (Oroud, 2015). At the same time, developing measurement methods or methodologies for estimating water balance is a significant challenge, especially in areas with few or no gauging stations. This is because it is only possible to directly measure some water balance components, as many of the water balance processes take place in the sub-surface and atmosphere, and their point measurements are only possible with measured data; calibration of the mathematical models for estimation is also possible.

Kerala, one of the southern states of India, has been facing severe drought in the past few decades, and many rivers have very lean flow during the summer months. After abundant rain during the monsoon season, the state experiences water shortages of severe magnitude. The state's average annual rainfall is very close to 3000 mm, with more than 70 per cent falling during the South-West monsoon,

which usually begins in June and lasts until September. The state receives rains from the North-East monsoon from October through November and very few summer showers from December to May. The state has 41 west-flowing and three east-flowing rivers originating from the Western Ghats. The total annual yield of all these rivers is 78.04 Million Cubic Meters (MCM), of which 70.32 MCM is within the state. The speciality of the rivers flowing across the state of Kerala is that they are short in length with a high relief ratio, leading to the quick outflow of water collected from the catchment into the sea. As a result, the state has yet to utilise the surface and shallow groundwater resources effectively. A significant portion of the river runoff occurs during the monsoon seasons, with the flow pattern closely matching rainfall with very little lag time.

The Bharathapuzha River, flowing through the central part of Kerala and the state's second largest and most Holy River, is a typical example. One of the significant issues faced by the river basin is the acute shortage of water in the summer season (Varughese and Hajilal, 2022). Many micro watersheds drain into the main river Bharathapuzha, but unfortunately, none carry summer flows (Tejaswini and Sathian, 2018). As the river dries during summer, all economic activities within the basin, particularly the agricultural activities, are severely impacted. Hydrological studies at the micro watershed scale are essential for finding a solution to the water scarcity scenario of the river basin. No previous studies have been reported in the literature on detailed water balance studies at the micro watershed scale in this river basin.

A water balance study of a micro watershed based on field measurements of various watershed processes would throw much insight into the water input, storage and output of the watershed. Such a study can provide vital information for planning scientific water management activities. Also, developing a relationship between rainfall and other water balance components will help in predicting watershed processes from easily measurable hydrological processes (usually rainfall), which are otherwise very hard to estimate or predict.

Considering the points mentioned earlier, a water balance study has been undertaken in a small sub-watershed of river Bharathapuzha with an outlet at Perassanur near Kuttippuram with the following specific objectives:

1. To determine the monthly water balance of a selected micro watershed.

2. To develop the relationship between monthly rainfall and water balance components.

3. To suggest scientific water management practices for the watershed.

CHAPTER - II
REVIEW OF LITERATURE

This Chapter critically reviews the previous research work related to the present study. The reviews are classified as determination of the significant water balance components like rainfall, runoff, evapotranspiration, soil moisture, and water table; estimation of the water balance; modelling used for the analysis of water balance; the relation between rainfall and other water balance components, and suggestions for improved water management practices.

2.1 DETERMINATION OF THE WATER BALANCE COMPONENTS

2.1.1 Determination of Rainfall

Upton and Rahimi (2003) detected errors in tipping bucket rain gauges at Bolton in northwest England. They quoted that tipping bucket rain gauges can produce misleading reports. They asserted that disruptions in the gauge could cause rapid tip occurrences, improper bucket positioning, or sudden snowmelt. In contrast, extended tipping events might be the outcome of partial blockages. Also, the absence of tips would indicate a significant problem. They cited that it is comparatively easy to identify a malfunctioning gauge in a relatively small region. The authors employed readily programmable diagnostic tests to detect these issues, utilising data from a single gauge or supplementary information from nearby gauges. The reviews were motivated by the need to process two years of data. The checks were then tested on archived data, finding 90% of confirmed faults. Finally, they suggested a correlation-based comparative test to identify the problems in rain gauges.

The rainfall with high temporal resolution from a tipping bucket rain gauge from Chilbolton in Southern England was retrieved by Song *et al.* (2016). The authors noted that the commonly used tipping bucket rain gauge often overlooks temporal variations, particularly during periods of low rainfall intensity. This research delved into an investigation of high temporal resolution rainfall rate estimation from 2007 to 2009, utilising the Artificial Neural Networks (ANN)

approach in conjunction with the traditional Cubic Spline Algorithm (CSA) and Multiple Linear Regression (MLR). The authors observed that they incorporated the Supervised Levenberg-Marquardt back-propagation algorithm and the K-folds cross-validation method into a feed-forward neural network to capture intricate nonlinear relationships and prevent model over fitting implicitly. The results indicated that, following training, the ANN performed equally well with the CSA. They also suggested that MLR could serve as an alternative method for estimating rainfall rates, contingent upon the quality of the available data.

Al-Wagdany (2020) derived the intensity-duration-frequency (IDF) curve from different rain gauge records at the Namman catchment in western Saudi Arabia. The researcher analysed rainfall to assess how the choice of rain gauge types affects the construction of Intensity-Duration-Frequency (IDF) curves. Rainfall data spanning 13 years were gathered from two different recording rain gauges, and the annual maximum rainfall values were extracted for calculating IDF curves. Additionally, it was pointed out that the underestimation of rainfall measurements by tipping-bucket rain gauges had a notable impact on IDF curves and the characteristics of design storms. To address this issue, adjusted rainfall intensity values were employed to create more accurate IDF curves. The study concluded that understanding rainfall intensities obtained from IDF curves can be effectively used for designing hydro-meteorological, hydro-climatological, and hydraulic structures such as canals, culverts, pipes, and dam spillways.

Hwang *et al.* (2020) compared and evaluated four commonly used spatial interpolation methods to estimate areal means of short-duration rainfalls in small catchments using rain gauge and radar data in South Korea. The researchers examined how the size of a catchment area influences various spatial interpolation methods and conducted simulations using hypothetical storms. They also assessed the performance of different spatial interpolation techniques by comparing their results with precipitation data from weather radar. Their findings revealed that the Mean Absolute Percentage Discrepancy (MAPD) for areal mean precipitation between the Thiessen polygon method and three other interpolation methods

(inverse distance weighting, multiple quadratic interpolations, and Kriging) increased significantly as the catchment area decreased in size, mainly when the catchment area was less than 500 km^2. The study emphasised that a smaller number of rain gauges used to calculate the areal mean rainfall resulted in a higher MAPD. In conclusion, the study highlighted that the temporal distribution of areal mean rainfall, derived from rain gauge and weather radar data, varied depending on the direction of rainfall movement, particularly in sparsely monitored catchment areas. Consequently, the research provided recommendations for the appropriate placement and number of rain gauges for accurately estimating areal mean rainfall in small catchment areas. Additionally, it assessed the impact of rainfall movement and direction in determining areal mean rainfall.

The specifications, installation, and analysis of the tipping bucket rain gauge were done by a study by Meeravali *et al*. (2020). They claimed that the tipping bucket rain gauge worked efficiently, accurately, and economically among all rain gauges (recording and non-recording). A tipping bucket rain gauge with GPRS-based data logger DL-2016 was placed on top of the roof at a height of 1 m. Hypertrm software was used to retrieve the precipitation recordings from the data logger. Hydrographs were drawn from precipitation data and were calibrated and analysed. They estimated peak discharge as 28.89 m^{3}s^{-1}, less than the maximum flood discharge of 31.56 m^{3}s^{-1} calculated from the empirical formula. The unit hydrograph method was employed to forecast the peak flood hydrograph when certain conditions were met, viz., the rainfall that caused the flood, data on the catchment's infiltration properties were available, and a suitable unit hydrograph was at hand. In the design context, extreme rainfall scenarios were utilised to create what is known as the design storm. This design storm, which represents the rainfall excess responsible for significant flooding, was then applied to the catchment's known or calculated unit hydrograph to produce the intended flood hydrograph.

Liu *et al*. (2021) employed measurement report (MR) data from time-division long-term evolution networks to estimate rainfall in the Andunshui River Basin, China. They noted that traditional rainfall monitoring methods, including rain

gauges, weather radars, and satellites, have been developed for rainfall measurement. The authors specifically utilised MR data and reports sent to user terminals for instructions. Their study concluded that rainfall estimation based on MR data represents a potential alternative or supplementary approach for estimating rainfall. Moreover, they found that MR data could be used with acceptable accuracy (greater than 0.8) in runoff simulations. They recommended adopting this proposed rainfall estimation method, particularly in areas that are rarely monitored or lack rain gauges, for flood simulation purposes.

2.1.2 Determination of Runoff

Spruill *et al*. (2000) simulated daily and monthly stream discharge for a small watershed in central Kentucky using Soil and Water Assessment Tool (SWAT) model. In contradiction to usual practice, they used streamflow data from 1996 to calibrate the model and streamflow data from 1995 for evaluation. During this timeframe, it was noted that the model effectively captured the patterns in daily streamflow. Given the limited knowledge about how the SWAT model responds to different inputs, a calibration process was developed to assess the parameters that impact stream discharge predictions. The sensitivity analysis revealed that a significantly larger area influenced streamflow compared to what was defined by topographic boundaries. As a result, the researchers concluded that the SWAT model had the potential to be a valuable tool for characterising monthly runoff in smaller watersheds. However, they stressed the importance of having calibration data for channels that either drain into or out of the topographic watershed.

Carlesso *et al*. (2011) estimated runoff based on Smith's modified model and the curve number method in southern Brazil. They aimed to assess and model runoff for different soil classes under varying precipitation intensities (30, 60, 120 mm h^{-1}). They utilised a portable rainfall simulator equipped with multiple nozzles to replicate these precipitation levels. For each type of soil, they gathered data on factors such as initial time to runoff and runoff rate, characteristics of the rainfall (including total duration and intensities), surface slope, crop residue quantity and coverage, soil densities (bulk and particle), soil porosity (bulk, macro, and micro),

textural fractions (clay, silt, and sand), and initial and saturated soil water content. The researchers then compared the observed runoff with Smith's modified curve number models (USDA-SCS-CN). The findings showed that cumulative runoff losses accounted for 67%, 45%, and 27% of the total precipitation for Rhodic Paleudalf, Typic Quartzipsamment, and Rhodic Hapludox soils, respectively. They noted an inverse relationship between initial runoff and runoff rate, regardless of soil surface and rainfall conditions. Furthermore, increasing rainfall intensity reduced the time to runoff and increased the runoff rate, leading to higher runoff losses, irrespective of soil surface conditions.

Le Coz *et al*. (2012) estimated uncertainty in open-channel discharges measured with the velocity-area method. The researchers pointed out that a significant portion of the discharge measurements in open channels rely on the velocity-area method. This method involves sampling the flow velocity and depth across the cross-section to calculate the total discharge. They introduced a new technique to assess the uncertainty associated with discharge measurements using the velocity-area method. To estimate these uncertainties, they proposed direct computation methods that involve vertical integration of velocity and transverse integration of velocity and depth. The authors applied the new uncertainty analysis method to varied stream discharge measurements and found similar results for standard measurements conducted in natural sections. It was observed that the new process appeared to be more versatile and could be easily implemented in discharge computation software.

Kaletova and Nemetova (2017) determined surface runoff from the modelled area at the Slovak University of Agriculture, Nitra. In a laboratory, they carried direct measurements on an experimental site with three different slopes. The results of direct measurements with the estimates of the models Simulation Model of Overland Flow and Erosion Processes (SMODERP) and Natural Resources Conservation Service (NRCS) were in the Geographic Information System (GIS) environment. A mathematical equation calculated the velocity of surface runoff. It was observed that the results of surface runoff volume obtained using GIS

techniques were equal in all cases, but not the velocity. The results of the SMODERP simulation and direct measurements were similar. The calculated velocity was highest, with a slope of 18.28% and a lower slope of 28% and 40.28%. The results indicated that the differences in the velocity varied in the range of 1.10 to 11.06%. The volume of surface runoff changed more, mainly the results of the NRCS Curve Number method in GIS (up to 41%). They concluded that the runoff velocity and volume are also high if the slope is high.

The streamflow was modelled using SWAT for the Thuthapuzha River basin in Kerala by Fousiya and Varughese (2020). They cited that managing water resources in a single river basin system is the best way to address water-related issues. They have considered data for calibration from 1989 to 2009 and the validation period from 2010 to 2017, and the simulation has been done daily. The first three years (1989-1991) were a warm-up period. The SWAT Calibration and Uncertainty Programs (SWAT-CUP) uncertainty analysis considered two indices, viz., p-factor and r-factor. In the calibration phase, the model exhibited p-factor and r-factor values of 0.77 and 0.64, respectively. During the validation phase, these values were 0.85 for the p-factor and 0.56 for the r-factor. The model's performance was evaluated using metrics such as Nash-Sutcliffe Efficiency (NSE), coefficient of determination (R^2), and per cent bias (PBIAS). For the calibration period, the R^2, NSE, and PBIAS values were 0.88, 0.88, and -1.4, respectively, while for the validation period, they were 0.8, 0.8, and 5.4, respectively. The study concluded that the streamflow simulations were reliable by the model based on the statistical performance parameters.

Liu *et al*. (2020) estimated the runoff and its contribution to large Asian rivers for the Qinghai-Tibetan Plateau. They stated that the quantity of water flowing in this region was not known because of a lack of observations. Consequently, they incorporated a velocity-based routing method within the Global Land Data Assimilation System (GLDAS) model to direct runoff to the basin outlet. According to their findings, the GLDAS model underestimated dry season runoff compared to observed values. Many hydrological models typically consider

potential evapotranspiration (ET) while neglecting the impact of water constraints. Their analysis revealed that, for the monthly precipitation and runoff data, the relative error fell within 5%, the correlation coefficient and the Nash-Sutcliffe Efficiency (NSE) were 0.95 and 0.76, respectively.

The surface runoff of the Sind River basin was estimated using integrated Soil Conservation Service Curve Number (SCS-CN) and GIS techniques by Kumar *et al*. (2021). The researchers opted for the SCS-CN method, considering its widespread popularity and frequent application. In the SCS-CN method, the runoff curve number (CN) plays a pivotal role, and it is influenced by factors such as land use/land cover (LULC), soil type, and Antecedent Moisture Content (AMC). Their dataset consisted of daily runoff data from the Sind River basin, covering ten years from 2005 to 2014. It was found that the average annual surface runoff was 133.71 mm. The average runoff volume was 35.04×10^8 m^3, representing 17.21% of the yearly rainfall.

Molenat *et al*. (2021) conducted a study in the Kamech catchment in Tunisia to explore the potential use of small reservoirs for monitoring stream runoff. The research involved estimating runoff at various temporal resolutions and assessing the impact of different factors related to reservoir water balance (including evaporation, precipitation, infiltration, reservoir level, and level-area-volume relationships) on the accuracy of river runoff estimation. A global sensitivity analysis was also performed. The findings indicated that a mass balance approach could be reliably used to estimate stream runoff based on data from small reservoirs. Furthermore, it was observed that the error and overall uncertainties in stream runoff estimation decreased as the temporal resolution increased. In general, the study's conclusions suggested that small reservoirs could serve as dependable stream runoff gauges at shorter temporal resolutions, provided that the reservoir level measurements have limited uncertainty. Additionally, at more extended temporal resolutions, reliability can be maintained as long as there is little uncertainty in the percolation rate from the reservoir.

Gholami *et al*. (2022) calculated the cost of runoff computation and sensitivity analysis of topological attributes for the Zarrineh River watershed in Iran. The research aimed to assess the impact of various Digital Elevation Models (DEMs) from different sources and with differing cell sizes on the accuracy of a hydrological model's output. The SWAT model was employed, and sequential uncertainties were utilised to identify the most influential input parameters. The findings revealed that parameters such as reach lengths, reach slopes, the number of sub-basins, and the quantity of Hydrologic Response Units (HRUs) had the most significant impact on runoff simulation by the SWAT model. Importantly, these parameters displayed variations based on changes in the source and resolution of the Digital Elevation Model (DEM). The study noted that the simulated results tended to overestimate runoff during periods of low precipitation and underestimate it during high precipitation periods. Furthermore, it was observed that reducing the DEM resolution led to a decrease in the accuracy of the simulated results. Ultimately, the study highlighted that finer resolution input data improved the performance of the SWAT model, particularly in predicting parameters such as runoff yield, hydrological response, and terrain morphology estimation.

2.1.3 Estimation of Evapotranspiration

Stancalie *et al*. (2010) estimated actual evapotranspiration using earth observation data and the Crop Water and Irrigation Requirements Program (CROPWAT) model for the year 2000 in agro-meteorological conditions at two test areas, Craiova and Alexandria of Romania. The methodology in this study revolved around simplifying the surface's energy balance, focusing on connecting evapotranspiration, net radiation, and the temperature difference between the surface and the air. This was done by measuring these parameters around 2:00 PM local time, coinciding with the satellite overpass. By applying this approach, they could derive daily crop evapotranspiration values. To validate these values, they compared them to the results generated by the CROPWAT model. The comparative analysis revealed that the method based on the surface energy balance generally yielded higher crop evapotranspiration (ET_c) values than those simulated by the CROPWAT model. The authors emphasised that satellite data could play a significant role in

comparing and validating model outputs, particularly for parameters like daily crop evapotranspiration.

The total available water in the soil layer was estimated by integrating actual evapotranspiration data in a remote sensing-based soil water balance by Campos *et al.* (2016). The study used an inverted formulation of a one-layer soil water balance model performed in the root zone. The daily precipitation was measured using a tipping bucket rain gauge, volumetric soil moisture content using Time Domain Reflectometry (TDR), and reference evapotranspiration using the Food and Agriculture Organization Penman-Monteith (FAO-PM) method. The study optimised the total available water to minimise the difference between measured and modelled ET. An optimisation procedure was adopted by using a continuous dataset of the year 2004 of daily ET measurements and 16 sets of 8 daily ET measurements, resulting in total available water values of 325 and 305 mm, respectively. The validation period was 2005–2008, during which Root Mean Square Error (RMSE) was 0.48 mm day^{-1}. They found that the model satisfactorily reproduced the water stress process. This analysis indicated relatively little influence from the evaporation component and the need for adequate knowledge about moisture stress for estimating total available water.

Li *et al*. (2018) studied an improved approach for estimating ET using a water balance equation for the Yangtze River basin. The authors highlighted the significance of evapotranspiration (ET) in the water cycle, underlining its crucial role in global water exchange and energy transfer. They acknowledged the challenges of accurately estimating regional ET and, in response, developed an enhanced approach for regional ET estimation. This new method was based on the water balance equation and utilised data from the Gravity Recovery and Climate Experiment (GRACE), daily precipitation records, and discharge data. The validity of the method and algorithm was confirmed through a simulation study. Compared to previous ET estimation methods, the results obtained with the GRACE-based approach exhibited considerable improvement, indicated by a correlation coefficient exceeding 0.9. Additionally, the study calculated the spatially averaged ET over the

Yangtze River basin from 2003 to 2013. They further compared these ET estimates with independent data on meteorological factors and soil moisture across the entire Yangtze River basin. The research also delved into the relationship between mean annual ET and atmospheric demand for seven sub-catchments within the Yangtze River basin. The analysis revealed that the spatial distribution characteristics of ET, as estimated by the proposed method, were influenced by atmospheric conditions. The authors anticipated that this methodology could find applications in assessing ET variations over shorter intervals (e.g., weekly or every ten days). Such an approach could enhance our understanding of hydrological processes, especially in regions with complex environmental factors.

An increase in the Economic Efficiency of Water Use (EEWU) caused by crop structure adjustment at Heihe River in arid areas of northwestern China was studied by Tan and Zheng (2019). They modified CROPWAT model input parameters based on farmer survey data, simulated the amount of water use after deducting the influences of climate, seeds, and irrigation systems, and finally analysed the variation of EEWU induced by crop structure adjustment from 2001 to 2012. The study determined that the CROPWAT model accurately simulated maize evapotranspiration, aligning well with observed data. They observed a significant increase in EEWU in the study area from 2001 to 2012, amounting to approximately 40%. Furthermore, they asserted that in the arid regions of northwest China, adjusting the crop structure had significant potential for enhancing EEWU and boosting agricultural income.

Falalakis and Gemitzi (2020) developed a straightforward method for estimating water balance, which relied on empirical relationships and remote sensing data for evapotranspiration (ET). They introduced a simplified approach that established empirical links between remotely sensed ET data from the Moderate Resolution Imaging Spectroradiometer (MODIS), Groundwater Recharge (GR), and readily accessible monthly precipitation data. This methodology was tested in seven catchments in northeastern Greece using precipitation and remotely sensed ET data from 2009 to 2019. The effectiveness of this method in accurately estimating the

water balance was assessed by comparing its components with modelled values. The results indicated an average ET fraction of approximately 54% of precipitation, an average groundwater recharge of 24%, and an average surface runoff of about 22% of rainfall in the study area. Notably, this approach utilised freely available remote sensing products and the R software for statistical analysis and graphing. As a result, it offers a cost-effective and practical alternative for estimating water balance, even in watersheds with limited data resources. The authors concluded that this methodology provides a dependable and economical solution for monthly water balance calculations at the catchment level, particularly in regions with few or no gauging stations.

Wang *et al.* (2021) modelled the coupling processes of ET and soil water balance in agroforestry systems. The researchers conducted a comprehensive study that combined modelling techniques with field experiments to explore the interaction between evapotranspiration (ET) and soil water conditions in agroforestry on the Loess Plateau of China from 2016 to 2018. Their research involved the development of a multi-source ET model tailored for intercropping systems, which took into account the impact of varying heights of different plant species in agroforestry on water vapour resistance. This enhanced ET model was then integrated with a soil water balance model to simulate the partitioning of ET. To validate the model, they used data on soil water content in the 0-200 cm layer, seasonal ET calculated with the soil water balance model, and directly measured understory ET. The results demonstrated that the root mean square error (RMSE) for simulated soil water content ranged from 7.3% to 10.1%. In comparison, the RMSE for simulated total ET and understory ET were notably low at 3.9% and 4.2%, respectively. The study suggested that the water transportation model they developed could also be applied to assess water utilisation and enhance the planning and management of various other agroforestry systems.

2.1.4 Determination of the Soil Moisture

Ladekarl (1998) estimated the components of soil water balance in a Danish oak standing Denmark from soil moisture measurements using Time Domain

Reflectometry (TDR). The study was carried out to determine spatial and temporal variability in soil water content and also choose water balance components. The study involved the placement of 56 TDR probes in a specific arrangement. These probes were positioned along two orthogonal lines at four different distances from a single tree trunk and at depths up to 2 meters. The probes were inserted both vertically and horizontally into the soil. One notable finding was that the variation in soil water content measurements between probes was more pronounced for the vertically inserted inquiries than the horizontally inserted ones. This difference was attributed to the varying thickness of soil horizons. Additionally, it was observed that the initial month following probe installation in the arid forest soil led to significant fluctuations in the measured soil moisture levels due to soil disturbance caused by the installation process. To estimate percolation, evapotranspiration, and soil water content, the study employed a simple conceptual evapotranspiration model. The model demonstrated an excellent performance in simulating soil water content. The findings indicated that, on average, annual evapotranspiration accounted for 50% of gross precipitation. Transpiration represented 88% of gross rainfall during the dry summer of 1992, while in the wetter summers of 1993 and 1994, transpiration constituted 52% and 64% of gross precipitation, respectively.

Walker *et al*. (2004) compared the techniques for in situ soil moisture measurement from the Nerrigundah catchment in eastern Australia. They cited that, in recent decades, various automated methods for measuring soil moisture content at specific points have been developed. This study evaluated different soil moisture sensors, including the Virrib®, Campbell Scientific CS615 reflectometer, Soil Moisture Equipment Corporation TRASE® sensors (both buriable and connector-type), and compared the connector-type TDR sensor with thermo-gravimetric measurements over a 2-year field study. The comparison involved qualitative and quantitative assessments using a basic water balance model and a model based on Richards's equation. The results indicated that the connector-type TDR sensors, when calibrated according to the manufacturer's specifications, provided soil moisture measurements that fell within the manufacturer's specified accuracy of $\pm2.5\%$ volume/volume, outperforming the other tested sensors. The research

findings suggest that connector-type TDR sensors offer the most accurate measurements of soil moisture content compared to the other sensors assessed.

Skierucha *et al*. (2008) calibrated a TDR probe for low soil water content measurements. They remarked that the TDR probes are increasingly employed for assessing soil moisture content in both field and laboratory settings. The typical calibration media for these probes are air, which has a low dielectric constant, and water, which has a high dielectric constant. However, the range of soil dielectric permittivity that is measured is considerably narrower than what the calibration media imply. The authors of this study argued that calibrating a short TDR probe using air could lead to calibration errors due to the overlap of the incident and reflected pulses in the reflectogram, a phenomenon referred to as the convolution effect. To address this issue, they proposed an alternative approach that reduces dielectric permittivity measurement errors. This approach involves selecting a calibration medium with dielectric permittivity values that closely match the boundaries of the measurement range. Additionally, it allows for using TDR probes of various lengths to improve accuracy.

The soil moisture was estimated using electrical resistivity and TDR methods by Calamita *et al.* (2012) at the Vallaccia catchment in central Italy. The research aimed to assess the suitability of the resistivity method in studying variations in soil moisture over time and space. Over more than one year, the investigators conducted extensive correlation and regression analyses, simultaneously measuring soil electrical resistivity and soil moisture. This analysis covered the entire dataset and was performed separately for each sampling day, each sampling location, and spatially averaged data. The results demonstrated a strong correlation between resistivity and soil moisture measurements, indicating that resistivity measurements could effectively capture spatial and temporal changes in soil moisture. It was noted that compared to TDR, the resistivity method provided information integrated over a larger soil volume and was more efficient and quicker to carry out. As a result, the resistivity method could serve as a valuable alternative tool for both qualitative and quantitative monitoring of soil moisture in small to medium-sized watersheds.

Alvarez-Garreton *et al*. (2014) accessed the impacts of assimilating satellite soil moisture into a rainfall–runoff model in a semi-arid catchment at Wyandra River in Queensland, Australia. The study emphasised the significant role of soil moisture in the mechanisms that generate runoff, and it highlighted that incorporating soil moisture data into rainfall-runoff models is considered a means to enhance the accuracy of predictions. In this research, a continuous streamflow modelling approach was employed within the watershed, effectively harnessing satellite-derived soil moisture observations to improve prediction capabilities. The authors observed the non-linear relation between runoff and soil moisture and identified their threshold values. They found total runoff as the primary component. Further, they suggested that antecedent soil moisture exerted an essential control in the runoff generation mechanisms. Finally, the study concluded that effective pre-processing of observed soil moisture data is crucial to data assimilation, and the quality of the model calibration significantly influences its performance.

A comprehensive calibration of Time Domain Reflectometry (TDR) was carried out by Zanetti *et al*. (2015) to evaluate soil moisture in tropical soils using Artificial Neural Network (ANN) for five distinct soil types. This calibration incorporated physical properties such as bulk density, sand, silt, clay, and organic matter. All five soils were simultaneously calibrated utilising a TDR device, with at least one of these physical properties in addition to the apparent dielectric constant (K_a). The findings revealed that the statistical metrics for the ANNs slightly outperformed third-order polynomial equations (resembling Topp equations) specifically tailored to each soil type. Notably, the results indicated that the inclusion of organic matter content, in combination with K_a, in the ANN calibration of TDRs yielded favourable outcomes, with Root Mean Square Error (RMSE) values ranging from 0.0126 to 0.0237 g g^{-1} and coefficient of determination (R^2) values ranging from 0.9083 to 0.9891. Finally, it was concluded that TDR calibration using ANN suits sandy soils.

Deng *et al*. (2020) suggested a method of electrical conductivity compensation in a low-cost soil moisture sensing measurement, which was based on

capacitance. They stated that, at present, the detection of soil dielectric constant is the most effective and convenient method to measure soil moisture content. However, the production cost of the measurement circuit is very high, and it also requires a large-scale deployment of sensors in agricultural fields. So, as a price advantage, a low-frequency capacitance detection method was used. However, it needed higher measurement accuracy and hence, the application needed to be improved. The study aimed to enhance the precision and applicability of low-frequency capacitance moisture sensors by correcting the relationship between low-frequency capacitance and soil moisture content by assessing soil conductivity. The authors examined three modified models (logistic, exponential, and polynomial) to estimate moisture content by comparing their results with values obtained from the oven-drying method calibration. The findings revealed that the logistic model produced the best results, with a Maximum Absolute Measurement Error (MAME) and Mean Absolute Error (MAE) below 3.55% and 2.50%, respectively. These levels of accuracy meet the requirements for soil moisture detection in most agricultural production scenarios. Consequently, the study offered an effective and cost-efficient method for low-cost soil moisture detection in soils with low salinity and organic matter, making it suitable for large-scale development.

Wyatt *et al*. (2020) focused on the impact of in-situ soil moisture data on improving the accuracy of seasonal streamflow forecasts in rainfall-dominated watersheds. The study aimed to assess the potential enhancements achieved by integrating in-situ soil moisture information into seasonal streamflow forecasting models. The researchers utilised precipitation and soil moisture data from four watersheds in the United States of America (USA). They applied a modified principal components analysis and regression method to predict seasonal streamflow totals with lead times of 0, 1, 2, and 3 months. The findings revealed that forecasts based solely on antecedent precipitation often needed more statistical significance and could explain less than 30% of the variability in seasonal streamflow, as indicated by the NSE coefficient. In contrast, forecasts incorporating soil moisture data exhibited an average reduction of 55% in RMSE compared to those relying solely on antecedent precipitation. This led the authors to suggest that this

innovative forecasting approach holds significant potential for application in managing surface water in regions characterised by rainfall domination.

The soil moisture in Oxisols was assessed by Ferreira *et al.* (2021) in the central Brazilian savanna using electrical resistivity. The study recognised the importance of determining the spatial distribution of soil moisture in the field and acknowledged the substantial challenges associated with this task. The investigation aimed to establish relationships between moisture levels and electrical resistivity for a typical tropical soil, evaluating the reliability of this approach as a method for predicting soil moisture. The results revealed a non-linear and inverse relationship between soil electrical resistivity and volumetric moisture. Moreover, it was observed that Archie's law, in its generalised form, could be utilised for estimating the water content of these soils. When represented on a semi-logarithmic graph, the resistivity-to-volumetric soil moisture relationship exhibited a two-step pattern with significant changes occurring around the moisture level associated with the wilting point. Through field validation, the study concluded that electrical resistivity was a viable method for measuring soil moisture and mapping its subsurface horizons.

Villoro *et al*. (2021) used a TDR wireless device for volumetric water content sensing. The study noted that Time Domain Reflectometry (TDR) is a widely adopted method for estimating soil volumetric water content (θ) and bulk electrical conductivity (σ). The authors introduced TDR-WiFi, a wireless, portable, and cost-effective interface designed to facilitate the measurement of θ and σ using a smartphone connected to a TDR cable tester. TDR-WiFi consisted of a microprocessor with a WiFi microcontroller (M5 Stack unit) linked to the TDR device through an RS232-TTL adapter. The firmware for the M5 stack was programmed in MicroPython to function as a server, enabling communication between the user and the TDR device via a web page accessible through any smartphone web browser. TDR-WiFi was compatible with the Campbell TDR100 device and could store TDR waveforms while estimating θ and σ. A complementary web page was created for subsequent analysis of the TDR waveforms. The authors successfully demonstrated the system's functionality both in a laboratory setting and

in field trials, where it allowed for water content measurements even on steep slopes. They concluded that TDR-WiFi proved effective in the field and anticipated its satisfactory use in hard-to-reach areas.

2.1.5 Determination of the Water Table

Glendenning *et al*. (2012) reviewed balancing watershed and local scale impacts of rainwater harvesting in India. They claimed that the depletion of groundwater resources in India is mainly because agricultural production increasingly relies on groundwater. They confirmed that Rain Water Harvesting (RWH) for groundwater recharge is one of the solutions to solve the groundwater problem. They quoted water level measurements as a preferred method for measuring RWH recharge as a water table fluctuation method coupled with a water balance approach. They also suggested modelling as a possible tool to extend limited field data. The authors reported that remote sensing and advanced statistical techniques are new opportunities for evaluation for the RWH part of watershed development. They suggested the SWAT model to analyse the benefits and potentials of RWH, especially for ungauged watersheds.

A novel approach for mapping groundwater recharge in irrigated regions in a changing climate, specifically in the Lower Chenab Canal area of Pakistan was developed by Awan and Ismaeel (2014). To achieve this, the researchers used a Soil and Water Assessment Tool (SWAT) model to simulate both groundwater recharge and actual evapotranspiration (ET_a). They then compared these ET_a estimates derived from the SWAT model with those obtained through the Surface Energy Balance Algorithm (SEBAL), calibrated based on data from 2005-2009. The study successfully demonstrated that the ET_a estimates generated by the SWAT model exhibited a strong level of agreement with those derived from SEBAL, with statistical measures including an R-squared (R^2) value of 0.85±0.05 and a Nash-Sutcliffe Efficiency (NSE) of 0.83±0.07. The authors concluded that by using remote sensing data, the SWAT model can effectively estimate groundwater recharge at a high spatial and temporal resolution.

Mohammadi *et al*. (2014) aimed to assess groundwater recharge in a semi-arid groundwater system in the Zagros Orogen region of Southern Iran, emphasising the critical role of accurately estimating groundwater recharge, particularly in semi-arid areas. The research employed a straightforward water balance equation to calculate the total annual groundwater recharge for eight water years from 2002 to 2010. The study highlighted that the water balance equation is a widely utilised method for quantifying groundwater recharge, and the reliability of results depends on the quality of data used to compute various components of the water balance. Two approaches were employed to estimate the total annual groundwater recharge: (1) summing the known inflow components to the aquifer system and (2) summing the outflow components from the aquifer along with the annual change in aquifer storage. A comparison of results between these two approaches revealed a significant difference, with an average annual recharge estimate of 91.30 million cubic meters. The study suggested that this difference may stem from potential errors in quantifying the inflow components and the possibility of an unidentified inflow component. Sensitivity analysis indicated that the disparity in the estimated annual recharge exceeded the estimated 20% error in quantifying the components of the water balance equation. The contribution of this unidentified inflow component to annual groundwater recharge ranged from 33.25 to 132.90 million cubic meters per year, with an average of 91.30 million cubic meters per year.

2.2 ESTIMATION OF THE WATER BALANCE FOR A WATERSHED

Flerchinger and Cooley (2000) computed a ten-year water balance of a mountainous semi-arid watershed at Upper Sheep Creek Watershed, which was a 26-ha semi-arid mountainous sub-basin within the Reynolds Creek Experimental Watershed in southwest Idaho, USA. The approach presented by the researchers involved calculating a partial water balance for each of the three distinct landscape units and then aggregating these to compute a water balance for the entire watershed. Notably, the study observed that it took much work to differentiate between runoff and changes in groundwater storage within these landscape units. Precipitation was directly measured within each landscape unit, with adjustments for any measurement drift. The study also noted that the spatial variability of adequate

precipitation was more pronounced in years with higher overall precipitation levels. Evapotranspiration, accounting for nearly 90% of proper rainfall, was estimated using the Simultaneous Heat and Water (SHAW) method. The authors established a correlation between runoff in the watershed and precipitation exceeding a critical threshold of approximately 450 mm, which was necessary to generate runoff. The research indicated that the average water balance error was 46 mm, equivalent to about 10% of the estimated adequate precipitation over ten years. This error was primarily attributed to deep percolation losses through fractures in the basalt rock underlying the watershed. The study found that the simulated percolation of water beyond the root zone closely matched the measured runoff, primarily originating from subsurface flow. Above a threshold of 50 mm, approximately 67% of water percolating beyond the root zone contributed to runoff, with the remainder presumed to be lost to deep percolation through the basalt. In conclusion, the study highlighted the significant implications of these findings for understanding subsurface flow and losses in simulating runoff and hydrological processes within the watershed.

Fowler (2002) assessed the validity of using mean Potential Evaporation (PE) in computations of the long-term soil water balance in Auckland, New Zealand. He mentioned that mainly precipitation data is used for such work but can substitute climatological representation to estimate PE. He predicted that if a climatological estimate is used in the water balance, errors will tend to cancel out. The author's approach aimed to validate climatological PE in long-term water balance studies. This was achieved by comparing time series of water deficit using a daily water balance model. Over more than 13 years at the chosen location, modelling experiments were conducted, explicitly comparing the model's performance during wet and dry years. The findings revealed that when climatological PE estimates were substituted into the daily water balance model, it yielded a soil water pattern similar to that obtained using actual PE values. The study's conclusion emphasised that the most favourable results were achieved when a reduction in PE was applied to account for the suppression of PE on rainy days.

The water balance over the Tigris–Euphrates watershed was assessed by Kavvas *et al*. (2011). The researchers conducted an extensive assessment of the watershed, encompassing land use and land cover, vegetation, soil characteristics, and the existing hydraulic infrastructure. They also developed a regional hydro-climate model, RegHCM-TE, to reconstruct historical precipitation data. This data was used to calculate various hydrological components such as infiltration, soil water storage, actual evapotranspiration, and direct runoff, which served as inputs for streamflow calculations. Additionally, the model was employed to estimate irrigation water requirements. Furthermore, the study included creating a hydrological model for routing streamflows within the watershed's river network. The researchers applied an algorithm to manage the reservoirs within the watershed, enabling them to conduct dynamic water balance assessments under different scenarios of water supply and demand. This approach aimed to optimise utilising the watershed's water resources to fulfil water demands efficiently. In conclusion, the study highlighted the utility of this dynamic water balance framework, which allowed for the assessment and quantification of the impact of sequential river flows on the chronologically evolving water balances across the watershed.

Kumar and Srinivasan (2016) examined the climatic water balance and drought conditions in the Kallar Watershed of Tamil Nadu, India. The researchers emphasised that studying the water balance of a watershed is crucial for comprehending its hydrology, which, in turn, informs the development of water resources for various beneficial purposes. To conduct their analysis, the study used three key parameters: precipitation, temperature, and water-holding capacity. These primary parameters were used to derive secondary water balance components, including potential evapotranspiration, actual evapotranspiration, water deficit, and water surplus. Additionally, the research introduced four water balance indices: the index of aridity, the index of humidity, the index of moisture, and the index of moisture adequacy, which were computed from the secondary water balance components. By employing these derived indices, the authors were able to assess drought conditions, climatic variations, and the agricultural potential of the region. The study's findings revealed a persistent water deficit throughout the year, except

during October and November. In light of these results, the study recommended the implementation of sustainable water management practices for areas facing such prolonged water deficits.

The water budget was assessed by Oroud (2015) for semi-arid watersheds in the eastern Mediterranean. It was noted that there needed to be more comprehensive data regarding evapotranspiration, runoff, and deep recharge in these catchments, primarily due to insufficient meteorological and hydrological measurements. Therefore, establishing meteorological, hydrological, and geomorphological measures was deemed essential to create a dependable database for comprehending the dynamics of rainfall and runoff/sediment yield. To address this data scarcity, the author utilised a transient model and integrated field measurements into the model, particularly in areas with limited hydro-meteorological data. The study also compared the simulated results and long-term flow observations, which revealed that the model performed satisfactorily. The results demonstrated that evapotranspiration, surface runoff, and deep recharge accounted for 87.5%, 7.5%, and 5% of the areal precipitation, respectively. The study concluded that significant runoff predominantly occurred in steep terrains with limited vegetation cover, adversely impacting water quality and the lifespan of dams constructed in these catchment areas.

Lv *et al*. (2017) conducted a study on the closure of the water budget in two large and densely-populated mid-latitude basins, namely the Yellow River basin and Changjiang River basin, using Gravity Recovery and Climate Experiment (GRACE) measurements. They emphasised that GRACE-derived terrestrial water storage change (TWSC) offered an opportunity to achieve closure in the terrestrial water budget. However, it was noted that achieving this balance was a challenge without considering human water use factors, such as irrigation and inter-basin water diversion, when estimating other water budget terms like evapotranspiration (ET). To address this, the study reconstructed ET using the Global Land Data Assimilation System (GLDAS) land surface models, considering naturalised streamflow and irrigation water, with absolute relative errors of less than 1.9%. The total basin

discharge was calculated as the residual from the water budget, incorporating observation-based precipitation and TWSC. The authors evaluated budget closure by comparing the difference between the total basin discharge and the observed total basin discharge while considering inter-basin water diversion. After reconstructing ET, the mean absolute imbalance values were significantly reduced, from 3.31 cm year^{-1} to 1.69 cm year^{-1} in the Yellow River basin and from 15.40 cm year^{-1} to 1.96 cm year^{-1} in the Changjiang River basin. The authors analysed the naturalised streamflow, consumed irrigation water, and inter-basin water diversion at annual time scales and suggested future studies for monthly time scales. They urged the proposed ET reconstruction method to be applied to other human-managed river basins to provide an alternative estimation.

Noviadi *et al*. (2019) analysed the water balance in the Bera watershed of area 164.6 km^2 in the Sumbawa River basin, Indonesia. They recorded the rainfall using 11 automatic rainfall recorders and interpolated the data with the isohyet method and inverse distance weighted analysis. The evaporation was estimated using data from the climate station located in Plampang. The water available was calculated using the net field requirement method. Finally, the water balance was calculated using Excel software by comparing the demand and supply of water that could be provided based on water availability. The study found that the rainfall in the region ranged from 0-124.30 mm, and the evaporation ranged from 3.94-7.92 mm while the discharge ranged from 0.32 l s^{-1} to 1221.60 l s^{-1} for a ten-day interval. The water requirements, calculated using the net field requirement method, had a discharge ranging from 0.15 l s^{-1} to 2036.30 l s^{-1}. It was found that the average water supply was 60% of rainfall, which indicated the need for better arrangements in water collection buildings and irrigation networks.

The impact of watershed characteristics on long-term annual and intra-annual water balances in India was investigated by Sinha *et al*. (2019). To accomplish this, the researchers developed a model using multiple linear regression methods and machine learning techniques, including Artificial Neural Network (ANN) and Relevance Vector Machine (RVM). This analysis encompassed 793

locations, including 25 major river basins and 768 watersheds across India, collectively covering approximately 90.32% of the country's total land area. They estimated the watershed parameter 'ω' that represented intrinsic watershed attributes. It was observed that the ANN and RVM models performed better in estimating ω than the Multiple Linear Regression (MLR) models. Moreover, the Normalized Difference Vegetation Index (NDVI) was more involved in explaining water distribution processes during inter-annual periods of low NDVI than periods of high NDVI. Furthermore, the study observed that the newly improved models closely mimicked the inherent characteristics of the individual basins and significantly enhanced the functionality of the Budyko framework for estimating water availability. This enhancement was pivotal for evaluating hydrological processes in ungauged watersheds across India.

2.3 MODELING USED FOR ESTIMATION OF THE WATER BALANCE

Xu and Singh (1998) reviewed monthly water balance models since the 1940s and discussed the relevance of various aspects of the practical application of such models for water resources investigation. The study examines the introduction of monthly water balance models, initially developed to assess the significance of various hydrological parameters across different hydrological conditions. These models were categorised based on their primary objectives and further grouped according to the input data requirements. The research also highlighted that, in some cases, monthly data on precipitation, temperature, and evaporation proved to be adequate, with precipitation data alone being sufficient at times. These monthly water balance models are advantageous because they typically require fewer parameters to describe hydrological phenomena. This results in a higher level of information per parameter, enabling a more precise determination of parameters and more reliable correlations between parameter values and catchment characteristics. As a result, these models can be applied effectively to ungauged catchments. The authors identified two practical reasons for using monthly models. First, they are valuable for water resource planning and predicting the impacts of climate change. Second, monthly hydro-climatological data are readily accessible. The study reports that current applications of water balance models focus on three main areas:

reconstructing the hydrology of catchments, evaluating the effects of climate change, and assessing the seasonal and geographical variations in water supply and irrigation requirements.

Muttiah and Wurbs (2002) studied the scale-dependent soil and climatic variability effects on the watershed water balance of the SWAT model for large watersheds in Texas, USA. They used land use and land cover from the United States Geological Survey (USGS) at 200 m resolution. The penman-Monteith method was used to estimate evapotranspiration using 30 years of daily climatic data. The study provided a concise overview of the SWAT model and its approximation method for assessing the sensitivity to the mean and variance of water balance components. To examine the alterations in the mean and variance of water balance components resulting from variations in soil and climate, the research encompassed six distinct watersheds. Soil parameters such as bulk density, available water capacity, and moist soil albedo were selected, and soil heterogeneity in the watersheds was analysed based on textural classes. Additionally, the research quantified the spatial variability of precipitation between nearby weather stations using power spectra. It investigated how changes in the geographic scale influenced the mean of water balance components. The authors proposed the existence of scale-dependent uncertainty laws related to water balance. They emphasised the critical role of precipitation in regulating the water balance of large watersheds. They concluded that climatic and soil variability had the most significant impact on water balance components.

Tripathi *et al*. (2006) investigated the impact of subdividing the Nagwan watershed in eastern India on the simulation of water balance components using the SWAT model. The research utilised meteorological and hydrological data, including daily rainfall, temperature, relative humidity, and runoff, from 1995 to 1998. Geospatial information, such as watershed and sub-watershed boundaries, slope, and soil texture maps, was generated through GIS. Land use/cover classification for 1996 was performed using a supervised classification method on satellite imagery. The study spatially divided the watershed into three schemes: a single watershed, 12

sub-watersheds, and 22 sub-watersheds, to investigate the effects of watershed subdivision. The simulation using the SWAT model was conducted over four years, from 1995 to 1998. The findings indicated that the water balance remained consistent across all three subdivision schemes. Notably, the number and size of sub-watersheds had minimal influence on surface runoff. However, variations were observed in other water balance components, with evapotranspiration ranging from 5% to 48%, percolation from 2% to 26%, and soil water content from 0.30% to 22%. In conclusion, the study emphasised that subdividing the watershed had a significant impact on water balance components.

The potential effects of climate change on the water balance of a semi-arid watershed situated in the Zarqa River Watershed (ZRW) of Jordan was evaluated by Abdulla *et al.* (2009). The methodology involved simulating how the basin's hydrological response would change under various climate change scenarios. To accomplish this, the researchers utilised the U.S. Environmental Protection Agency's (EPA) BASINS-HSPF modelling environment, specifically designed for simulating the primary hydrological processes affecting the spatial and temporal distribution of water. They applied this modelling environment to develop a hydrological model for the ZRW, incorporating digital elevation, land use, soil, and hydro-meteorological data. The model's calibration for the ZRW was carried out using a 15-year data record from 1980 to 1994. Validation of the model was conducted against an independent data record spanning seven years from 1995 to 2002. The quality of calibration and verification results was assessed through linear regression analysis of monthly and daily flow data. Monthly calibration and validation exhibited strong fits with regression coefficient (r) values of 0.928 and 0.923, respectively, while daily records showed an r value of 0.785. The study's conclusion highlighted the potential for climate warming to impact runoff and groundwater recharge in the ZRW significantly. However, the researchers emphasised that substantial changes could heavily influence the extent of this warming's influence on rainfall volume.

Ghandhari and Moghaddam (2011) reviewed water balance principles for five watersheds in Iran. They cited that the water balance models were introduced to

evaluate the different hydrologic parameters, but presently, they are widely used for water resource management. It was stated that though water balance is a simple concept, it can cause huge errors. They specifically mentioned that most of the models in the country used in water resource planning were extracted from different climatic conditions and needed to be concentrated while using models for achieving effective water management. Ghandhari and Moghaddam investigated five separate watersheds in the northeast region of Iran and compared their results with two other published results. They found significant deviations between supposal and actual values of water balance parameters. Their conclusion emphasised that achieving more effective water resource management could be facilitated by establishing minimum standards, specifying the necessary parameters and estimation methods for distinct local zones, ensuring reliability, adopting new cost-reduction techniques and tools, and enhancing field measurements.

The hydrological processes in the Arrio Lino Watershed in Southern Brazil was assessed by Bonuma *et al*. (2013), employing the SWAT model while considering the measurement uncertainty. They utilised measured discharge data from the watershed outlet to evaluate the sensitivity of selected parameters for streamflow calibration and validation from 2001 to 2005. To account for measurement uncertainty, they adapted the statistical indicators. Their findings indicated that the monthly streamflow predictions closely matched the observed values, yielding NSE coefficients 0.87 during calibration and 0.76 during validation. It was noted that the daily goodness-of-fit indicators were initially lower but showed improvement when incorporating the uncertainty in measured data. As a result, the study suggested that the SWAT model held promise as a valuable tool for assessing hydrological processes in Brazilian watersheds.

Touhami *et al*. (2015) assessed the influence of climate change on soil water balance and groundwater recharge in a semi-arid region of southeastern Spain. To achieve this, they employed the HYDROBAL hydrological model, designed to estimate water balances in ecosystems dominated by various vegetation types by integrating meteorological conditions, vegetation characteristics, and soil processes.

The HYDROBAL model calculated water flows across vegetation canopies and soil water balance through a straightforward mass balance equation on a daily time scale. The necessary input data included soil information, climate data, vegetation data, and reference evapotranspiration. The model's outputs encompassed variables such as interception, net precipitation, surface runoff, soil water reserves, actual evapotranspiration, direct percolation, infiltration, and potential recharge. The researchers conducted a General Linear Model univariate analysis based on these output variables to examine the water balance outcomes. Their findings indicated that, during the selected years for running the HYDROBAL model, there were declines in various water balance components, including precipitation, actual evapotranspiration, groundwater recharge, and runoff, compared to the baseline of 1961-1990. The authors concluded that this method proves valuable for assessing the impacts of projected climate change on groundwater recharge and can assist water resource managers and planners in developing strategies for the efficient utilisation and conservation of freshwater resources.

The effects of climate change on water balance components were examined by Leta *et al.* (2016) within the Heeia watershed in Hawaii, USA, utilising the SWAT model. The researchers employed a calibrated model to evaluate how alterations in rainfall, temperature, and carbon dioxide concentration would impact the watershed's water balance. One key observation was the high initial abstraction of rains in the Heeia watershed, attributed to the soils substantial initial infiltration capacity. Furthermore, the study revealed that the simulated streamflows closely matched the observed data, indicating significant agreement and satisfactory model performance. This underlined the suitability of SWAT for assessing small island watersheds characterised by substantial variations in topography, precipitation, and land use. In addition, the researchers introduced methods to address issues related to data scarcity, further enhancing the model's utility in these challenging settings. The authors predicted that the overall decrease in water balance components was due to climate change scenarios, which showed a decline in rainfall during the wet season and a marginal increase in the dry season.

Sandra and Sathian (2016) conducted a comprehensive assessment of the water balance within the Kurumali sub-basin of the Karuvannur River basin for water resources management. To achieve this, they gathered various thematic maps and attribute data for the watershed from multiple government agencies. Then, they established and configured the SWAT model, incorporating digital thematic maps, soil properties, and climate parameters as inputs. Within the catchment, they identified six distinct land use categories and eight different soil types. The model underwent calibration and validation, comparing its river flow predictions with observed values. Impressively, the model exhibited high-performance metrics, with NSE and R^2 values reaching 0.88 and 0.96 during calibration and 0.90 and 0.99 during validation, respectively. Using the calibrated model, they predicted crucial hydrologic processes, including surface runoff, lateral flow, base flow, and evapotranspiration. Their findings indicated that base flow accounted for 64% of annual rainfall, lateral flow contributed 12%, and surface runoff constituted 9%. As a result of their study, the authors proposed that the SWAT model could be effectively employed for simulating river flow and forecasting the water balance of a river basin within the humid tropics.

Kundu *et al*. (2017) analysed the separate and combined impacts of anticipated climate and land use changes on the water balance within a section of the Narmada River basin in Madhya Pradesh. They underscored the significant influence of land use changes on a basin's water balance and sub-watersheds, affecting various parameters like water yield, surface runoff, and evapotranspiration (ET). Using the SWAT model, the researchers examined how the future water balance would be affected by both the independent and integrated consequences of climate and land use alterations. Their study involved projecting changes in water balance for 12 sub-watersheds within the basin. The findings revealed that, in the future, these sub-watersheds would experience increased water yield and reduced ET. The sub-watersheds 1 to 7 exhibited comparatively higher surface runoff and water yield, primarily due to bare lands, agricultural areas, and settlements. In contrast, the southern sub-watersheds, from 8 to 12, displayed lower water yield and

surface runoff but higher ET, primarily because of the more fabulous presence of vegetation and forested areas in these regions.

The water balance and water yield for the Reedy Fork-Buffalo Creek Watershed in North Carolina was estimated by Ayivi and Jha (2018), utilising the SWAT model. The study aimed to assess the SWAT model's performance in analysing watershed hydrology and the streamflow variability within the watershed. By examining graphical results, the researchers noted that the SWAT model effectively tracked monthly flow patterns during calibration and validation periods. One key observation was that evapotranspiration (ET) was the most significant contributor to water loss from the watershed, accounting for 65.4% of the total. The total annual water yield was estimated to be 343 mm, with 132 mm attributed to surface runoff and 215 mm to baseflow. The researchers employed statistical model performance measures, including R^2 and NSE, to assess the correlation between observed and simulated monthly streamflow. Their analysis indicated strong agreement between observed and simulated flow, with both NSE and R^2 exceeding 0.7 for the calibration and validation periods. In conclusion, the study suggested that the SWAT model holds promise as a decision-support tool for predicting water balance and water yield, particularly in the context of sustainable water management, where both water quality and quantity are critical concerns.

Tejaswini and Sathian (2018) assessed hydrological processes within a small watershed in Valancheri, a sub-basin of the Bharathapuzha river basin in Kerala. To tackle the challenge of working with an ungauged watershed, the researchers employed a regionalisation technique. Calibration of the SWAT model was performed in the Kunthipuzha basin, which shared similar characteristics with the study area, and the calibrated parameters were subsequently applied to the Valancheri watershed. The model calibration was executed from 2000 to 2006, and validation occurred from 2007 to 2009. The model's performance was satisfactory, with performance metrics of Nash-Sutcliffe Efficiency (NSE) at 0.81 and Coefficient of Determination (R^2) at 0.82 during the calibration period. In the validation period, R^2 was at 0.95, and NSE was at 0.82. Using this well-calibrated

model, the researchers made predictions at the micro-watershed level for various hydrological elements in the Valancheri watershed. Their findings and simulation results were deemed highly valuable for the planning and developing of water resources in the local area.

Abdulla and Al-Shurafat (2020) conducted rainfall-runoff modelling in a semi-arid region with trans-boundary characteristics, specifically within the Yarmouk River basin, spanning two countries, Jordan and Syria. They investigated the capability of the SWAT model to simulate streamflow for the Yarmouk River basin. They used the available daily precipitation, ET, and runoff data with an optimisation technique to calibrate SWAT. For the pre-development condition (i.e. basin without artificial changes), the model performed well for the Yarmouk River basin, for which the R^2 was 0.87 and 0.81 for both the calibration period (1986-1995) and validation (1996-2000) period, respectively. The study involved a comparison of the model-generated average monthly runoff with observed data, and the results were deemed satisfactory. Furthermore, the model performed well under post-development conditions, achieving R^2 values of 0.89 during calibration and 0.81 during validation. The researchers concluded that the SWAT model could effectively simulate hydrological processes with a high level of accuracy, making it a viable choice for water hydrology studies. In their final remarks, they emphasised that the modelling outcomes from this study could be a valuable resource for water authorities in improving water resources management within the Yarmouk River basin.

Eini *et al.* (2020) developed an alternative SWAT-based model to simulate water budget components and streamflow in a watershed influenced by karst characteristics. Their study focused on the Maharlu Lake catchment in the southwest province of Fars, Iran. They explored two innovative approaches to model the hydrological processes of a karst system within the Zagros Mountains in Iran. The significant modifications made in these two methods involved adjusting percolation rates in karst Hydrologic Response Units (HRUs) through the SWAT-Maharlu Lake (SWAT-ML) model and altering the crack flow module using the SWAT-Crack

Flow (SWAT-CF) model. They used hydrological datasets from 1980 to 2013 for calibrating and validating various parameters, including surface runoff, baseflow, crop yields, and actual evapotranspiration. Both of the modified models outperformed the standard SWAT model in simulating runoff. The average Nash-Sutcliffe Efficiency (NSE) values for the original SWAT, SWAT-ML, and SWAT-CF were 0.64, 0.68, and 0.66. Moreover, the results indicated that the modified models provided more accurate estimates of deep aquifer infiltration for karst HRUs, resulting in improved recharge assessments of the deep aquifer. However, the findings also revealed that the presence of karst conditions and the geometry of sinkholes in karst regions did not have a significant impact on the generation of runoff.

Gebru and Tesfahunegn (2020) focused on estimating water balance components in the Dura sub-catchment in Northern Ethiopia by employing a flexible, physical, and GIS-based WetSpass water balance model. To analyse various data, they utilised Descriptive and Inverse Distance-weighted methods and calculated actual evapotranspiration (ET), surface runoff, and groundwater recharge. They also determined the Potential Evapotranspiration (PET) for the area, and their performance assessment demonstrated an error of less than 2%, indicating the robustness of the model for supporting decision-making. Their findings revealed that the model-estimated annual actual ET accounted for 78.4% of the mean annual rainfall. However, they also observed spatial and temporal variations in ET across the sub-catchment. Notably, a significant portion, approximately 77.5%, of the annual actual ET occurred during the summer season. Moreover, the study indicated that about 7.9% and 13.7% of the mean yearly precipitation effectively contributed to groundwater recharge and surface runoff, respectively. The researchers concluded that the water balance components estimated using the WetSpass model closely aligned with observed data, as evidenced by high R-squared values ($R^2 > 0.90$) and slight percentage differences (D < 5%). These results demonstrated the importance of the model outputs for facilitating decision-making processes. Furthermore, the authors affirmed that the WetSpass model proved to be a robust tool for assessing the temporal and spatial variability of water balance components when integrated

with GIS, even in ungauged sub-catchments with diverse resources such as soil types, Digital Elevation Models (DEM), land use categories, and management practices. Lastly, they recommended the implementation of site-specific integrated soil and water management schemes, such as water conservation structures, to enhance groundwater retention and reduce runoff.

The SWAT model was applied to estimate runoff of the Nethravathi river basin in the Dakshina Kannada district of Karnataka, India by Krishnan *et al.* (2018). They remarked that this region faced water scarcity during the summer and severe runoff during the rainy season, using 36 years of data (1970-2005). The study utilised SWAT-CUP in combination with the Sequential Uncertainty Fitting (SUFI-2) technique to assess the model's sensitivity, calibration, and validation. Calibration was carried out from 1995 to 1999, and verification was conducted from 2000 to 2005. Central Water Commission discharge data collected at the Bantwal station were used for both monthly and daily discharge data to validate the model. The findings indicated that the monthly time step yielded superior results compared to the daily time step for both calibration and validation. For monthly simulations, the R-squared (R^2) and Nash-Sutcliffe Efficiency (NSE) values were 0.96 and 0.94, respectively, during the calibration period and 0.91 for both during validation. In contrast, for daily calibration, the R^2 and NSE values were 0.88 and 0.84, respectively, and 0.80 and 0.79 during validation. The study revealed that the average annual runoff equated to 30% of the average yearly rainfall for the entire river basin. In conclusion, the authors emphasised the necessity of implementing suitable soil and water conservation structures to promote sustainable management practices in the study area.

The water balance components were estimated by Mestry *et al.* (2020) within watersheds in the Manjira River basin using the SWAT model and GIS. Specifically, two watersheds were selected, identified by the codes MNJR008 and MNJR011 specified by the Central Ground Water Board. The research utilised various SWAT input data, including Digital Elevation Model (DEM), Land Use/Land Cover (LULC) data, soil classification, slope, and weather data, to calculate different water

balance components. These components encompassed variables such as rainfall, baseflow, surface runoff, evapotranspiration (ET), Potential Evapotranspiration (PET), and water yield for each of the selected watersheds. The evaluated data were subsequently validated through regression analysis, comparing two datasets. Specifically, simulated rainfall data from the SWAT simulations was compared to observed rainfall data obtained from global weather data for SWAT. The analysis demonstrated a substantial similarity between the SWAT-simulated data and the observed data, with R-squared (R^2) values of 0.96 for watershed MNJR008 and 0.92 for MNJR011. These results indicated that the data generated from the SWAT simulations aligned closely with the observed data. The researchers suggested that this dataset could be instrumental in various water resource management programs, as it allowed for predicting actual usable water availability, mainly through the water yield component.

Nasiri *et al*. (2020) simulated the water balance components in the Samalqan watershed in Iran. They used the SWAT model for this 1148 km^2 watershed, and the streamflow simulation was considered for 13 years. The study simulated water balance components, including surface runoff, lateral flow, base flow, and evapotranspiration. These results were then calibrated using the SWAT-CUP program, and the model's performance was subsequently assessed. A sensitivity analysis was conducted, considering 26 SWAT parameters. Calibration took place over the period from 2004 to 2012, while validation occurred from 2012 to 2014. The study revealed that the model exhibited good performance, with R-squared (R^2) and Nash-Sutcliffe Efficiency (NSE) values falling within the ranges of 0.60–0.80 and 0.80–0.95 for calibration and 0.70–0.90 and 0.70–0.80 for validation periods. These results indicated that the model's outputs were satisfactory. The researchers demonstrated that the SWAT model could effectively be employed in semi-arid regions to support the development of water management policies and sustainable water management strategies. They concluded that understanding the existing water potential was crucial for water planning and managing water resources within the watershed. Furthermore, they recommended using the SWAT model for watersheds with similar characteristics and requirements.

Nyatuame *et al*. (2020) conducted a study to assess the Land Use and Land Cover (LULC) impacts on the water balance within the Tordzie watershed. The research highlighted that changes directly influenced the presence of water in the watershed in LULC. To evaluate water availability, the study employed the SWAT model integrated into ArcGIS, with a calibration period from 2000 to 2003 and validation from 2004 to 2006. The model was calibrated and validated using discharge data from the Tordzinu location within Tordzie, covering a study area of 1278.3 square kilometres. In evaluating the model's performance on a monthly timescale, the researchers utilised performance metrics such as Nash-Sutcliffe Efficiency (NSE), Coefficient of Determination (R^2), and Percent Bias (PBIAS) as evaluators. The findings indicated that under the different LULC scenarios, simulated surface flow (SUR_Q) increased by 24.65%, while water yield decreased by 6.7%. The annual simulated water yield was estimated at 132.21 mm and 123.30 mm. Consequently, the study concluded that LULC changes had a significant impact on the hydrology of the Tordzie watershed. In light of these findings, the authors recommended implementing sustainable land management techniques to mitigate the influence of LULC changes on the watershed's hydrology.

2.4 RELATION BETWEEN RAINFALL AND OTHER WATER BALANCE COMPONENTS

Tuset *et al*. (2016) investigated rainfall, runoff, and sediment transport in a Mediterranean mountainous catchment in Ribera Salada. They reported that the relation between these parameters was highly variable, and so they measured the flow discharge continuously. Rainfall data were collected from both direct rain gauges and daily rainfall reconstructions using radar information. An analysis revealed that, in comparison to other Mediterranean mountain catchments, Ribera Salada exhibited lower levels of geomorphological and hydrological activity. The researchers also conducted Pearson correlations between precipitation, runoff, and sediment transport variables. The results indicated a correlation between sediment load and the volume of direct runoff. Furthermore, through a multivariate analysis, it was predicted that the total suspended load could be estimated by considering a

combination of rainfall and runoff variables. Ultimately, they concluded that land use and climate change could significantly change water harvesting cycles.

The spectral analysis of temporal variability of nonlinear and non-stationary rainfall-runoff processes were studied by Chang *et al.* (2019). They reported that converting rainfall input to runoff output over a catchment is a complex hydrologic process. They also mentioned that the hydrological processes involved in runoff generation include rainfall, evaporation, transpiration, infiltration, groundwater, and surface runoff. The study aimed to assess the time-dependent and nonlinear response of catchments to variations in rainfall. In this context, both the rainfall and runoff discharge fields were considered to exhibit non-stationary behaviour over time. To capture the nonlinear relationship between the input (rainfall) and the output (runoff), the researchers employed a functional series representation. They utilised the Fourier-Stieltjes representation approach to analyse the variance of runoff discharge in the spectral frequency domain. The results of the analysis, based on the spectral solution for the runoff discharge variance, revealed that larger values of the catchment size parameter related to rainfall characteristics led to increased variability in the runoff discharge. Conversely, a more significant catchment scale parameter contributed to reduced variability in the runoff discharge. The authors concluded that the catchment scale parameter impacts a reduction in the cross-correlation of runoff discharge and rainfall rate, resulting in reduced runoff discharge variability.

Pravalie *et al.* (2019) analysed the spatio-temporal variations in the climatic water balance in Romania in response to trends in precipitation and reference evapotranspiration from 1961 to 2013. They pointed out that changes in precipitation (P), evapotranspiration (ET), and the Climatic Water Balance (CWB) have yet to receive sufficient in-depth analysis in many parts of the world. To address this gap, the researchers investigated the spatio-temporal changes in CWB, representing the difference between precipitation (P) and reference evapotranspiration (ET_0) in Romania. They utilised a wide range of climatic data from 70 weather stations nationwide, applying the FAO-56 Penman-Monteith

method. The study employed statistical tests, including the Mann–Kendall test and Sen's slope method, to analyse CWB trends. Additionally, the Spearman correlation procedure was used to evaluate the impact of atmospheric circulation on the variability of this index across different time scales. The results indicated a decrease in CWB for most of the study area, with reductions of up to 2 mm per year, suggesting an overall intensification of drier conditions across all time scales. The researchers attributed these negative CWB trends to a partial, statistically insignificant decrease in precipitation (P) and a statistically significant increase in reference evapotranspiration (ET_0). In light of these findings, the study underscored the importance of adapting human and ecological systems to anticipated trends of increased dryness, which could be exacerbated by the climate changes expected to occur by the end of the century.

Zhang *et al*. (2019) conducted a study to investigate the relative impacts of precipitation (P), evapotranspiration (ET), and runoff (R) on changes in terrestrial water storage across 168 river basins. The research focused on analysing three primary water fluxes: P, ET, and R. Utilizing hierarchical partitioning analysis, they quantified the respective relative contributions of P, ET, and R to Terrestrial Water Storage Changes (TWSC). The study covered the period from January 2003 to December 2011 and observed significant increases in Terrestrial Water Storage Anomalies (TWSA) in 49 basins, while 42 basins showed notable decreases in TWSA. Notably, a strong positive correlation was identified between P and TWSC in low-latitude basins, whereas mid- and high-latitude basins exhibited a strong negative correlation between TWSC and ET and R. On average, across the 168 basins and considering all possible combinations of P, ET, and R, the three independent variables collectively contributed to 61.4% of TWSC. Among these contributions, P, ET, and R accounted for 42.6%, 43.2%, and 4.2%, respectively. Spatially, low-latitude basins demonstrated a more substantial contribution of P to TWSC, while mid- and high-latitude basins exhibited a more significant contribution of ET and R. The authors concluded that the insights gained from this study hold important relevance for enhancing our comprehension of global responses in terrestrial water storage to the influences of climate change.

A study was carried out by Heerspink *et al.* (2020) on the trends in streamflow, ET, and groundwater storage across the Amazon Basin linked to changing precipitation and land cover. The authors conducted an extensive investigation into the alterations in various components of the water balance across the entirety of the Amazon Basin. Their study encompassed an analysis of how changes in land cover and precipitation impact streamflow, as well as how these factors influence the water balance components of evapotranspiration (ET) and groundwater storage. They also delved into how modifications in the partitioning of the water balance might subsequently affect streamflows. The research revealed significant changes in streamflow, with an average annual variation of ±9.5 mm across the Amazon Basin. These alterations in streamflow exhibited a spatially variable pattern, characterised by increased discharge in the northern and western regions of the basin and reduced discharge in the southern and eastern basins. Furthermore, substantial changes in ET, with an annual variation of ±29 mm and an increase in groundwater storage by 7.1 mm per year, were observed. In light of these findings, the authors emphasised that studies examining changes in streamflow should be viewed within the context of the entire water budget, encompassing the often overlooked aspects of groundwater storage. They suggested that alterations in the water balance partitioning also influence streamflows. Moreover, given the limited data available to quantify changes in groundwater storage and ET over the complete discharge record, the authors recommended using model-based investigations to gain a more comprehensive understanding of how the water balance responds to changes in climate and landscape. Ultimately, they underscored the importance of preserving the water, food, energy, and ecological resources of the Amazon Basin for a more thorough comprehension of how the water balance evolves in response to a changing environment.

Safari *et al.* (2020) delved into rainfall-runoff modelling, employing the Regression in the Reproducing Kernel Hilbert Space (RRKHS) algorithm. They applied this non-linear regression approach for rainfall-runoff modelling. This approach was chosen when conventional linear methods failed to deliver satisfactory results. The authors demonstrated the calibration and verification processes of

RRKHS for forecasting rainfall-runoff models, both for one-day and multi-day ahead predictions. They utilised daily data on rainfall and streamflow collected from a mountainous catchment in the Black Sea region of Turkey. The research outcomes showcased the superiority of the RRKHS approach over alternative methods. The relative peak error fell within the range of 0.009 to 0.299, underscoring the high accuracy of RRKHS in estimating peak streamflow. As a recommendation, the authors proposed employing the RRKHS model for modelling the daily rainfall-runoff process, particularly for generating forecasts of streamflow time series for 1, 2, and 3 days ahead. They attributed the superior performance of the RRKHS model to its formulation within a very high-dimensional space, potentially extending to infinity, thus enabling a more precise regression analysis.

Song *et al*. (2020) experimented to explore the potential of using soil moisture observations to estimate rainfall. The experiment occurred in a soil tank at Hohai University in Jiangsu Province, China, within the State Key Laboratory of Hydrology, Water Resources, and Hydraulic Engineering. In this endeavour, they designed a specialised loamy sand soil tank to carry out artificial rainfall-runoff experiments, during which they continuously monitored various parameters, including soil moisture (SM), rainfall, surface runoff (SR), and subsurface runoff (SSR). The study encompassed the analysis of 28 rainfall-runoff events, intending to assess the capability of estimating rainfall from SM observations. This estimation was achieved by applying the SM2RAIN algorithm, which was further adapted to the conditions of the artificial rainfall-runoff experiment, resulting in the creation of SM2RAIN-exp. The primary objective was to gain insights into the fundamental processes governing the relationship between SM and rainfall. The research findings indicated that SM2RAIN-exp exhibited a satisfactory performance in estimating rainfall. Interestingly, it was observed that combining SM data from both 10 cm and 30 cm depths led to better performance than utilising sensors at either depth in isolation. This highlighted the importance of selecting an appropriate soil depth for optimal results. Additionally, the authors suggested that accounting for the contribution of surface runoff could help address critical issues related to estimating precipitation using satellite surface SM data.

A study was conducted by De Almeida *et al.* (2021) highlighting the influence of rainfall event duration and intensity on sediment yield and runoff rates. Their research was carried out on arable land located in the municipality of Seropedica, Rio de Janeiro, Brazil. The conventional approach in simulated rainfall experiments often involves applying precipitation at a constant intensity for a fixed duration. In contrast, this study introduced a different system. The researchers implemented twenty-five distinct rainfall events on micro-scale runoff plots covered with corn straw to assess runoff rates. These rainfall events were constructed by combining various durations and intensities while maintaining the same erosivity value. These rainfall events ranged from 38 to 106 minutes, and their passions varied from 75.0 to 44.6 mm per hour. The resulting runoff rates fell from 16.9 ± 8.74 mm to 32.63 ± 10.67 mm, with the highest rates observed during events with high intensity and low duration. The time it took for surface runoff to commence ranged from 14 to 19.2 minutes, and this initiation was delayed for events with longer durations and lower rain intensities. Notably, the study revealed that varying the intensity and duration of rainfall while maintaining the same erosivity had a significant impact on the quantity and timing of runoff. In conclusion, the findings of this study offer insights that could lead to new perspectives in designing water erosion experiments involving simulated rain. Specifically, it emphasises the importance of considering both the duration and intensity of rainfall events when assessing soil erosion capacity.

Nour *et al.* (2021) conducted an extensive study to assess the relationship between rainfall and discharge and to analyse the water balance in the Chari-Logone sub-basins within the Lake Chad basin over the past six decades. Their research aimed to estimate the average hydrological balances for different geographic areas to pinpoint the most productive regions within the basin. The study involved comparing the rainfall-runoff relationship between the wettest and driest decades during the study period. This analysis helped identify the specific areas that had the most significant impact on amplifying the hydrological response to variations in rainfall. Additionally, the researchers evaluated the long-term stability of the rainfall-runoff relationship under climatic conditions that closely resembled the

average situation. The authors found that the average water flow in the Chari-Logone basin was 823 m^3 s^{-1} or 42 mm $year^{-1,}$ which consisted of only 5% of precipitation. This meagre discharge ratio indicated that the basin was highly sensitive to variations in rainfall. The findings revealed a substantial 75% difference in average flow despite only a 15% decrease in precipitation. The hydro-climatic data did not show evidence of human-induced factors responsible for the flow reduction or alterations in the hydrological regime within the Chari-Logone basin. The study also characterised the spatial disparities, temporal fluctuations, and the individual sensitivities of various sub-watersheds to climatic variations based on the hydro-climatic data. In summary, this research provided valuable insights into the dynamics of the Chari-Logone sub-basins and their responses to climatic variations, shedding light on the factors contributing to changes in the hydrological regime over time.

Alavinia *et al.* (2019) conducted a study to assess how variations in rainfall patterns affect runoff and rainfall-induced erosion. They noted that the temporal changes in rainfall intensity during natural rainstorms are a common occurrence. Yet, there needs to be more information available to comprehend their impact on runoff fully. In response to this knowledge gap, the researchers designed and implemented four different simulated rainfall patterns, namely constant, increasing, decreasing, and increasing-decreasing, while keeping the total kinetic energy consistent. These rainfall patterns were applied to two types of soil, sandy and sandy loam, using 15 cm $\times$ 30 cm long detachment trays under conditions allowing infiltration. Throughout each simulation, runoff samples were collected at regular intervals. Their observations revealed no significant difference in runoff between the two soil types. This research shed light on the impact of varying rainfall patterns on runoff and erosion, indicating that the specific temporal variation in rainfall intensity may not be a primary factor affecting runoff differences between the selected soil types. Also, they plotted the relation between rainfall intensity and runoff rate, for which R^2 was 0.93. The direct influence of rainfall intensity on runoff rate showed that the runoff rate was affected by the occurrence time and duration of the maximum rainfall intensity during a storm with varying intensity rainfall patterns.

The study noted that the temporal variations of runoff rates exhibited distinct ways depending on the type of rainfall. In constant-intensity rainfall patterns, runoff rates experienced a rapid initial increase, followed by a period of stability. However, when considering other rainfall patterns, the runoff rates displayed variations at different stages. The researchers emphasised that the insights gained from this investigation could be valuable for comprehending the influence of rainfall patterns on runoff. Furthermore, these findings might be instrumental in developing predictive models to assess the impact of varying rainfall patterns on runoff dynamics.

A study was conducted by Zheng *et al*. (2021) focusing on identifying the most effective ridge practices for managing runoff from sloping farmland in a humid subtropical region of Southern China, particularly under various types of rainfall. They categorised a total of 253 natural rainfall events spanning the years 2012 to 2018 into three distinct rainfall types based on critical parameters such as rainfall depth, maximum-30 min rainfall intensity, and rainfall duration, using K-means clustering. The study aimed to assess the impact of these rainfall types on surface runoff under different ridge management practices. The results revealed a notable reduction in annual runoff, ranging from 18.9% to 62.0%, across all rainfall events. The rainfall events were classified into three primary categories: intense, normal, and long-duration. Among these, intense and normal rainfall was responsible for most water loss, accounting for 75.0% to 83.8%. Interestingly, the runoff efficiency during long-duration rainfall events was the lowest, sometimes even showing negative values, particularly on farmlands equipped with only downslope ridges. Of note, a relatively small subset of the total rainfall events, approximately 20%, contributed significantly to both the total rainfall depth (29-33%) and total runoff depth (68-89%). These events were primarily intense and normal rainfall events. In summary, the authors concluded that rainfall depth was pivotal in influencing runoff generation in this region.

2.5 SUGGESTIONS FOR IMPROVED WATER MANAGEMENT PRACTICES

Cullum *et al*. (2006) combined the effects of best management practices on water quality in lakes from agricultural watersheds. They examined the water quality conditions in three watersheds before and after best management practices (BMPs). Before the adoption of BMPs, it was noted that the lakes suffered from ecological stress and damage caused by an excessive inflow of sediment. Subsequently, applying cultural and structural BMPs resulted in noticeable enhancements in water quality. It was observed that the most significant improvements in water quality were observed in the two watersheds where cultural practices and a combination of cultural and structural measures were in place. As a result, they concluded that cultural BMPs, more so than structural BMPs, have a pivotal role in improving lake water quality and are essential in conjunction with structural measures to ensure enhanced water quality in lakes impacted by agricultural runoff.

An integrated impact of Soil and Water Conservation (SWC) structures on runoff through measurements and modelling was assessed by Melaku *et al*. (2018a) in the Northern Ethiopian highlands. They investigated two smaller watersheds that were adjacent to each other. One of the watersheds (treated sub-watershed) had an area of 27.1 ha with SWC structures constructed, while the other was without SWC structures (untreated sub-watershed) with an area of 31.7 ha. They observed runoff in both watersheds and compared it using GeoWEPP model simulations. The results of the simulation indicated that the daily runoff was adequately predicted for both sub-watersheds, with a satisfactory fit (R^2=0.68 and NSE=0.43 for the untreated sub-watershed, and R^2=0.61 and NSE=0.84 for the treated sub-watershed). The authors noted that the implementation of SWC structures had the effect of reducing the slope gradient and altering flow accumulation. Consequently, they concluded that the surface runoff in the treated sub-watershed was decreased by approximately 19% in comparison to the untreated sub-watershed.

Melaku *et al*. (2018b) predicted the SWC impacts on runoff using the SWAT model in Northern Ethiopian highlands. From 2011 to 2015, an evaluation was conducted in the Gumara-Maksegnit watershed involving two neighbouring

watersheds. In one of these watersheds, referred to as the "treated watershed (TW)," soil and water conservation (SWC) structures were implemented, while the other served as a reference watershed with no SWC structures, known as the "untreated watershed (UW)." For both watersheds, separate projects were established using the SWAT and SWAT-CUP models to simulate daily runoff. The runoff simulations demonstrated that SWAT effectively reproduced the hydrological patterns for both watersheds. During the daily flow calibration period from 2011 to 2013, the results showed a strong correlation between predicted and observed data, with R^2 values of 0.78 for the TW and 0.77 for the UW. Similarly, the validation results for 2014 to 2015 also exhibited good correlations, with R^2 values of 0.72 for the TW and 0.70 for the UW. This study provided evidence that SWAT performed well in both watersheds and holds promise as a valuable tool for scaling up and assessing the impact of SWC structures in the highlands of Ethiopia.

Wolka *et al*. (2018) studied the benefits, limitations, and sustainability of soil and water conservation structures in the Toni and Bokole watersheds of the Omo-Gibe basin in Southwest Ethiopia. A household survey was conducted, involving 201 households selected through a multistage sampling approach encompassing six rural kebeles. The researchers observed that farmers displayed selectivity in their acceptance and adoption of soil and water conservation (SWC) structures, with their decisions influenced by the specific characteristics of the local land. Stone and soil bunds were widely adopted; however, the labour-intensive nature of constructing and maintaining SWC structures posed challenges in certain areas. The study's conclusion emphasised the critical importance of considering biophysical factors, including land characteristics, environmental conditions within the watershed, and the types of SWC structures, to ensure the effective implementation and long-term sustainability of these measures.

Sith *et al*. (2019) assessed water quality and evaluated the BMPs in a small agricultural watershed adjacent to the Coral Reef area in Japan. The researchers employed the SWAT model, coupled with the MODFLOW groundwater model, to simulate streamflow. Their findings demonstrated the model's ability to accurately

predict hourly streamflow, making it a valuable tool for assessing scenarios involving best management practices (BMPs). The study identified effective measures for water quality improvement; however, the authors acknowledged that the practical implementation of these measures might present real-world challenges.

Uniyal *et al*. (2020) identified critical areas and evaluated the BMPs for sustainable watershed management using the SWAT model for the Baitarani catchment in Odisha, India. They conducted calibration and validation of the SWAT model, followed by an assessment of the effectiveness of eight agricultural and structural management practices, both individually and in combinations, to evaluate their impact on various water balance components. They observed that combining these best management practices (BMPs) yielded better results than implementing them individually. In their comparative analysis, they found that at the watershed level, structural BMPs (ranging from 66% to 70%) outperformed agricultural BMPs (ranging from 2% to 7%). Furthermore, the simulation results regarding BMPs' effects on water balance components showed a reduction in annual average surface runoff by 4% to 14% across the three scenarios. Conversely, there was an increase in aquifer recharge (ranging from 6.8% to 8.7%), baseflow (ranging from 8% to 10.5%), and percolation (ranging from 1.2% to 3.9%) due to the implementation of BMPs. In conclusion, the authors highlighted the significance of this study in promoting sustainable land and water resource management at a catchment scale.

Critique of Reviews

Based on the reviews, it is inferred that there is a need to analyse water balance, particularly for ungauged watersheds, as they dominate most areas. This work is limited to ungauged watersheds due to the lack of data availability and the need for data generation. There is sufficient work on the relation between rainfall and runoff, but the result is limited when other significant parameters like ET, soil moisture, and the water table are considered. Thus, there is a need for implementing water management practices in these regions, which needs to be highlighted. Hence, the research work of 'Determination of water balance components of a micro watershed for improved water management practices' is undertaken.

CHAPTER - III
MATERIALS AND METHODS

This Chapter deals with the study area, data used, and the methodology adopted to fulfil the study's objectives. It describes the location and characteristics of the study area and the various instruments used for recording the water balance components, viz., rainfall, runoff, soil moisture storage, and groundwater storage. The procedure to determine ET through water balance and its estimation through climatic parameters has been described. Various softwares used are also described. The application of the SWAT model to determine more detailed water balance components, along with its sensitivity and calibration, is explained. The methodology for determining the relationship between rainfall and water balance components is also presented. Further, procedures to suggest improved water management practices are also described in this Chapter.

3.1 DESCRIPTION OF THE STUDY WATERSHEDS

A micro watershed of Bharathapuzha River (the second longest river of Kerala), which joins laterally with the mainstream of the river, has been chosen for the study. The micro watershed has an outlet at Perassannur near Anjukannu Railway Bridge, and hence, it is named the 'Perassannur watershed'. The delineated watershed of the study area lies within the range of 10º50'27" and 10°58'12" North latitude and 76º02'21" and 76º07'16" East longitude. It is located between 5 to 161 m above mean sea level. Most of the study area falls within a radial distance of about 4 km from Valanchery municipal town. The location map of the Perassannur watershed is shown in Fig. 3.1. The area of the Perassannur watershed is 79.66 km^2.

The water balance study has been replicated in a smaller area, which is a sub-watershed of the Perassannur watershed, by delineating the catchment area at the Painkanoor outlet, as discharge details for this outlet have also been monitored, and it is named 'Painkanoor sub-watershed'. The location map of the Painkanoor sub-watershed is shown in Fig. 3.2 and has an area of 35.21 km^2. It is located within the range of 10º51'04" and 10º58'12" North latitude and 76º02'34" and 76º05'57"

East longitude. The elevation of the watershed ranges between 8 to 151 m above MSL.

The average annual rainfall of the area is 2582 mm. The water year is divided into four seasons: southwest monsoon (June to September), northeast monsoon (October to December), post-monsoon (January to March), and pre-monsoon (April to May). Gridded data of India Meteorological Department (IMD) shows that approximately 65-70% of the annual rainfall occurs during the southwest monsoon season, 15-20% during the northeast monsoon season, and the rest during the pre-monsoon and post-monsoon periods. The mean annual minimum and maximum temperature of the study area were 22.79⁰C and 31.96⁰C, respectively. The mean annual minimum and maximum humidity was 63.31% and 90.78%, respectively. Also, the mean yearly wind velocity was 2.16 km h^{-1}. The mainstream flows nearly along the centre of the watershed, which is the primary source of water for agriculture and other activities.
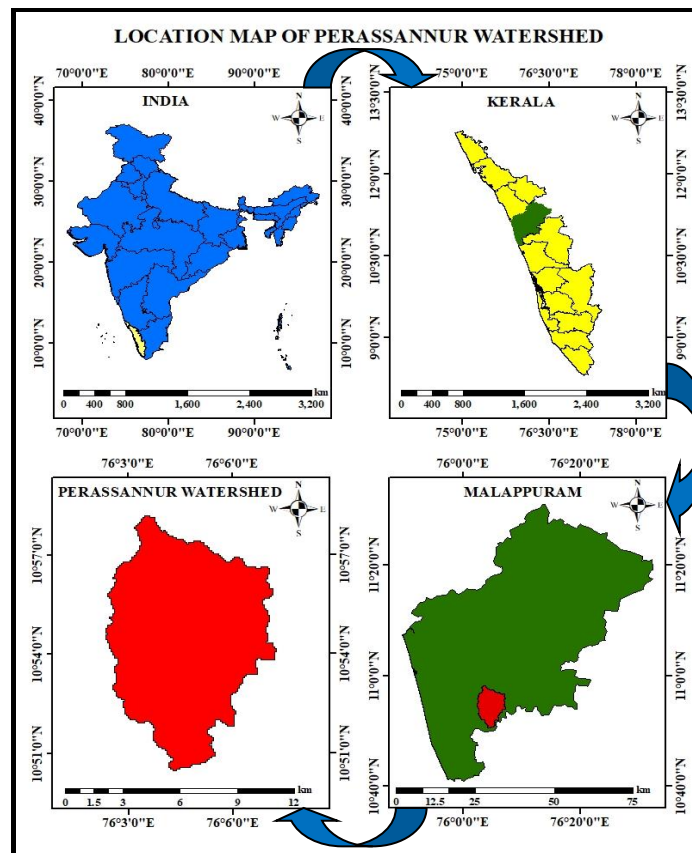
Fig. 3.1. Location Map of the Perassannur Watershed
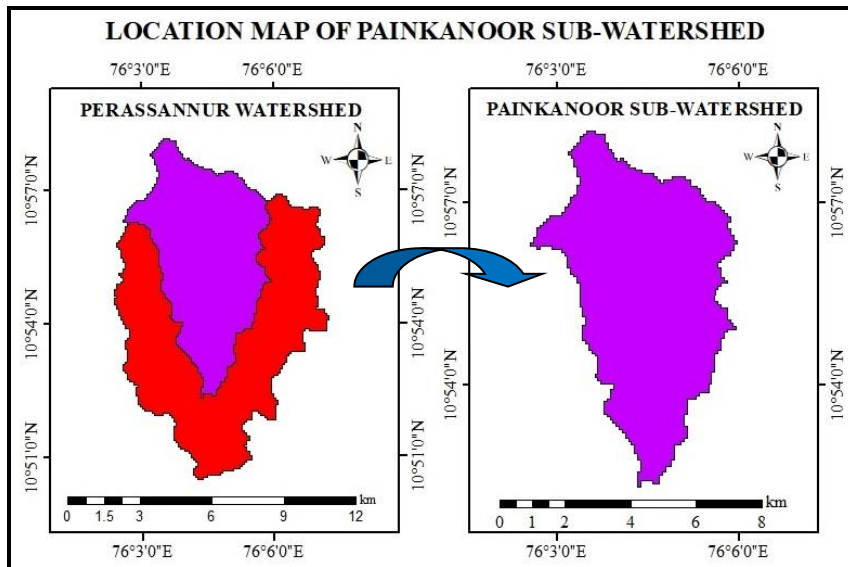
Fig. 3.2. Location Map of the Painkanoor Sub-watershed
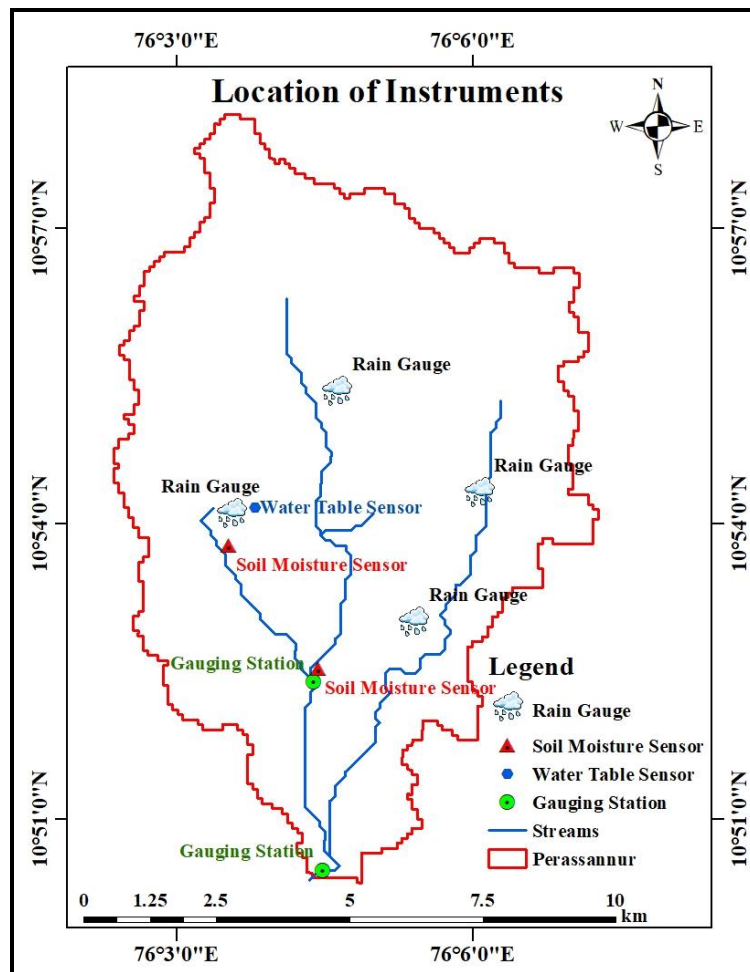
Fig. 3.3. Locations of Instrumentation for the Measurements of the Water Balance Components

3.2 DETERMINATION OF THE WATER BALANCE COMPONENTS

The water balance components of the study watersheds were measured by installing various hydro-meteorological instruments for measuring rainfall, runoff, soil moisture storage, and groundwater storage. Four automatic rain gauges were installed for recording rainfall, two stream gauging stations for recording runoff, two soil moisture sensors for recording soil moisture, and one water table recorder for monitoring the groundwater table in the study watershed. Locations of all these hydro-meteorological stations are shown in Fig. 3.3.

3.3 MEASUREMENT OF RAINFALL

To record rainfall with high spatial resolution, four automatic Tipping Bucket Rain gauges (TBRs) were installed in the watershed in a distributed manner such that they can measure the rainfall received by the catchment very accurately, including its spatial variation. The network of four rain gauges was with a spatial separation of about 3 km. For this research, automatic TBR manufactured by Rain Wise Industrial, USA, was used to record the rainfall. It is a well-designed and manufactured rain gauge that combines durable construction at a very reasonable cost. It offers less resistance to airflow than most previous designs, which helps to reduce the sampling errors that may occur during wind-driven rain. This is a digital rainfall recorder based on a microcontroller system. It includes a rain sensor connected to a data logger to collect real-time data automatically. The device features a funnel and a rocker mechanism equipped with two small buckets situated below the funnel. When raindrops enter the funnel, they are funnelled into one of the small buckets on the rocker mechanism. After receiving 0.20 mm of rain, the rocker tips over, emptying the bucket and shifting the other under the funnel. A recording mechanism within the gauge records each tip along with the corresponding timestamp. The specifications of the rain gauge are shown in Table 3.1.

The installation of the rain gauge was carried out in selected places by considering the following points:
  i. The ground should be free from sloping levels.
  ii. The site should take away from the heavy winds.

iii. The site should be away from large obstructions like trees and high-rise buildings.

iv. The minimum clearance should be 1.5 times the height of the significant obstacles.

Table 3.1. Specifications of the Tipping Bucket Rain Gauge

Sr. No.	Specification	Description
1.	Housing	High-impact polypropylene
2.	Collector diameter	203.2 mm
3.	Weight	1 kg
4.	Resolution	0.5 mm
5.	Power Specification	Two 1.5V AAA Batteries
6.	Clock Accuracy	±1 min month^{-1}
7.	Communication	USB 2.0
8.	Maximum Input Frequency	100 Hz
9.	Minimum Pulse Width	10 ms
10.	Logging Interval	60 seconds
11.	Sensor	Tipping Bucket Rain gauge
12.	Least Count	0.20 mm
13.	Accuracy	2% @ 25mm h^{-1}
14.	Temperature:	
	a. with Lithium Batteries	-40 - 60°C
	b. with Alkaline Batteries	-18 - 55°C
15.	Humidity	0 - 100% Non-Condensing

TBR was set up on the elevated platform made of metal plates and iron poles so the water would drain freely after falling from the bucket. It was set up at a height of 1.5 m (India Meteorological Department [IMD], 2021) so that there would not be any clogging or error by the splashing of rainwater. Proper care was taken to level the platform using a spirit level. The rain gauge was placed on a platform with four corner screws. Fig. 3.4 shows the installed tipping bucket rain gauge in the study area. After setting up the rain gauge, a power supply was given by installing batteries. The data logger was connected with the help of a USB cable

using RL-Loader (Version 2.4) to export the data in Microsoft Excel format. The following maintenance procedures were adopted for the rain gauges:

i. Inspect and clean the sensor at regular intervals, e.g. every month. Clean any accumulated dust, etc., using a soft cloth dampened with water.

ii. The calibration of the sensor may drift with time and exposure to radiation.

iii. Replace the batteries after one year.

Fig. 3.4. Tipping Bucket Rain Gauge Installed in the Study Area

3.3.1 Mean Rainfall over the Catchment

Mean rainfall received by the watershed was calculated using the Thiessen polygon method and the Inverse Distance Weighted (IDW) method in the GIS platform.

3.3.1.1 Thiessen Polygon Method

Thiessen polygon method is a popular method of weighing the rain gauge observation according to the area represented by each rain gauge. It assumes that the rainfall at any point within the polygon is the same as that of the nearest gauge. In this method, polygons are drawn perpendicular bisectors to the lines joining the rain gauge stations. The average depth of rainfall is calculated by taking a weighted average of the area of each polygon and the rainfall received in that area, as given in Eq. 3.1.

$$Q = \frac{\sum\limits_{i=1}^{n} A_i\,R_i}{\sum\limits_{i=1}^{n} A_i} \quad \text{..... (Eq. 3.1)}$$

Where,

Q is the average rainfall (mm)

i is the counter for observations

n is the number of observations

A is the area represented by rainfall (km^2)

R is the rainfall at the station (mm)

3.3.1.2 Inverse Distance Weighted (IDW) Method

Inverse Distance Weighting (IDW) represents a deterministic technique for multivariate interpolation when dealing with scattered data points. This method assumes that each input point exerts a local influence that diminishes as distance increases. It places a greater emphasis on points closer to the target location than those farther away. To calculate the output value for a given area, points within a certain radius are considered. IDW interpolation allows for the adjustment of the relative impact of sample points. The power value in IDW interpolation determines how much input points affect the output. The influence is more substantial for points nearby, resulting in a more detailed surface. As the distance increases, the effect diminishes, leading to a smoother texture. Increasing the power value localises the cell's output and lowers the average value. In contrast, decreasing the power value widens the influence and raises the average, resulting in a smoother surface. The weight for the average is determined by a distance function measuring the distance between the sample point and the interpolated point (Watson and Philip, 1985).

The general weighting function used in IDW is the inverse of the distance squared, represented by Eq.3.2 in the inverse distance weighted method.

$$Z^* = \sum\limits_{i=1}^{n} w_i\,Z_i \quad \text{..... (Eq. 3.2)}$$

Where,

Z^* is the weighting general function

Z_i (i= 1, 2, 3, ..., n) is the data height value interpolated by several n points

w_i is the weight which is given in Eq. 3.3.

$$w_i = \frac{h_i^{-p}}{\sum\limits_{j=1}^{n} h_j^{-p}} \quad \text{..... (Eq. 3.3)}$$

Where,

p is a changeable positive value called the power parameter

h_j is the distance from the point distribution to the interpolation point (km)

h_i is given in Eq. 3.4.

$$h_i = \sqrt{(x - x_i)^2 + (y - y_i)^2} \quad \text{..... (Eq. 3.4)}$$

Where,

(x,y) are coordinates of the interpolation point

(x_i, y_i) are coordinates for each spread point

The weight variable's function transforms the entire distribution of data points, gradually approaching a value close to zero as the distance from the reference point increases. The IDW interpolation method offers several advantages. It allows for the control of interpolation characteristics by limiting the selection of input points used in the interpolation process. This means that points located far from the sample point but estimated to exhibit spatial correlations can be excluded from the calculation. The choice of issues to be utilised can either be directly determined or selected based on the desired interpolation distance. However, one notable drawback of the IDW interpolation method is that it cannot estimate values exceeding the maximum or falling below the minimum values of the sample points.

3.3.2 Statistical Analysis of the Rainfall

Rainfall characteristics of the watershed were analysed by computing various descriptive statistical measures such as mean, standard deviation and coefficient of variation. Further, the variability of the rainfall data recorded by different rain gauge stations was also analysed using analysis of variance (ANOVA) (Girden, 1992). The weight variable's behaviour changes across the entire dataset, gradually approaching

a value close to zero as the distance from the reference point increases. The IDW interpolation method comes with several advantages. It allows for manipulating interpolation characteristics by controlling the selection of input points employed in the interpolation process. This means that distant points, presumed to have spatial correlations with the sample point, can be omitted from the calculation. The choice of points to include can be determined directly or based on the desired interpolation distance.

However, a significant limitation of the IDW interpolation method is its inability to estimate values that exceed the maximum or fall below the minimum values in the sample points. Suppose the within-groups variance is smaller than the between-groups variance. In that case, the F-test will detect higher F-values, thus increasing the likelihood that the observed differences are genuine and not random. In addition, the rainfall intensities were computed from the rain gauge data, and the event frequency was analysed.

3.4 MEASUREMENT OF RUNOFF OF THE MAIN STREAM

In this research, the total runoff was quantified using a widely employed technique, which involves the discrete integration of flow velocity across the cross-section of a channel. This method entails sampling velocities and water depths at specific locations along vertical lines distributed across the channel. The area-velocity method for determining runoff in open channels requires measurements of stream velocity, flow depth, and the distance between observation points on the channel. Velocity is typically measured at one or more points within each vertical using a current meter. This meter is commonly mounted on a wading rod or deployed from a cableway or a bridge. Subsequently, an average velocity is calculated for each vertical segment.

In this study, an automatic water level sensor (Fig. 3.5), a rotor-type current sensor attached to a wading rod (Fig. 3.6) with a data logger (Fig. 3.7) manufactured by Environmental Measurements and Control (EMCON) Kochi was used. The specifications of the automatic water level recorder and sensor are provided in Table 3.2. An automatic water level sensor, along with a discharge recording system, was

used to measure and record the depth and velocity of water in the channel continuously. Both the water level sensor and rotor-type current meter were installed at the outlet located in the Perassannur watershed (Fig. 3.8). The cross-section of the channel was determined by a total station survey (Fig. 3.9). The runoff was obtained from the sum of the product of mean velocity and the cross-sectional area of the channel.

Fig. 3.5: Automatic Water Level Sensor

Fig. 3.6: Rotor Type Current Sensor Attached to a Wading Rod

Fig. 3.7: EMCON Data Logger

Table 3.2. Specifications of Automatic Water Level Sensor with Discharge Recording System

Sr. No.	Specification	Description
A. Automatic Water Level Sensor		
1.	Measurement type	Capacitance
2.	Range	0 to 20 m
3.	Accuracy	±1%
4.	Sensing method	Hydrostatic pressure sensor
5.	Cable length	10 m
6.	Material	Delrin
B. Savanious Rotor Type Current Sensor (Wading Rod)		
1.	Measurement type	The average number of counts accumulated for 7.5 seconds can present the velocity
2.	Water current	Direct reading in cm s^{-1}
3.	Range of current/velocity	1 to 400 cm s^{-1}
4.	Accuracy	±1%
5.	Threshold value	< 1.5 cm s^{-1}
6.	Water current sensing method	Savanious rotor for sensing at very low velocities
7.	Cable length	10 m
8.	Rod length	3 m
9.	Material	Stainless steel, Delrin and Brass
C. EMCON Data Logger		
1.	Display	LED
2.	Power	7.4 Volt Lithium-ion rechargeable battery
3.	Operational switch	5-way toggle switch
4.	Power switch	Piano switch
5.	Data storage	SD card
6.	Download Format	Microsoft Excel/CSV
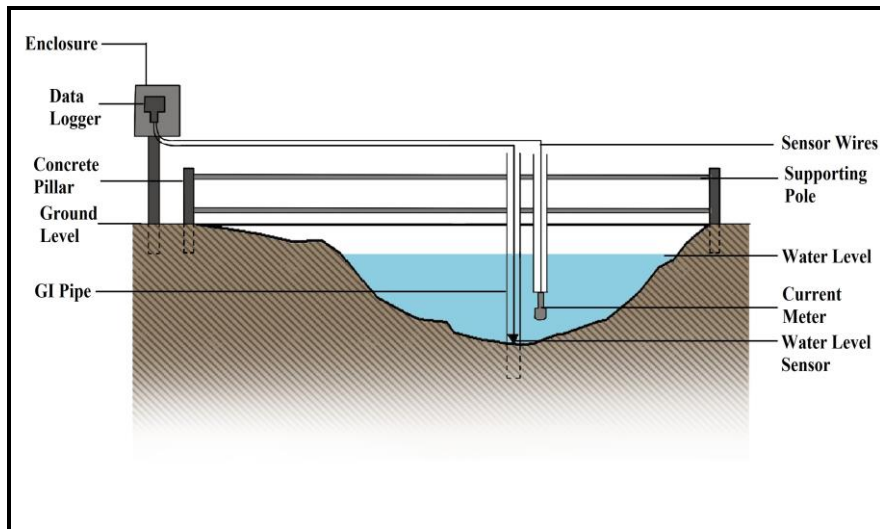
Fig. 3.8. Schematic Diagram of Depth and Velocity of Flow Measurement at Perassannur

Fig. 3.9. Determination of Channel Cross-section using Total Station

Runoff was also monitored at the outlet of the sub-watershed Painkanoor. Here, the water level was monitored continuously, and the flow velocity was measured by a cup-type current meter. The rating curve was prepared for the channel section. Then, using the continuous water level recording, the discharge monitoring was also done.

Also, an automatic water level sensor manufactured by EMCON was installed at the outlet of the Painkanoor sub-watershed to measure and record continuously the depth of water flowing from the channel (Fig. 3.10). Here, the cup-type water current meter shown in Fig. 3.11, manufactured by Balaji Hydromet Roorkee; specifications shown in Table 3.3, was used to measure the velocity at different instants. The cross-section of the channel was determined using a total station instrument. The stage-discharge relationship determined the runoff. The runoff for both sections was recorded from August 2021 to December 2022 at 4 hours.
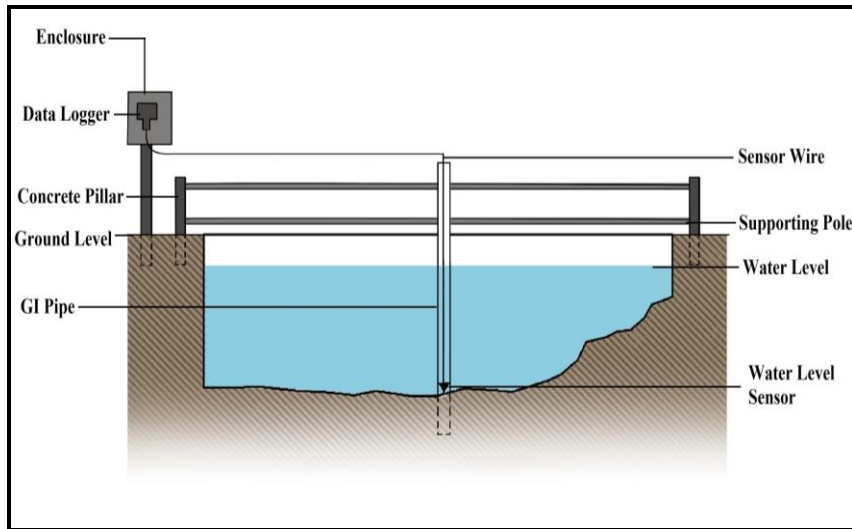
Fig. 3.10. Schematic Diagram of Depth of Flow Measurement at Section Painkanoor
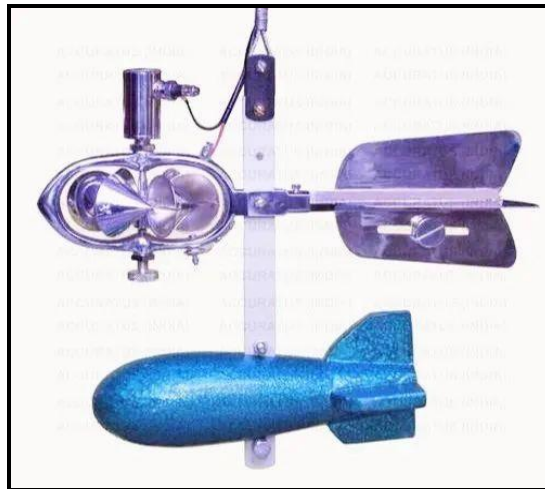
Fig. 3.11. Cup-type Water Current Meter with Fish Weight

Table 3.3. Specifications of Cup-type Water Current Meter

Sr. No.	Specification	Description
1.	Sensor	6 Cup Wheel
2.	Current Meter Body	All parts of brass, chrome plated
3.	Operating Range	0.1 to 3.5 meters per second
4.	Accuracy For velocity up to 0.3 m/s For velocities > 0.3 m/s	 ±1% ±0.5%
5.	Contact Chamber	Magnetic or Fibre Optic
6.	Dimension	Bucket Wheel Diameter: 127 mm Bucket diameter: 50 mm
7.	Rates Spin Test	>75 second
8.	Connection cable	10 m

3.5 MEASUREMENT OF SOIL MOISTURE

The measurement of soil moisture is crucial for enhancing the accuracy of predictions in hydrological balance studies because it significantly influences runoff generation processes.

In this research, in-situ soil volumetric moisture content was measured using two soil moisture sensors. One was the TEROS 12 soil moisture sensor, a capacitance-based manufactured by METER Group, Inc. USA. There were three such sensors, which were installed at 0.25 m, 0.75 m, and 1.25 m. As the root zone depth of most of the horticultural crops in the study area was about 1.5 m, it was decided to determine the soil moisture storage in the soil column of 1.5 m (Kuriakose *et al*., 2009; Sreenath, 2013; Shaw *et al*., 2023). To get the average soil moisture in the root zone depth, the soil column was divided into three vertical depth sections of 0.50 m each, and the sensor was placed in the centre of each 0.50 m vertical section.

The other was a resistance-based TDR sensor manufactured by Campbell Scientific Ltd., UK, having model name CS650. This had only one sensor, which was installed at a depth of 0.75 m, which was again the centre of 1.5 m considering

root zone depth. These sensors were installed horizontally at two different locations in the study area. In both the soil moisture meters, one-minute data were averaged every hour, and the hourly data were averaged to obtain the daily mean for each soil depth. Table 3.4 and Table 3.5 gives details of soil moisture sensors and their data logger used in this study.

3.5.1 TEROS 12 Soil Moisture Sensor

The TEROS 12 sensor is a precise instrument that employs capacitance/frequency-domain technology to monitor Volumetric Water Content (VWC). These sensors assess soil moisture levels between Needle 1 and Needle 2, measure Electrical Conductivity (EC) between Needle 2 and Needle 3, and have an embedded thermistor for temperature measurement. These sensors are well-suited for long-term placement within the soil due to their low power consumption, and they continuously record data with the help of a data logger.

The sensor supplies an oscillating wave of 70 MHz to the sensor needles, which get charged depending on the dielectric property of the medium. The TEROS 12 microprocessor logs the charge time of the needle and generates a RAW value, which is derived from the substrate's dielectric properties. This RAW value is then transformed into VWC through the application of Topp's equation (Topp *et al*., 1980) using the ZL6 data logger (Hilhorst, 2000).

The equation of VWC for soil is given by the manufacturer as shown in Eq. 3.5:

$$\theta\,(\mathrm{m^3\ m^{-3}}) = 3.879 \times 10^{-4} \times \mathrm{RAW} - 0.6956 \quad ..... (\mathrm{Eq.}\ 3.5)$$

Where,

θ is the VWC (in $\mathrm{m^3\ m^{-3}}$)

RAW is the raw sensor output

The TEROS 12's resistance to fluctuations in soil texture and electrical conductivity (EC) can be attributed to its operation at a high measurement frequency. It works seamlessly with METER data loggers. Fig. 3.12 presents the TEROS 12 soil moisture sensor, and its specifications are given in Table 3.4.
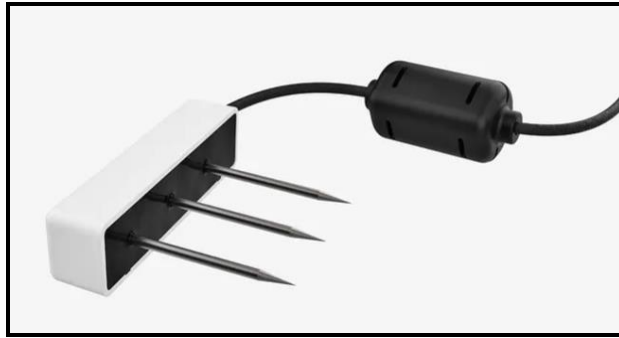
Fig. 3.12. TEROS 12 Soil Moisture Sensor

Table 3.4. Specifications of TEROS 12 Soil Moisture Sensor

Sr. No.	Specification	Description
1.	Dimensions: Length Width Height	94 mm 24 mm 75 mm
2.	Prong Length	55 mm
3.	Supply Voltage (VCC) to GND	4.0 VDC to 15.0 VDC
4.	Operating temperature	−40 to 60 °C
5.	Cable Length	5 m
6.	Connector Types	3.5-mm stereo plug connector
7.	Volumetric Water Content (VWC)	0.00-0.62 m^3 m^{-3}
8.	Resolution	0.001 m^3 m^{-3}
9.	Accuracy	±0.03 m^3 m^{-3}

Fig. 3.13. Calibration of TEROS 12 Soil Moisture Sensor

3.5.1.1 Calibration

The soil was collected from the study site, air-dried for 24 hours, and then passed through a sieve of 2 mm in size. A rigid plastic container was taken, and the mass and volume of the clean, dry and empty container was recorded. Approximately 10 g of soil was taken in a moisture box and kept in the oven for gravimetric moisture content determination. The air-dried soil was filled in the container so that it approximately matched the field bulk density of the soil. The soil was added in layers and gradually compacted after every layer was laid to minimise the voids. Then, the container was weighed along with the soil. TEROS 12 moisture sensor was inserted vertically in the container filled with soil, avoiding any air gaps, and RAW sensor reading was recorded from the sensor.

Ten per cent water of the total soil volume was added to the dry soil and mixed thoroughly to get a homogeneous mixture, which now became 10% VMC. The soil sample was again filled in the container, matching the field bulk density; the sensor was inserted in the container, and the RAW value of sensor data was noted. This procedure was repeated to yield five calibration points. RAW data from the sensor obtained via ZENTRA Utility was tabulated in the calibration chart. These calibration values were added to ZENTRA Cloud software, and the sensors were ready to install in the field. Fig. 3.13 represents the calibration of TEROS 12 soil moisture sensor.

3.5.1.2 Installation

A trench was dug using a spade and other digging tools up to a depth of 1.25 m. Then, the three sensors were installed carefully by hand into the undisturbed soil of the trench sidewall at a depth of 0.25 m, 0.75 m, and 1.25 m from the ground level. The trench was carefully backfilled to preserve the soil's bulk density and avoid dislodging the installed sensors by any accidental pull of the connecting chord. Fig. 3.14 shows the TEROS 12 soil moisture sensors installed in the study area.

Fig. 3.14. TEROS 12 Soil Moisture Sensors Installed in the Study Area

3.5.1.3 Data Logger of the capacitance-based soil moisture sensor

The data logger of the sensor is a plug-and-play device having six sensor input ports which can support six different METER analogue, digital, or pulse sensors at the same time. ZENTRA Utility, a user-friendly interface software, was downloaded from metergroup.com and configured the data logger. ZENTRA Utility can set all the configuration parameters required for the logger and perform real-time sensor measurements. The calibrated TEROS 12 soil moisture sensor was connected to the data logger. ZL6 data logger was placed in an enclosure of UV-resistant polymer, making the device compatible with long-term outdoor operations (metergroup.com). The specifications of the ZL6 data logger are shown in Table 3.5, and Fig. 3.15 shows the view of the ZL6 data logger. Fig. 3.16 shows the ZL6 data logger installed in the study area.

Fig. 3.15. ZL6 Data Logger

Fig. 3.16. ZL6 Data Logger Installed in the Study Area

The volumetric water content thus obtained from Zentra Utility software is downloaded in the Microsoft Excel format and is converted to gravimetric water content using Eq. 3.6:

$$\theta_g = \frac{\theta_v}{\rho} \quad \text{..... (Eq. 3.6)}$$

Where,

θ_g is the gravimetric water content (kg kg^{-1})

θ_v is the volumetric water content (m^3 m^{-3})

ρ is the bulk density (kg m^{-3})

The bulk density is determined by the core sampler method (Black, 1965) using Eq. 3.7:

$$\text{Bulk density} = \frac{\text{Dry mass of soil core (kg)}}{\text{Volume of core sampler (m}^3)} \quad \text{..... (Eq. 3.7)}$$

Table 3.5. Specifications of ZL6 Data Logger

Sr. No.	Specification	Description
1.	Dimensions Length Width Height	 149 mm 63 mm 250 mm
2.	Enclosure material	Weather-impact, UV-resistant polymer
3.	Sensor input ports	6 (METER analogue, digital, or pulse sensors)
4.	Sensor port type	3.5 mm stereo plug connector
5.	Memory type	Nonvolatile flash, full data retention with loss of power
6.	Data storage	2 MB (20,000 to 30,000 records)
7.	Battery capacity	6 AA alkaline batteries
8.	Operating temperature	−40 to 60 °C

3.5.2 CS650 Soil Moisture Sensor

The CS650 soil water content reflectometers employ cutting-edge methods to observe soil volumetric water content, electrical conductivity, and temperature. These devices comprise two stainless-steel rods linked to a printed circuit board.

CS650 instruments gauge propagation time, signal attenuation, and temperature. Subsequently, they calculate dielectric permittivity, volumetric water content, and bulk electrical conductivity based on these initial readings. The measured signal attenuation is employed to compensate for the loss effect in reflection detection, consequently improving the precision of propagation time measurements. This correction for the loss effect allows for precise water content measurements in soils without needing soil-specific calibration. Horizontal installation of the sensor provides better accurate volumetric water content. The specifications of the CS650 soil moisture sensor are shown in Table 3.6. Fig. 3.17 represents the CS650 soil moisture sensor.

Table 3.6. Specifications of CS 650 Soil Moisture Sensor

Sr. No.	Specification	Description
1.	Dimensions Length Width Height	 85 mm 63 mm 18 mm
2.	Prong Length	300 mm
3.	Supply Voltage (VCC) to GND	6 VDC to 18 VDC
4.	Operating temperature	−50 to 70 °C
5.	Cable Length	10 m
6.	Connector Types	3.5 mm stereo plug connector
7.	Volumetric Water Content (VWC)	$0.00 - 1.00 \ m^3 \ m^{-3}$
8.	Resolution	$0.005 \ m^3 \ m^{-3}$
9.	Accuracy	$\pm 0.03 \ m^3 \ m^{-3}$
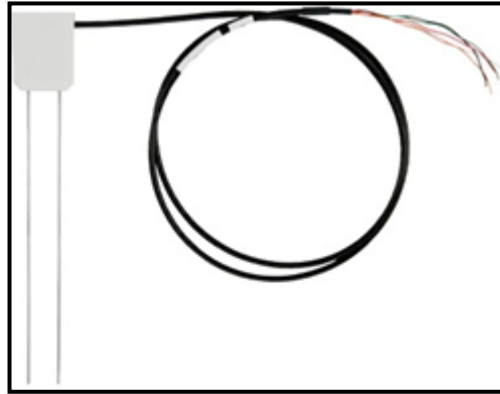
Fig. 3.17. CS 650 Soil Moisture Sensor

3.5.2.1 Installation of the CS650 Soil Moisture Sensor

A trench was dug using a spade, excavator, and other tools up to a depth of 0.75 m. A pilot hole was created, smaller than the sensor rod, into the undisturbed soil of the trench sidewall at a depth of 0.75 m. The sensor was pushed into this pilot hole by hand. The trench was carefully backfilled to preserve the soil's bulk density and avoid dislodging the installed sensor by any accidental tension on the connecting cable. Fig. 3.18 shows the installation of the CS650 soil moisture sensor, and Fig. 3.19 shows the CS650 soil moisture sensor installed in the study area.

Fig. 3.18. Installation of CS650 Soil Moisture Sensor

Fig. 3.19. CS650 Installed in the Study Area

3.5.2.2 CR300 Data Logger of the CS650 Soil Moisture Sensor

The CR300 is a versatile and compact data logger for measurement and control purposes. It boasts fast communication, minimal power consumption, a built-in USB interface, and impressive analogue input accuracy and resolution. This data logger is particularly well-suited for small-scale applications that demand extended remote monitoring and control. The CR300 is capable of concurrently handling measurement and communication tasks. It is compatible with a wide range of sensors with electrical responses, facilitates direct communication and telecommunications, processes data into statistical values, performs calculations, and can even control external devices. Following data collection, the measurements are securely stored in nonvolatile memory on board.

CS650 soil moisture sensor was connected to the CR300 data logger. PC200W software was used to connect the data logger to the computer and view and download the data. The data logger was placed in an enclosure of UV-resistant polymer, making the device compatible with long-term outdoor operations. CR300 data logger is shown in Fig. 3.20, and its specifications are shown in Table 3.7. Fig. 3.21 represents the CR300 data logger installed in the study area. The volumetric water content, thus obtained from PC200W software, was downloaded in Microsoft Excel format and converted to gravimetric water content.

Fig. 3.20. CR 300 Data Logger

Table 3.7. Specifications of CR300 Data Logger

Sr. No.	Specification	Description
1.	Dimensions Length Width Height	 140 mm 76.2 mm 45.6 mm
2.	Enclosure material	Weather-impact, UV-resistant polymer
3.	Sensor input ports	25
4.	Sensor port type	SDI-12 (Serial Digital Interface at 1200 baud)
5.	Memory type	Serial flash
6.	Data storage	30 MB
7.	Charger Input	Solar panel input (16 to 32 VDC)
8.	Battery capacity	12 VDC, lead-acid 7 Ah battery
9.	Operating temperature	−40 to 70 °C

Fig. 3.21. CR300 Data Logger Installed in the Study Area

Fig. 3.22. EMCON Automatic Water Level Sensor Installed in the Open Well

3.6 DETERMINATION OF HEIGHT OF THE WATER TABLE

An automatic water level sensor and a data logger manufactured by EMCON, Kochi, were used to record the depth of the water column. It senses the water depth based on hydrostatic pressure and records the water depth in the well with an accuracy of ±1%. A cable of the required length is used to connect the sensor with the data logger. Measurements were made continuously at an interval of 4 hours, and the daily mean was obtained by averaging the height of the water level from the ground surface. Finally, the height of the water table from MSL was determined by knowing the elevation of the ground surface from MSL. The measurements of the height of water table from the ground surface were also recorded using a manually operated water level sensor to check the accuracy of the readings recorded by the EMCON data logger. Fig. 3.22 shows an automatic water level sensor installed at an open well in the study area. Fig. 3.23 shows a v-guard water level sensor, and Fig. 3.24 shows the manual recording of the height of the water table.

Fig. 3.23. V-guard Water Level Sensor

Fig. 3.24. Manual Recording of the Height of the Groundwater Table

3.7 ESTIMATION OF ET USING THE WATER BALANCE EQUATION

The FAO Penman-Monteith (PM) method was selected by the Food and Agriculture Organization (FAO) of the United Nations, the International Commission on Irrigation and Drainage, and the American Society of Civil Engineers as the standard procedure for computing reference evapotranspiration (ET_0). It is defined as the atmospheric evaporative demand from a reference surface consisting of a hypothetical reference crop with a height of 0.12 m, a fixed surface resistance of 70 s m^{-1}, and an albedo of 0.23. The reference surface resembles an extensive green grass of uniform height, actively growing, well-watered, and completely shading the ground.

Daily meteorological variables (wind speed, solar radiation, air temperature, and relative humidity) that were used to estimate ET_0 by the FAO Penman-Monteith method were recorded by the KCAET meteorological observatory, a nearby weather station, nearly 10 km from the study area. The meteorological parameters that were used as input were prepared using MS Excel, and the calculation procedure was followed as described in FAO Irrigation and Drainage Paper No. 56. The equation for FAO-PM is given below (Eq. 3.8) (Allen, 1998):

$$ET_0 = \frac{0.408\Delta\,(R_n - G) + \gamma\,\dfrac{900}{T + 273}\,u_2\,(e_s - e_a)}{\Delta + \gamma\,(1 + 0.34\,u_2)} \quad \ldots\ldots \text{(Eq. 3.8)}$$

Where,

ET_0 is reference evapotranspiration (mm day^{-1})

Δ is the slope vapour pressure curve (kPa °C^{-1})

Rn is net radiation at the crop surface (MJ m^{-2} day^{-1})

G is soil heat flux density (MJ m^{-2} day^{-1})

γ is psychrometric constant (kPa °C^{-1})

T is the mean daily air temperature at 2 m height (°C)

u_2 is the wind speed at 2 m height (m s^{-1})

e_s is saturation vapour pressure (kPa)

e_a is actual vapour pressure (kPa)

es-ea is saturation vapour pressure deficit (kPa)

Crop evapotranspiration under standard conditions (ET_c), represents the total evapotranspiration from healthy, well-fertilized crops cultivated in extensive fields. This occurs when soil moisture levels are optimal, and the crops achieve maximum yield under specific climatic conditions. ET_c can be determined by incorporating climatic data and directly integrating factors like crop resistance, albedo, and air resistance within the Penman-Monteith approach. Experimentally determined ratios of ET_c/ET_0, called crop coefficients (K_c), are used to relate,

$$ET_c = K_c \times ET_0 \ ..... \ (Eq. \ 3.9)$$

ET_c was computed using CROPWAT 8.0 model and was used for determining the water balance of the study area. The detailed CROPWAT 8.0 model is extensively described by Smith (1992), Stancalie *et al*. (2010), and Tan and Zheng (2019).

3.8 DETERMINATION OF EVAPOTRANSPIRATION USING WATER BALANCE EQUATION

ET of a watershed can be determined using the water balance equation, which is given as Eq. 3.10. Many previous studies have utilised the water balance equation to estimate ET from a watershed (Li *et al*., 2018; Paciolla *et al*., 2021; Fu *et al.*, 2022).

$$ET = P - R \pm \Delta SM \pm \Delta GW \ ..... \ (Eq. \ 3.10)$$

Where,

    ET is evapotranspiration

    P is precipitation

    R is runoff

    ΔSM is a change in soil moisture storage

    ΔGW is a change in groundwater storage

3.9 SOFTWARES AND TOOLS USED

Different softwares and tools were used for this study, and their brief description is given below.

3.9.1 ArcGIS

ArcGIS is a privately owned geographic information system that visualises geographic data on maps. It was developed by the Environmental Systems Research Institute (ESRI) and was initially released in New York in 1999. Its primary use involves map creation and utilisation, the compilation of geographic data, the analysis of mapped data, the sharing and exploring geographic information across various applications and managing geographic data within a database. ArcGIS offers a unified framework for handling diverse spatial data from multiple origins. This study made use of ArcGIS in multivarious ways, such as to delineate the watershed boundary to prepare thematic maps, viz. drainage, land use, and soil. Also, the watershed model SWAT used in this study use ArcGIS as a platform for designing many of the spatial analysis.

3.9.2 Google Earth Engine (GEE)

In this study, Google Earth Engine (GEE) was used for land use classification. GEE is a cloud-based platform designed for the extensive processing of satellite imagery, enabling the detection of changes, trend mapping, and quantifying variations on Earth's surface. It leverages a vast library of satellite imagery, amounting to multiple petabytes, to identify alterations, map patterns, and measure distinctions on the planet's surface. GEE seamlessly merges this extensive catalogue of analysis-ready satellite imagery and remote sensing data with Google's powerful computational capabilities, enabling users to conduct planetary-scale analyses directly within their web browsers (Gorelick *et al*., 2017; Tamiminia *et al*., 2020; Yang *et al*., 2022).

3.9.3 SPAW Model

The SPAW (Soil-Plant-Atmosphere-Water) model developed by Keith Saxton, United States Department of Agriculture (USDA) - Agricultural Research Service (ARS) is a daily hydrologic model used for calculating the characteristics of soil. SPAW is a program that estimates hydraulic conductivity, soil water tension, and water holding capacity based on organic matter, soil texture, gravel content, salinity, and compaction. In this study, the soil characteristics such as hydraulic

conductivity, available water, electrical conductivity, and bulk density were obtained using this model to prepare the soil database (De Jong and Zentner, 1985; Saxton and Willey, 2005).

3.9.4 CROPWAT

In this study, CROPWAT was used to determine the evapotranspiration of the study area. CROPWAT is a decision support system available for DOS or Windows platforms, created to assist agro-meteorologists, agronomists, and irrigation engineers in conducting essential calculations related to evapotranspiration and crop water usage. Its primary focus is facilitating tasks related to the design and administration of irrigation systems. CROPWAT enables users to assess the impact of applying recommendations to enhance irrigation practices, plan irrigation schedules while considering fluctuating water supply, and evaluate production outcomes under scenarios involving rainfed conditions or limited irrigation (Smith, 1992).

3.9.5 SWAT Model

SWAT has been used in studies to estimate more detailed water balance components of the hydrological processes taking place in the watershed. A detailed description of the SWAT is given in Section 3.10 of this Chapter.

3.9.6 SWAT-CUP

Soil and Water Assessment Tool Calibration and Uncertainty Programme (SWAT-CUP) is an automated calibration tool for the SWAT model, and a detailed description of the same is provided in Section 3.11 of this Chapter.

3.9.7 R Software

R software package was used for determining the relationships between rainfall and other water balance components. R-Studio is a suite of robust and cost-effective software designed for disk recovery. Initially created by R-Tools Technology, Inc. for data recovery experts, it serves as an Integrated Development Environment for the R programming language, which is used for statistical computing and graphics. The software is partially built using the C++ programming

language and utilises the Quasar Technologies (Qt) framework for its graphical user interface. A significant portion of the code is also written in Java and JavaScript. R-Studio has been revamped to offer a scalable and user-friendly data recovery solution that combines cutting-edge file recovery and disk repair technology with an intuitive interface. This redesign caters to the needs of both enterprise and professional-level data recovery specialists while ensuring that entry-level users can also benefit from its features without any difficulty (Lalanne and Mesbah, 2016; Shedlock and Stumpo, 2022; Favero *et al*., 2023).

3.10 HYDROLOGIC MODEL DESCRIPTION FOR ESTIMATION OF WATER BALANCE

3.10.1 SWAT Model Overview

Dr. Jeff Arnold developed the SWAT model for the USDA Agricultural Research Service (ARS) (Arnold *et al*., 1998). SWAT is a basin-scale, process and physically-based, continuous-simulation, semi-distributed, eco-hydrological model, which is a promising tool to analyse hydrological parameters in a wide range of watershed scales with varying weather conditions, soil properties, stream channel characteristics, land use, and management conditions, in both gauged and ungauged watersheds. SWAT is coupled with the ArcGIS platform via the ArcSWAT interface. It requires various spatial data, such as land use maps, soil maps, digital elevation models (DEM), and meteorological data. SWAT 2012 was used in this study with the ArcSWAT 2012 extension of ArcGIS as an interface for the model.

3.10.2 SWAT Model Inputs

The essential inputs required for a SWAT simulation include a Digital Elevation Model (DEM), land-use map, soil map, and weather data (Arnold *et al*., 2012). Many researchers around the World have used these essential inputs for SWAT model simulation. The model is used to determine various hydrologic cycle components like evapotranspiration (ET), runoff, base flow, groundwater recharge, etc., using the water balance equation (Neitsch *et al*., 2011). This study includes determining water balance components through measurements and estimation of the same and additional features through SWAT simulation.

3.10.2.1 Digital Elevation Model (DEM)

A Digital Elevation Model (DEM) is a 3D representation of a specific geographical area, offering comprehensive positional information in all three dimensions, x, y, and z, at each set of latitude and longitude coordinates. DEMs can be visualised as a grid of squares (raster) or a Triangular Irregular Network (TIN) in a vector format. The TIN is the primary or directly measured dataset, while the Raster DEM is the secondary or computed version. DEMs are generated using various techniques such as satellite remote sensing, photogrammetry, and land surveying.

The Shuttle Radar Topography Mission (SRTM) 30 m resolution DEM was used in this study for physiographic analysis due to its lower root mean square error. SRTM, an international initiative led by the National Aeronautics and Space Administration (NASA) and the National Geospatial-Intelligence Agency, provides data accessible at no cost through the United States Geological Survey (USGS) in collaboration with NASA. The data can be obtained by visiting the website *https://earthexplorer.usgs.gov.* The datum and projection used were WGS_1984 and UTM Zone 43, respectively. Many researchers have used SRTM DEM for estimating water balance and obtained satisfactory results (e.g. Awan and Ismaeel, 2014; Sandra and Sathian, 2016; Mestry *et al*., 2020; Nasiri *et al*., 2020; Nyatuame *et al*., 2020; Varughese and Hajilal, 2020).

3.10.2.2 Digital Land Use Land Cover (LULC) Map

The term "land use" pertains to the human activities or economic functions associated with a specific land area, whereas "land cover" refers to the type of surface feature found on the Earth (Lillesand and Kiefer, 2000). The Land Use Land Cover (LULC) map is a crucial input for the SWAT model. The accuracy of LULC classification relies on the precision of remote sensing imagery. To attain the desired accuracy and reliability, a ground-truthing campaign is essential, as emphasised by Tripathi *et al.* (2006) and Awan and Ismaeel (2014). To achieve this, a GPS survey was conducted in the study area, recording 455 points and defining nine distinct land

use classes. Careful consideration was given to ensure these points represented the entire area and included the selected classes.

Preparing the Land Use Land Cover (LULC) map involved the utilisation of the Google Earth Engine (GEE). GEE encompasses a vast catalogue of analysis-ready data, amounting to multiple petabytes, seamlessly integrated with a high-performance, inherently parallel computing service. This resource is accessible and manageable through an internet-accessible Application Programming Interface (API) and an associated web-based Interactive Development Environment, facilitating swift prototyping and visualisation of outcomes. Within the data catalogue, an extensive collection of publicly available geospatial datasets encompassing data from various satellite and aerial imaging systems, spanning both optical and non-optical wavelengths. These datasets also contain environmental variables, weather and climate forecasts and hindcasts, land cover information, topographic data, and socio-economic datasets.

This extensive dataset is preprocessed to a readily accessible format that preserves the information, making it efficiently available and eliminating many challenges associated with data management. Users can retrieve and analyse data from both the public catalogue and their private data through a set of operators offered by the Earth Engine API. These operations are executed within a robust parallel processing system that automatically subdivides and distributes computations, ensuring high-throughput analysis capabilities. To initiate the process, users create an account on the Earth Engine homepage at *https://earthengine.google.com* and access the user interface. The program was written as shown in Appendix A. The results were downloaded, which gave an LULC map.

3.10.2.3 Digital Soil Map

The morphologic characteristics of the soil and soil map of the study area were collected from the Directorate of Soil Survey and Soil Conservation of Kerala State. Other studies in Kerala have also used the same data source (e.g., Sandra and Sathian, 2016; Tejaswini and Sathian, 2018; Varughese and Hajilal, 2022).

The soil properties which were not available at the soil survey and soil conservation department were computed using Soil Plant Atmosphere Water (SPAW) software. The soil characteristics required for the model, such as hydraulic conductivity, electrical conductivity, and bulk density, were also obtained from SPAW. Many researchers have also used the SPAW model for getting soil properties (e.g. De Jong and Zentner, 1985; Rao and Saxton, 1995; Yetukuri *et al*., 1996; Saxton and Willey, 2006; Nandgude *et al*., 2014).

The soil map was digitised and converted to a grid file using ArcGIS 10.3. The soil information was added to the ArcSWAT user interface, and then the soils were classified according to different textural characteristics.

3.10.2.4 Slope Map

In SWAT, a slope map is used to create HRU. The slope map was prepared from SRTM DEM utilising the appropriate tools of the ArcGIS. The whole watershed area was classified using guidelines laid down by the soil survey manual of the United States Department of Agriculture (USDA). The slope categories were measured from the map scale and were used for preparing the slope map that gives various group categories of the slope of the watershed area.

3.10.2.5 Weather Data

The rainfall data were obtained from the four tipping bucket rain gauges installed within the watershed. The PM method employed in this research necessitates weather data such as daily maximum and minimum air temperature, wind speed, solar radiation, and relative humidity. To obtain this data, information was gathered from the nearest weather station, specifically, the Kelappaji College of Agricultural Engineering and Technology in Tavanur, affiliated with Kerala Agricultural University, located approximately 10 kilometres from the study area. Similarly, other researchers have also used climatic data from nearby weather stations for running the SWAT model (e.g. Tejaswini and Sathian, 2018; Eini *et al*., 2020; Nyatuame *et al*., 2020). The meteorological data collected were converted into text format and then provided to the SWAT model as input.

3.10.3 Water Balance Equation by the SWAT model

In SWAT, the hydrological simulations of a watershed are divided into two primary phases: the land phase and the routing phase. The land phase, which corresponds to the hydrological cycle, regulates the quantities of water, sediment, nutrients, and pesticides that are transported to the main channel within each sub-basin. This phase relies on the water balance equation for its calculations. On the other hand, the routing phase focuses on transporting water, sediment, and agricultural chemicals through the network of channels leading to the outlet of the watershed (Arnold *et al*., 2012).

The water balance equation adopted by SWAT is given as Eq. 3.11.

$$SW_t = SW_0 + \sum_{i=1}^{t}(R_i - Q_{surf} - E_a - W_{seep} - Q_{gw}) \quad .....(Eq.\,3.11)$$

Where,

SW_t is the final soil water content (mm H_2O)

SW_0 is the initial soil water content on the day i (mm H_2O)

t is the time (days)

R_i is the amount of precipitation on the day i (mm H_2O)

Q_{surf} is the amount of surface runoff on the day i (mm H_2O)

E_a is the amount of evapotranspiration on the day i (mm H_2O)

W_{seep} is the amount of water entering the vadose zone from the soil profile on the day i (mm H_2O)

Q_{gw} is the amount of return flow on the day i (mm H_2O)

3.10.4 SWAT Simulation

Fig. 3.25 shows the schematic view of the hydrological cycle and SWAT simulation processes (Neitsch *et al*., 2005). Fig. 3.26 shows the flow chart for the simulation of the SWAT model. The data collected from various sources such as DEM, LULC map, soil map and slope map are overlayed. The delineation of the watershed and sub-watersheds is carried out using DEM. The HRU analysis is carried out using all these data. In the next step, input tables are written along with

the weather data in SWAT-compatible form. Then, these input tables are edited, and finally, the simulation of the SWAT model is carried out.
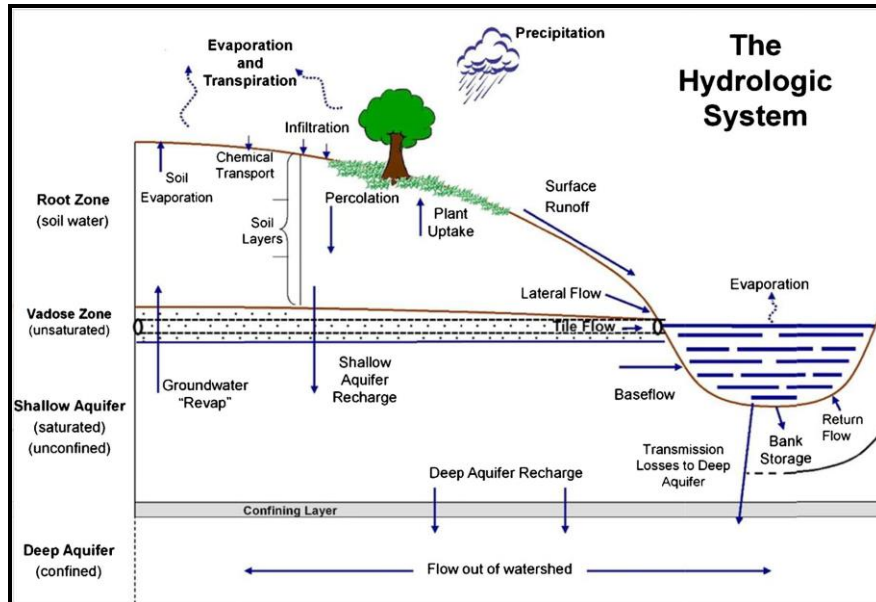

Fig. 3.25. Schematic View of the Hydrological Cycle and SWAT Simulation Processes (Neitsch *et al*., 2005)

3.10.5 SWAT Model Output

3.10.5.1 Watershed Delineation

The first step in using the SWAT model is to delineate the watershed corresponding to the outlet chosen in the mainstream. The watershed delineation process consists of five significant steps: DEM setup, stream definition, outlet and inlet definition, selection and definition of watershed outlets and calculation of sub-basin parameters. The watershed boundary corresponding to the highest point of the area was delineated in ArcSWAT following these steps. Watershed delineation for any outlet chosen in the stream outlet is possible in the model.

3.10.5.2 Surface Runoff

SWAT provides two approaches for calculating surface runoff: the Soil Conservation Service Curve Number (SCS-CN) method (USDA, 1972) and the Green and Ampt infiltration method (Green and Ampt, 1911). The SCS-CN method is frequently employed by researchers within the SWAT model to estimate surface runoff. It determines surface runoff by considering the hydrologic soil group, land

use, and Antecedent Moisture Content (AMC) for each Hydrologic Response Unit (HRU) in the area (Melaku *et al*., 2018a; Eini *et al*., 2020; Gholami *et al*., 2022).
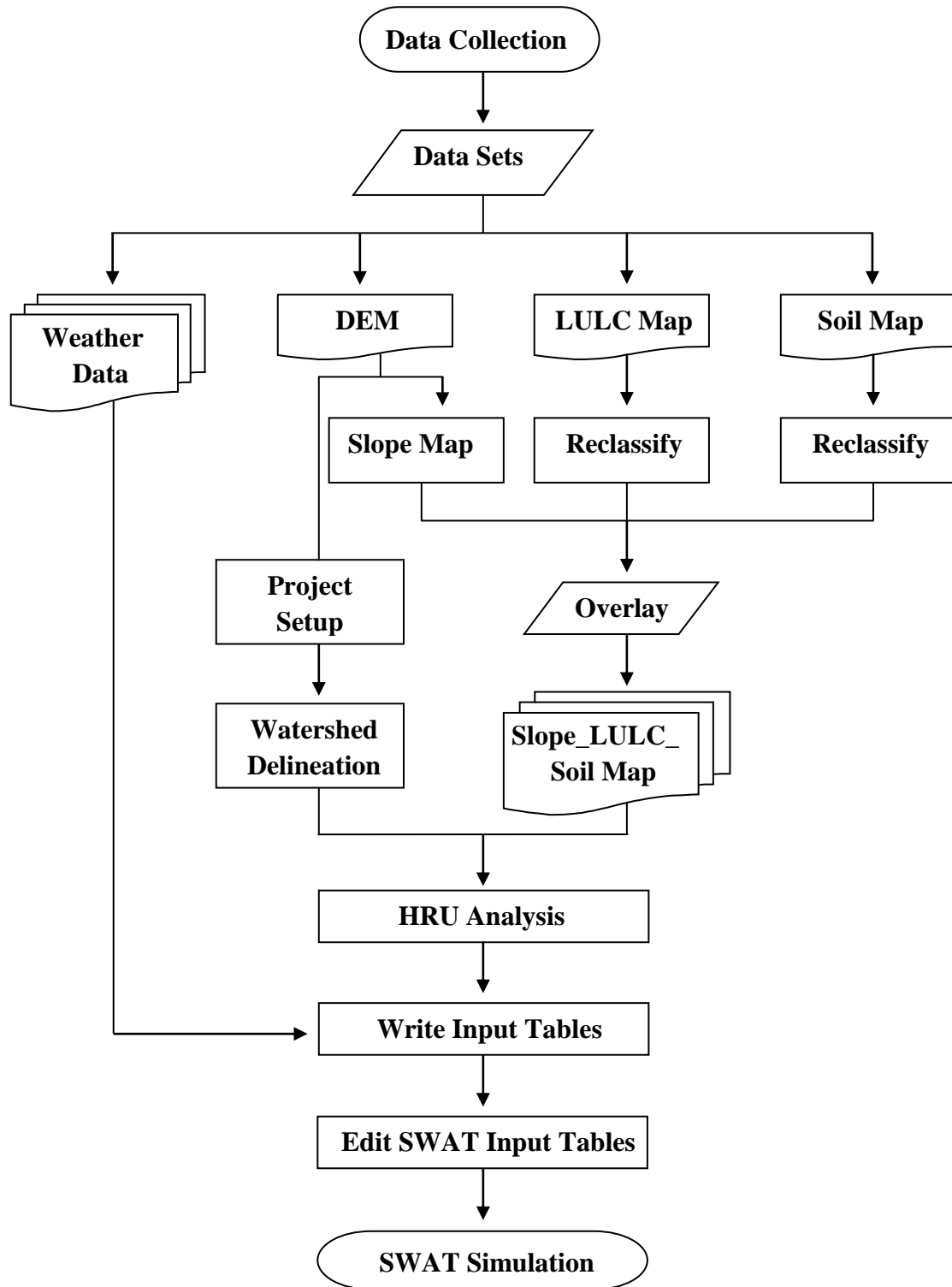

Fig. 3.26. Flow Chart for Simulation in SWAT Model

The Soil Conservation Service Curve Number method is a simple, proficient, and extensively used method to determine the approximate amount of runoff resulting from a rainfall event from a specific area. The SCS technique was initially developed for watersheds of 15 km² but has been adapted for use in larger watersheds or basins by adjusting curve number values. Extensive research has demonstrated its effectiveness in various hydrological conditions (Gassman *et al.*, 2007; Nyatuame *et al.*, 2020).

The runoff curve number is determined by a combination of land-use type, soil group, and Antecedent Soil Moisture Condition (AMC), resulting in values ranging from 0 to 100. Soil types are categorised into four Hydrologic Soil Groups (HSG): Group A, Group B, Group C, and Group D. Soils falling under the "Group A" hydrologic soil group exhibit high infiltration rates and minimal surface runoff, while "Group D" comprises soils with low infiltration rates.

The general equation for the SCS-CN method is given in Eq. 3.12 (USDA, 1972):

$$Q_{surf} = \frac{(R_{day} - 0.2S)^2}{(R_{day} + 0.8S)}, R > 0.2S \quad ..... \text{ (Eq. 3.12)}$$
$$Q_{surf} = 0, R \leq 0.2S$$

Where,

Q_{surf} is the depth of accumulated runoff or rainfall excess (mm H_2O);

R_{day} is the rainfall depth for the day (mm H_2O);

S is the depth of potential maximum water retention (mm H_2O)

The retention parameter exhibits spatial variations attributed to alterations in land surface characteristics, including changes in soils, land use, slope, and management practices. Additionally, temporal fluctuations in soil water content can also influence this parameter. It is related to CN by the SCS equation (Eq. 3.13) (USDA, 1972):

$$S = 254\left(\frac{100}{CN} - 1\right) \quad ..... \text{(Eq. 3.13)}$$

Where,

CN is the curve number for the day

The initial abstraction, denoted as I_a, is often estimated as 0.2 times the value of S. This includes factors like surface storage, interception, and pre-runoff infiltration and is represented by Eq. 3.14.

$$Q_{surf} = \frac{(R_{day} - I_a)^2}{(R_{day} - I_a + S)} \quad ..... (Eq. 3.14)$$

Where,

I_a is the initial abstraction of water (mm H_2O)

3.10.5.3 Lateral flow

Lateral flow is the movement of water under gravitational forces parallel to the slope of the land. Lateral subsurface flow in the soil profile can be calculated simultaneously with percolation. For estimating lateral flow, SWAT incorporates a kinematic storage model equation, which uses kinematic approximations for its derivation, which is shown in Eq. 3.15:

$$q_{lateral} = 0.024 \left[\frac{2s \times k_{sat} \times \sin\alpha}{\theta_d \times L} \right] \quad ..... (Eq. 3.15)$$

Where,

s = drainable volume of soil water per unit area of the saturated thickness (mm day^{-1})

k_{sat} = saturated hydraulic conductivity (mm h^{-1})

θ_d = drainable porosity

L = flow length (m)

α = slope of the land

3.10.5.4 Base flow

Groundwater discharges into streams when the water table rises above the stream bed is called base flow. Base flow can be referred to as the volume of stream flow originating from the groundwater. SWAT simulates base flow by using the Eq. 3.16:

$$Q_{gw,i} = Q_{gw,i-1} \times \exp.(-\alpha_{gw}.\Delta t) + W_{rchrg,sh} \times [1 - \exp.(-\alpha.gw.\Delta t)], \text{if } aq_{sh} > aq_{shthrq}$$

$$Q_{gw,i} = 0, \quad .aq_{sh} \leq aq_{shthrq} \qquad \qquad ....(Eq.\,3.16)$$

Where,

$Q_{gw,\,i}$ = groundwater flow into the main channel on the day i (mm H_2O)

$Q_{gw,\,i-1}$ = groundwater flow into the main channel on day i-1 (mm H_2O)

α_{gw} = base flow recession constant

Δt = time step

$W_{rchrg,sh}$ = amount of recharge entering the shallow aquifer on the day i (mm H_2O)

aq_{sh} = amount of water stored in the shallow aquifer at the beginning of the day (mm H_2O)

$aq_{shthr,q}$ = threshold water level in the shallow aquifer for groundwater contribution to the main channel to occur (mm H_2O)

3.10.5.5 Evapotranspiration (ET)

The estimation of Evapotranspiration (ET) depends on the interplay of Potential Evapotranspiration (PET) and the leaf area index, representing the ratio of plant leaf area to the soil surface area. This estimation integrates various components that consider the energy required for evaporation, the driving force behind vapour removal, and factors related to aerodynamics and surface resistance. Actual soil water evaporation is calculated using exponential functions considering soil depth and water content. Plant transpiration is modelled as a linear function of PET and the leaf area index, as outlined by Arnold and Allen (1996).

The model provides three choices for calculating Potential Evapotranspiration (PET): the Hargreaves method (Hargreaves and Samani, 1985), the Priestley-Taylor method (Priestley and Taylor, 1972), and the Penman-Monteith method (Monteith, 1965). The Penman-Monteith method was used for PET estimation as many researchers have successfully used it in the SWAT model (e.g. Muttiah and Wurbs, 2000; Bonuma *et al.*, 2013; Sith *et al.*, 2019). Also, it is suitable for the study area, referring to other research in similar climatic conditions (e.g.

Tejaswini and Sathian, 2018; Varughese and Hajilal, 2022; Pasha, 2022). The detailed Penman-Monteith method is explained in Section 3.2.5 of this Chapter.

3.10.5.6 Groundwater Storage

One of the significant outcomes generated by the SWAT model is its ability to estimate groundwater in unconfined (shallow) aquifers, as discussed by Arnold *et al*. (1993). In the model, the groundwater storage within an unconfined aquifer is regarded as the water that has percolated through and moved beyond the soil's root zone, a concept also emphasised by Tripathi *et al*. (2006) and Awan and Ismaeel (2014). Over an extended period, this percolated water will eventually reach the phreatic surface within the saturated zone, as outlined by Neitsch *et al*. (2005) and further corroborated by Awan and Ismaeel (2014).

3.10.5.7 Deep Aquifer Recharge

SWAT estimates deep aquifer recharge as the difference between the precipitation depth and the cumulative depth of other water balance components, viz., ET, runoff, change in soil moisture and change in groundwater storage.

3.11 SWAT-CUP DESCRIPTION

SWAT-CUP (Soil and Water Assessment Tool Calibration and Uncertainty Programme) is an automated calibration tool for the SWAT model developed by Eawag - Swiss Federal Institute of Aquatic Science and Technology (Abbaspour *et al.*, 2015). The SWAT-CUP is a public domain program using a generic interface. It attempts to account for all sources of uncertainty from input variables, conceptual models, parameters, and measured data. The main advantage of SWAT-CUP is that it performs different sensitivity analyses, calibration, validation, and uncertainty analyses. It has made the calibration procedure more straightforward and faster for professionals and students (Rohtash *et al*., 2018; Fousiya and Varughese, 2020; Varughese and Hajilal, 2022).

The SWAT-CUP systematically modifies uncertain model parameters, and the model is run. The required outputs are then extracted from the model output files and compared with the observed data. The program uses five different uncertainty

algorithms: SUFI-2 (Sequential Uncertainty Fitting), GLUE (Generalized Likelihood Uncertainty Estimation), PARASOL (Parameter Solution), MCMC (Markov Chain Monte Carlo), and PSO (Particle Swarm Optimization) (Abbaspour *et al.*, 2015). Each SWAT-CUP project contains one calibration method and allows the user to run the procedure many times until convergence is reached. Referring to previous studies, the SUFI-2 algorithm was found to be very efficient for sensitivity analysis of small watersheds (e.g. Abbaspour *et al.*, 2007; Krishnan *et al.*, 2018; Shivhare *et al.*, 2018; Nasiri *et al.*, 2020; Hosseini and Khaleghi, 2020). Thus, in this study, the SUFI-2 algorithm was used for sensitivity analysis, calibration, and validation of the model using monthly data.

SUFI-2 uses Latin-Hypercube sampling to generate a separate set of parameters. This method allows for setting ranges for parameters of interest and running multiple simulations with different parameters sampled by Latin-Hypercube. The SUFI-2 algorithm employs two key indicators to assess the quality of model calibration and the degree of uncertainty. These indicators are the p-factor and the r-factor. The p-factor signifies the percentage of observed data falling within the 95% Per cent Prediction Uncertainty (95PPU). At the same time, the r-factor represents the average width of the 95PPU band divided by the standard deviation of the measured data. A p-factor of 1 and an r-factor of zero indicate a simulation that precisely matches the observed data, as described by Krishnan *et al.* in 2018. Once acceptable values for the p-factor and r-factor are achieved, the parameter uncertainties align with the desired parameter ranges. Graphical and statistical evaluation techniques assess how closely the simulated results align with the observed data. The SWAT and SWAT-CUP calibration tools offer a range of statistical criteria for model evaluation, allowing for selecting an objective function for model calibration and validation. Fig. 3.27 illustrates the workflow of the SWAT-CUP model simulation using the SUFI-2 algorithm.

Sensitivity analysis can be defined as the procedure for determining how the parameters of a model's output change in response to variations in the parameters of the model's input. The initial step in the calibration and validation process involves

conducting sensitivity analysis. Two types of sensitivity analysis are commonly used: "one-at-a-time" sensitivity analysis and "global" sensitivity analysis, facilitated by Latin-Hypercube sampling. In "one-at-a-time" sensitivity analysis, the sensitivity of a single parameter is assessed while maintaining the values of the other parameters at constant and reasonable values. In contrast, "global" sensitivity analysis considers the collective impact of all input parameters on the variability of the output, and it is based on running numerous model simulations.

After conducting an initial sensitivity analysis, which involved sequentially altering one parameter while holding all others constant (one-at-a-time sensitivity analysis) and then utilising global sensitivity analysis (simultaneously varying all parameters), the selection of parameters for the model calibration was determined. The global sensitivity analysis was carried out for the study area, specifically for simulating streamflow, as done in previous research by other scholars, such as Eini *et al.* (2020), Varughese and Hajilal (2020), and Pasha (2022). This analysis considered fourteen hydrologic parameters.

3.11.1 Model Calibration

Before employing physically based distributed watershed models in simulating hydrological processes, it is essential to undergo a calibration process to minimise the uncertainties linked to model predictions. The calibration of hydrological models is a thorough procedure that is influenced by factors such as the number of input parameters and model intricacy. Diligent calibration is crucial for achieving precise simulation of hydrological processes.

3.11.2 Model Performance Evaluation

There are many methods to assess and evaluate the accuracy of results produced by the model through graphical comparison and statistical analysis of the values. Usually, multiple evaluation criteria are used as the single statistical metric only evaluates a specific part of model performance. The statistics for performance evaluation used in this study included coefficient of determination (R^2), Nash-Sutcliffe Efficiency (NSE), Percent Bias (PBIAS) and RMSE-observations Standard deviation Ratio (RSR).
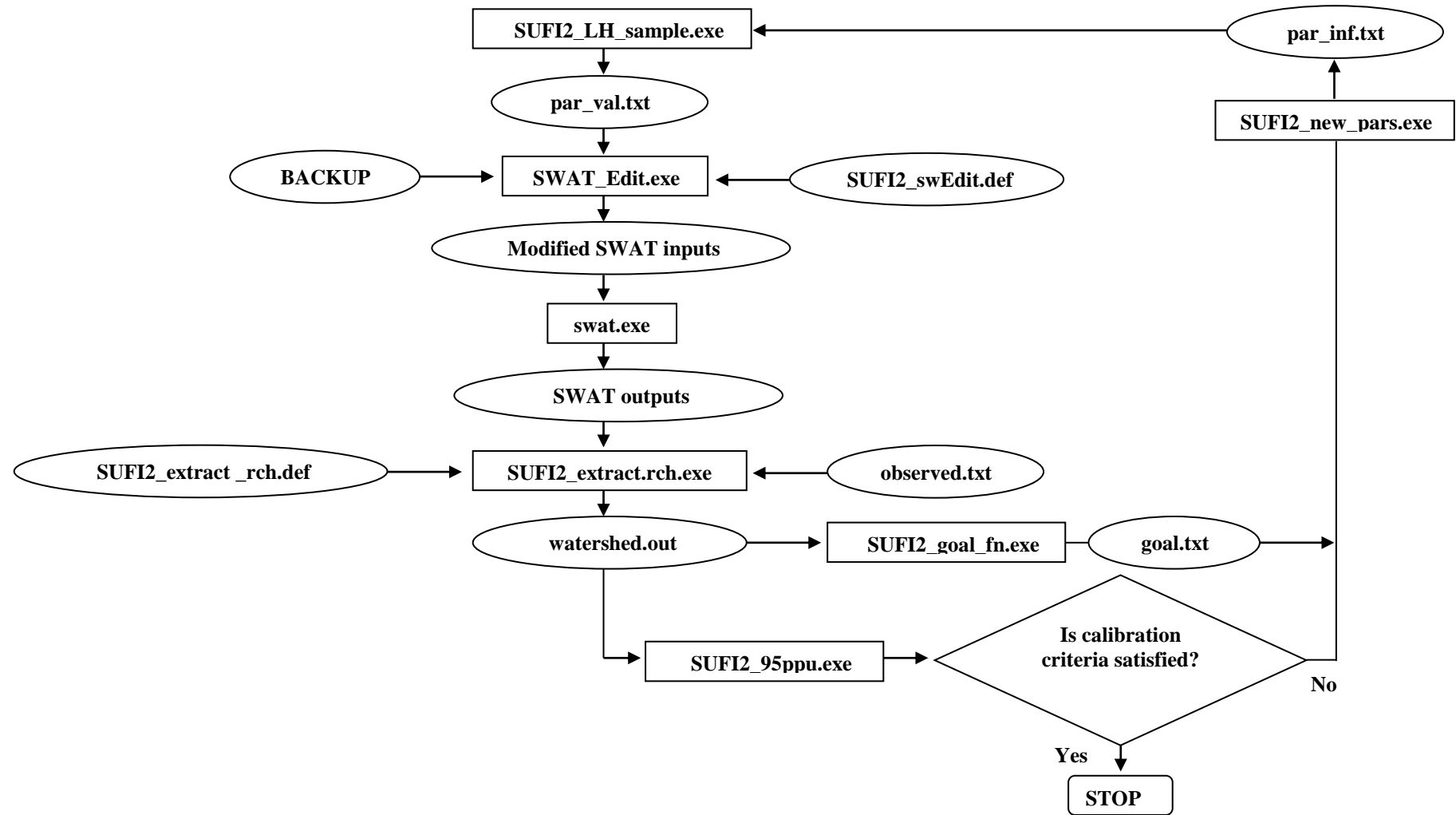
Fig. 3.27. Flow Chart for SWAT-CUP Model

3.11.2.1 Coefficient of Determination (R^2)

The coefficient of determination (R^2) is defined as the variance ratio in the dependent variable, which is predictable from the independent variable. The R^2 value indicates the strength of the relationship between the simulated and observed values, and the range of values falls between 0 and 1, with 1 indicating that the predicted value matches the observed value perfectly and 0 signifying no correlation between the predicted and observed values. Generally, values exceeding 0.5 are deemed acceptable (Santhi *et al*., 2001; Van Liew *et al*., 2003; Moriasi *et al*., 2007). R^2 is given by Eq. 3.17 (Krause *et al*. 2005):

$$R^2 = \left\{ \frac{\sum\limits_{i=1}^{n} \left[(O_i - \overline{O}) \times (P_i - \overline{P}) \right]}{\sqrt{\left[\sum\limits_{i=1}^{n} (O_i - \overline{O})^2 \times \sum\limits_{i=1}^{n} (P_i - \overline{P})^2 \right]}} \right\}^2 \quad .....(Eq. 3.17)$$

Where,

i is the counter for individual observed and predicted values

n is the number of observations

O_i is the observed values

$\overline{O}$ is the mean of observed values

P_i is the predicted values

$\overline{P}$ is the mean of predicted values

3.11.2.2 Nash–Sutcliffe Efficiency (NSE)

The Nash-Sutcliffe Efficiency (NSE) is a normalised statistic that assesses the extent to which the variance of residuals ("noise") relates to the variance of measured data ("information"), as outlined by Nash and Sutcliffe (1970). It is commonly employed to evaluate the predictive capabilities of hydrological models. The NSE provides insight into how well the simulated data aligns with actual measurements and can take on values ranging from -∞ to 1. Values falling within the range of 0.0 to 1.0 are generally considered satisfactory indicators of model performance, while values below 0.0 suggest that the mean observed value

outperforms the simulated value. Typically, values exceeding 0.4 are deemed acceptable. The NSE is given by Eq. 3.18.

$$NSE = 1 - \frac{\sum_{i=1}^{n}(P_i - O_i)^2}{\sum_{i=1}^{n}(O_i - \overline{O})^2} \quad ..... (Eq.\,3.18)$$

Where,

   i is the counter for individual observed and predicted values

   n is the number of observations

   P_i is the predicted values

   O_i is the observed values

   $\overline{O}$ is the mean of observed values

3.11.2.3 Percent Bias (PBIAS)

The PBIAS is a statistical metric that assesses the average tendency of the simulated data compared with the experimental observations. PBIAS, ranging from -10 to 10, is characterised by an ideal zero value, where lower magnitude values signify precise model simulation. Negative PBIAS values indicate a bias toward overestimation in the model, while positive values point to a bias involving model underestimation (Gupta and Kapoor, 2020). The PBIAS is given by Eq. 3.19.

$$PBIAS = \left[\frac{\sum_{i=1}^{n}(O_i - P_i) \times 100}{\sum_{i=1}^{n}(O_i)} \right] \quad ..... (Eq.\,3.19)$$

Where,

   i is the counter for individual observed and predicted values

   n is the number of observations

   O_i is the observed values

   P_i is the predicted values

3.11.2.4 RMSE-observations Standard-Deviation Ratio (RSR)

The RMSE (Root Mean Square Error) observations standard deviation ratio (RSR) is defined as the ratio of the RMSE and standard deviation of measured data

(Singh *et al.*, 2005). RSR ranges from an ideal value of zero to a relatively high positive value. A lower RSR signifies a smaller RMSE and, consequently, reflects superior model simulation performance. Typically, values lower than 0.7 are considered acceptable. It is expressed by Eq. 3.20 (Singh *et al.*, 2005):

$$RSR = \frac{RMSE}{STDEV_{obs}} = \left[\frac{\sum\limits_{i=1}^{n}(O_i - P_i)^2}{\sqrt{\sum\limits_{i=1}^{n}(O_i - \overline{O})^2}} \right] \quad ..... (Eq. 3.20)$$

Where,

   i is the counter for individual observed and predicted values

   n is the number of observations

   P_i is the predicted values

   O_i is the observed values

   $\overline{O}$ is the mean of observed values

3.12 DEVELOPMENT OF RELATIONSHIPS BETWEEN RAINFALL AND WATER BALANCE COMPONENTS

The relationship between rainfall and other hydrological components has yet to be fully understood. Establishing such a connection is a complex procedure, as numerous direct and indirect factors, including precipitation distribution, evaporation, transpiration, abstraction, topography, and soil types impact it. It has been recognised that converting rainfall input to hydrological components over the catchment is an exceptionally complex hydrologic process influenced by various storm and drainage characteristics. Understanding this relationship is a necessary step to quantify the hydrological parameters in any watershed. These relations are valuable tools for engineers dealing with water management. The R software was used in this study to determine the relationship between rainfall and other water balance components.

3.12.1 Pearson's Correlation Coefficient

Pearson's correlation assesses the intensity of the linear association between two variables, and its value can range from -1 to +1. A value of -1 indicates a

complete negative linear correlation, 0 signifies no correlation, and +1 represents an absolute positive linear correlation. Pearson's correlation coefficient ("r") can be calculated using Eq. 3.21 (Gupta and Kapoor, 2020).

$$r = \frac{\sum\limits_{i=1}^{n}\left[(O_i - \overline{O}) \times (P_i - \overline{P})\right]}{\sqrt{\left[\sum\limits_{i=1}^{n}\left(O_i - \overline{O}\right)^2 \times \sum\limits_{i=1}^{n}(P_i - \overline{P})^2\right]}} \quad ..... (Eq. 3.21)$$

Where,

i is the counter for individual observed and predicted values

n is the number of observations

O_i is the observed values

$\overline{O}$ is the mean of observed values

P_i is the predicted values

$\overline{P}$ is the mean of predicted values

The Pearson's correlation coefficient has been determined between all the determined water balance components for monthly and weekly time scales using R software.

3.12.2 Regression Model

Regression analysis is a valuable method for revealing the connections between observed variables in data, although it may not readily indicate causation. In statistical modelling, regression analysis is a set of statistical processes for estimating the relationships between a dependent variable and one or more independent variables. In this study, the regression model was developed after testing the relationship for linear, polynomial, exponential, logarithmic, and power functions in the R-Studio software. The model was selected based on the coefficient of determination (R^2), shown in Eq. 3.17, and the p-value obtained from R software.

3.12.3 Residual versus Fitted Plot

A common type of residual plot used in residual analysis is the "residuals versus (vs.) fitted plot." This plot displays the residual values on the vertical axis and the predicted or fitted values (estimated responses) on the horizontal axis. This

particular plot is frequently employed to identify issues such as non-linearity, unequal error variances, and outliers in the data. The residuals are calculated from the Eq. 3.22.

$$e_i = y_i - \overline{y}_i \quad ..... (Eq. 3.22)$$

Where,

   i is the counter for individual observed and predicted values

   e_i is the residual

   y_i is the predicted value

   $\overline{y}_i$ is the observed value

3.12.4 Normal Q-Q (Quantile-Quantile) Plot

A Normal Q-Q plot is a valuable tool for visually comparing and analysing two probability distributions by plotting their quantiles against each other. When the two distributions are identical, the points on the Q-Q plot will form a perfect straight line. This plot enables the identification of data points that diverge significantly from this reference line. By examining the points on the Normal Q-Q plot, one can assess the univariate normality of the dataset. If the data follows a normal distribution, the points will closely align with the 45-degree reference line. However, if the data deviates from normality, the points will exhibit deviations from this reference line.

3.13 PLANNING SCIENTIFIC WATER MANAGEMENT PRACTICES

To plan scientific water management measures for a watershed, it is required to analyse the morphometric information, water balance components and the water demands of the watershed. A flow chart of such a plan is presented in Fig 3.28. The morphometric report provides topographic information on the watershed, subsoil details and geological characteristics. Water balance components include all water-related inflow, storage and outflow from the watershed. Water demand depicts all information about water requirements for all socio-economic activities, including agriculture. The most crucial morphometric information includes an elevation map of the area, slope map, soil map, land use, drainage network map and geological map.

The elevation map provides the MSL value of each place, and this information is vital to assess the feasibility and effectiveness of the water harvesting measures. It also offers the viability of land treatment measures. Land slope maps provide valuable input to identify various land treatment measures suitable for different slope groups. Land uses have a very high role in deciding the infiltration and percolation characteristics of the soil. Further, the land use of an area determines the ET of a particular place, which is one of the critical water balance components. A drainage line map gives the spatial distribution of all channels and streams in a watershed. All drainage line treatments will be associated with the drainage channels. A geological map provides information on the stability of the subsurface, which is essential for formulating groundwater recharge plans and locating surface water storage.

The most crucial water balance data include rainfall, runoff, soil moisture and groundwater. Daily or at least weekly rainfall data is required to know the temporal receipt of water in the catchment. More rain gauge stations are necessary if the watershed area is more prominent to account for the spatial variability of rainfall. Runoff provides quantitative information on the outflow of water from the watershed. The difference between rainfall and the sum of ET and runoff shows how much rainwater is stored in the surface and subsurface of the watershed. Again, it is required to know the component-wise runoff such as surface runoff, lateral flow and baseflow. Separate assessment of these runoff components has its significance from the point of view of planning appropriate interventions for the conservation of surface and groundwater.

Water demand required by various sectors is also necessary to know the extent of water harvesting and conservation needed in the watershed. Agricultural water demand is the most important one. The other demands, such as domestic and industrial, also assume significance as they are there throughout the year, and generally, they take higher priority than irrigation water. Assessing all the above-said information pertaining to the sub-watershed or micro watershed, appropriate soil and water conservation measures are planned.
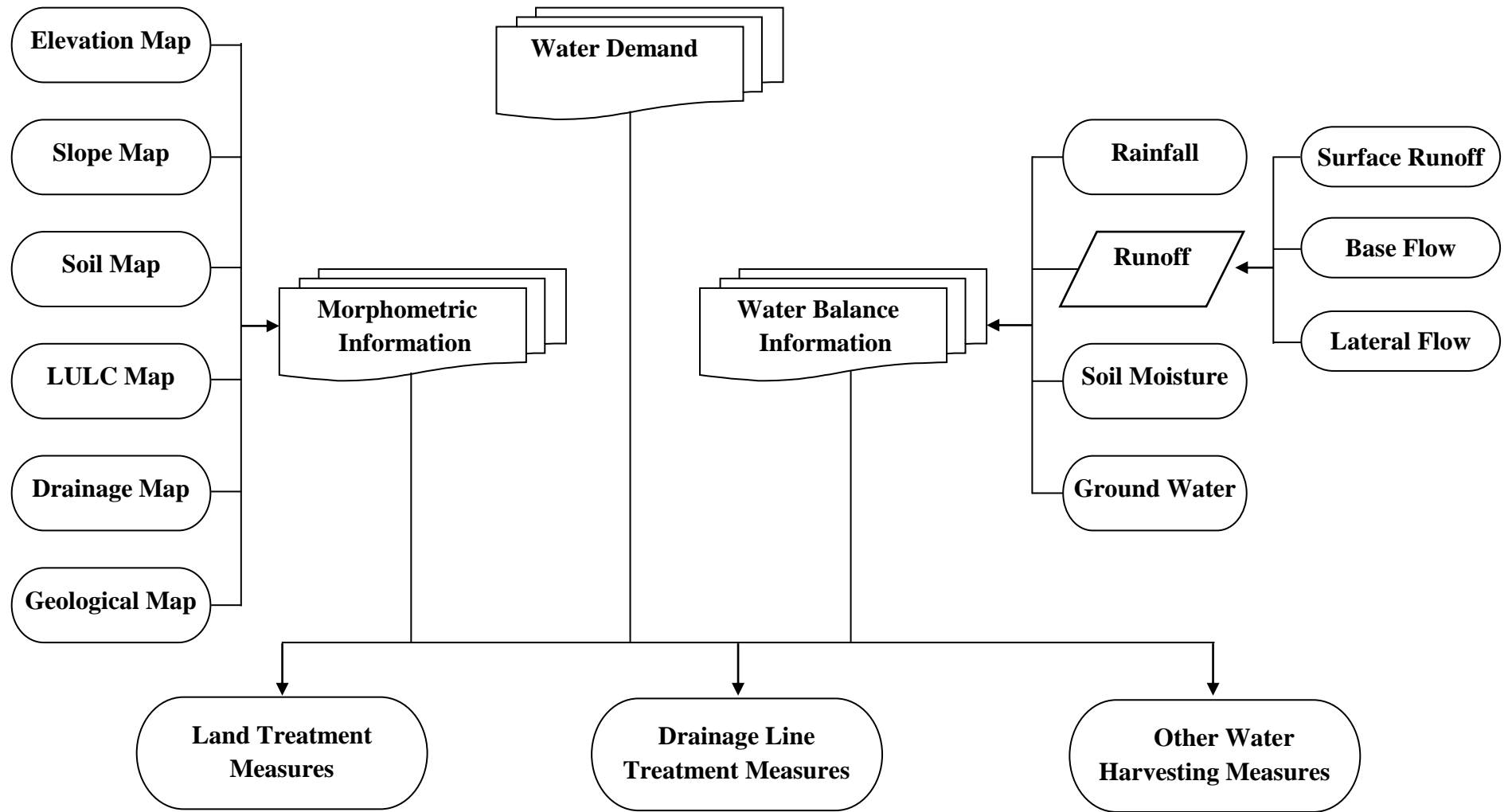
Fig. 3.28. Flow Chart for Planning Scientific Water Management Practices

3.14 GUIDELINES FOR THE SELECTION OF WATER CONSERVATION MEASURES

The standard guidelines issued by the Integrated Mission for Sustainable Development (IMSD) (IMSD, 1995); FAO (Jahn *et al*., 2006); Central Ground Water Board (CGWB) (Saha and Ray, 2019) as given in Table 3.8, have been used.

Table 3.8: Criteria for Selection of Different Soil and Water Conservation Measures

Sr. No.	Structure	Slope	Land use	Soil permeability
1.	Vented Cross Bars (VCB)	< 15	Agricultural lands	Medium to high permeable soils
2.	Stone/soil bunds	< 15	Agricultural lands	Medium to high permeable soils
3.	Graded contour bunds	< 6	Agricultural lands	Medium to high permeable soils
4.	Staggered contour trenches	10-33	Open scrub or wastelands	Medium permeable soils
5.	Bench terraces	< 33	Open scrub or wastelands	Medium permeable Soils
6.	Farm ponds	< 5	Agricultural lands	Medium to high permeable Soils
7.	Roof water harvesting	< 5	Urban lands	Medium to high permeable Soils

3.14.1 Procedure for Planning VCB and Stone/Soil Bunds

The storage height of VCB was taken as 2 m, and hence, the contours were plotted at an interval of 2 m. The streams were digitised using the polygon feature in ArcGIS up to the intersection of the following contour line. Using the 3D Analyst tool from ArcGIS, the volume of water stored behind each bund was calculated. The total amount of water held by all bunds was also determined.

3.14.2 Procedure for Planning Soil and Water Conservation Structures

The slope map was digitised in ArcGIS based on the slope criteria for each structure. The structures, viz. graded contour bunds, staggered contour trenches, bench terraces, farm ponds, and roof water harvesting structures, were suggested based on the slope map, land use, soil and geology.

CHAPTER - IV
RESULTS AND DISCUSSIONS

The study "Determination of water balance components of a micro watershed for improved water management practices" was conducted at the Perassannur sub-watershed of the River Bharathapuzha of Kerala state. The study has been replicated in one more sub-watershed, delineated corresponding to the outlet at Painkanoor. Topographic and hydrologic data pertaining to the watershed was collected, analysed, and the results are presented, interpreted, and discussed in the following sections of this Chapter.

4.1 PHYSIOGRAPHY OF THE STUDY AREA

The linear, areal, and relief characteristics of the study watersheds were extracted from DEM. The watershed boundary with the drainage network is presented in Fig 4.1. The area and perimeter of the Perassannur watershed were obtained as 79.66 km^2 and 56.60 km, respectively. The maximum length of the basin was 14.45 km, and the width was 9.06 km. The watershed was identified as fern-shaped. The streams were evenly distributed within the watershed and had the highest stream order of four. The mainstream was nearly along the centre of the watershed.

The area and perimeter of the Painkanoor sub-watershed were 35.36 km^2 and 38.90 km, respectively; the maximum length of the basin was 10.95 km, and the width was 6.19 km. This sub-watershed was also fern-shaped, as shown in Fig. 4.2. The highest stream order was 3, and the main stream flowed nearly along the centre of the watershed.

The maximum elevation was observed as 161 m for the Perassannur watershed, as shown in Table 4.1. The maximum percentage area of the Perassannur watershed was 27.43% which was within the elevation band of 30-50 m, followed by 17.93% area in the elevation range of 15-30 m, while the lowest area of 2.80% was seen in the elevation class of 130-161 m. The area covered by each elevation class from the classified DEM of the Perassannur watershed is shown in Fig. 4.3.
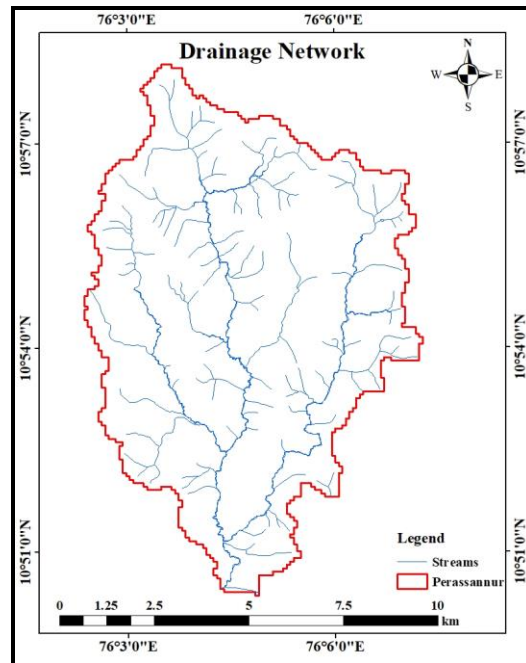
Fig. 4.1. Perassannur Watershed with Boundary and Drainage Network
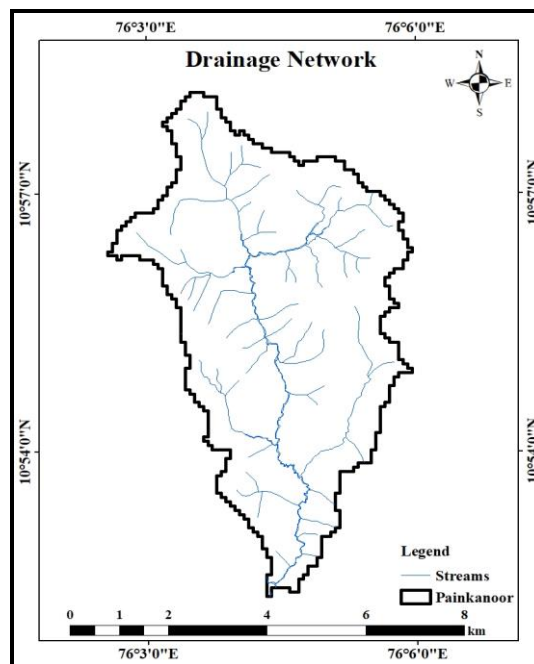
Fig. 4.2. Painkanoor Sub-watershed with Boundary and Drainage Network

The hypsometric curve was plotted, as shown in Fig. 4.4, to analyse the distribution of land elevations. The curve is a concave-up curve, which indicates a youthful or actively tectonic landscape where erosion has not had sufficient time to smooth out the terrain.
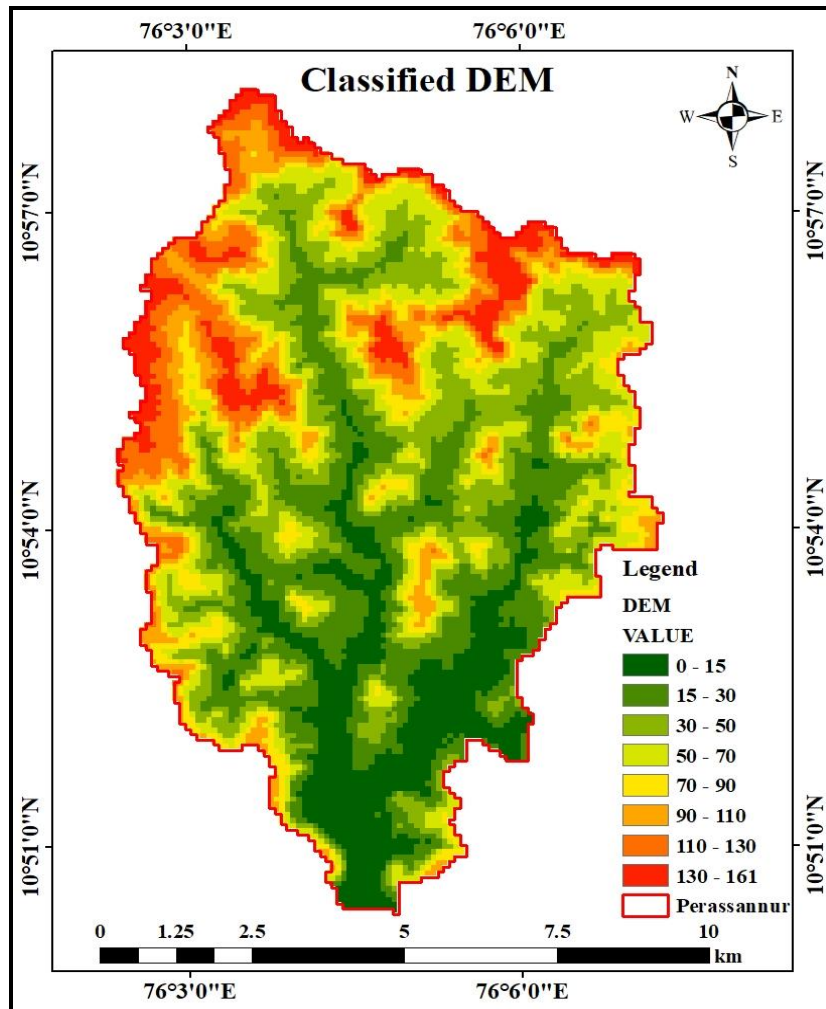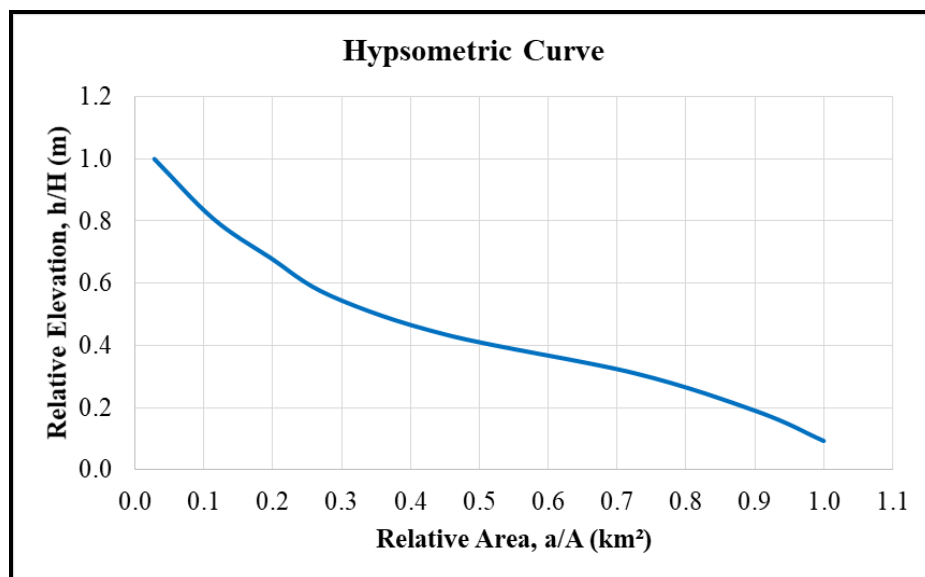
Fig. 4.3. Classified DEM of the Perassannur Watershed

Fig. 4.4. Hypsometric Curve for the Perassannur Watershed

Table 4.1. Area Covered by Different Elevation Classes for the Perassannur Watershed

Sr. No.	Elevation (m)	Area (km^2)	Area (%)
1.	0-15	7.54	9.46
2.	15-30	14.28	17.93
3.	30-50	21.85	27.43
4.	50-70	13.30	16.69
5.	70-90	7.09	8.89
6.	90-110	6.54	8.21
7.	110-130	6.83	8.58
8.	130-161	2.23	2.80
Total		**79.66**	**100.00**

The maximum elevation of the Painkanoor sub-watershed was 151 m, as shown in Table 4.2. The maximum percentage area of 29.43% was lying in the elevation band of 30-50 m, followed by an 18.00% area in the elevation range of 50-70 m, while the lowest area of 2.88% was observed in the elevation class of 0-15 m. The area covered by each elevation class is depicted in the classified DEM of the Painkanoor sub-watershed, as shown in Fig. 4.5. The hypsometric curve was plotted, as shown in Fig. 4.6, and the significant portion of land at higher elevations suggests a rugged terrain.

Table 4.2. Area Covered by Different Elevation Classes for the Painkanoor Sub-watershed

Sr. No.	Elevation (m)	Area (km^2)	Area (%)
1	0-15	0.99	2.88
2	15-30	4.93	14.36
3	30-50	10.11	29.43
4	50-70	6.19	18.00
5	70-90	3.26	9.49
6	90-110	3.54	10.30
7	110-130	4.21	12.24
8	130-151	1.14	3.31
Total		**34.36**	**100.00**
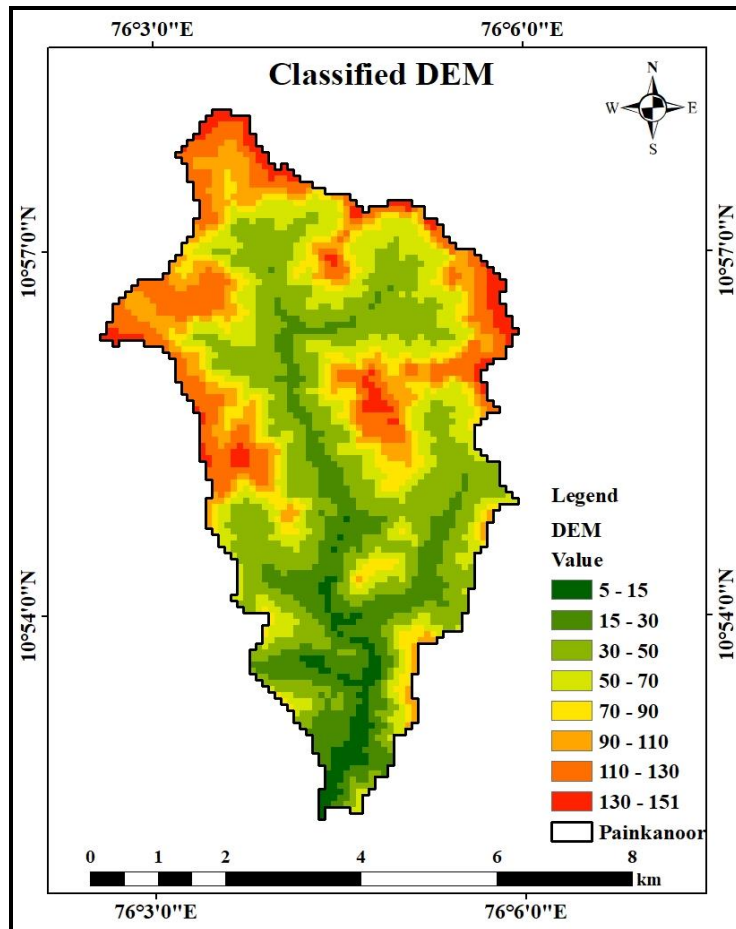
Fig. 4.5. Classified DEM of the Painkanoor Sub-watershed
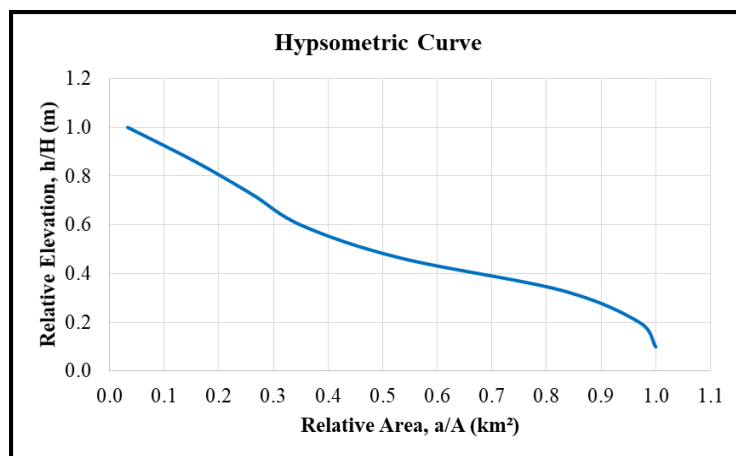
Fig. 4.6. Hypsometric Curve for the Painkanoor Sub-watershed

Elevation contours of the Perassannur sub-watershed, plotted at an interval of 20 m, is shown in Fig. 4.7 for the study area. It can be seen that the entire area has been divided into small hillocks and valleys.

The land slope of the Perassannur watershed varied from 0 to 35 per cent, as shown in Fig 4.8 and Table. 4.3. It is seen that 24.36% of the area lies within the slope group of 3-6%, followed by 22.34% of the area lying in the slope range of 6-9%, while the lowest percentage area of 2.37% was within the slope range of 25-35%.

Table 4.3. Slope Classification of the Perassannur Watershed

Sr. No.	Slope (%)	Area (km^2)	Area (%)
1.	0-3	9.93	12.47
2.	3-6	19.40	24.36
3.	6-9	17.79	22.34
4.	9-12	11.55	14.50
5.	12-15	7.82	9.82
6.	15-20	7.08	8.89
7.	20-25	4.19	5.26
8.	25-35	1.89	2.37
Total		**79.66**	**100.00**

The land slope of the Painkanoor sub-watershed varied from 0 to 35 percent, as shown in Fig 4.9 and Table. 4.4. It is seen that 23.99% of the area lies within the slope range of 3-6%, followed by 22.77% area in the slope group of 6-9%, while the lowest percentage area of 1.70% within the slope range of 25-35%.

Table 4.4. Slope Classification of the Painkanoor Sub-watershed

Sr. No.	Slope (%)	Area (km^2)	Area (%)
1.	0-3	3.05	8.87
2.	3-6	8.24	23.99
3.	6-9	7.83	22.77
4.	9-12	5.49	15.97
5.	12-15	3.66	10.66
6.	15-20	3.47	10.10
7.	20-25	2.04	5.95
8.	25-35	0.58	1.70
Total		**34.36**	**100.00**
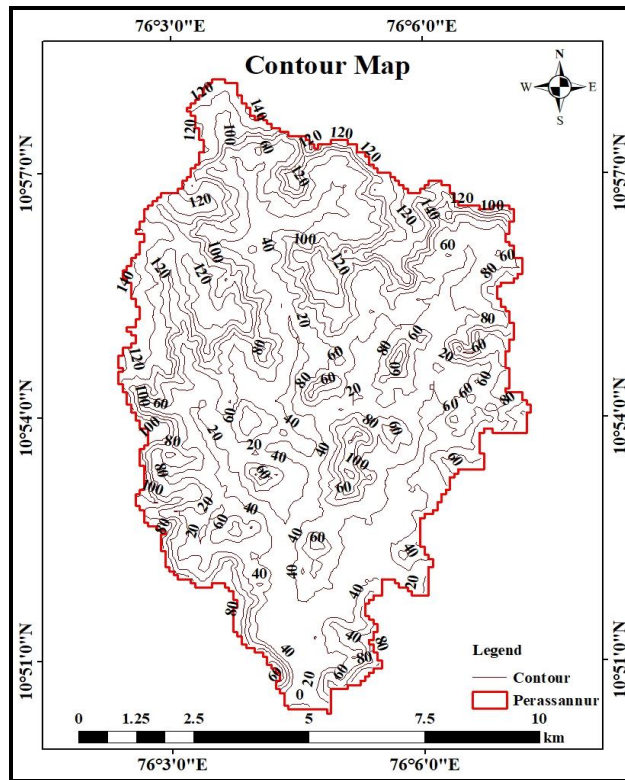
Fig. 4.7. Contour Map of the Perassannur Watershed
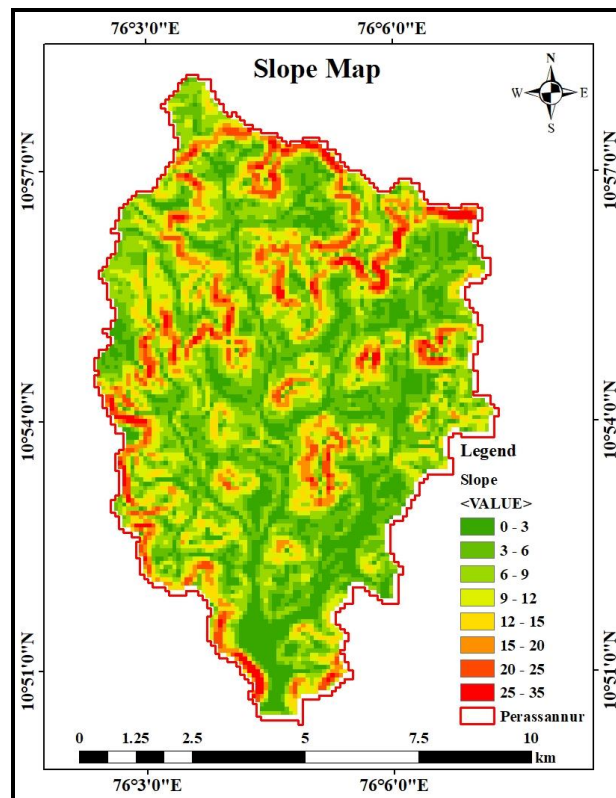
Fig. 4.8. Slope Map of the Perassannur Watershed
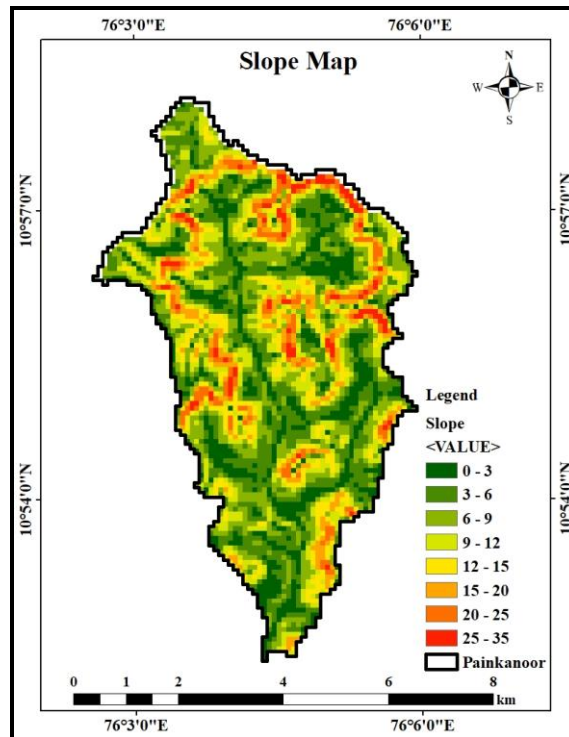
Fig. 4.9. Slope Map of the Painkanoor Sub-watershed

The geological map of the Perassannur watershed prepared in the ArcGIS platform is shown in Fig 4.10. The geological classification of the Perassannur watershed is shown in the Table. 4.5. It is observed that 55.33% of the Perassannur watershed has Neogene sedimentary rock, while 44.67% of the area has undivided Precambrian rock.

The Neogene sedimentary rocks are extremely weathered sandstones (i.e., wacke, arkose, litharenite, iron sandstone, and quartz arenite) enriched through sediment recycling (Nagarajan *et al*., 2014). The undivided Precambrian rocks include various rock assemblages such as khondalite, charnockite, gneiss and meta-sedimentary rocks (Nandakumaran and Balakrishnan, 2020).

Table 4.5. Geological Classification of the Perassannur Watershed

Sr. No.	Geology	Area (km^2)	Area (%)
1.	Neogene Sedimentary Rock	44.08	55.33
2.	Undivided Precambrian Rock	35.58	44.67
Total		**79.66**	**100.00**
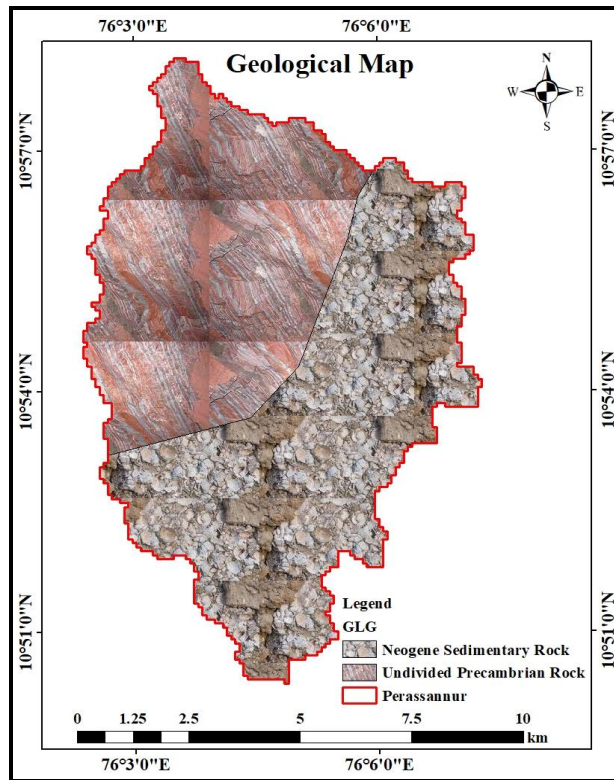
Fig. 4.10. Geological Map of the Perassannur Watershed
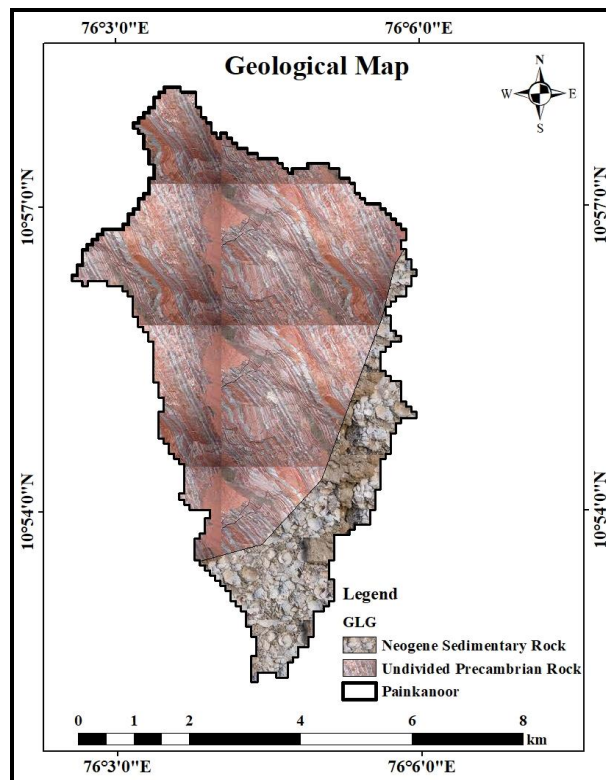
Fig. 4.11. Geological Map of the Painkanoor Sub-watershed

The geological classification of the Painkanoor sub-watershed is shown in Fig 4.11 and Table. 4.6. It is observed that 78.67% of the area of the Painkanoor sub-watershed has undivided Precambrian rock, while 21.33% of the area has Neogene sedimentary rock.

Table 4.6. Geological Classification of the Painkanoor Sub-watershed

Sr. No.	Geology	Area (km^2)	Area (%)
1.	Neogene Sedimentary Rock	7.33	21.33
2.	Undivided Precambrian Rock	27.03	78.67
Total		**34.36**	**100.00**

4.2 REVENUE DIVISIONAL DISTRIBUTION OF THE WATERSHED AREA

The areal distribution of the watershed in various Grama Panchayaths has also been determined, as this information is essential for the implementation of the interventions and to facilitate the people's participation. The distribution of the area of the Perassannur watershed in various Grama Panchayaths is given in Table 4.7 and that of Painkannur in Table 4.8. The total geographical area of the Perassanur watershed is distributed in 10 Grama Panchayaths and that of Painkannur sub-watershed in 8 Grama Panchayaths. This creates challenges in implementing the development interventions for natural resources management.

Perassannur watershed as shown in Fig. 4.12 has an area of 28.80 km^2 in Edayur (36.15%), 22.06 km^2 in Valanchery (27.69%), 12.38 km^2 in Irimbiliyam (15.54%), 10.61 km^2 in Marakkara (13.32%), 3.48 km^2 in Kuttippuram (4.36%), and some marginal areas in Kuruva, Athavanad, Ponmala, Moorkanad, and Kottakkal Gram Panchayats.

Table 4.7. Area of Perassannur Watershed Embedded in Various Gram Panchayats

Sr. No.	Gram Panchayats	Area (km^2)	% Area
1.	Athavanad	0.21	0.26
2.	Edayur	28.80	36.15
3.	Irimbiliyam	12.38	15.54
4.	Kottakkal	0.03	0.04
5.	Kuruva	1.91	2.40
6.	Kuttippuram	3.48	4.36
7.	Marakkara	10.61	13.32
8.	Moorkanad	0.06	0.07
9.	Ponmala	0.15	0.18
10.	Valanchery	22.06	27.69
Total		**79.66**	**100.00**

Similarly, the Painkanoor sub-watershed covers an area of 15.59 km^2 in Edayur (45.37%), 8.63 km^2 in Marakkara (25.12%), 8.05 km^2 in Valanchery (23.43%), and marginal areas in Kuruva, Irimbiliyam, Ponmala, Kottakkal, and Kuttippuram Gram Panchayats as shown in Fig. 4.13.

Table 4.8. Area of Painkanoor Sub-watershed Embedded in Various Gram Panchayats

Sr. No.	Gram Panchayat	Area (km^2)	% Area
1.	Edayur	15.59	45.37
2.	Irimpiliyam	0.90	2.62
3.	Kottakkal	0.05	0.15
4.	Kuruva	0.95	2.76
5.	Kuttippuram	0.04	0.12
6.	Marakkara	8.63	25.12
7.	Ponmala	0.15	0.44
8.	Valanchery	8.05	23.43
Total		**34.36**	**100.00**
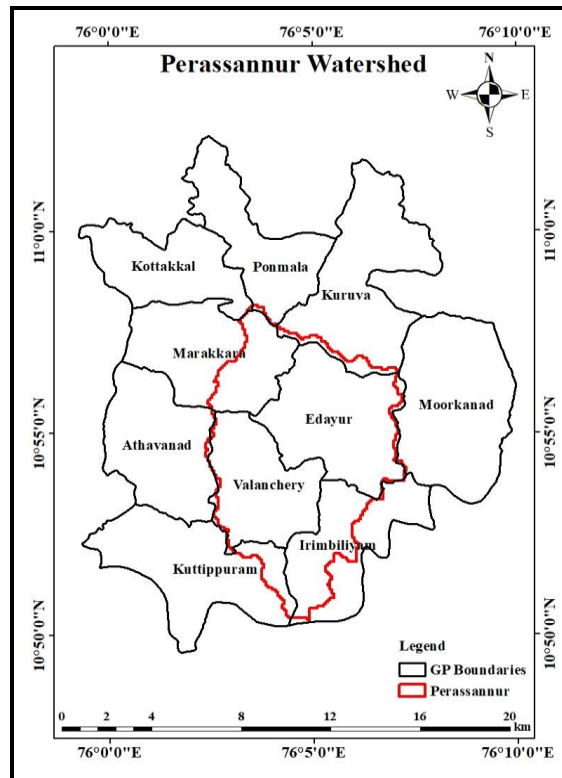
Fig. 4.12. Perassannur Watershed Embedded in Various Gram Panchayats
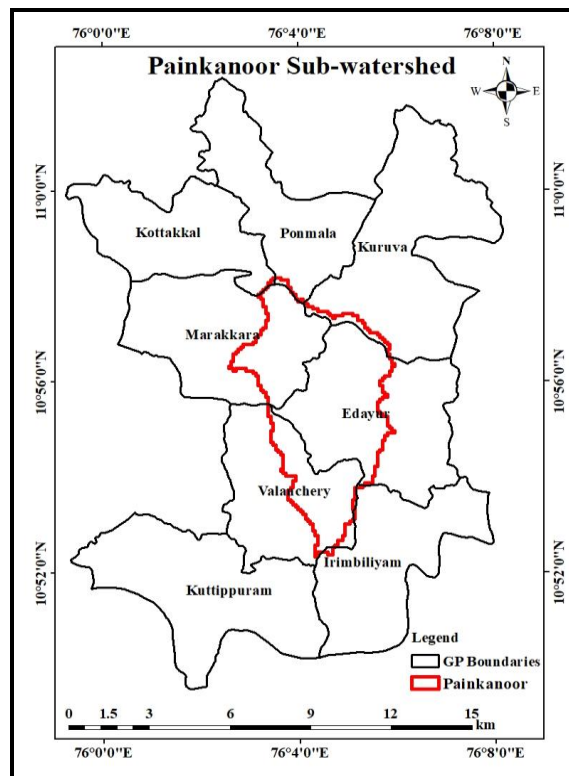
Fig. 4.13. Painkanoor Sub-watershed Embedded in Various Gram Panchayats

4.3 WATER BALANCE COMPONENTS OF THE STUDY WATERSHED

The study area's water balance components were assessed by setting up a range of instruments to measure rainfall, runoff, soil moisture storage, and groundwater storage. The following presents the outcomes of these measurements and the quantification of the study area's water balance components.

4.4 MEAN AREAL RAINFALL OF THE CATCHMENT

The rainfall was measured by four tipping bucket rain gauges in the study area at Edayur, Irimbiliyam, Marakkara, and Valanchery. The rain gauge at Valanchery was in operation from January 2021, while the rest were operated from August 2021 to December 2022. The mean annual rainfall of the watershed determined using the Thiessen Polygon method is shown in Fig 4.14. The polygon represented by Marakkara has a maximum area of 27.96 km^2, while Edayur has a minimum area of 14.26 km^2. The mean annual rainfall depths received by the stations Valanchery, Marakkara, Edayur, and Irimbiliyam were 2642.95 mm, 2578.45 mm, 2576.95 mm, and 2534.75 mm, respectively. This indicates that annual rainfall received by different rain gauge stations were at random.

The mean annual areal rainfall computed by the inverse distance method is presented in Fig. 4.15 to Fig. 4.17. The mean annual rainfall of the different watershed locations has been calculated for the years 2021 and 2022 separately. For the year 2021, it was observed that maximum rainfall was recorded at rain gauge station Marakkara and minimum at Valanchery, shown in Fig. 4.15. However, in 2022, maximum rainfall was recorded at rain gauge Valanchery and minimum at Marakkara and Irimbiliyam, as shown in Fig. 4.16. Also, the mean rainfall distribution map of the study area is shown in Fig. 4.17.
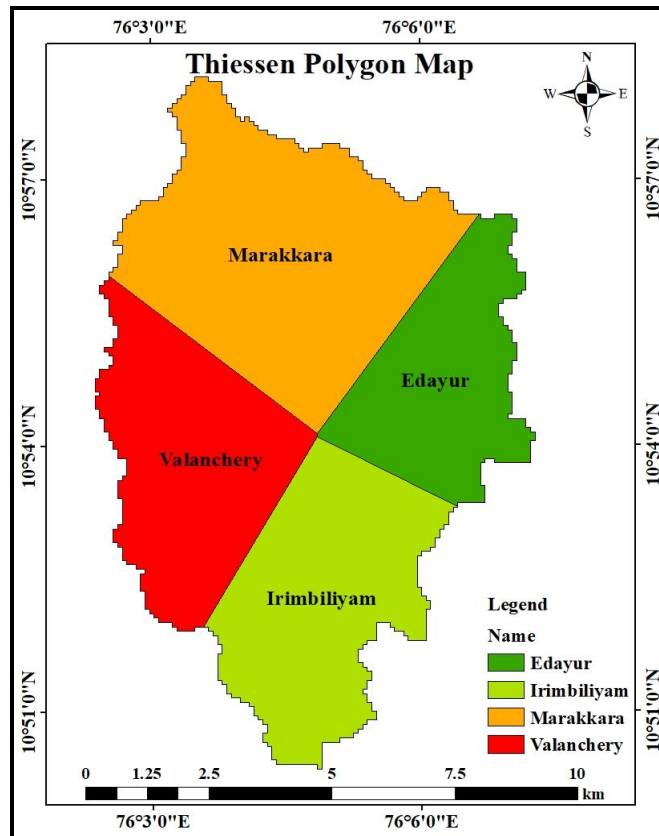
Fig. 4.14. Thiessen Polygon Map of the Perassannur Watershed
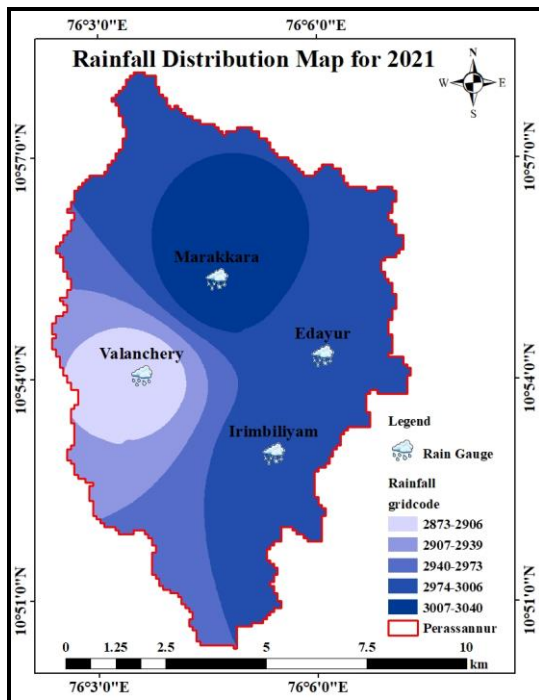
Fig. 4.15. Rainfall Distribution Map of the Study Area for the Year 2021
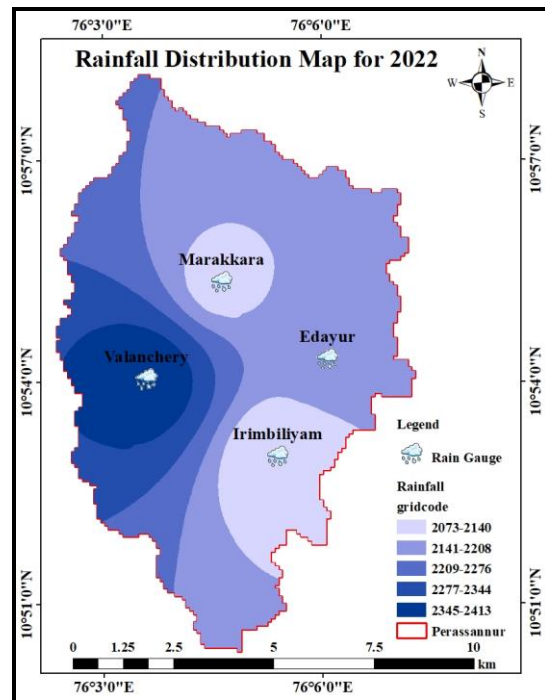
Fig. 4.16. Rainfall Distribution Map of the Study Area for the Year 2022
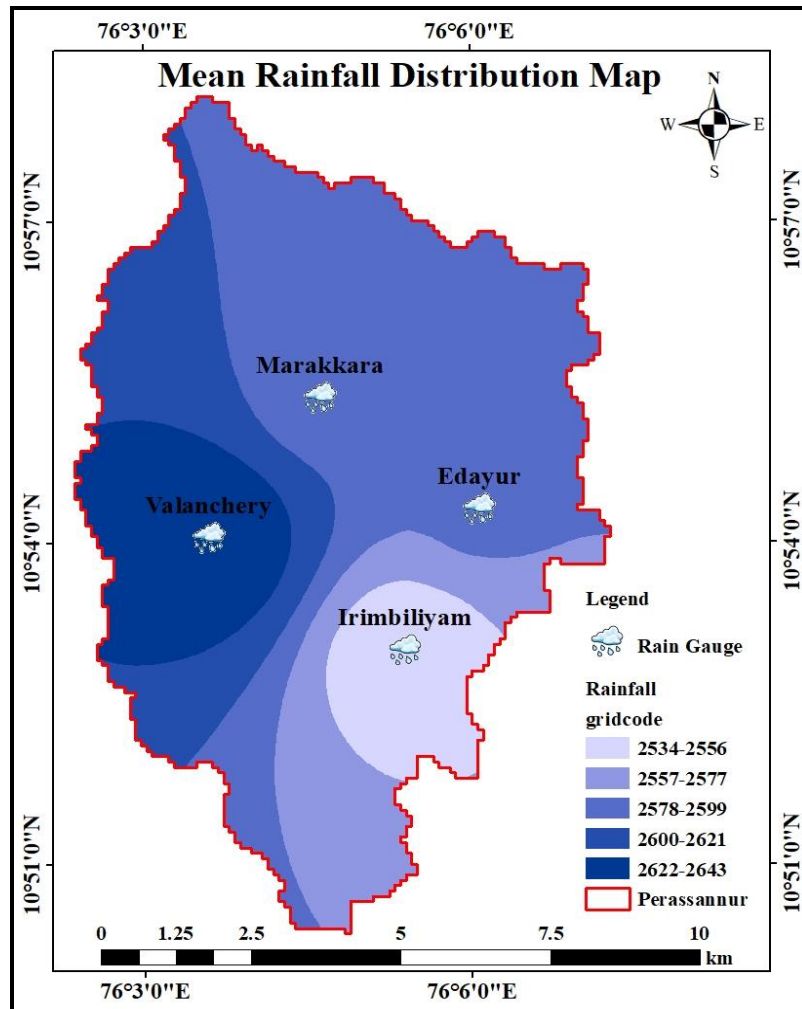
Fig. 4.17. Mean Rainfall Distribution Map of the Study Area

4.5 MONTHLY AND WEEKLY RAINFALL OF THE CATCHMENT

Fig. 4.18 shows the average monthly rainfall recorded by all four rain gauges in the study area from August 2021 to December 2022. It was observed that the highest rainfall of 529 mm was recorded in the month of October 2021, followed by 503 mm in the month of July 2022. At the same time, during January and February of 2022, there was no rainfall. Similarly, Fig. 4.19 shows the mean weekly rainfall recorded by all the rain gauges in the study area from the 33rd week of 2021 to the 52nd week of 2022. For 2021, the highest rainfall of 250 mm was recorded in the 41st week, followed by 168 mm in the 39th week. In 2022, the highest rainfall of 236 mm was recorded in the 27th week, followed by 209 mm in the 31st week, while for ten weeks, there was no rainfall at all.
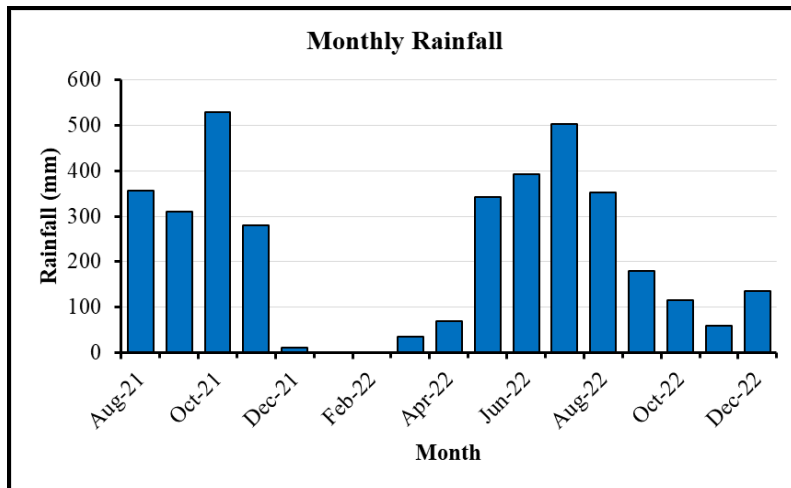
Fig. 4.18. Monthly Rainfall of the Perassannur Watershed
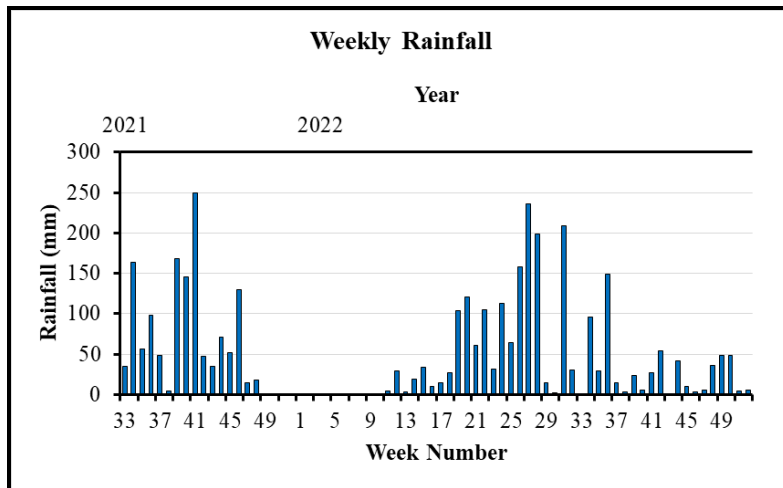
Fig. 4.19. Weekly Rainfall of the Perassannur Watershed
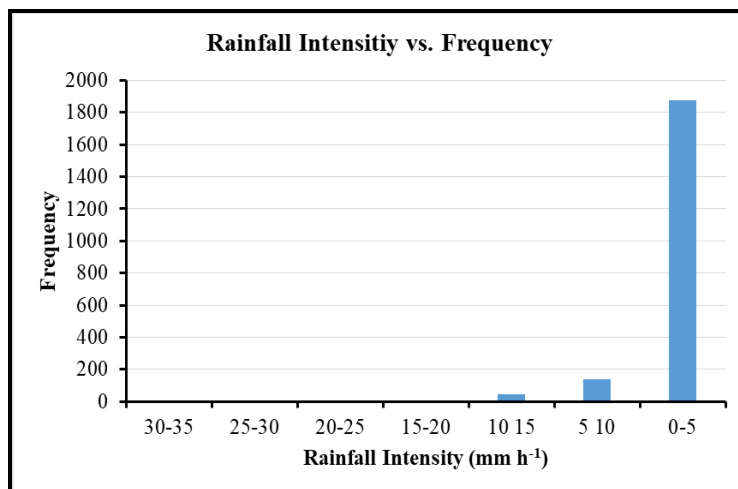
Fig. 4.20. Rainfall Intensity vs. Frequency of the Study Area

4.5.1 Frequency of the Rainfall Intensity in the Study Area

Rainfall has been recorded during every one-hour interval. The frequency of one hour rainfall received by the catchment is given in Table 4.9 and Fig. 4.20. It is observed that the highest rainfall intensities lying in the range of 30-35 mm h^{-1} was observed once during the study duration. Two rainfalls have occurred within the intensity class of 25-30 mm h^{-1}, 43 numbers of rainfall have been received within the moderate intensity class of 10-15 mm h^{-1}, and it is seen that the majority of the rainfall incidents have happened with an intensity ranging between 0-5 mm h^{-1}.

Table 4.9. Rainfall Intensity vs. Frequency of the Study Area

Sr. No.	Rainfall Intensity (mm h^{-1})	Frequency
1.	30-35	1
2.	25-30	2
3.	20-25	4
4.	15-20	7
5.	10-15	43
6.	5-10	136
7.	0-5	1878

4.5.2 Spatial Variability of the Rainfall

It is seen that there is variation between the rainfall received by various rain gauge stations, though the geographical separation between them was less. The monthly and weekly descriptive statistics of the spatial variation of rainfall are given in Tables 4.10 and 4.11, respectively. In certain months, the variation, as indicated by the coefficient of variation (CV), is very high. Similarly, the CV value is more than 1 for many weeks. Figs. 4.21 and 4.22 represent monthly and weekly spatial variability of the rainfall.

Table 4.10. Statistical Analysis for Monthly Rainfall Variability

Sr. No.	Month	Mean	Standard Deviation (SD)	CV
1.	January	17.61	49.82	2.83
2.	February	1.80	5.09	2.83
3.	March	24.63	21.85	0.89
4.	April	43.68	41.34	0.95
5.	May	230.05	196.22	0.85
6.	June	233.73	198.45	0.85
7.	July	311.78	255.77	0.82
8.	August	353.83	14.86	0.04
9.	September	244.85	68.81	0.28
10.	October	322.03	221.83	0.69
11.	November	166.38	116.02	0.70
12.	December	74.03	69.23	0.94
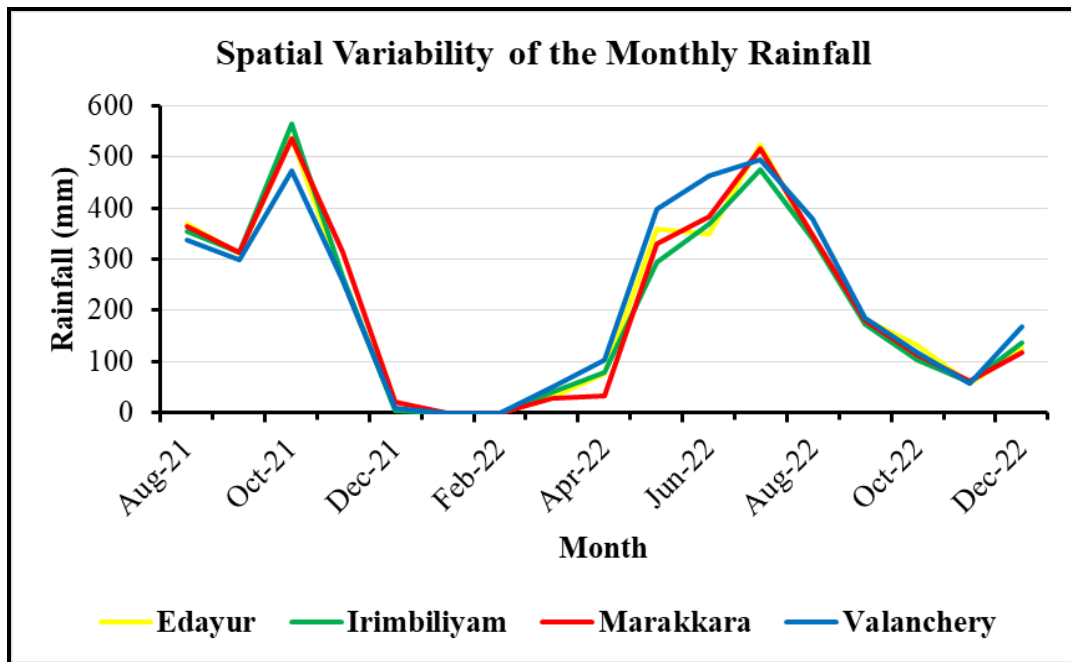
Fig. 4.21. Spatial Variability of the Monthly Rainfall

Table 4.11. Statistical Analysis for Weekly Rainfall Variability

Week No.	Mean	SD	CV	Week No.	Mean	SD	CV
1	0.08	0.21	2.83	27	125.28	119.65	0.96
2	16.85	47.66	2.83	28	128.10	107.35	0.84
3	0.00	0.00	0.00	29	21.05	36.10	1.72
4	0.00	0.00	0.00	30	9.35	13.42	1.44
5	0.00	0.00	0.00	31	142.50	70.93	0.50
6	1.00	2.83	2.83	32	46.18	18.34	0.40
7	0.80	2.26	2.83	33	17.55	18.94	1.08
8	0.00	0.00	0.00	34	129.60	37.18	0.29
9	0.00	0.00	0.00	35	42.60	15.05	0.35
10	5.10	14.42	2.83	36	123.55	27.43	0.22
11	2.45	6.05	2.47	37	31.38	18.54	0.59
12	15.68	15.47	0.99	38	3.73	1.26	0.34
13	1.40	3.64	2.60	39	96.03	78.37	0.82
14	9.38	11.74	1.25	40	75.50	75.89	1.01
15	19.23	23.14	1.20	41	138.50	119.35	0.86
16	9.68	12.62	1.30	42	50.85	10.62	0.21
17	7.44	8.22	1.10	43	17.38	18.70	1.08
18	18.53	18.10	0.98	44	56.33	18.30	0.32
19	81.90	83.26	1.02	45	30.90	23.95	0.77
20	70.09	60.13	0.86	46	66.25	68.39	1.03
21	42.40	38.54	0.91	47	10.05	6.26	0.62
22	62.88	54.65	0.87	48	26.85	11.70	0.44
23	20.93	19.66	0.94	49	24.28	28.48	1.17
24	77.95	67.86	0.87	50	24.35	26.13	1.07
25	33.43	33.98	1.02	51	2.05	2.20	1.07
26	83.73	80.58	0.96	52	2.65	2.85	1.08
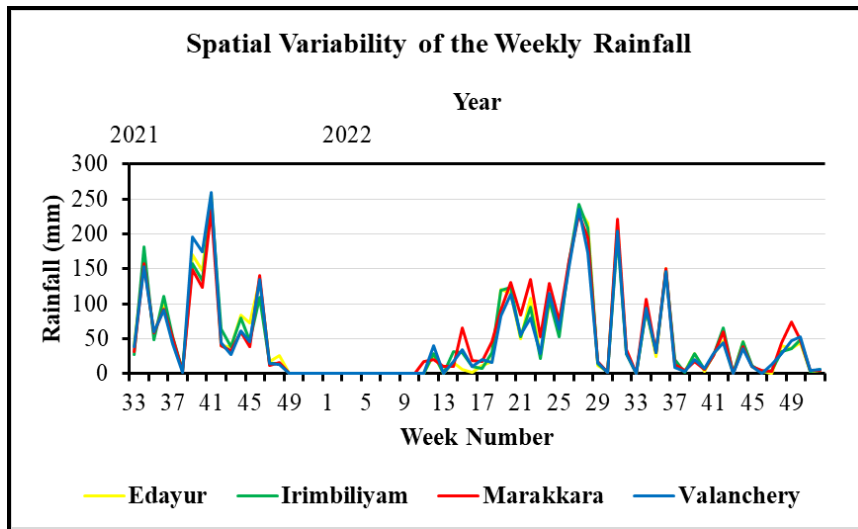
Fig. 4.22. Spatial Variability of the Weekly Rainfall

Table 4.12 shows the ANOVA table prepared to understand the statistical significance of rainfall variability, and it is observed that since the P-value is greater than or equal to 0.05, we do not have sufficient evidence to reject the null hypothesis. This suggests a lack of statistical support for a significant difference between the means of the four rain gauges.

Table 4.12. ANOVA Table for Monthly Rainfall Variability

ANOVA: Single Factor Summary					
Groups		**Count**	**Sum**	**Average**	**Variance**
Edayur		17	3660	215.2941	32352.6
Irimbiliyam		17	3576	210.3294	31103.1
Marakkara		17	3663	215.4706	33573.3
Valanchery		17	3792	223.0588	31362.0
ANOVA					
Source of Variation	**SS**	**df**	**MS**	**F**	**P-value**	**F crit**
Between Groups	1406.84	3	468.95	0.0146	0.9976	2.7482
Within Groups	2054257.10	64	32097.77			
Total	**2055663.94**	**67**				

Table 4.13 shows the ANOVA table for weekly rainfall variability, and it was observed that the P-value is not less than 0.05. This means there is no statistically significant difference between the mean rainfall values of the four rain gauges.

Table 4.13. ANOVA Table for Weekly Rainfall Variability

ANOVA: Single Factor Summary					
Groups		**Count**	**Sum**	**Average**	**Variance**
Marakkara		74	3788.2	51.19189	3806.868
Edayur		74	3659.2	49.44865	4092.657
Valanchery		74	3570.2	48.24595	3888.42
Irimbiliyam		74	3656.4	49.41081	3897.475
ANOVA					
Source of Variation	**SS**	**df**	**MS**	**F**	**P-value**	**F crit**
Between Groups	327.3497	3	109.1166	0.0278	0.9937	2.6355
Within Groups	1145036	292	3921.355			
Total	**1145363**	**295**				

4.6 TOTAL RUNOFF

4.6.1 Cross-sectional Area and Rating Curve

The cross-section of the Perassannur watershed and the Painkanoor sub-watershed were determined using total station equipment. The readings were plotted, and the cross-sectional area was determined using ArcGIS, as shown in Fig. 4.23 and Fig. 4.24, respectively. The cross sectional area was calculated for each 0.1 m width interval and then added to get the total cross-section up to the top of the bank height. Then, the cross-sectional area of the channel corresponding to every 0.2 m incremental height was also computed as it was necessary to get the cross-section corresponding to different stage heights, which was required to determine the total runoff. Table 4.14 shows the cross-sectional area of the drain with varying depths for the Perassannur watershed and Painkanoor sub-watershed for each 0.2 m. The maximum cross sectional areas were 33.39 m^2 and 18.33 m^2 for Perassannur and Painkanoor sections, respectively.
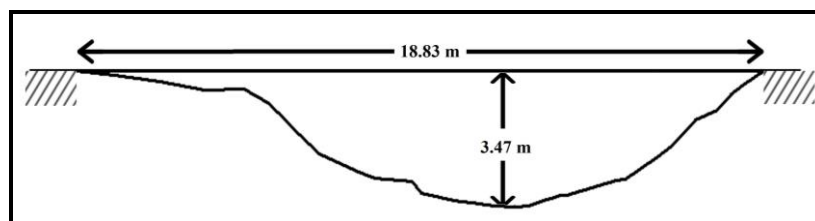
Fig. 4.23. Cross-section of the Main Stream at Perassannur
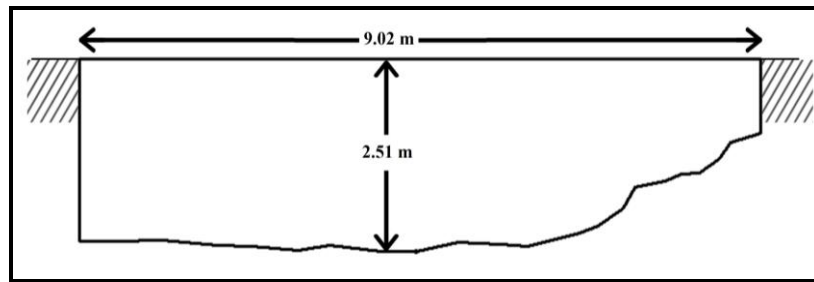
Fig. 4.24. Cross-section of the Main Stream at Painkanoor

Table 4.14. The Cross Sectional Area of the Drains with Varying Depths

Sr. No.	Depth (m)	Cross-Sectional Area (m²)	
		Perassannur Outlet	**Painkanoor Outlet**
1.	0.2	0.41	1.69
2.	0.4	1.10	3.05
3.	0.6	2.14	4.51
4.	0.8	3.47	6.06
5.	1.0	5.01	7.68
6.	1.2	6.73	9.37
7.	1.4	8.58	11.11
8.	1.6	10.53	12.88
9.	1.8	12.57	14.69
10.	2.0	14.69	16.51
11.	2.2	16.88	18.33
12.	2.4	19.18	-
13.	2.6	21.60	-
14.	2.8	24.18	-
15.	3.0	26.96	-
16.	3.2	30.01	-
17.	3.4	33.39	-

The flow velocity was measured by the current meter, and the water stage was determined from the automatic water level sensor. The discharge was calculated using the area-velocity method. Finally, the stage-discharge relationship (rating curve) was developed for the Perassannur watershed and Painkanoor sub-watershed, as shown in Fig. 4.25 and Fig. 4.26, respectively.
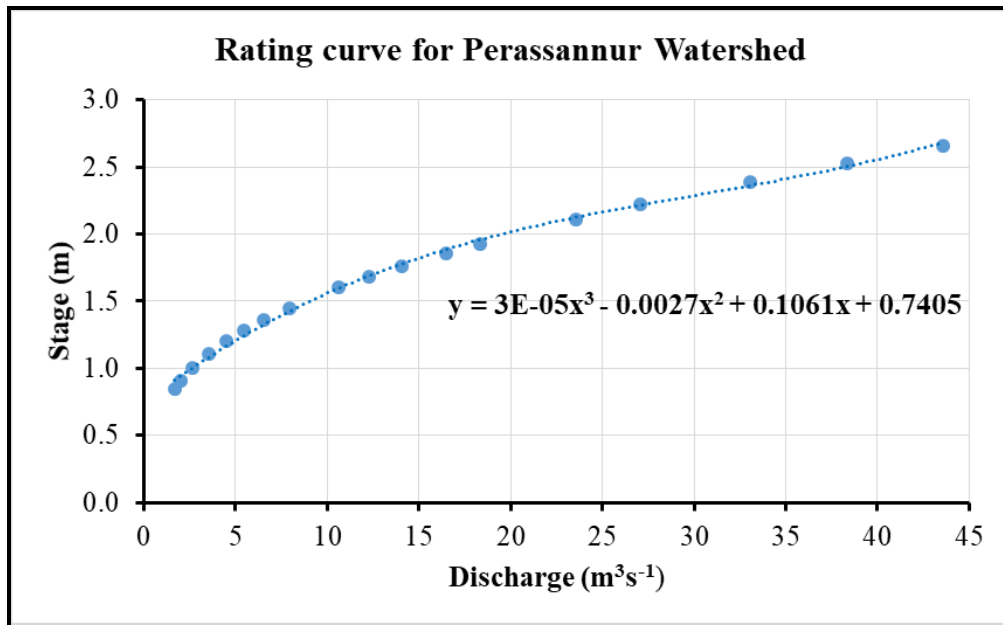
Fig. 4.25. Stage Discharge Relationship for Perassannur Outlet
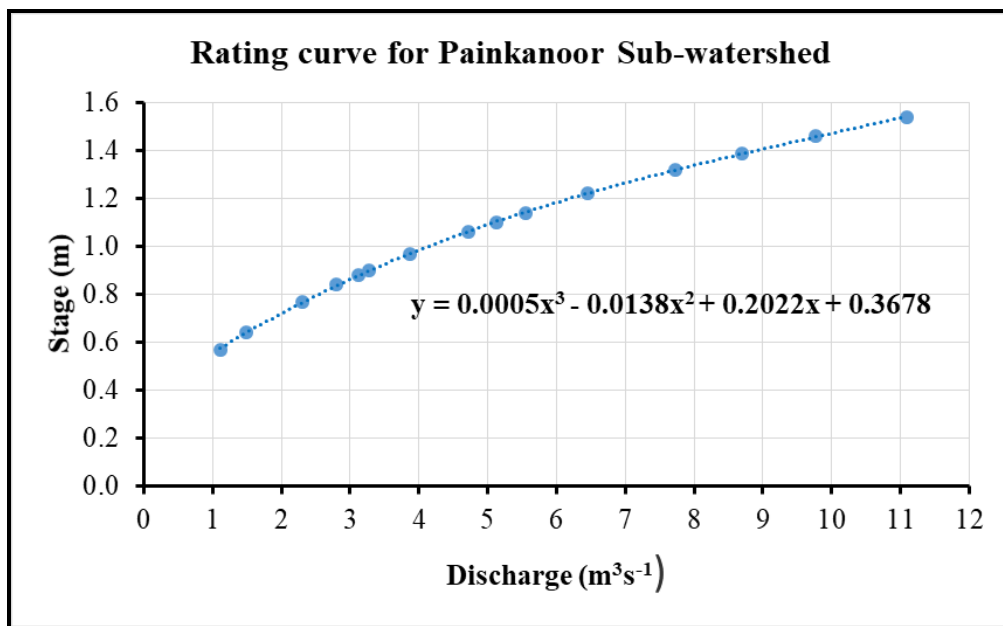
Fig. 4.26. Stage Discharge Relationship for Painkanoor Outlet

4.6.2 Monthly and Weekly Runoff of the Catchments

Fig. 4.27 shows the average monthly runoff recorded at the Perassannur outlet of the watershed from August 2021 to December 2022. A maximum runoff of 13.30 m^3s^{-1} was observed during October 2021, followed by 12.64 m^3s^{-1} in July 2022. There was no runoff during March and April 2022.
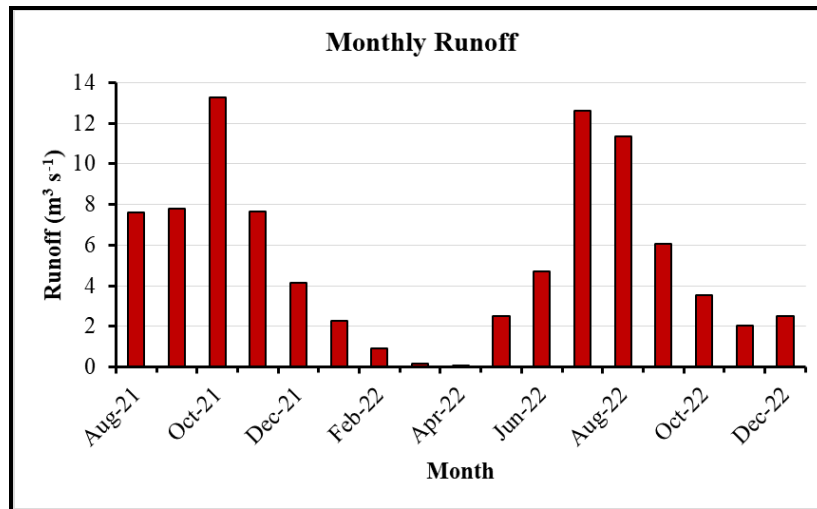
Monthly Runoff

Fig. 4.27. Mean Monthly Runoff at Perassannur Outlet

Fig. 4.28 shows the monthly runoff generated from the Painkanoor sub-watershed from August 2021 to December 2022. Maximum mean runoff of 9.95 m^3s^{-1} was observed during October 2021, followed by 7.88 m^3s^{-1} in July 2022. There was no runoff in the months of March and April 2022.
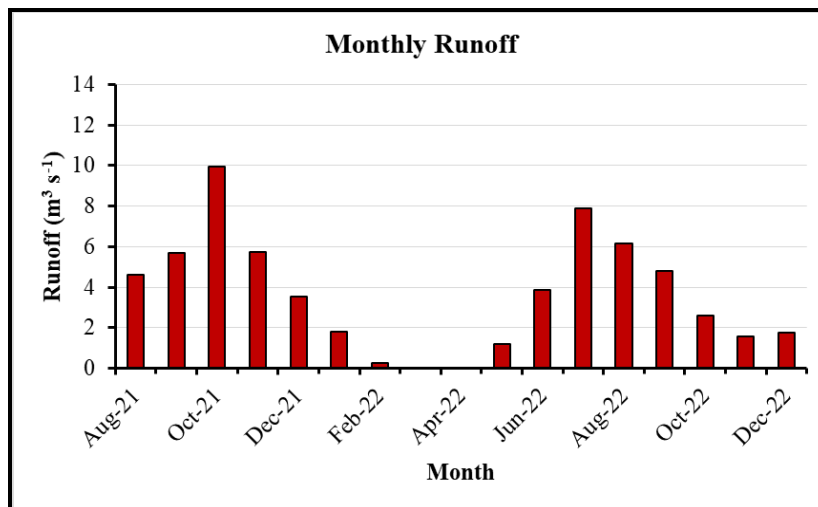
Monthly Runoff

Fig. 4.28. Mean Monthly Runoff at Painkanoor Outlet

Fig. 4.29 shows the mean weekly runoff recorded at the Perassannur outlet from the 33rd week of 2021 to the 52nd week of 2022. It was observed that for the year 2021, the mean weekly runoff was 18.42 m^3s^{-1} in the 41st week, followed by 15.33 m^3s^{-1} in the 42nd week. For 2022, the highest runoff of 18.52 m^3s^{-1} was observed in the 28th week, followed by 15.88 m^3s^{-1} in the 29th week.
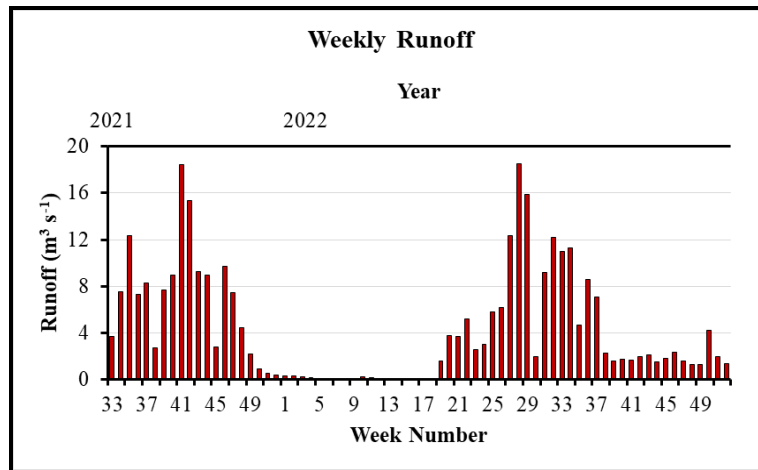
Fig. 4.29. Mean Weekly Runoff at Perassannur Outlet

Fig. 4.30 shows the mean weekly runoff recorded for the Painkanoor sub-watershed from the 33rd week of 2021 to the 52nd week of 2022. It was observed that for the year 2021, the mean weekly runoff of 7.88 m^{3}s^{-1} was observed in the 41st week, followed by 3.77 m^{3}s^{-1} in the 42nd week. For the year 2022, the highest runoff of 4.59 m^{3}s^{-1} was observed in the 28th week, followed by 3.55 m^{3}s^{-1} in the 29th week, whereas for 11 weeks, there was no runoff from the 7th week to the 18th week.
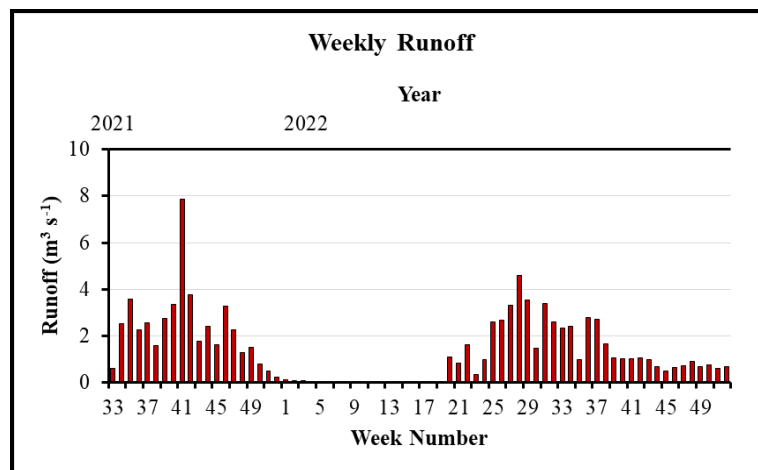
Fig. 4.30. Mean Weekly Runoff at Painkanoor Outlet

The observed runoff was converted into the depth of water in millimetres, considering the total area of the watershed. Fig. 4.31 and Fig. 4.32 show the monthly and weekly runoff as depth in mm for the Perassannur watershed and the Painkanoor sub-watershed, respectively.
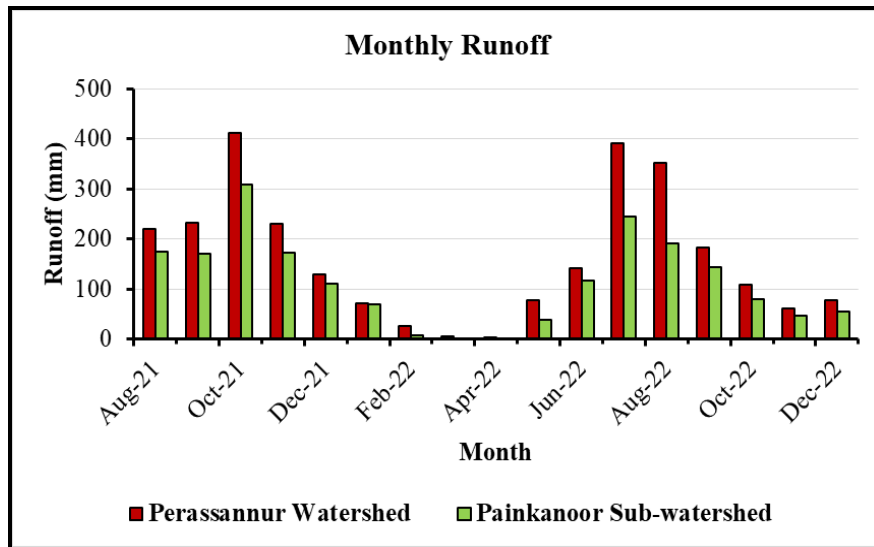
Fig. 4.31. Monthly Runoff in Depth at Perassannur and Painkanoor Outlets
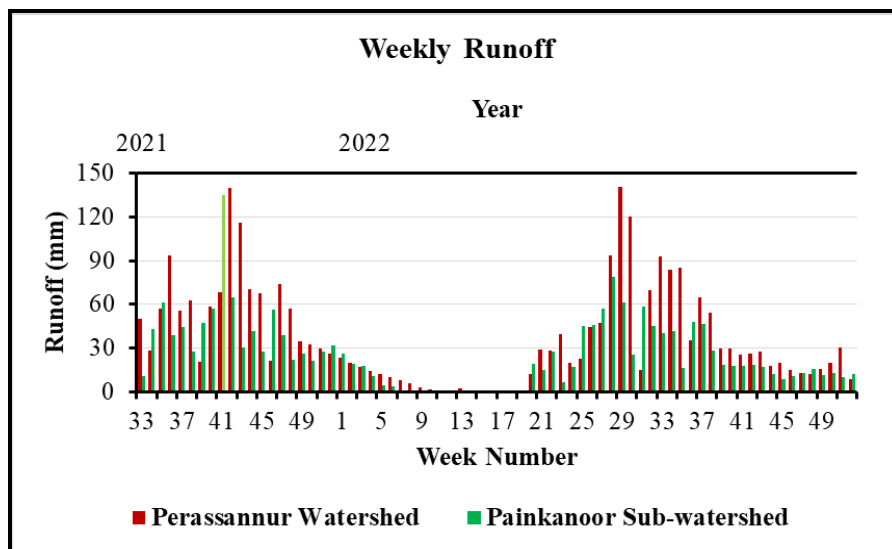
Fig. 4.32. Weekly Runoff in Depth at Perassannur and Painkanoor Outlets

4.7 SOIL MOISTURE CONTENT OF THE WATERSHED

ZL6 and CR300 data loggers recorded the soil moisture in the Perassannur watershed as volumetric soil moisture content, and the readings were recorded for one hour. These one-hour readings were averaged to obtain the mean soil moisture content daily. The average monthly soil moisture contents recorded by the ZL6 data logger at different depths of 0.25, 0.75 and 1.25 m are shown in Fig. 4.33. It was observed that for the soil moisture sensor at 0.25 m, the highest soil moisture of 30.57% was observed in October 2021. In 2022, the highest value was observed in

July and the lowest in February. For the sensor at a depth of 0.75 m, the highest soil moisture value of 33.07% was observed in November 2021, followed by 32.93% in October 2021. In the case of the sensor placed at a depth of 1.25 m, the highest soil moisture was observed in October 2021, and the lowest was 21.11% in February 2022. From Fig. 4.33, it is observed that during all seasons, the lowest soil moisture level was recorded by the soil moisture sensor placed at a depth of 0.25 m, while it was nearly the same for the soil moisture sensor at a depth of 0.75 m and 1.25 m. Further, the temporal variation of soil moisture was maximum at 0.25 m depth.
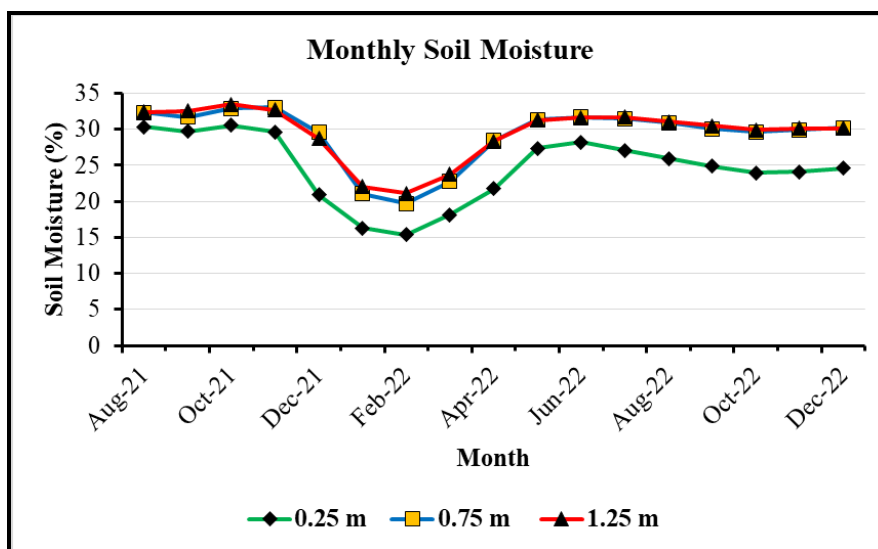
Fig. 4.33. Mean Monthly Soil Moisture by ZL6 Data Logger at Different Depths
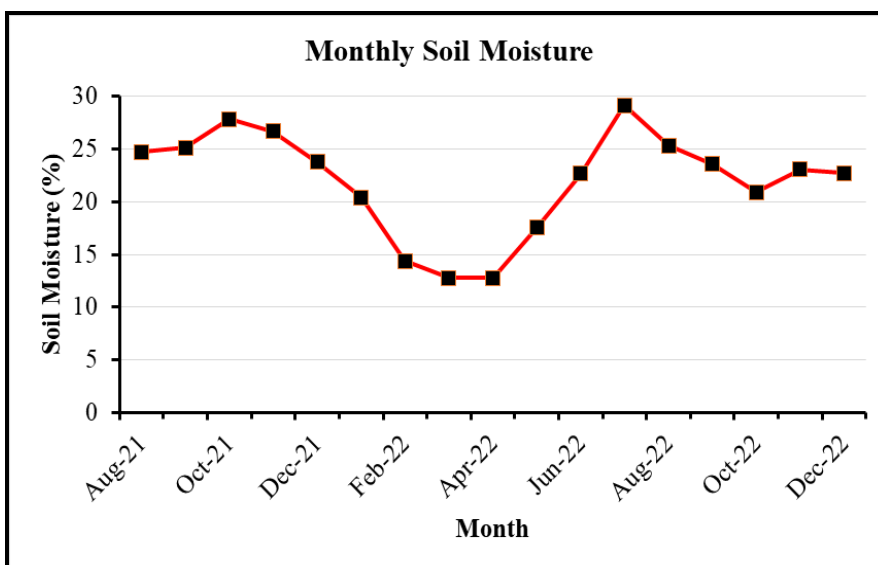
Fig. 4.34. Mean Monthly Soil Moisture by CR300 Data Logger

The soil moisture was recorded at another location using the CS650 soil moisture sensor at a depth of 0.75 m below the soil surface, which was connected to the CR300 data logger. Fig. 4.34 shows the average monthly soil moisture content recorded by the CR300 data logger. The highest soil moisture of 29.11% was observed in July 2022, followed by 27.85% in October 2021 and the lowest value of 12.78% in April 2022. The pattern of soil moisture fluctuation measured by the ZL6 sensor and that by the CS650 sensor is similar. However, the fluctuation is more vivid in the case of the latter.

The soil moisture recorded by the ZL6 data logger for the soil moisture sensor installed at a depth of 0.25 m represented the soil column of 0.50 m, and hence, the soil moisture was converted in terms of depth of water in mm. Similarly, the soil water was obtained for the soil column of 0.5 m height between depths of 0.5 m to 1 m, and soil column depth between 1 m and 1.5 m were added to get the soil water stored in the soil column of 1.50 m. Also, the soil moisture recorded by the CR300 data logger was converted in depth for the soil column of 1.50 m depth from ground surface. The mean soil moisture within the Perassannur watershed was obtained by taking the average of both these values.

Fig. 4.35 shows the mean monthly water content as the water depth per unit depth of soil. It was observed that the highest soil moisture storage in the root zone was 451.3 mm in October 2021, followed by 444.0 mm in July 2022, while it was lowest at 248.2 mm in February 2022. This goes by the expectation that the soil moisture storage is more for the months having higher rainfall and vice versa.

The soil moisture storage obtained daily was also averaged to get the average weekly soil moisture storage in the soil column of 1.50 m depth from ground surface. Fig. 4.36 shows the mean weekly water content as the water depth per unit depth of soil. It was observed that for the year 2021, the highest soil moisture storage was 474.29 mm in the 41st week, followed by 470.60 mm in the 33rd week, while it was lowest with a value of 337.78 mm in the 52nd week. For 2022, the highest soil moisture storage was 491.75 mm in the 27th week, followed by 486.33

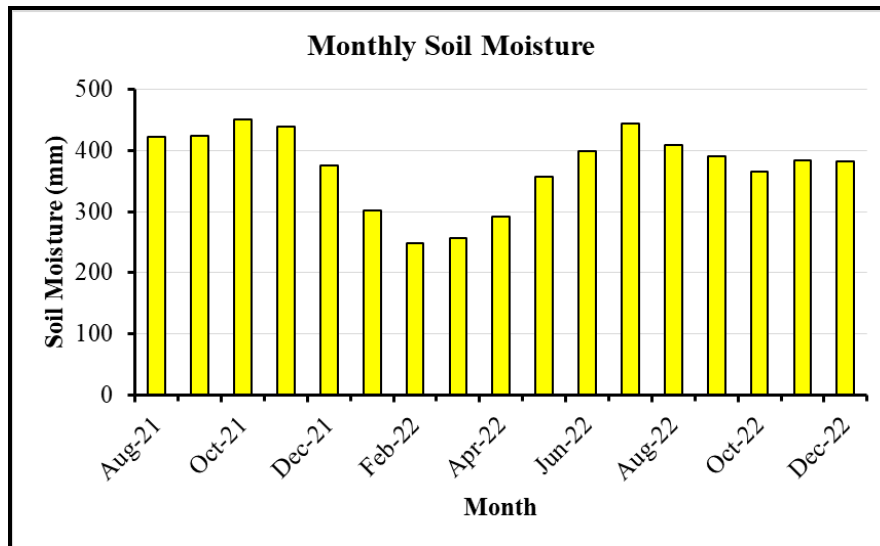mm in the 28th week, while the lowest soil moisture storage was observed as 235.05 mm in the 10th week.

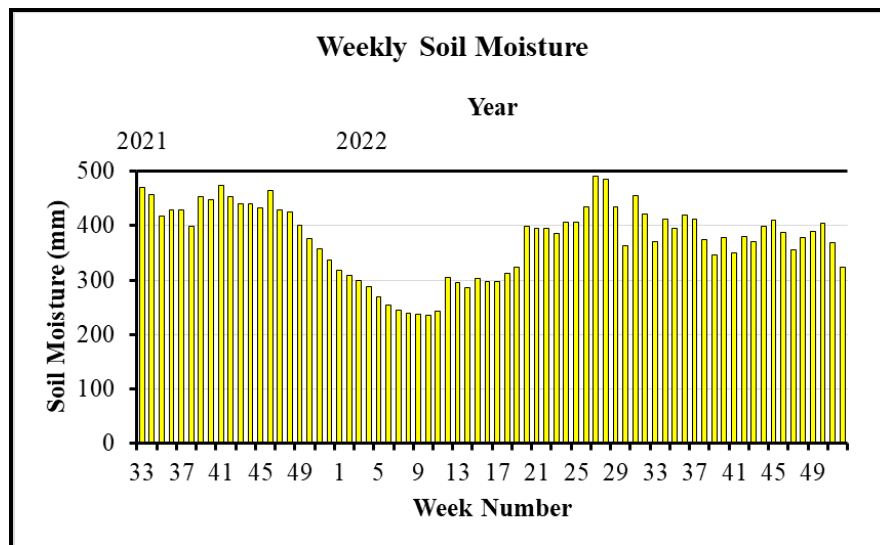**Fig. 4.35. Mean Monthly Soil Moisture as Depth per Unit Depth of Soil**

Fig. 4.36. Mean Weekly Soil Moisture as Depth per Unit Depth of Soil

4.8 GROUNDWATER STORAGE

Shallow groundwater storage was measured by monitoring the water table using an automatic water level sensor installed in the open well within the study area. Measurements were recorded at 4 hours, and the daily mean was taken to obtain the daily water table. The monthly water table was obtained by taking the average of the daily data and was converted to the height of the water table above

MSL. Fig. 4.37 shows the monthly height of the groundwater table above MSL. It was observed that the lowest height of the water table above MSL of 43.48 m was obtained in the month of April 2022, followed by 44.88 m in the month of March 2022. The maximum height of the water table above MSL of 45.95 m was observed in July 2022 and 45.63 m in October 2021. This data shows that the height of the water table above MSL is higher in the months having higher rainfall and vice versa.

Monthly Height of Groundwater Table from MSL
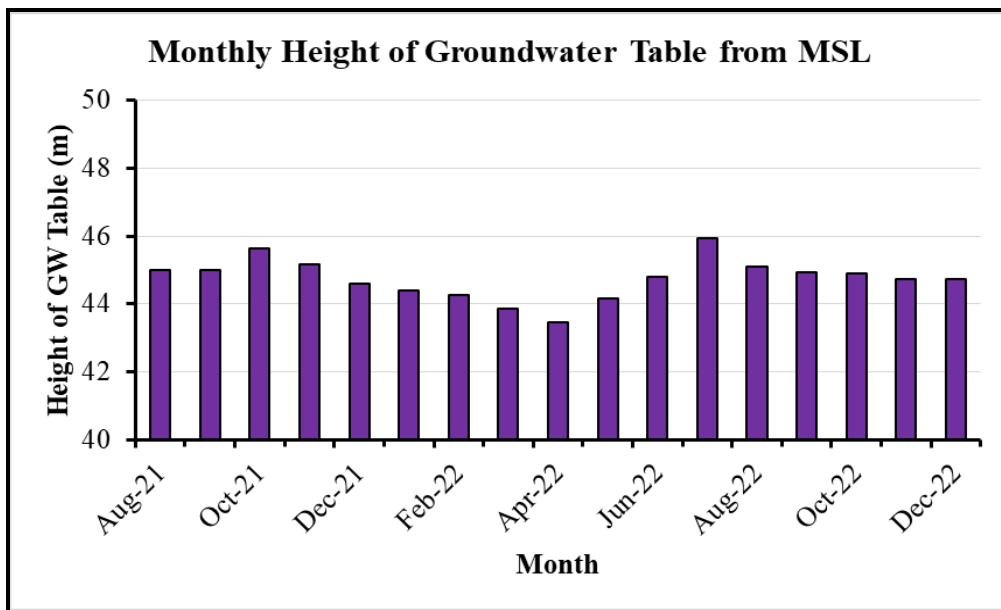
Fig. 4.37. Mean Monthly Height of Water Table from MSL

Weekly Height of Groundwater Table from MSL
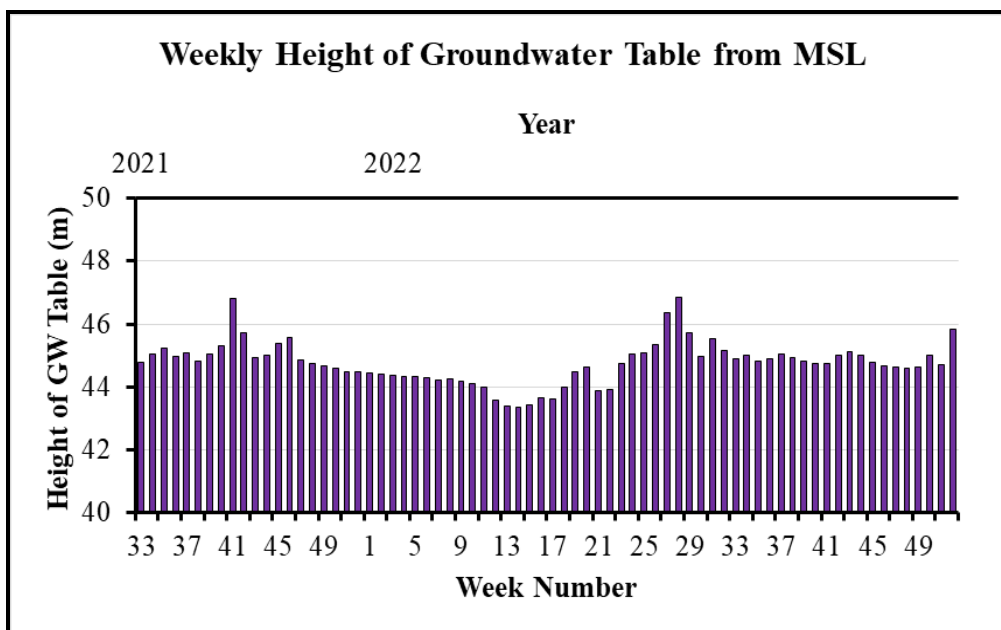
Fig. 4.38. Mean Weekly Height of the Water Table from MSL

The mean height of the water table was also obtained every week by taking an average of the daily data and was converted to the height of the water table above MSL. Fig. 4.38 shows the weekly height of the groundwater table above MSL. It was observed that for the year 2021, the lowest height of the water table above MSL was 44.46 m in the 51st week, followed by 44.49 m in the 52nd week, while it was highest at 46.81 m in the 41st week, followed by 45.72 m in the 42nd week. For the year 2022, the lowest height of the water table above MSL was 43.36 m in the 14th week, followed by 43.39 m in the 13th week, while it was at its maximum with a height of 46.84 m in the 28th week, followed by 46.34 m in the 27th week.

4.9 EVAPOTRANSPIRATION BY PENMAN MONTEITH METHOD

Monthly ET values of the watershed have been estimated by the FAO Penman-Monteith method by applying appropriate K_c values on ET_0, and the results are presented in Fig 4.39. It was observed that the highest ET was observed in the month of March 2022 at 127.17 mm, followed by 113.74 mm in April 2022. The lowest ET of 54.68 mm was observed in the month of August 2022, followed by 58.51 mm in the month of November 2021. In the monsoon months, the monthly ET is only a small percentage of the monthly rainfall. In the summer, the entire ET is met from the soil moisture storage.

ET for the study area was also estimated weekly by taking the cumulative value of the daily ET. Fig. 4.40 shows the weekly ET using the Penman-Monteith method. It was observed that for the year 2021, the highest ET was 20.26 mm in the 38th week, followed by 20.25 mm in the 52nd week, while it was lowest at 12.08 mm in the 45th week. For the year 2022, the highest ET was 32.55 mm in the 10th week, followed by 30.99 mm in the 9th week, while it was lowest at 8.10 mm in the 31st week, followed by 10.48 mm in the 27th week.
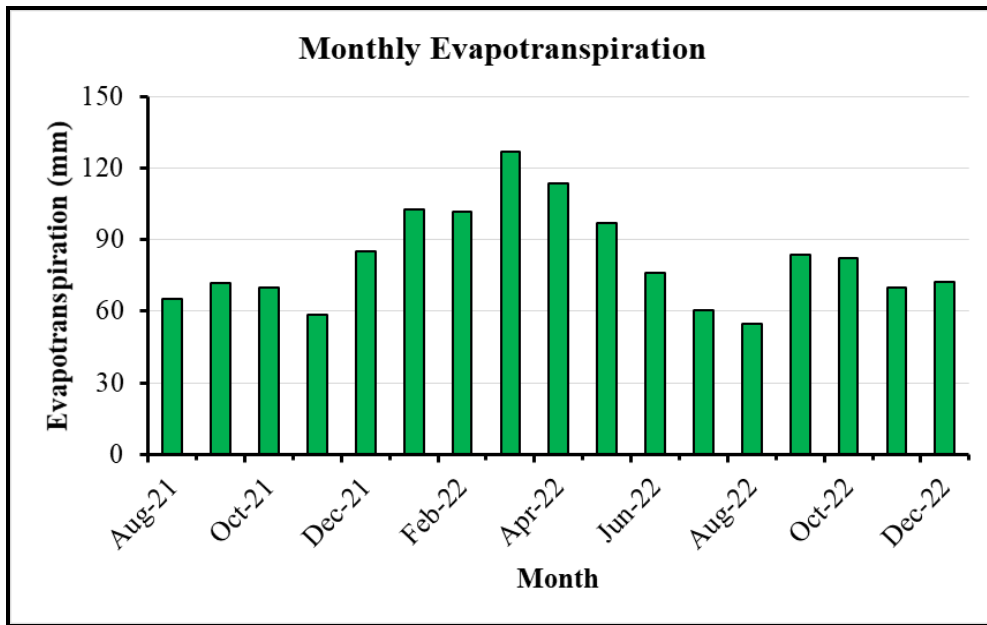
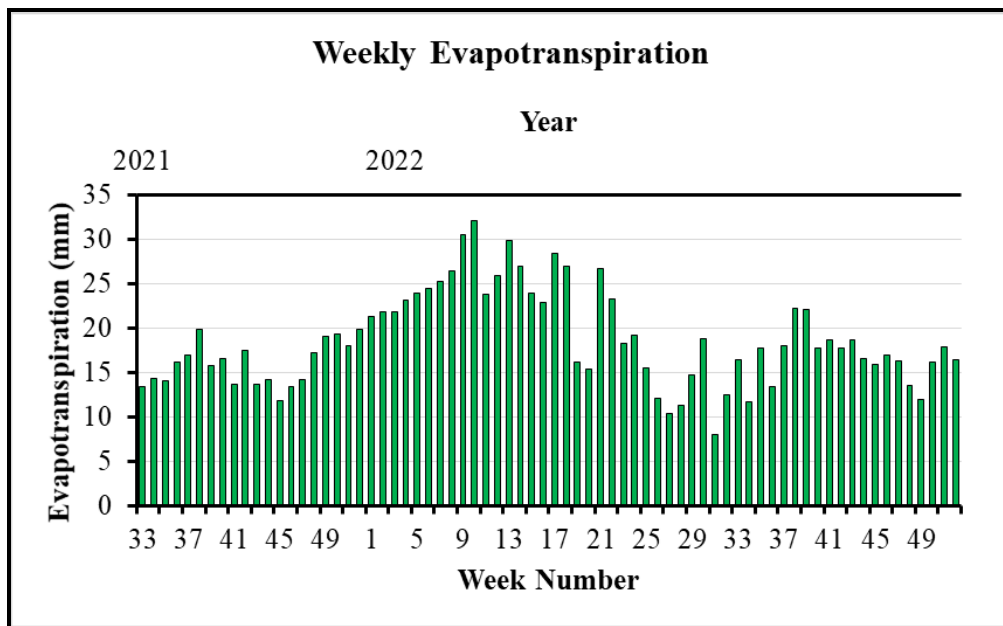**Fig. 4.39. Monthly Evapotranspiration using Penman-Monteith Method**

Fig. 4.40. Weekly Evapotranspiration using Penman-Monteith Method

4.10 WATER BALANCE COMPONENTS

The water balance components thus determined were plotted on a monthly and weekly time scale for both the Perassannur watershed and Painkanoor sub-watershed, as shown in Figs. 4.41 to 4.44. The rainfall, runoff and ET, along with the change in soil moisture storage and groundwater storage, were plotted.
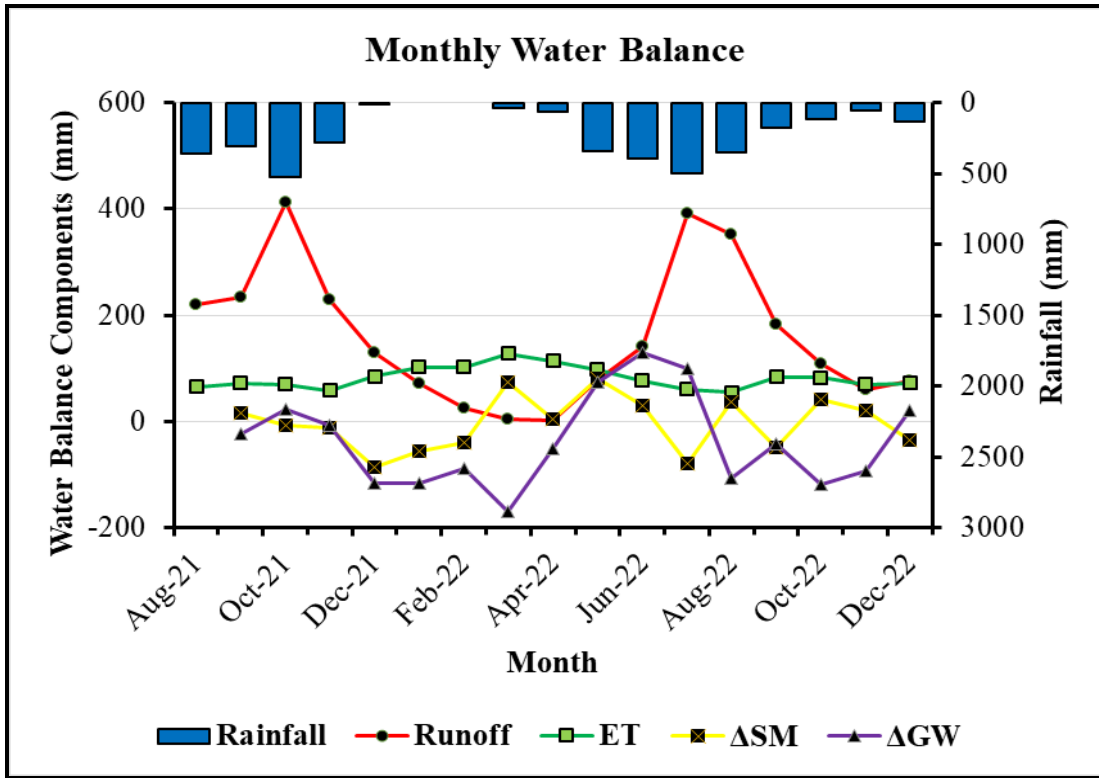
Fig. 4.41. Monthly Water Balance of the Perassannur Watershed
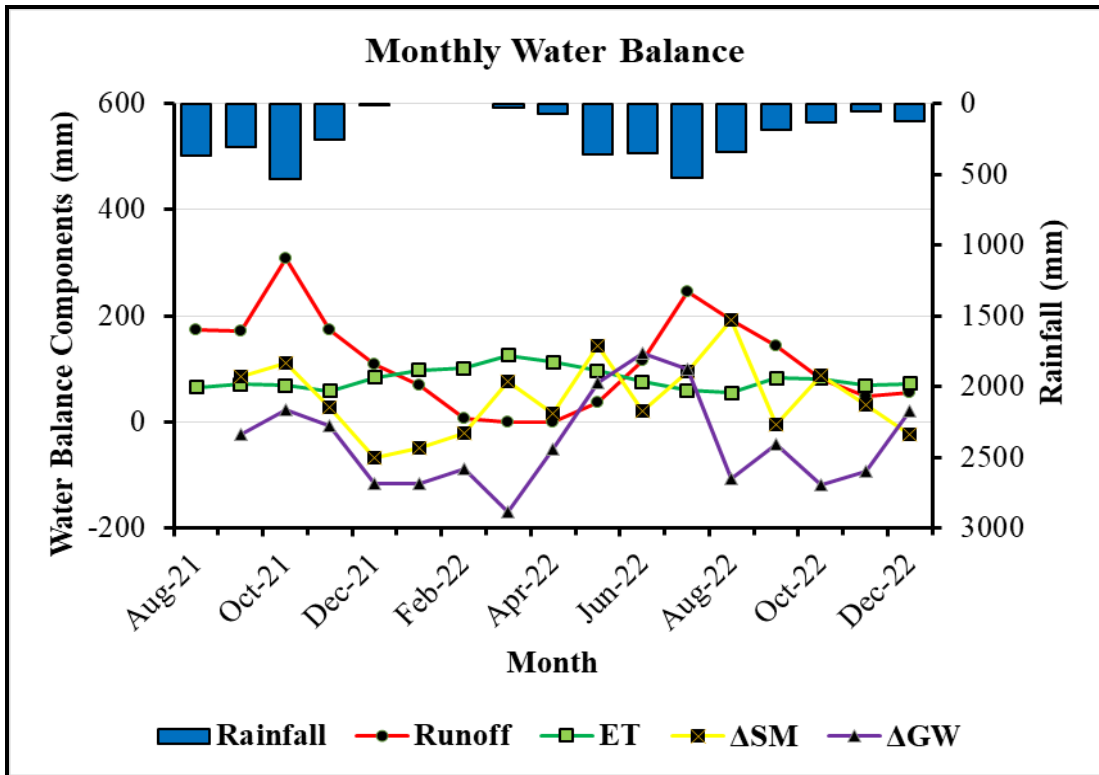
Fig. 4.42. Monthly Water Balance of the Painkanoor Sub-watershed
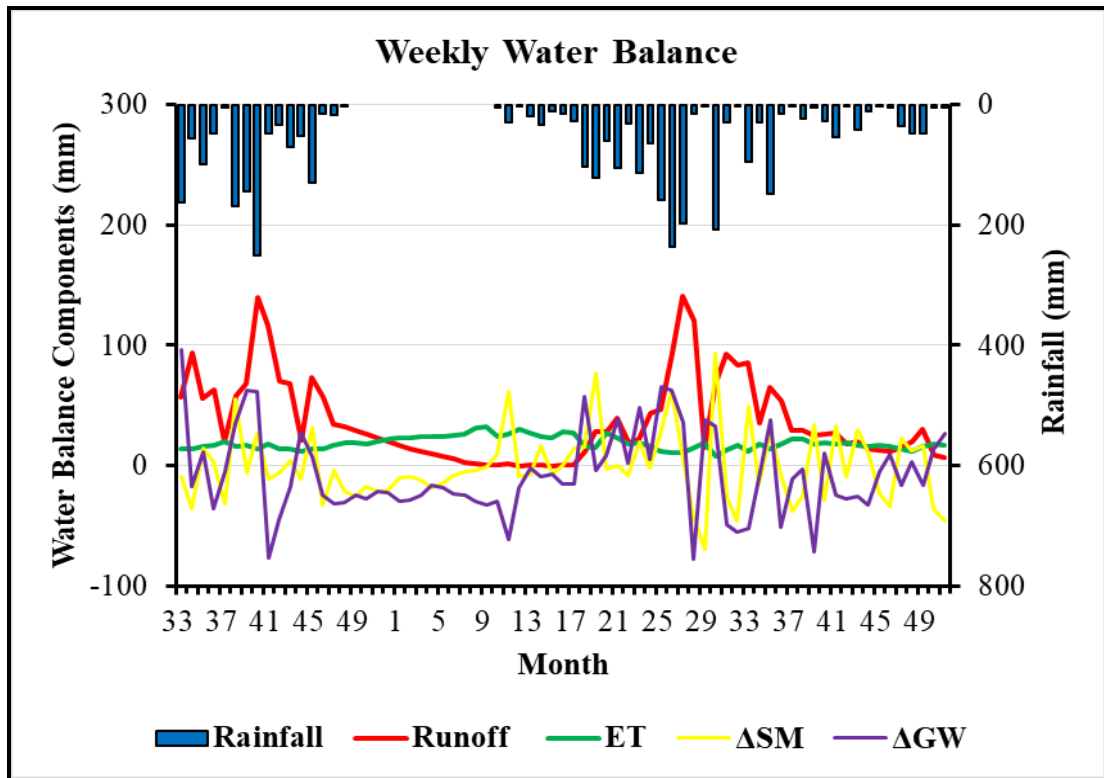
Fig. 4.43. Weekly Water Balance of the Perassannur Watershed
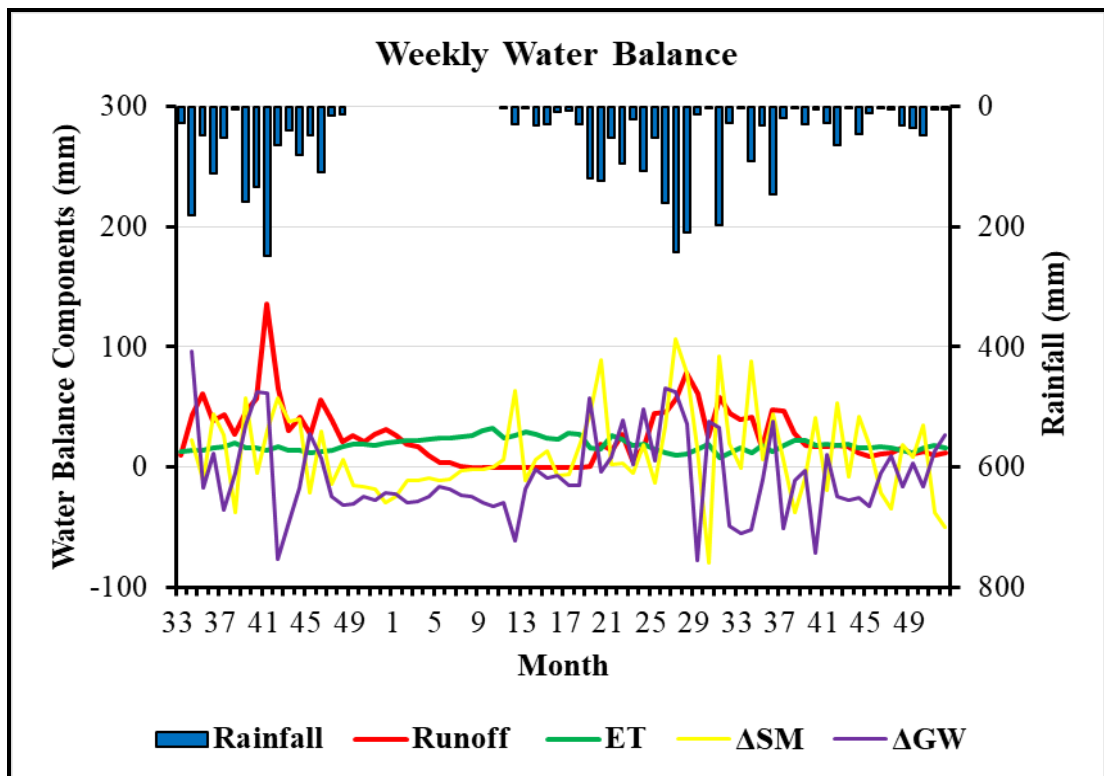
Fig. 4.44. Weekly Water Balance of the Painkanoor Sub-watershed

4.11 EVAPOTRANSPIRATION FROM WATER BALANCE EQUATION

ET has also been estimated by solving the Water Balance (WB) equation. The value of monthly ET for both watersheds as determined by the water balance equation is presented in Figs. 4.45 and 4.46, along with estimated ET from the Penman Monteith (PM) method. It is seen that there is a close comparison between the ET determined by the WB and PM methods.
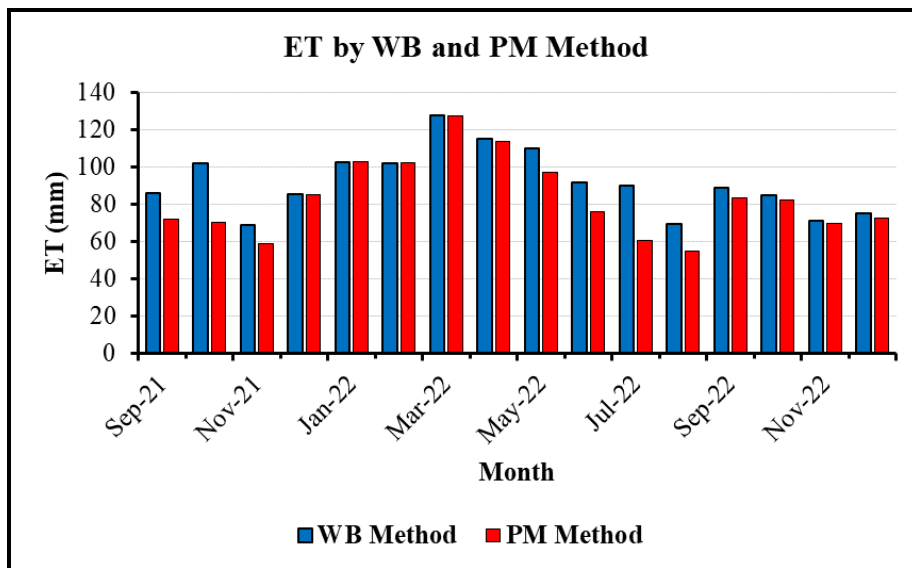
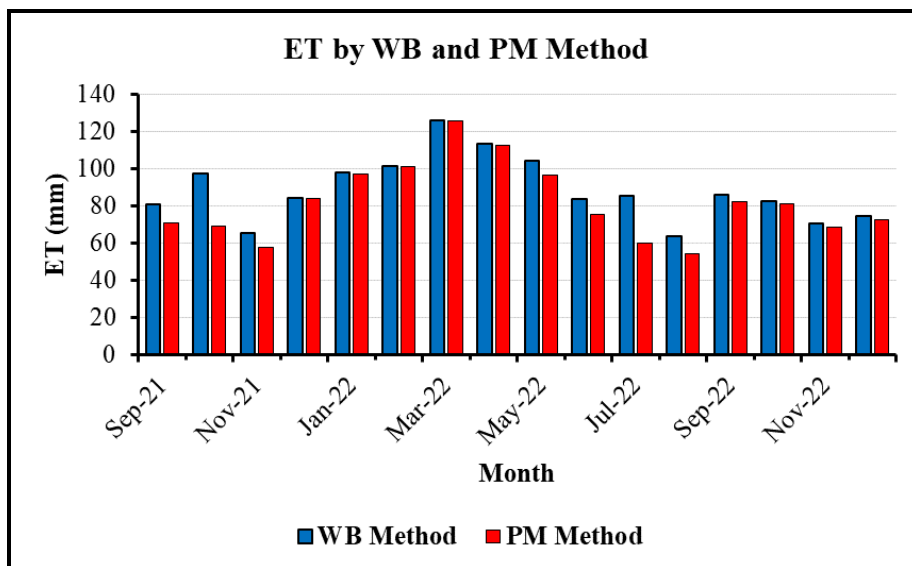**Fig. 4.45. Monthly ET by Water Balance and PM Method for the Perassannur Watershed**

Fig. 4.46. Monthly ET by Water Balance and PM Method for the Painkanoor Sub-watershed

Weekly ET has also been computed using WB method and PM method, and the same is presented in shown in Figs. 4.47 and 4.48 for Perassannur watershed and Painkanoor sub-watershed, respectively. For weekly ET, there is a close comparison of both methods.
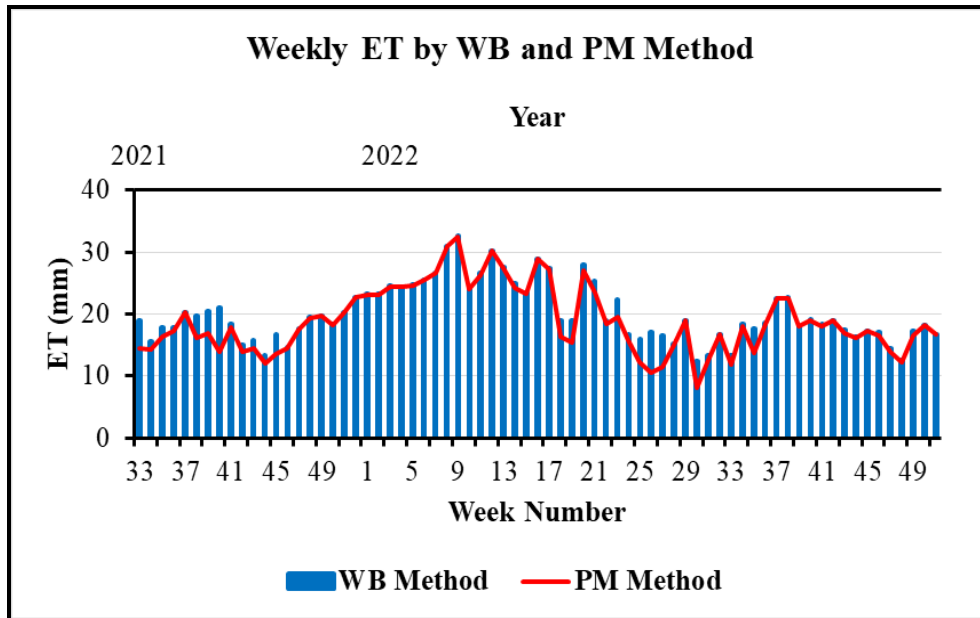

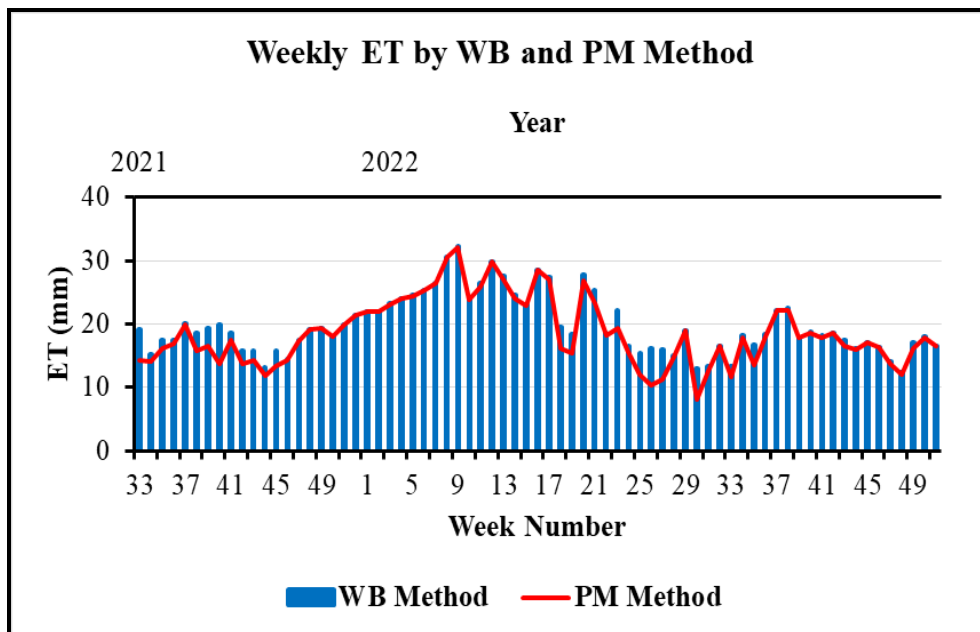**Fig. 4.47. Weekly ET by Water Balance and PM Method for the Perassannur Watershed**

Fig. 4.48. Weekly ET by Water Balance and PM Method for the Painkanoor Sub-watershed

Fig. 4.49 and Fig. 4.50 compare monthly ET from the WB equation and PM method for the Perassannur watershed and the Painkanoor sub-watershed, respectively. The coefficient of determination (R^2) for the Perassannur watershed was 0.75, and the R^2 for Painkanoor sub-watershed was 0.82. The high R^2 value in both cases indicates close matching between the ET computed through both approaches.
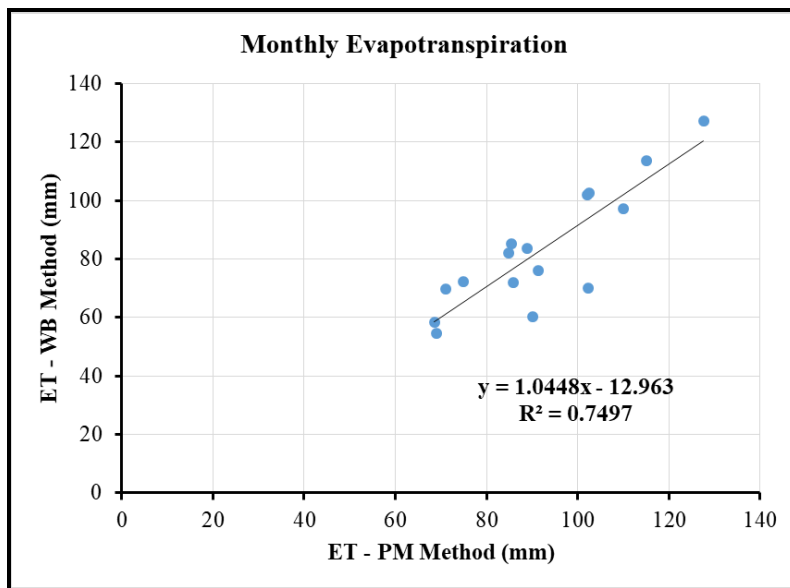

Fig. 4.49. Monthly ET by WB vs. PM Method for the Perassannur Watershed
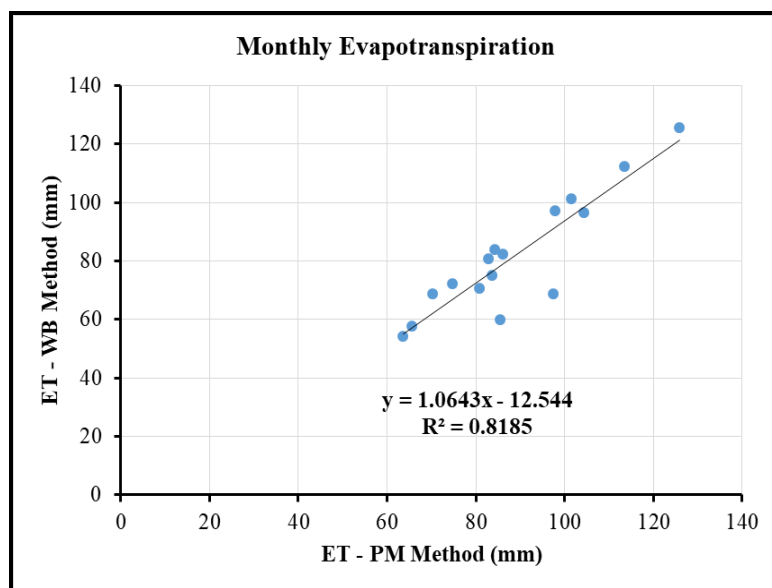

Fig. 4.50. Monthly ET by WB vs. PM Method for the Painkanoor Sub-watershed

The coefficient of determination (R^2) values for the Perassannur and Painkanoor watersheds were obtained as 0.91 and 0.92, respectively, as shown in Fig. 4.51 and Fig. 4.52. Thus, the computed ET by both methods offers a close comparison.
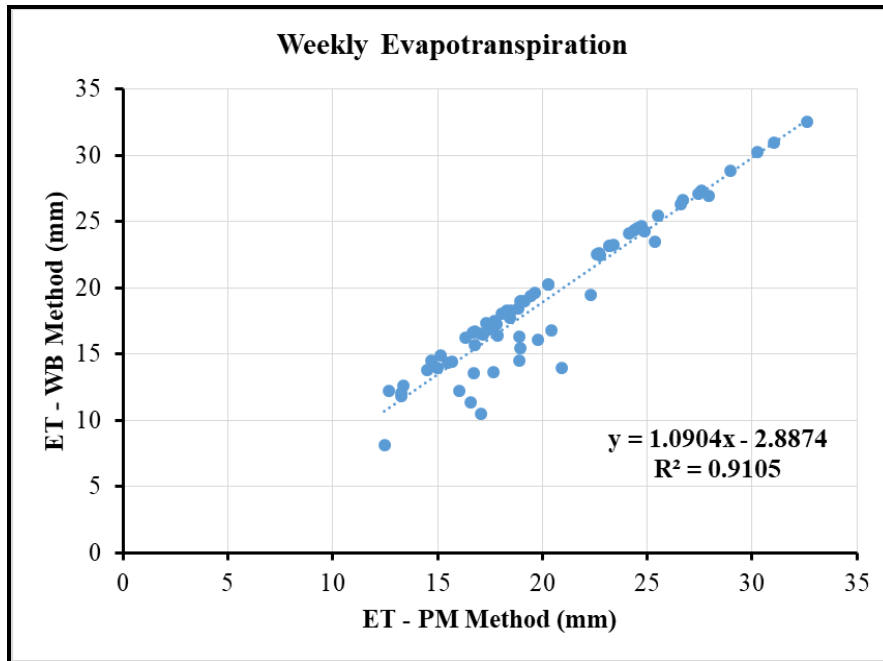

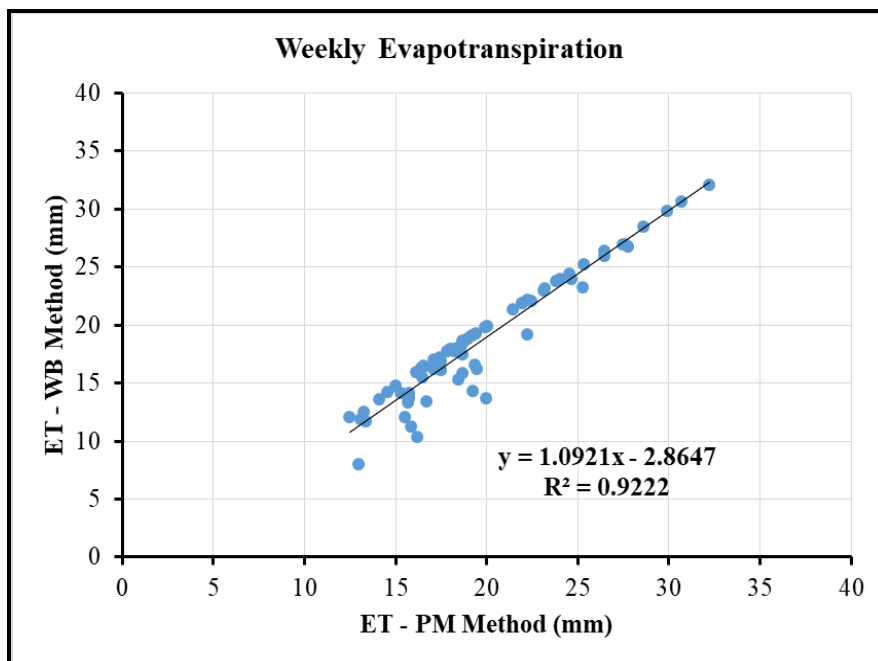**Fig. 4.51. Weekly ET by WB vs. PM Method for the Perassannur Watershed**

Fig. 4.52. Weekly ET by WB vs. PM Method for the Painkanoor Sub-watershed

4.12 WATER BALANCE BY SWAT

Water balance components of the watershed have also been determined using SWAT. A discussion on the spatial inputs required by the model is presented first and is followed by a description of the outputs of the model.

4.12.1 Digital Elevation Model (DEM)

The DEM prepared from the SRTM DEM of 30 m resolution and having defined the datum and projection is shown in Fig 4.53.

4.12.2 Land Use Map

The land use map, which is prepared in GEE and is projected UTM_Zone43, is shown in Fig 4.54, which has been classified into nine classes. According to the classification shown in Table 4.15, the Perassannur watershed had more area under paddy cultivation, i.e. 16.36 km^2 (20.54%), followed by mixed cropping at 15.71 km^2 (19.73%), whereas coconut cultivation was restricted to 12.45 km^2 (15.63%).

Table 4.15. Land Use Classification of the Perassannur Watershed

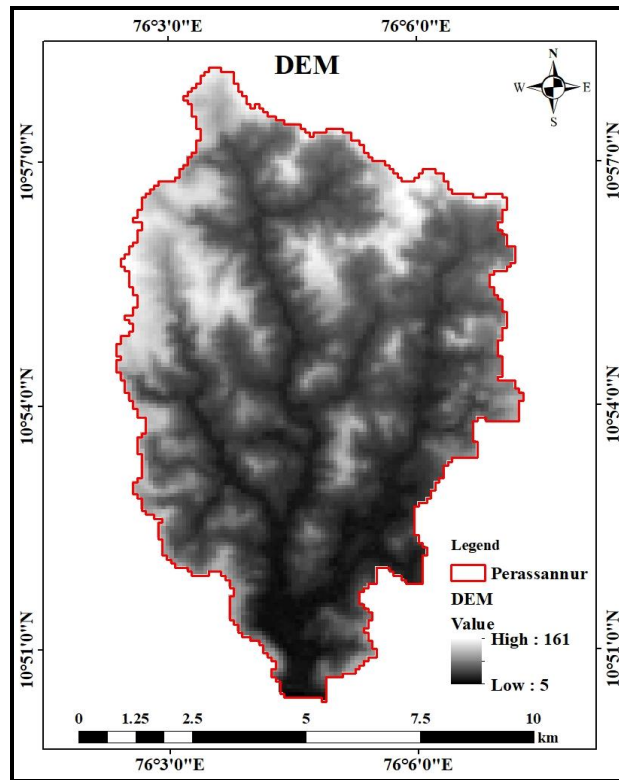| Sr. No.	Land Use Type	Area (km^2)	Area (%)
1.	Barren	5.04	6.33
2.	Coconut	12.45	15.63
3.	Forest	5.48	6.88
4.	Land with scrub	7.42	9.31
5.	Mixed Cropping	15.71	19.73
6.	Paddy	16.36	20.54
7.	Rubber	5.25	6.59
8.	Urban	6.76	8.49
9.	Water Bodies	5.18	6.51
Total		**79.66**	**100.00**

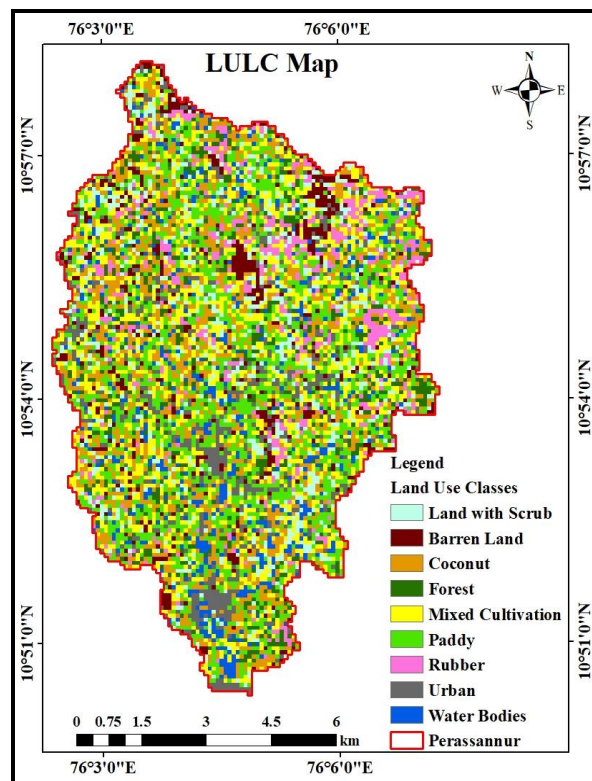**Fig. 4.53. DEM of the Perassannur Watershed**

Fig. 4.54. LULC Map of the Perassannur Watershed

4.12.3 Soil Map

Fig. 4.55 shows the digital soil map of the Perassannur watershed showing different soil series viz. Irumpiliyam, Vettakode, Perumanna, Mungilmada, Thuyyam and Water. It was found that a significant part of the study area falls under the soil series Irumpiliyam with an area of 51.83 km^2 (65.06%), followed by Vettakode soil series 14.53 km^2 (18.24%) and Perumanna soil series as shown in Table 4.16.

Table 4.16. Soil Series of the Perassannur Watershed

Sr. No.	Soil Series	Area (km^2)	Area (%)
1.	Irumpiliyam	51.83	65.06
2.	MannurSree	0.06	0.08
3.	Mungilmada	0.99	1.25
4.	Perumanna	11.93	14.98
5.	Thuyyam	0.31	0.38
6.	Vettakode	14.53	18.24
7.	Water	0.01	0.01
Total		**79.66**	**100.00**

4.12.4 Slope Map

The slope map was processed as a SWAT input model, as shown in Fig. 4.56 for the Perassannur watershed. It was found that 37.33 km^2 (46.86%) of the watershed area comes under the slope range of 0-6.9%, followed by 28.06 km^2 (35.23%) within the slope range of 7-13.9%, as shown in Table 4.17.

Table 4.17. Soil Slope Classes of the Perassannur Watershed

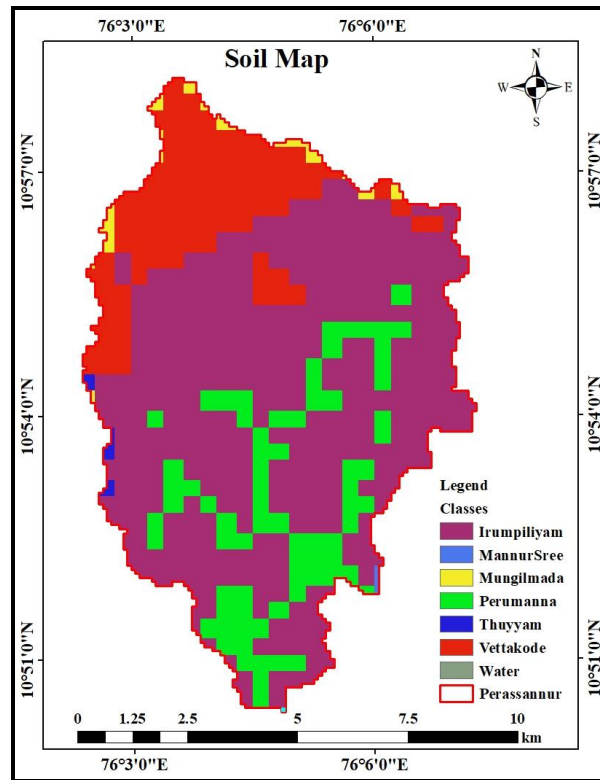| Sr. No.	Slope (%)	Area (km^2)	Area (%)
1.	0-6.9	37.33	46.86
2.	7-13.9	28.06	35.23
3.	14-20.9	9.96	12.50
4.	21-27.9	3.83	4.81
5.	28-35	0.48	0.60
Total		**79.66**	**100.00**

142

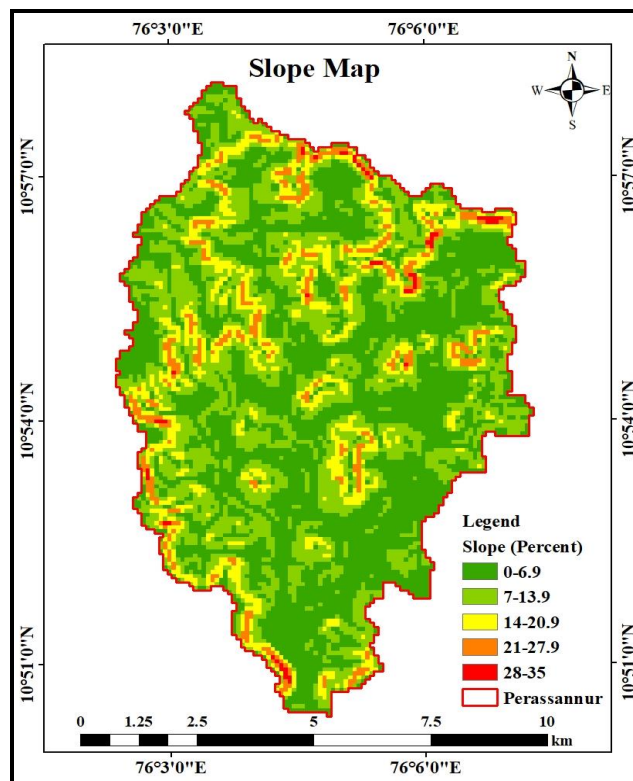**Fig. 4.55. Soil Map of the Perassannur Watershed**

Fig. 4.56. Slope Map of the Perassannur Watershed

4.13 SWAT MODEL SET-UP

      The setup of the SWAT model primarily involves four main steps: watershed delineation, HRU analysis, creation of input tables, SWAT input modification, and SWAT simulation. Further elaboration on the model setup process and the generation of outputs is provided below.

4.13.1 Watershed Delineation

      First, the main watershed corresponding to the Perassanur outlet was delineated. Then, seven sub-watershed boundaries were delineated, as shown in Fig. 4.57. The total area of the watershed was 79.66 km^2. The model also determined the area of the sub-watersheds delineated within the main watershed. The area of the sub-watersheds delineated is given in Table 4.18. The sub-watershed 1 had maximum area of 24.08 km^2, followed by 23.45 km^2 for sub-watershed 6, and the sub-watershed 7 had least area of 2.03 km^2.
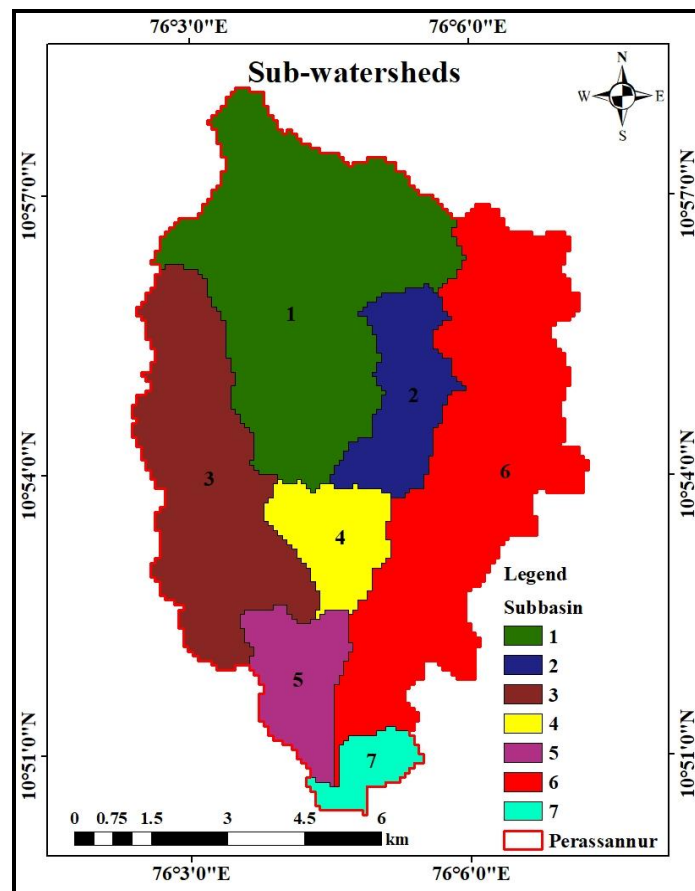

Fig. 4.57. Sub-watersheds of the Perassannur Watershed

Table 4.18. Sub-watershed Areas of Perassannur Watershed

Sub-watershed	Area (km^2)	Area (%)
1	24.08	30.23
2	5.77	7.24
3	15.19	19.07
4	4.32	5.42
5	4.81	6.04
6	23.45	29.44
7	2.03	2.55
Total	**79.66**	**100.00**

4.13.2 HRU Analysis

The model defined 339 HRUs based on land use, soil and slope map by assigning 5% as the threshold area. Thus, the unique areas below 5% were not considered in sub-basins. The use of SWAT threshold values helps in minimising the number of HRUs and enhances the SWAT model simulation efficiency.

4.14 SENSITIVITY ANALYSIS, CALIBRATION AND PERFORMANCE EVALUATION OF THE SWAT MODEL

4.14.1 Sensitivity Analysis

After the 'one at a time sensitivity analysis', fourteen parameters were selected initially for the 'global sensitivity analysis', viz. CN2 (Initial SCS curve number for moisture condition II), GW_REVAP (Groundwater revap coefficient), CH_K2 (Effective hydraulic conductivity in main channel alluvium), GWQMN (Threshold depth of water in the shallow aquifer required for return flow to occur), CH_N2 (Manning's n value for main channel), EPCO (Plant uptake compensation factor), ESCO (Soil evaporation compensation factor), ALPHA_BNK (Base flow alpha factor for bank storage), GW_DELAY (Groundwater delay time), REVAPMN (Threshold depth of water in the shallow aquifer for revap or percolation to the deep aquifer to occur), SOL_BD (moist bulk density), OV_N (Manning's 'n' value for overland flow), SOL_K (Saturated hydraulic conductivity), and SOL_AWC (Available water holding capacity of soil). The SUFI-2 method was selected, and

500 simulations were done. The global sensitivity analysis identified the most sensitive parameters as CN2, GW_REVAP, CH_K2, GWQMN, and CH_N2. The role of these parameters would be maximum in the calibration of the model.

4.14.2 Calibration of the Model

The sensitive parameters and their fitted values after calibration are shown in Table 4.19. The surface response of the model is influenced mainly by the curve number (CN2), which is sensitive to peak flow and discharge. The CN2 value was calibrated between 0.65 and 0.85, and it was fitted at 0.82, indicating that peak flow and discharge will increase. A high curve number indicates a higher runoff potential and depends mainly on the land use, soil, antecedent moisture conditions and basin slope. SWAT default values of curve numbers were adjusted based on these parameters during the calibration process (Khalid *et al*., 2016; Sao *et al*., 2020; Singh and Jha, 2021; Leta *et al*., 2022).

GW_REVAP was calibrated from 0.3 to 0.4, and it was fitted with 0.38. The calibrated value indicated a moderately high rate of groundwater transfer from the shallow aquifer to the overlying unsaturated zone (Singh and Saravanan, 2020; Juma *et al*., 2022; Lee *et al*., 2023).

CH_K2 was calibrated within 75 to 100 mm h^{-1}, and it was fitted with 80.98 mm h^{-1}. The calibrated value indicated the 'moderately high loss rate' alluvium material, and the basin response is mainly affected by it. The effective hydraulic conductivity of the stream is set to zero by default in the SWAT model, which means that there is no loss of water is expected from the stream bed. This is not the case concerning the humid tropics and semi-arid tropics (Neitsch *et al*., 2011), and hence, the value was increased based on suggested value ranges and was adjusted based on sensitivity analysis (Briak *et al*., 2016; Shivhare *et al*., 2018; Singh and Saravanan, 2020).

GWQMN was calibrated from 10 to 15 mm, and it was fitted with 11.44 mm. The calibrated value indicates that 0.11 m depth is required for return flow in the shallow aquifer. The water depth influences the subsurface response in the

shallow aquifer required for return flow to the stream. It depends on the hydraulic properties of the geologic formations and the depth to the water table (Dos Santos *et al*., 2020; Singh and Saravanan, 2020; Sanchez-Gomez *et al*., 2022).

CH_N2 was calibrated within 0.08 mm to 0.12 mm, and it was fitted with a 0.09 mm roughness coefficient. The sensitivity of CH_N2 indicates that the study area has a natural stream with a thick lining of the channel (Briak *et al*., 2016; Shivhare *et al*., 2018; Dakhlalla and Parajuli, 2019; Singh and Saravanan, 2020).

EPCO was calibrated within 4 to 5, and it was fitted with 4.08. ESCO was calibrated within 15 to 20, and it was fitted at 15.35. The calibrated value indicated the high soil evaporation demand in the lower layer of soil. The ESCO coefficient is a significant factor in channel flow routing, and it is employed to adjust the distribution of soil depth to satisfy evaporation requirements. With higher ESCO, a basin can extract less evaporative demand from lower levels. Thus, high ESCO should match low EPCO in a watershed and vice versa (Tang *et al*., 2012; Mengistu *et al*., 2019; Hosseini and Khaleghi, 2020; Sao *et al*., 2020).

The subsurface response is influenced by the factor ALPHA_BNK, which was fitted at 0.05. It characterises the bank storage recession curve. The value was adjusted such that the variation between observed and simulated flow is minimum (Liang *et al*., 2021; Li *et al*., 2021; Garna *et al*., 2023; Wang *et al*., 2023). GW_DELAY was found to be 215 days, which indicates the lag time taken by water to move past the lowest depth of the soil profile by percolation and flow through the vadose zone before becoming shallow aquifer recharge. It depends on the hydraulic properties of the geologic formations and the depth of the water table (Thavhana *et al*., 2018; Qi *et al*., 2019; Desai *et al*., 2021).

The REVAPM was calibrated within the range of 100 to 120 mm, and the final calibrated value was set at 112.46 mm. This calibrated value represents a threshold depth of water, which is 0.112 meters, for percolation from the shallow aquifer to the deep aquifer (Chauhan *et al*., 2020; Singh and Saravanan, 2020; Chiphang *et al*., 2022). SOL_BD was calibrated between 0.6 and 0.7 g cm^{-3} and was

fitted at 0.64 g cm^{-3}, which indicates very high soil porosity and low soil compaction (Khalid *et al*., 2016; Ha *et al*., 2018; Singh and Goyal, 2017; Singh and Saravanan, 2020; Chen *et al*., 2023).

OV_N was calibrated within 5 to 8 and was fitted at 5.29. The higher OV_N value suggests an expansion of agricultural activities and a decrease in the utilisation of forest and shrubland within the study area (Khalid *et al*., 2016; Teklay *et al*., 2019; Singh and Saravanan, 2020). SOL_K was calibrated within 0.8 mm h^{-1} to 1.2 mm h^{-1}, and it was fitted at 1.01 mm h^{-1}. SOL_K is closely associated with the flow of water through soil profiles. This is due to the study area's composition of sandy loam, which possesses a moderate percolation capacity. Consequently, water in the soil tends to move downward into the shallow aquifer, recharging the baseflow (Liu *et al*., 2017; Thavhana *et al*., 2018; Li *et al*., 2021).

SOL_AWC was calibrated within 0.08 mm to 0.12 mm, and it was fitted at 0.09 mm. The calibrated value indicated that the plant's available water was comparatively less than the default value of SOL_AWC. A lower value of SOL_AWC means a low capacity of soil to retain water, thereby causing more water available for percolation and surface runoff and vice versa. Different sub-basins will have variations in land use and structural and topographical changes in the area. This was also considered, and the value was adjusted accordingly for the area (Liu *et al*., 2017; Shivhare *et al*., 2018; Xueman *et al*., 2020; Moazenzadeh and Izady, 2022; Xiang *et al*., 2022)

There may be these model uncertainties due to significant variations in topography and rainfall and also some errors in data input sources like land use and soil, data preparation, etc. The uncertainties may also be due to human and instrumental errors during data processing.

Table 4.19. Sensitivity Parameters and their Ranking

Sensitivity Rank	Parameter	Description	Unit	Min. Value	Max. Value	Fitted Value	t-value	p-value
1.	r_CN2.mgt	Initial SCS curve number for moisture condition II	-	0.65	0.85	0.82	-2.92	0.00
2.	v_GW_REVAP.gw	Groundwater revap coefficient	-	0.30	0.40	0.38	-3.61	0.00
3.	v_CH_K(2).rte	Effective hydraulic conductivity in main channel alluvium	mm h^{-1}	75.00	100.00	80.98	-3.64	0.00
4.	v_GWQMN.gw	The threshold depth of water in the shallow aquifer required for return flow to occur	mm H$_2$O	10.00	15.00	11.44	-3.79	0.00
5.	v_CH_N(2).rte	Manning's 'n' value for the main channel	-	0.08	0.12	0.09	-4.35	0.00
6.	v_EPCO.hru	Plant uptake compensation factor	-	4.00	5.00	4.08	-4.62	0.00
7.	v__ESCO.hru	Soil evaporation compensation factor	-	15.00	20.00	15.35	-4.79	0.00
8.	v_ALPHA_BNK.rte	The baseflow alpha factor for bank storage	days	0.04	0.06	0.05	-5.11	0.00
9.	v_GW_DELAY.gw	Groundwater delay time	days	200.00	250.00	215.55	-6.11	0.00
10.	v_REVAPMN.gw	Threshold depth of water in the shallow aquifer for revap or percolation to the deep aquifer to occur	mm H$_2$O	100.00	120.00	112.46	-8.11	0.00
11.	r_SOL_BD(1).sol	Moist bulk density	g cm^{-3}	0.60	0.70	0.65	-10.43	0.00
12.	v_OV_N.hru	Manning's 'n' value for overland flow	-	5.00	8.00	5.29	-2.71	0.01
13.	R_SOL_K(1).sol	Saturated hydraulic conductivity	mm h^{-1}	-0.80	-1.20	-1.01	2.81	0.01
14.	r_SOL_AWC(1).sol	Available water capacity of the soil layer	mm H$_2$O mm^{-1} soil	0.08	0.12	0.09	-2.46	0.03

4.14.3 Evaluation of Model Performance

Graphical and statistical comparisons between the observed and simulated values evaluated the model performance. Observed and SWAT simulated monthly runoff values of the Perassanur watershed and Painkannur sub-watershed are graphically shown in Figs 4.58 and 4.59, respectively. Visual observation shows very close matching between observed and simulated runoff in both watersheds.
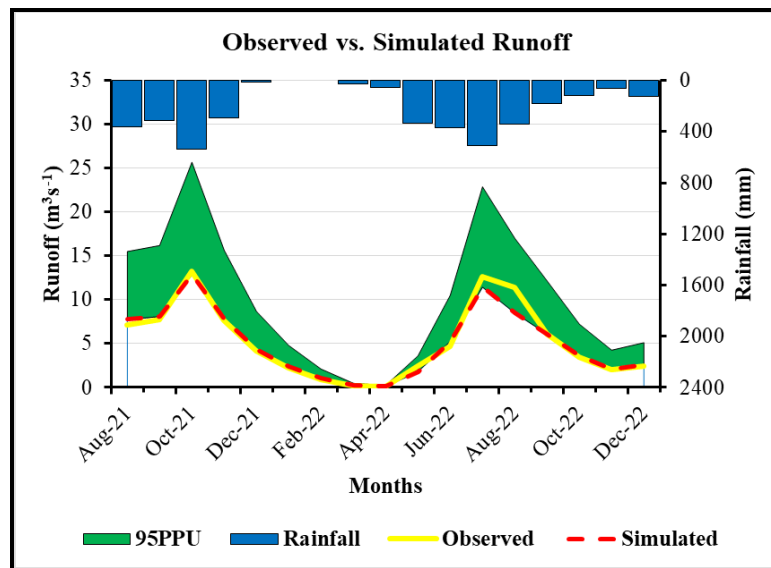

Fig. 4.58. Observed vs. Simulated Runoff using SWAT for the Perassannur Watershed
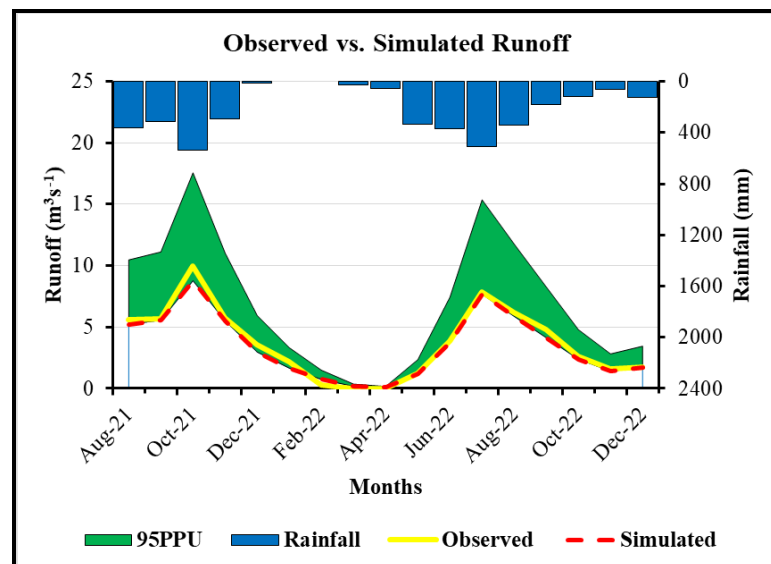
Fig. 4.59. Observed vs. Simulated Runoff using SWAT for the Painkanoor Sub-watershed

Statistical comparisons between the observed and simulated values involved the use of the coefficient of determination (R^2), Nash-Sutcliffe Efficiency (NSE), Percent Bias (PBIAS), and the RMSE-observations Standard Deviation Ratio (RSR). Fig. 4.60 and Fig. 4.61 shows the model performance indices for the Perassannur watershed and Painkanoor sub-watershed, respectively.
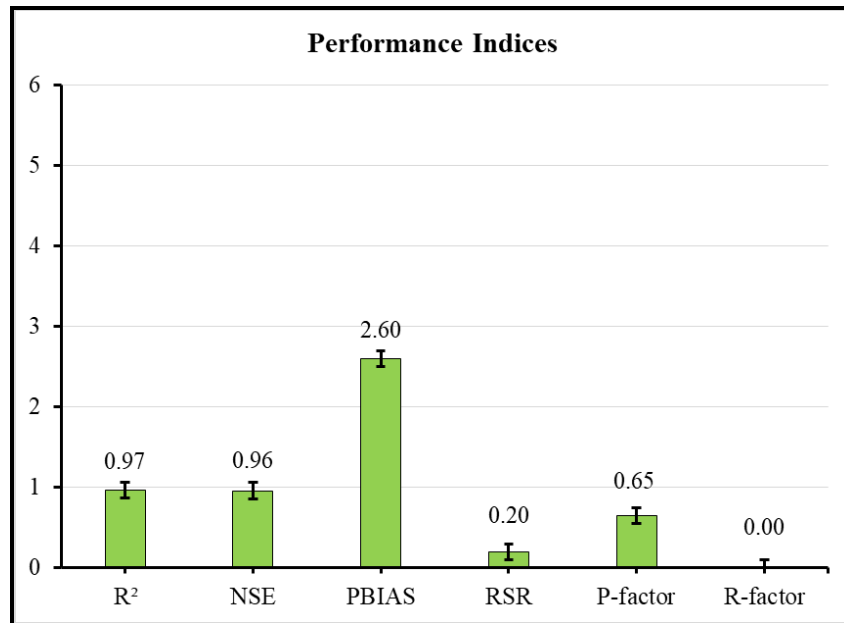

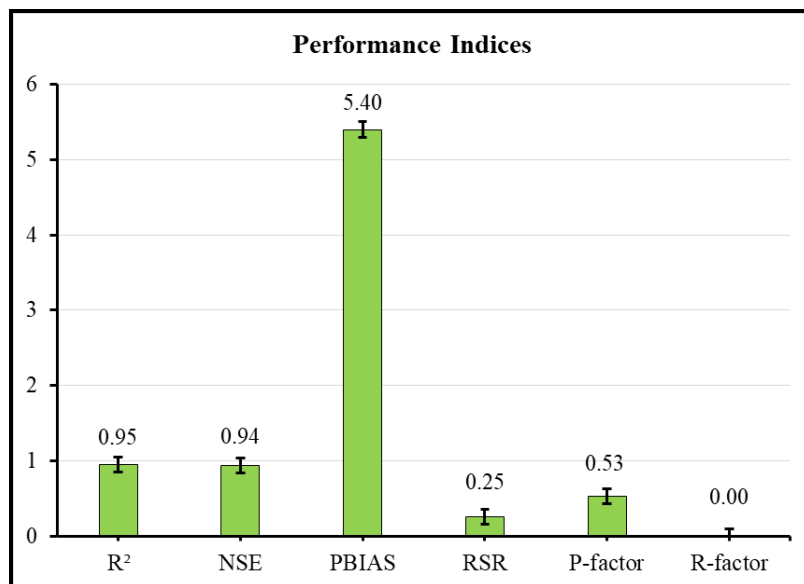**Fig. 4.60. SWAT Model Performance Indices for the Perassannur Watershed**

Fig. 4.61. SWAT Model Performance Indices for the Painkanoor Sub-watershed

The results of statistical analysis showed good performance indices. The R^2 was observed as 0.97 and 0.95 for the Perassannur watershed and Painkanoor sub-watershed, respectively. Other researchers have reported that an R^2 value greater than 0.90 can be considered a good model performance (Mestry *et al*., 2020; Li *et al*., 2021; Moazenzadeh and Izady, 2022). The NSE was 0.96 and 0.94 for the Perassannur watershed and Painkanoor sub-watershed, respectively. In the case of runoff prediction from a watershed, an NSE value greater than 0.80 is very acceptable (e.g. Sandra and Sathian, 2016; Krishnan *et al*., 2018; Molenat *et al*., 2021). The PBIAS was 2.60 and 5.40 for the Perassannur watershed and Painkanoor sub-watershed, respectively. The positive PBIAS indicates that the SWAT model over-predicted the runoff. However, its value ±15 indicates the model performance is 'very good.' Previous studies have also obtained PBIAS values within the range of ±15 as good (e.g. Moriasi *et al*., 2007; Uniyal *et al*., 2020). The RSR values were 0.20 and 0.25 for the Perassannur watershed and Painkanoor sub-watersheds, respectively. This value from 0 to 0.5 is very good (Moriasi *et al*., 2007).

The strength of the model calibration and uncertainty procedure were also analysed using the P factor, which was 0.65 for Perassannur and 0.53 for Painkanoor sub-watersheds. It has been reported that a p-value greater than 0.50 is acceptable (Moriasi *et al*., 2007). The R factor also indicates the strength of the model calibration. This value was 0.00 for both the Perassannur watershed and the Painkanoor sub-watershed. The R-value should be close to 0 for good model performance (Moriasi *et al*., 2007). All these indices showed very good results for the Perassannur watershed and the Painkanoor sub-watershed. To summarise, all model performance indices have demonstrated promising results in the Perassannur and Painkanoor sub-watersheds.

The ET obtained from the water balance method, and SWAT simulation for the Perassanur watershed and Painkannur sub-watershed are graphically shown in Figs 4.62 and 4.63, respectively. It is observed that the ET obtained by both methods has a considerable difference. The reason may be that the SWAT model considers HRUs, and hence, the land use may be reflected in the results.
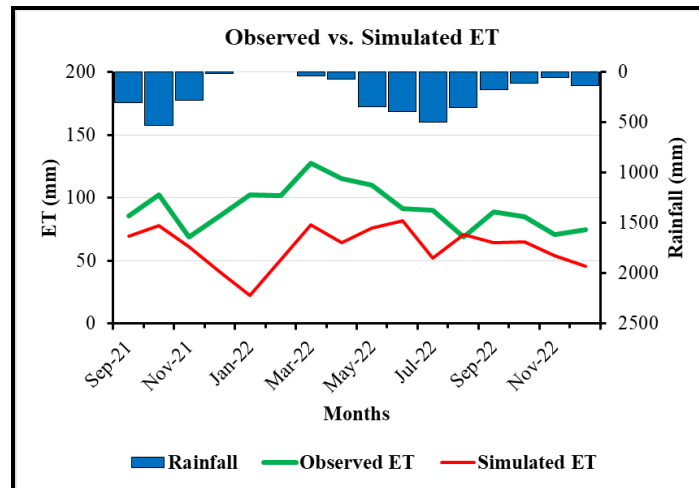
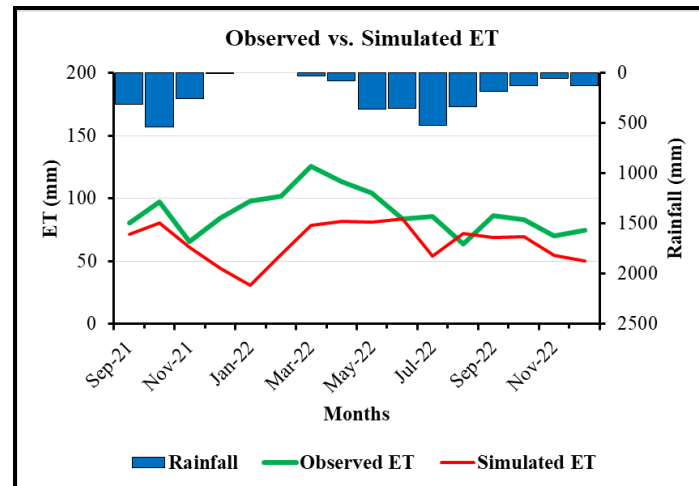**Fig. 4.62. Observed vs. Simulated ET using SWAT for the Perassannur Watershed**

Fig. 4.63. Observed vs. Simulated ET using SWAT for the Painkanoor Sub-watershed

4.14.4 Detailed Water Balance Components of the Basin by SWAT

The water balance components obtained by SWAT simulation for the Perassannur watershed and the Painkanoor sub-watershed are shown in Fig. 4.64 and Fig. 4.65, respectively. The water balance components viz. ET, surface flow, base flow, lateral flow, and deep aquifer recharge for both watersheds as a percentage of annual rainfall are shown as pie diagrams in Figs. 4.66 and 4.67. It is observed that for both watersheds, surface runoff is the major component, followed by ET. The deep aquifer recharge was 6.94% for the Perassannur watershed, while only 0.36% for the Painkanoor sub-watershed.
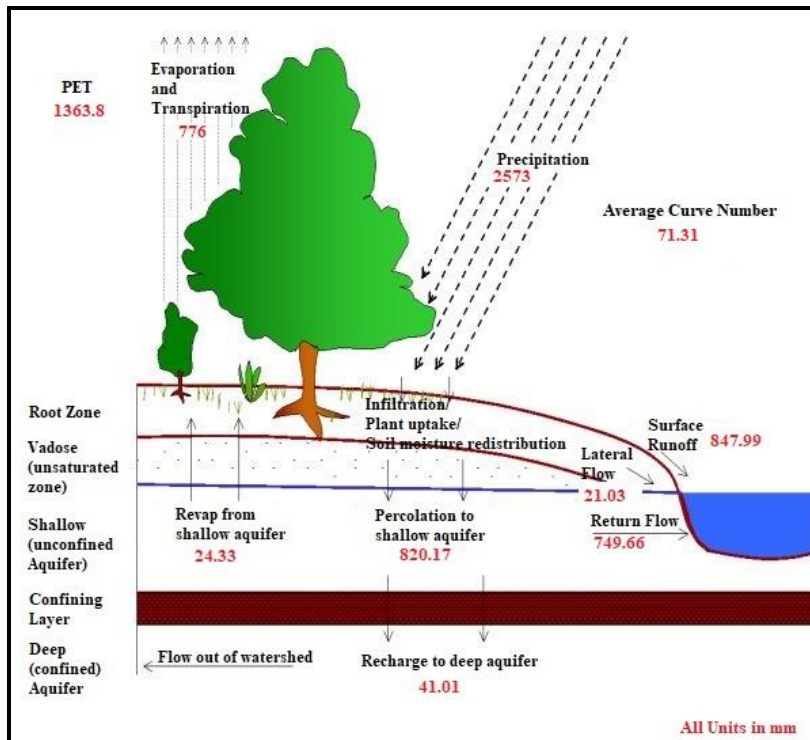
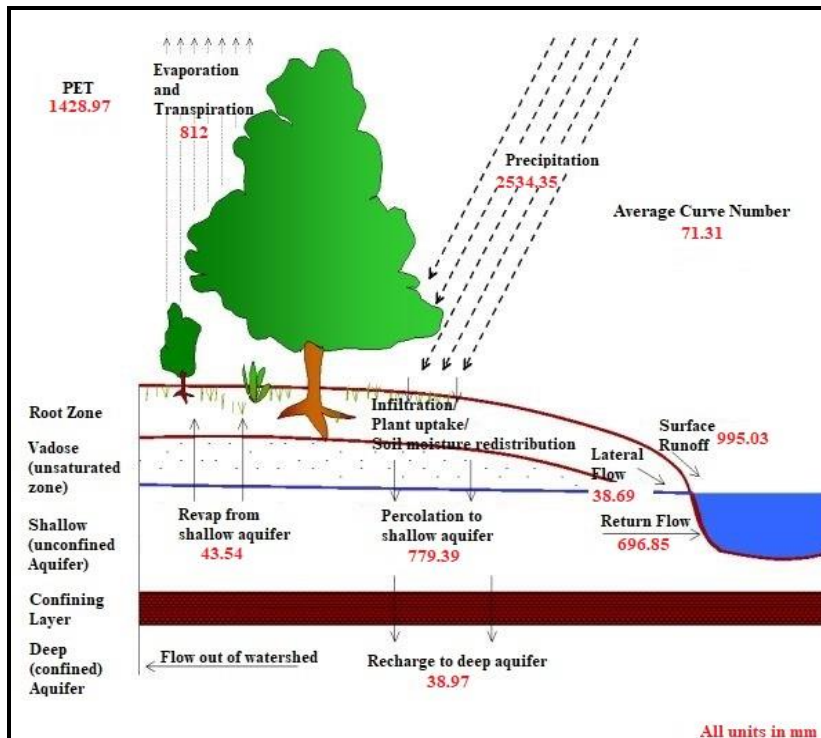**Fig. 4.64. Quantified Schematic Representation of the Hydrologic Cycle for the Perassannur Watershed**

Fig. 4.65. Quantified Schematic Representation of the Hydrologic cycle for the Painkanoor Sub-watershed
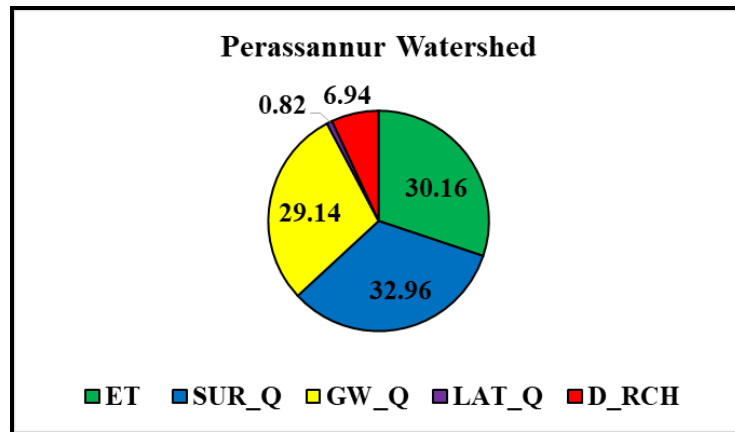
Fig. 4.66. Average Water Balance Components as a Percentage of Annual Rainfall for the Perassannur Watershed
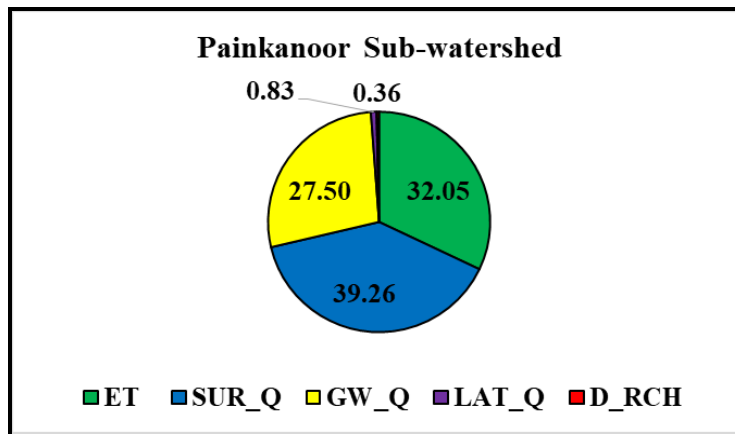

Fig. 4.67. Average Water Balance Components as a Percentage of Annual Rainfall for the Painkanoor Sub-watershed

The SWAT model simulated the water balance components for all sub-watersheds within the Perassannur watershed. The proportions of evapotranspiration, surface flow, base flow, lateral flow, and deep aquifer recharge as a percentage of annual rainfall for each sub-watershed are plotted in the pie diagrams and are presented in Fig. 4.68 to Fig. 4.74. It was observed that surface runoff was the major component of stream discharge in all the sub-watersheds. The base flow was the second highest component in sub-watersheds 1, 2, 3, and 6, whereas ET was the second highest in sub-watersheds 4, 5, and 7.

Similar results were also reported by other researchers where the major part of water balance was ET, surface flow, or base flow, whereas lateral flow and deep

aquifer storage were in marginal proportions (Bonuma *et al.*, 2013; Leta *et al.*, 2016; Kundu *et al.*, 2017; Ayivi and Jha, 2018; Tejaswini and Sathian, 2018; Nasiri *et al.*, 2020). The rise in surface runoff may be attributed to the reduced water infiltration capacity. Consequently, in areas with high surface runoff, it is essential to strategise and implement water conservation measures, as suggested by Bonuma *et al.* in 2013. Furthermore, the elevated evapotranspiration rate can be linked to the specific vegetation cover and the region's high temperatures, as indicated by Nasiri *et al.* in 2020. Additionally, the low value for deep aquifer recharge suggests that the water-yielding potential of the deep aquifers in the watershed will be limited.
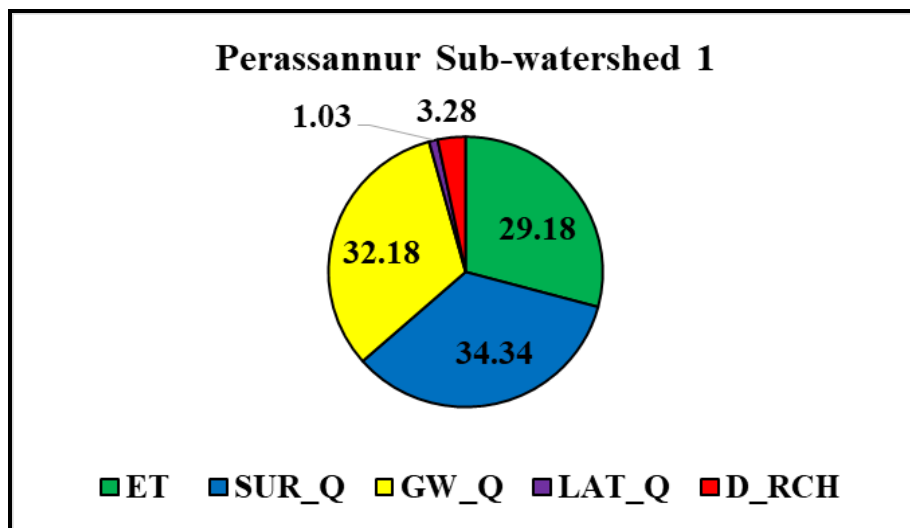

Fig. 4.68. Average Water Balance Components of the Perassannur Sub-watershed 1

Fig. 4.69. Average Water Balance Components of the Perassannur Sub-watershed 2

Fig. 4.70. Average Water Balance Components of the Perassannur Sub-watershed 3
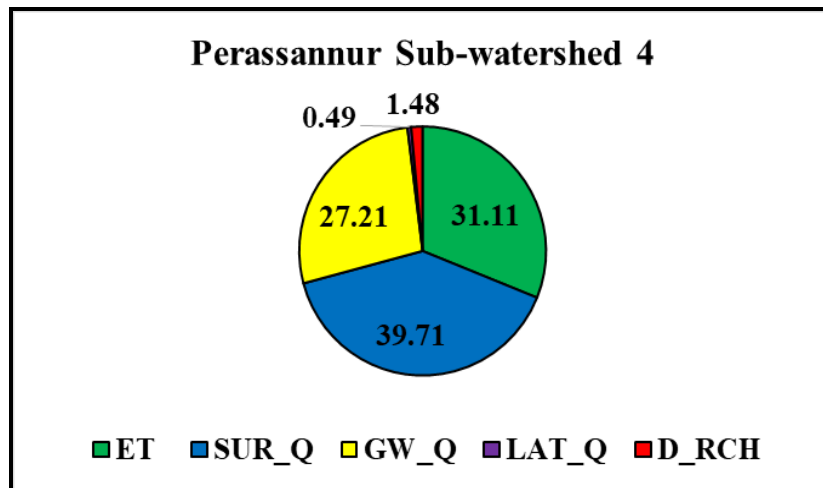
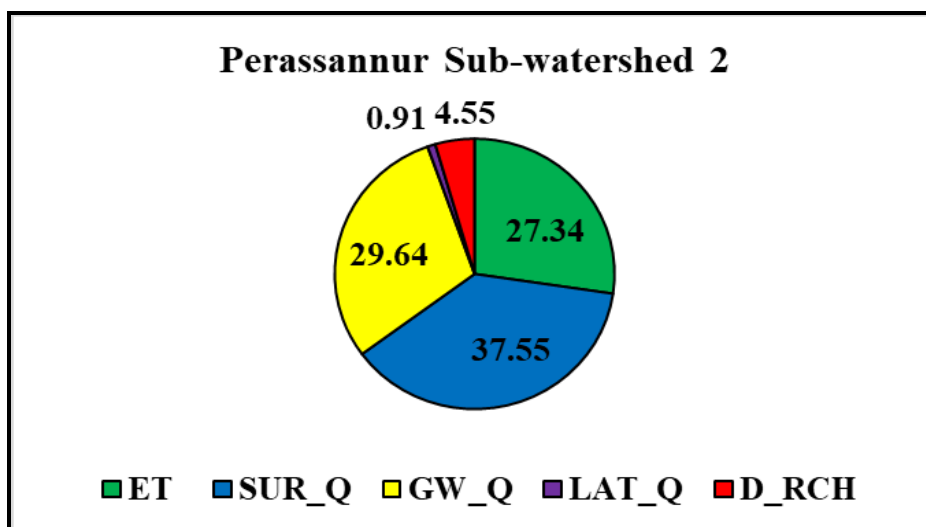**Fig. 4.71. Average Water Balance Components of the Perassannur Sub-watershed 4**
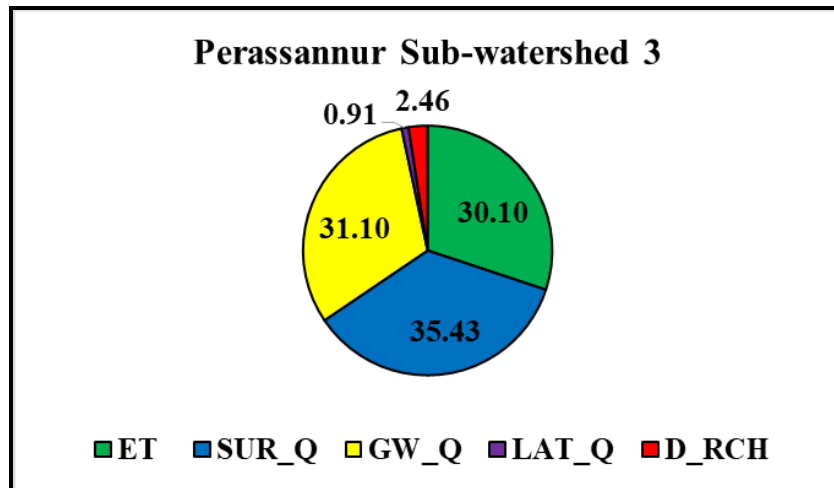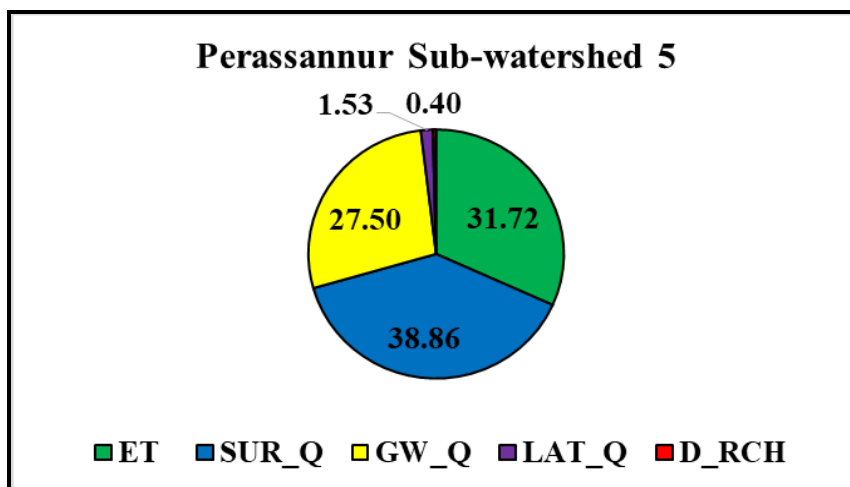

Fig. 4.72. Average Water Balance Components of the Perassannur Sub-watershed 5
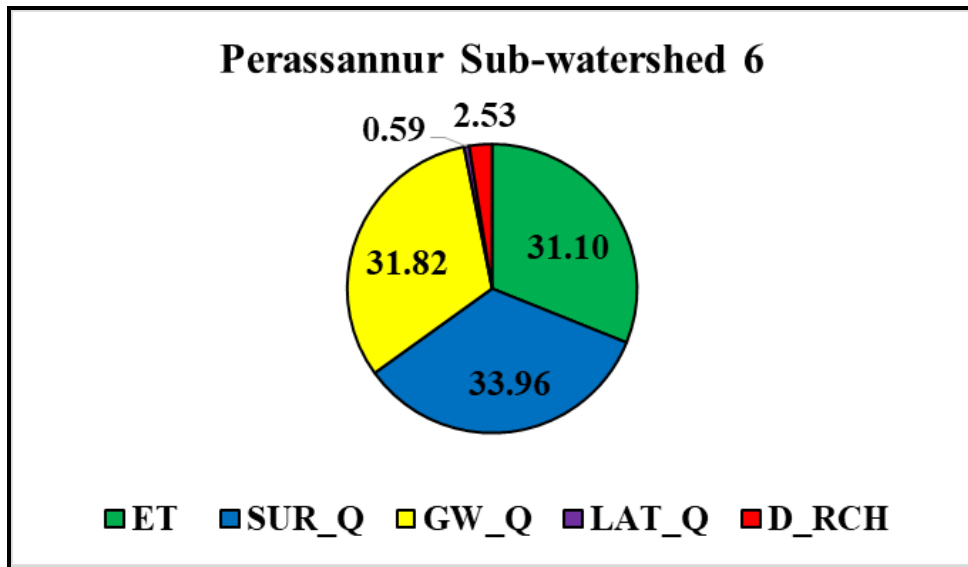
Fig. 4.73. Average Water Balance Components of the Perassannur Sub-watershed 6
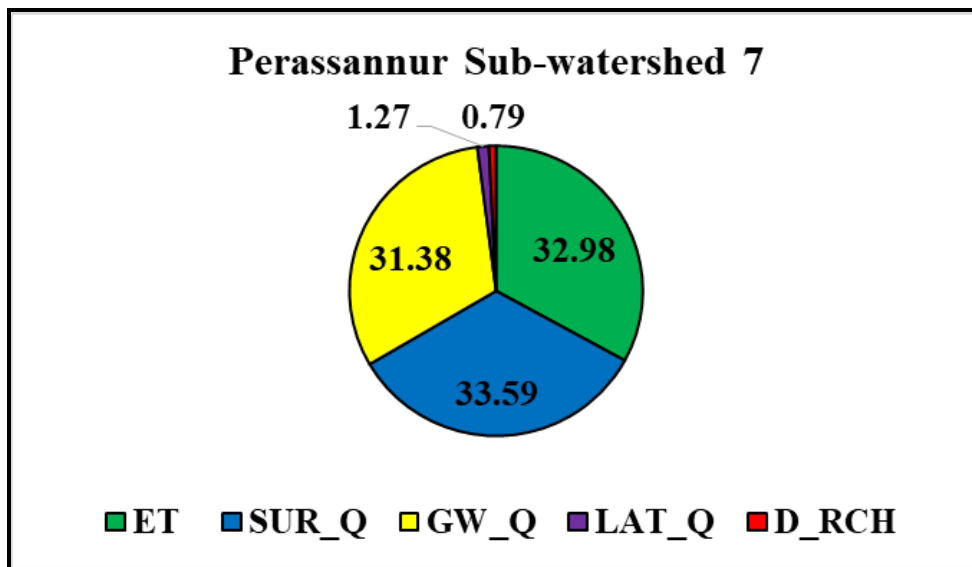
Fig. 4.74. Average Water Balance Components of the Perassannur Sub-watershed 7

Fig. 4.75 and Fig. 4.76 show the SWAT simulated monthly water balance components of the Perassannur watershed and Painkanoor sub-watershed. It is observed that the surface runoff, base flow and evapotranspiration are the major water balance components for both the watersheds. However, lateral flow is significantly less for the watersheds.

Fig. 4.75. SWAT Simulated Monthly Water Balance for the Perassannur Watershed

Fig. 4.76. SWAT Simulated Monthly Water Balance for the Painkanoor Sub-watershed

4.15 RELATION BETWEEN RAINFALL AND WATER BALANCE COMPONENTS

The relation between rainfall versus runoff, soil moisture, depth to groundwater table, and evapotranspiration were determined using R-Stuido software and the results are presented in the following sub-sections.

4.15.1 Monthly Rainfall vs. Water Balance Components for the Perassannur Watershed

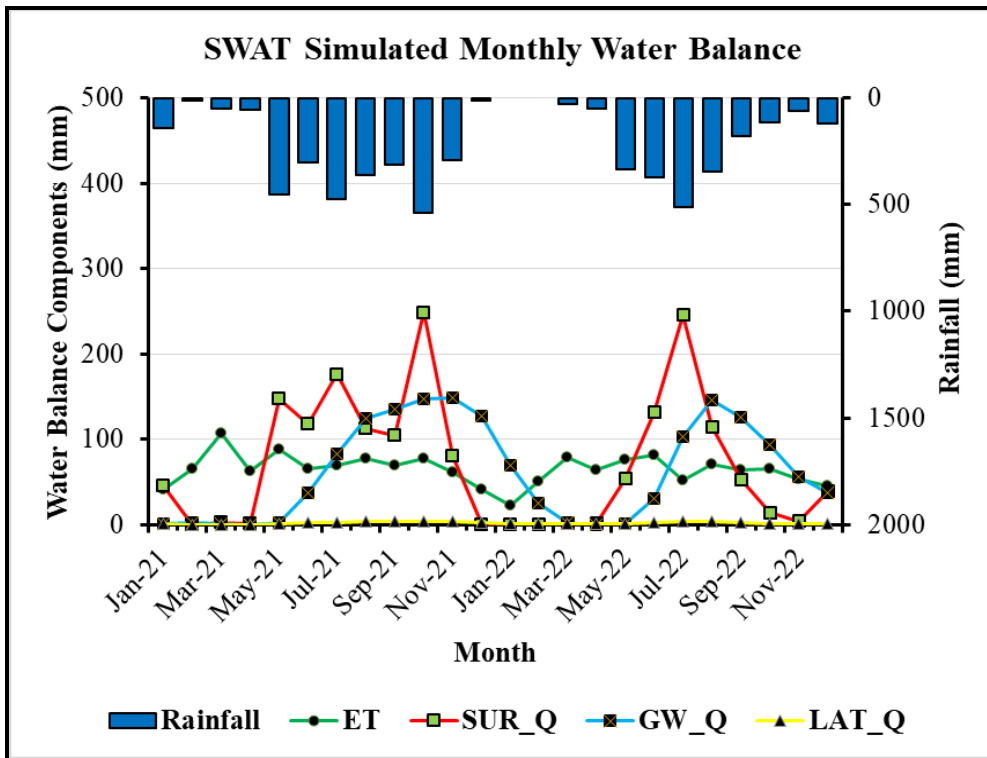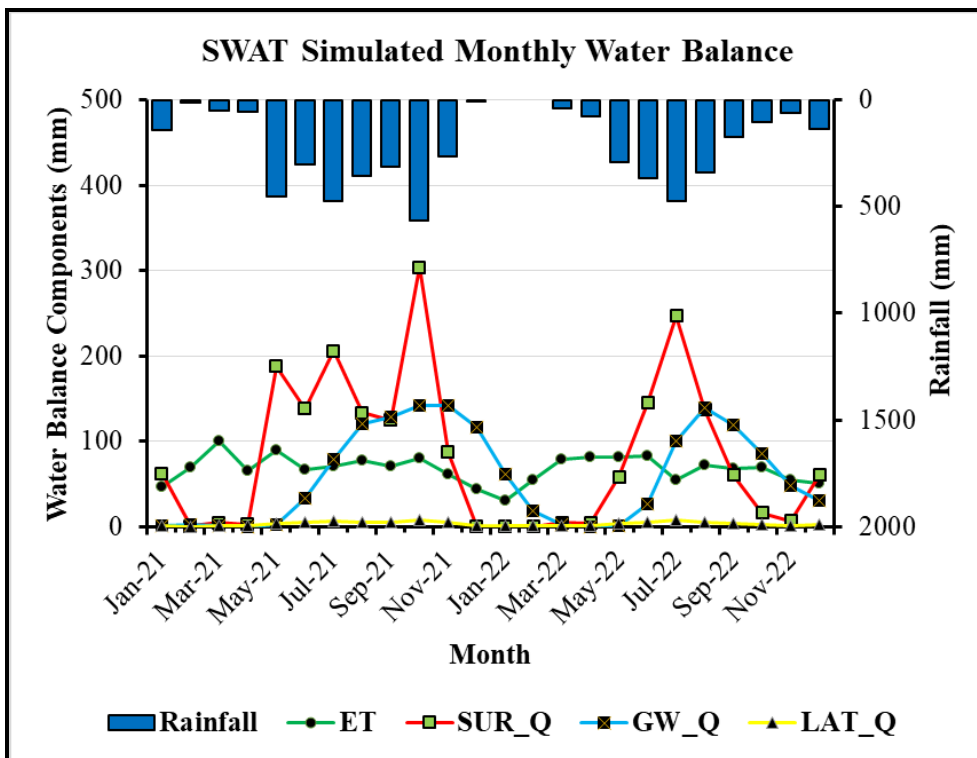Fig. 4.77 shows the Pearson's correlation coefficient (r) between the monthly water balance components of the Perassannur watershed. It was observed that 'r' between rainfall and runoff was 0.83, rainfall and soil moisture was 0.80, rainfall and height of GW table was 0.72, and rainfall and evapotranspiration was -0.64. Pearson's correlation coefficient was also observed as 0.76 between runoff and soil moisture, 0.89 between runoff and height of GW table, and -0.76 between runoff and ET. The 'r' value between soil moisture and height of GW table was 0.76, and between soil moisture and ET was -0.85. Also, the 'r' value between height of GW table and ET was -0.86. This indicates that ET has a negative correlation with other water balance components. The importance of 'r' between monthly rainfall vs. runoff and rainfall vs. soil moisture stated a very good correlation. Also, rainfall vs. height of GW table indicated a good correlation, while rainfall vs. ET showed a weak correlation.

The polynomial non-linear regression model was developed between monthly rainfall versus runoff, rainfall versus soil moisture, rainfall versus height of GW table, and rainfall versus ET with a 95% confidence interval for the Perassannur watershed as shown in Fig. 4.78, Fig. 4.79, Fig. 4.80, and Fig. 4.81, respectively. The relationship between monthly rainfall vs. runoff for the Perassannur watershed is given by Eq. 4.1, with R^2 of 0.78 and a p-value of 0.0006, having an F-statistic of 10.64 on 4 and 12 degrees of freedom.

$$121.55x^4 + 34.01x^3 + 85.13x^2 + 434.60x + 159.99 = 0 \quad ..... (Eq.\, 4.1)$$
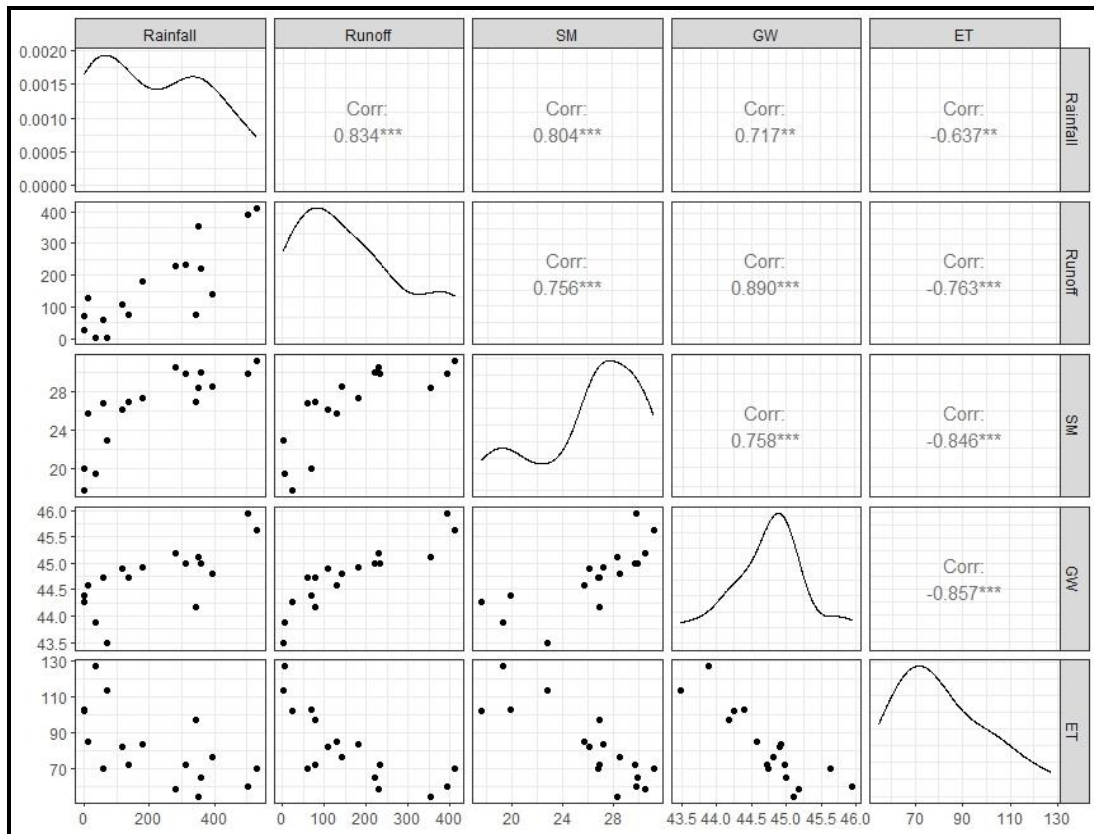
Fig. 4.77. Pearson's Correlation Coefficient for Monthly Water Balance Components for the Perassannur Watershed

The relation between monthly rainfall vs. soil moisture for the Perassannur watershed is given by Eq. 4.2, with R^2 of 0.77 and p-value of 0.0001, having F statistic of 14.99 on 3 and 13 degrees of freedom.

$$3.49x^3 - 4.72x^2 + 13.14x + 26.34 = 0 \quad ..... (Eq. 4.2)$$

The relation between monthly rainfall vs. height of GW for the watershed is given by Eq. 4.3, with R^2 of 0.69 and a p-value of 0.01, having an F-statistic of 4.84 on 5 and 11 degrees of freedom.

$$-0.69x^5 + 0.52x^4 + 0.40x^3 + 0.32x^2 + 1.73x + 44.75 = 0 \quad ..... (Eq. 4.3)$$

The monthly rainfall vs. evapotranspiration relationship for the Perassannur watershed is given by Eq. 4.4, with R^2 of 0.45 and p-value of 0.04, having an F-statistic of 3.62 on 3 and 13 degrees of freedom.

$$-4.93x^3 + 17.57x^2 - 52.06 + 81.93 = 0 \quad ..... (Eq. 4.4)$$
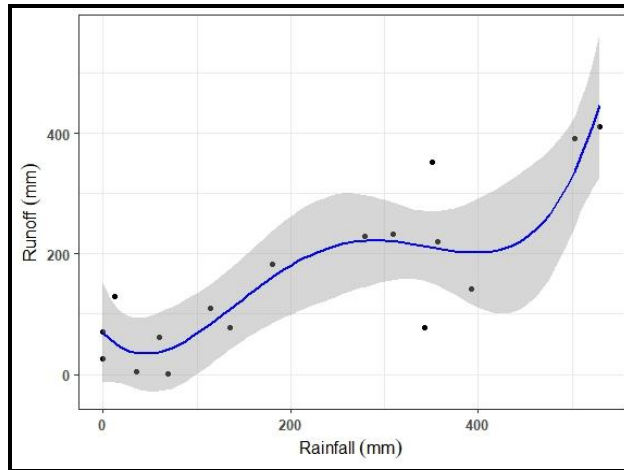
Fig. 4.78. Monthly Rainfall vs. Runoff for the Perassannur Watershed
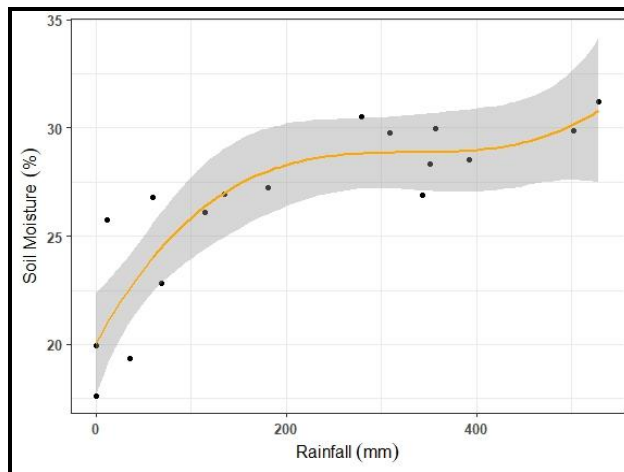
Fig. 4.79. Monthly Rainfall vs. Soil Moisture for the Perassannur Watershed
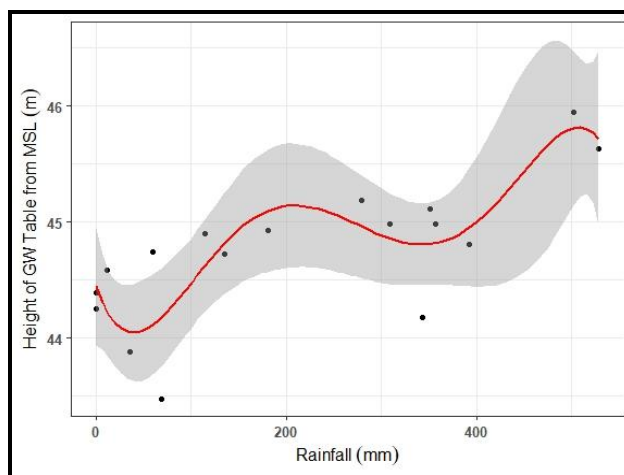
Fig. 4.80. Monthly Rainfall vs. Height of GW Table for the Perassannur Watershed
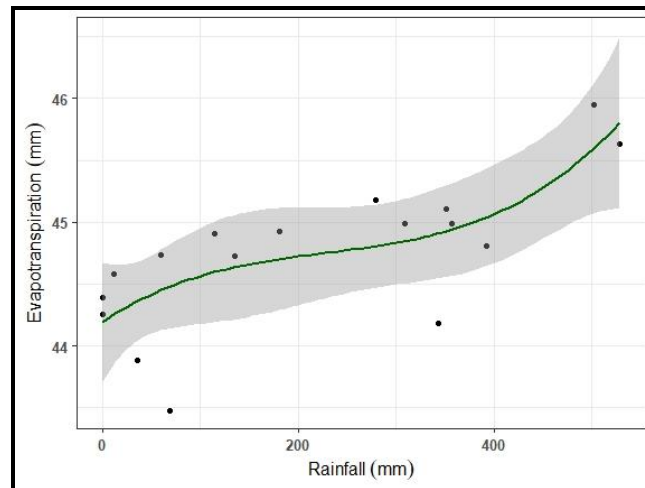
Fig. 4.81. Monthly Rainfall vs. ET for the Perassannur Watershed

Fig. 4.82, Fig. 4.83, Fig. 4.84, and Fig. 4.85 show the residual vs. fitted plot between rainfall and runoff, rainfall and soil moisture, rainfall and height of GW table, rainfall and evapotranspiration, respectively, for the Perassannur watershed. The x-axis indicates the monthly value of the water balance component, and the y-axis indicates the residuals. All these graphs show that the fitted line is not a straight line passing through zero residual, which suggests that there is non-linearity between the plotted variables. Also, the three outliers are shown in each graph, by the numbers which indicate the month starting from August 2021.
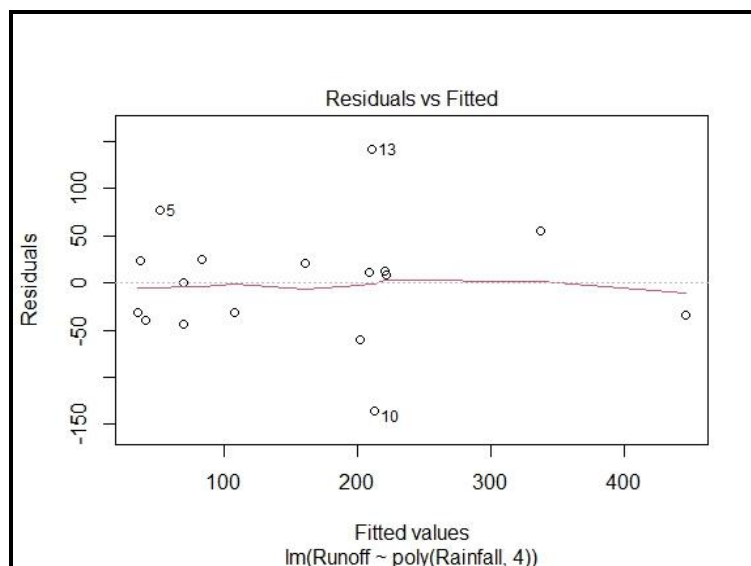
Fig. 4.82. The Residual vs. Fitted Plot between Rainfall and Runoff for the Perassannur Watershed
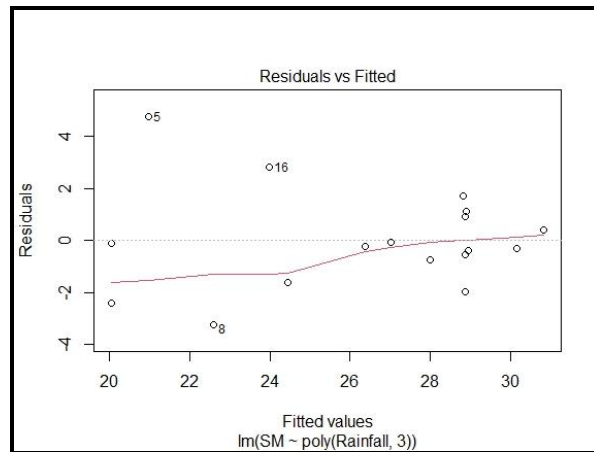
Fig. 4.83. The Residual vs. Fitted Plot between Rainfall and Soil Moisture for the Perassannur Watershed
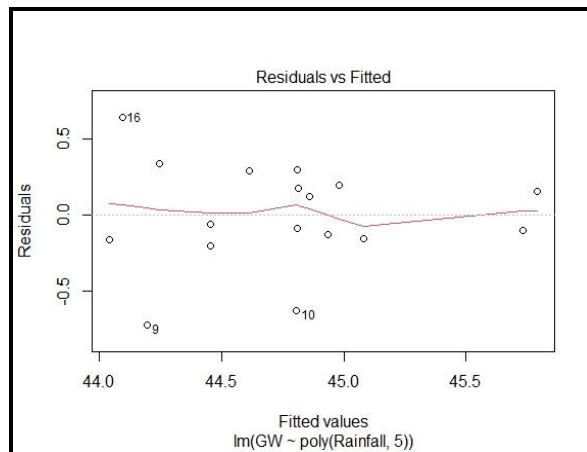
Fig. 4.84. The Residual vs. Fitted Plot between Rainfall and Height of GW Table for the Perassannur Watershed
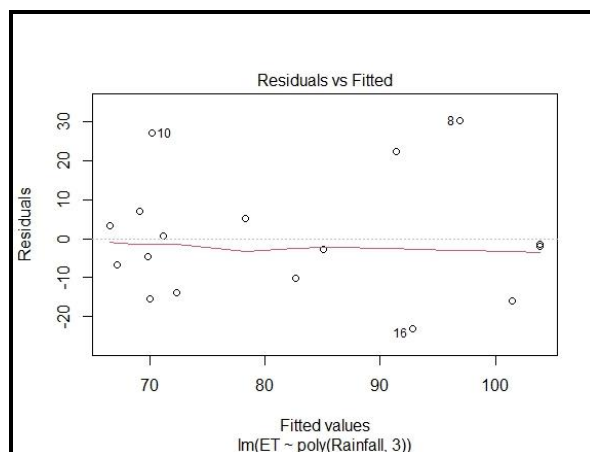
Fig. 4.85. The Residual vs. Fitted Plot between Rainfall and Evapotranspiration for the Perassannur Watershed

Fig. 4.86, Fig. 4.87, Fig. 4.88, and Fig. 4.89 show the Normal Q-Q plot between rainfall and runoff, rainfall and soil moisture, rainfall and height of GW table, rainfall and evapotranspiration, respectively, for the Perassannur watershed. The x-axis indicates the theoretical quantities of the water balance component, and the y-axis indicates the standardised residuals. All these figures show three outliers in each graph, by the numbers, which means the month starting from August 2021.
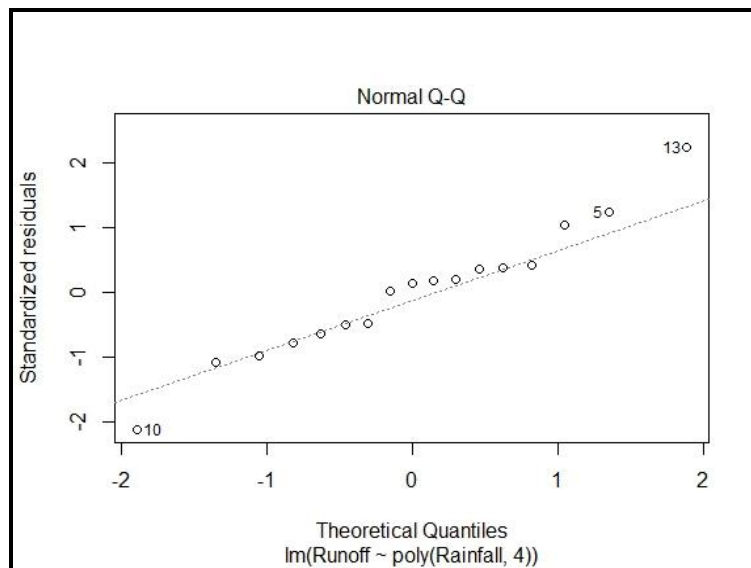
Fig. 4.86. The Normal Q-Q Plot between Rainfall and Runoff for the Perassannur Watershed
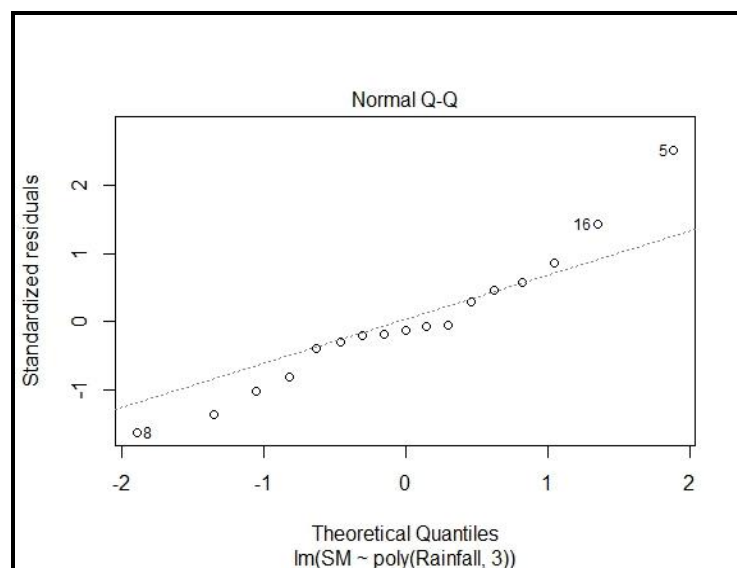
Fig. 4.87. The Normal Q-Q Plot between Rainfall and Soil Moisture for the Perassannur Watershed
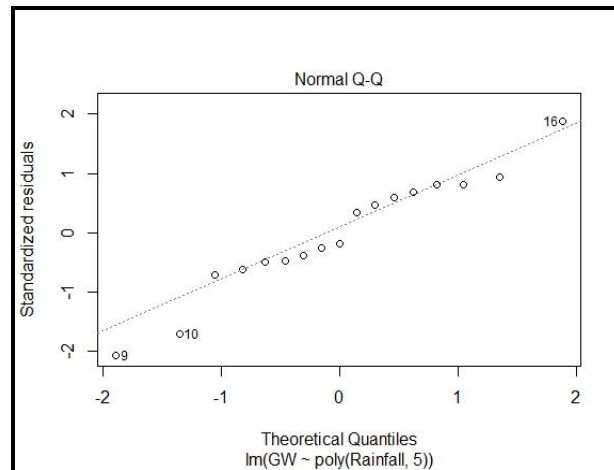
Fig. 4.88. The Normal Q-Q Plot between Rainfall and Height of GW Table for the Perassannur Watershed
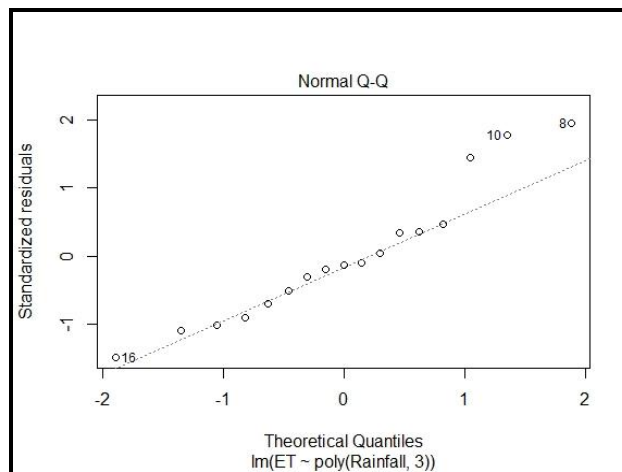
Fig. 4.89. The Normal Q-Q Plot between Rainfall and Evapotranspiration for the Perassannur Watershed

4.15.2 Monthly Rainfall vs. Water Balance Components for the Painkanoor Sub-watershed

Fig. 4.90 shows the Pearson's correlation coefficient (r) between the monthly water balance components for the Painkanoor sub-watershed. It was observed that 'r' between rainfall and runoff was 0.81, rainfall and soil moisture was 0.65, rainfall and height of GW table was 0.72, and rainfall and evapotranspiration was -0.61. Pearson's correlation coefficient was also observed as 0.88 between runoff and soil moisture, 0.90 between runoff and height of GW table, and -0.75 between runoff and ET. The 'r' value between soil moisture and height of GW table was 0.94, and between soil moisture and ET was -0.92. Also, the 'r' value between height of GW

table and ET was -0.86. This indicates that evapotranspiration has a negative correlation with other water balance components. The values of 'r' between monthly rainfall and runoff stated a very good correlation, rainfall and soil moisture indicated a good correlation and rainfall and height of GW table showed a good correlation. In contrast, rainfall and ET depicted a weak correlation.
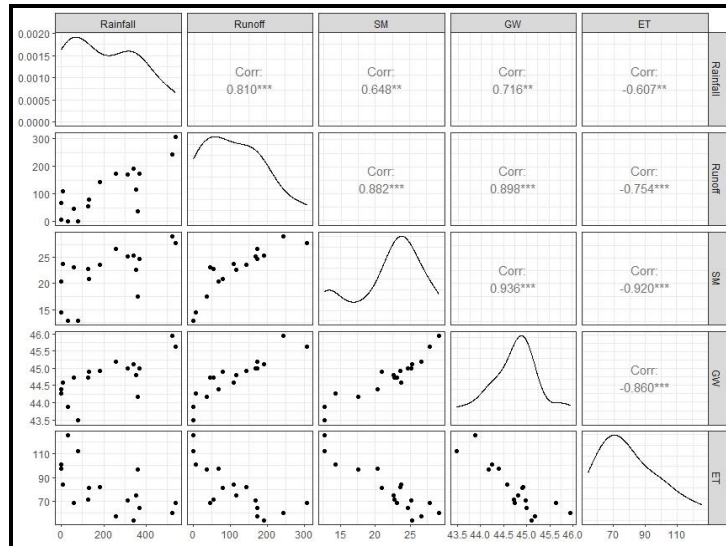
Fig. 4.90. Pearson's Correlation Coefficient for Monthly Water Balance Components for the Painkanoor Sub-watershed

The polynomial non-linear regression model was developed between monthly rainfall vs. runoff, rainfall vs. soil moisture, rainfall vs. height of GW table, and rainfall vs. ET with a 95% confidence interval for the Painkanoor sub-watershed as shown in Fig. 4.91, Fig. 4.92, Fig. 4.93, and Fig. 4.94, respectively.

The relationship between monthly rainfall vs. runoff for the Painkanoor sub-watershed is given by Eq. 4.5, with R^2 of 0.82 and p-value of 0.0002, F-statistic of 13.50 on 4, and 12 degrees of freedom.

$$127.59x^4 + 30.98x^3 + 56.92x^2 + 287.71x + 113.21 = 0 \quad ..... (Eq. 4.5)$$

The relation between monthly rainfall vs. soil moisture for the Painkanoor sub-watershed is given by Eq. 4.6, with R^2 of 0.53 and p-value of 0.04, F-statistic of 3.40 on 4, and 12 degrees of freedom.

$$6.21x^4 + 2.34x^3 - 0.10x^2 + 12.86x + 21.96 = 0 \quad ..... (Eq. 4.6)$$

The monthly rainfall vs. height of GW table relationship for the Painkanoor sub-watershed is given by Eq. 4.7, with R^2 of 0.66 and p-value of 0.008, F-statistic of 5.75 on 4, and 12 degrees of freedom.

$$0.75\,x^4 + 0.42\,x^3 + 0.31\,x^2 + 1.73\,x + 44.75 = 0 \quad ..... (Eq.\,4.7)$$

Monthly rainfall vs. evapotranspiration for the Painkanoor sub-watershed is given by Eq. 4.8, with R^2 of 0.41 and p-value of 0.02, F-statistic of 4.95 on 2, and 14 degrees of freedom.

$$17.19\,x^2 - 48.60\,x + 80.65 = 0 \quad ..... (Eq.\,4.8)$$
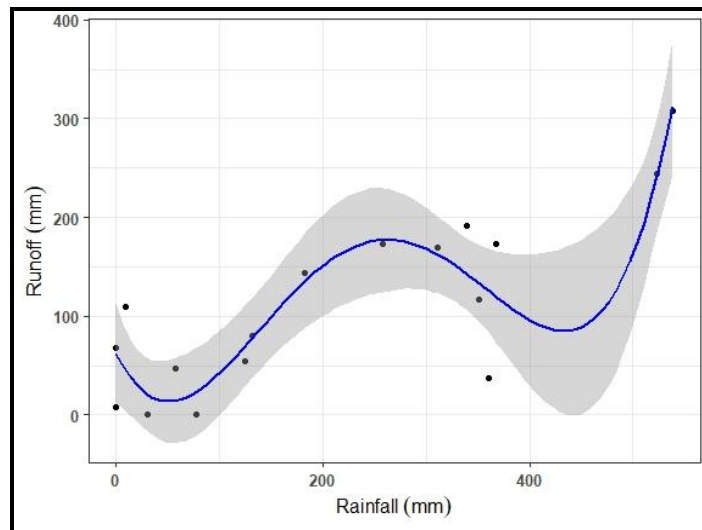
Fig. 4.91: Monthly Rainfall vs. Runoff for the Painkanoor Sub-watershed
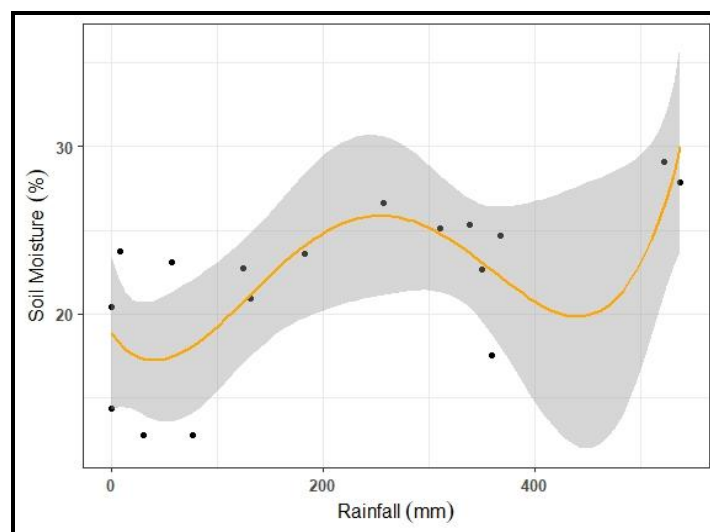
Fig. 4.92: Monthly Rainfall vs. Soil Moisture for the Painkanoor Sub-watershed
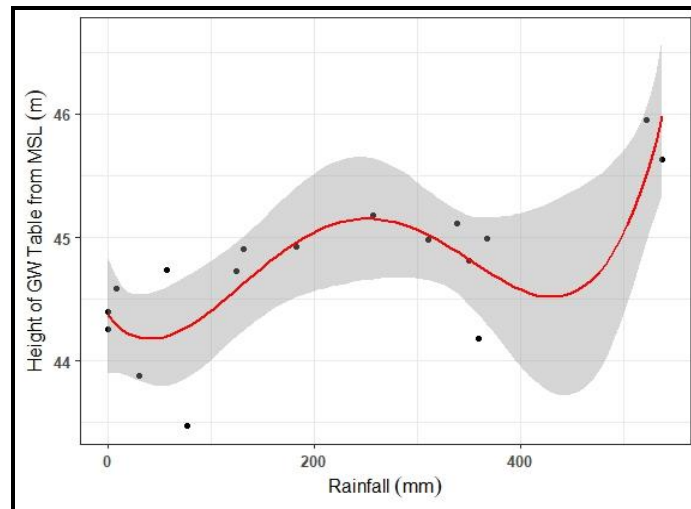
Fig. 4.93: Monthly Rainfall vs. Height of GW Table for the Painkanoor Sub-watershed
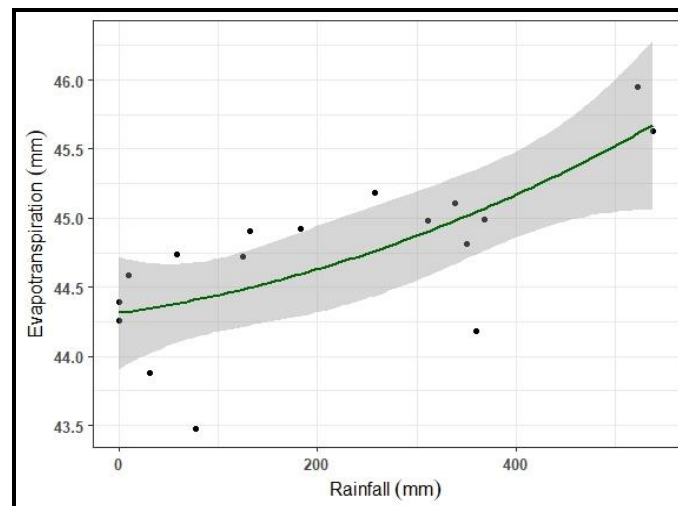
Fig. 4.94: Monthly Rainfall vs. ET for the Painkanoor Sub-watershed

Fig. 4.95, Fig. 4.96, Fig. 4.97, and Fig. 4.98 show the residual vs. fitted plot between rainfall and runoff, rainfall and soil moisture, rainfall and height of GW table, rainfall and evapotranspiration, respectively, for the Painkanoor sub-watershed. The x-axis indicates the monthly values of the water balance components, and the y-axis indicates the residuals. All these graphs show that the fitted line is not a straight line passing through zero residual, which suggests that there is non-linearity between the plotted variables. Also, the three outliers are shown in each graph, by the numbers which indicate the month starting from August 2021.
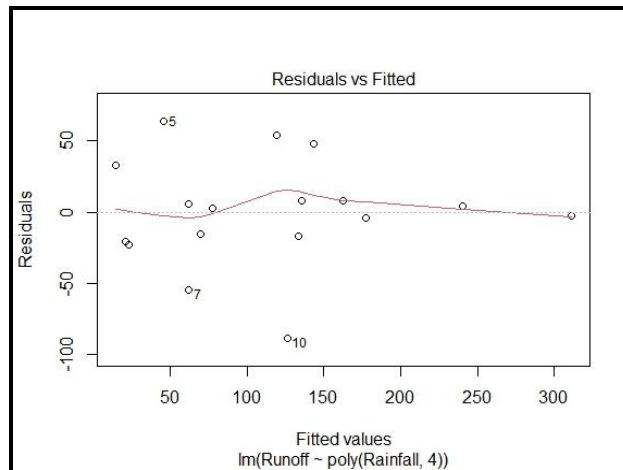
Fig. 4.95. The Residual vs. Fitted Plot between Rainfall and Runoff for the Painkanoor Sub-watershed
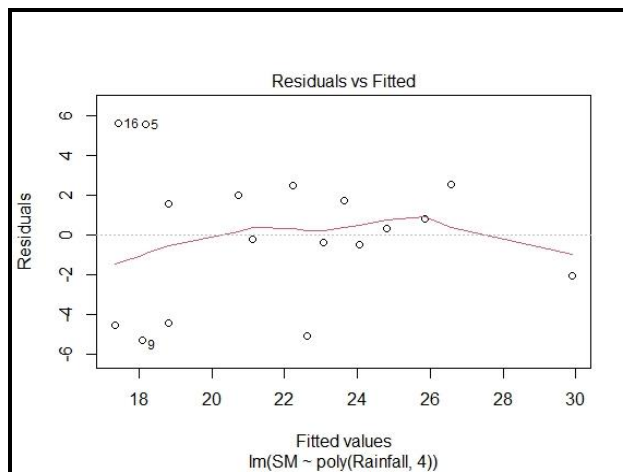
Fig. 4.96. The Residual vs. Fitted Plot between Rainfall and Soil Moisture for the Painkanoor Sub-watershed
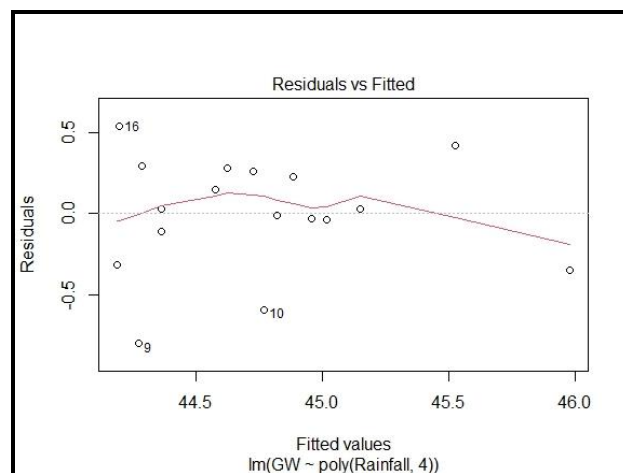
Fig. 4.97. The Residual vs. Fitted Plot between Rainfall and Height of GW Table for the Painkanoor Sub-watershed
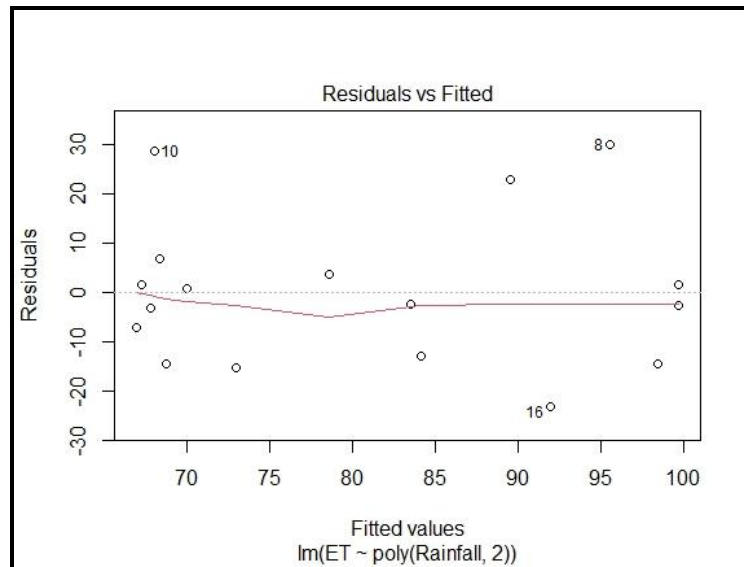
Fig. 4.98. The Residual vs. Fitted Plot between Rainfall and Evapotranspiration for the Painkanoor Sub-watershed

Fig. 4.99, Fig. 4.100, Fig. 4.101, and Fig. 4.102 show the Normal Q-Q plot between rainfall and runoff, rainfall and soil moisture, rainfall and height of GW table, rainfall and evapotranspiration, respectively. The x-axis indicates the theoretical quantities of the water balance component, and the y-axis indicates the standardised residuals. All these figures show three outliers in each graph, which means the month starting from August 2021
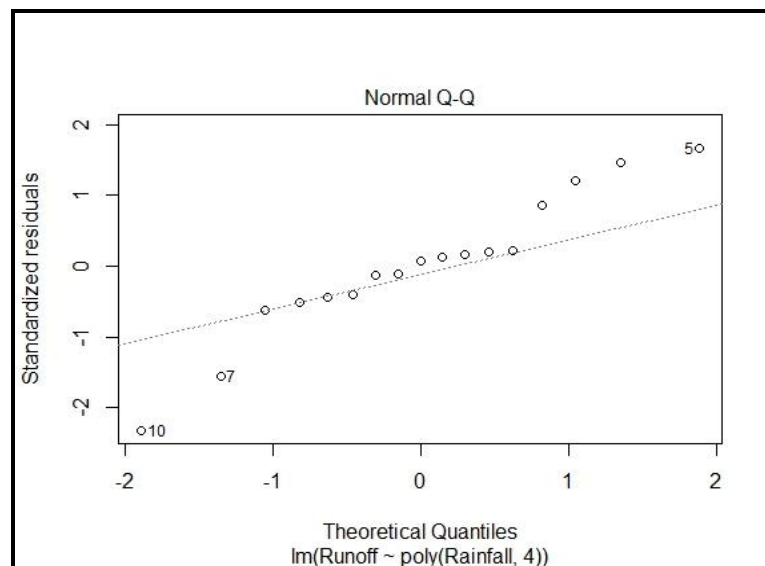
Fig. 4.99. The Normal Q-Q Plot between Rainfall and Runoff for the Painkanoor Sub-watershed
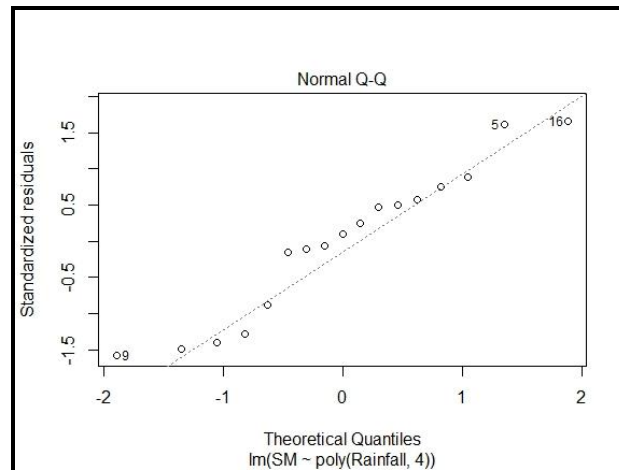
Fig. 4.100. The Normal Q-Q Plot between Rainfall and Soil Moisture for the Painkanoor Sub-watershed
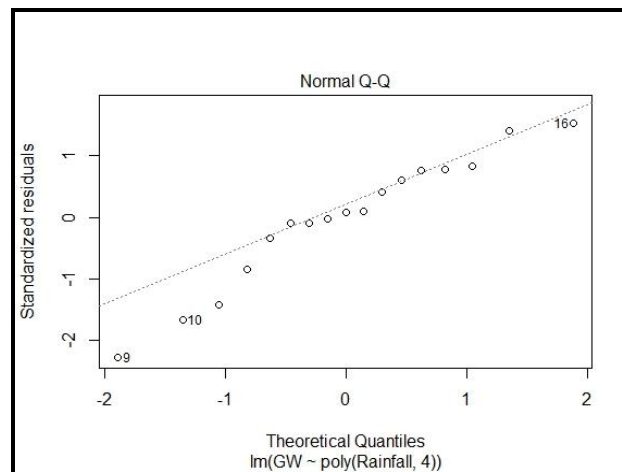
Fig. 4.101. The Normal Q-Q Plot between Rainfall and Height of GW Table for the Painkanoor Sub-watershed
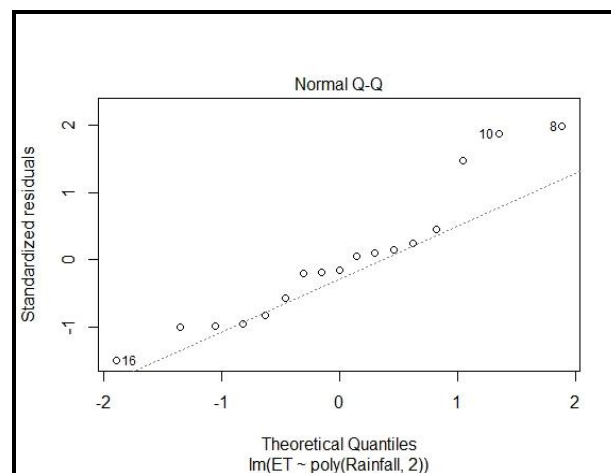
Fig. 4.102. The Normal Q-Q Plot between Rainfall and Evapotranspiration for the Painkanoor Sub-watershed

4.15.3 Weekly Rainfall vs. Water Balance Components for the Perassannur Watershed

Fig. 4.103 shows the Pearson's correlation coefficient (r) between the weekly water balance components for the Perassannur watershed. It was observed that 'r' between rainfall and runoff was 0.62, rainfall and soil moisture was 0.65, rainfall and height of GW table was 0.59, and rainfall and evapotranspiration was -0.56. Pearson's correlation coefficient was also observed as 0.70 between runoff and soil moisture, 0.78 between runoff and height of GW table, and -0.64 between runoff and ET. The 'r' value between soil moisture and height of GW table was 0.65, and between soil moisture and ET was -0.79. Also, the 'r' value between height of GW table and ET was -0.76. This indicates that evapotranspiration has a negative correlation with other water balance components. The values of 'r' between monthly rainfall and runoff, rainfall and soil moisture, rainfall and height of GW table, and rainfall and ET have a value of less than 0.7, which shows a weak correlation. Thus, it is not possible to develop an acceptable relationship between weekly rainfall and water balance components for the Perassannur watershed.
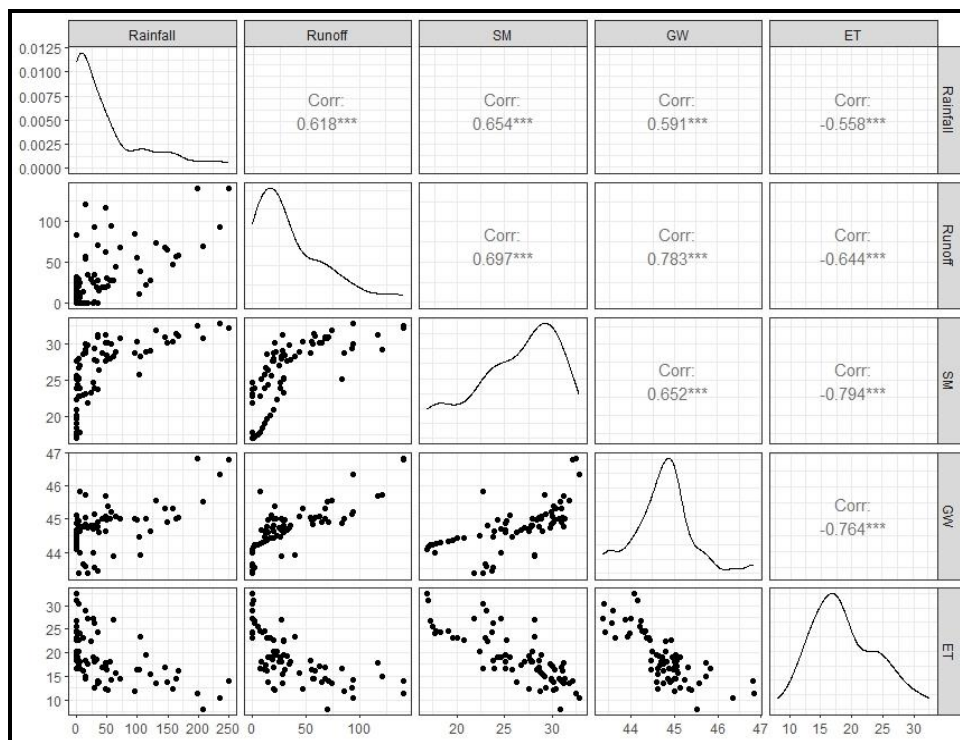
Fig. 4.103. Pearson's Correlation Coefficient for Weekly Water Balance Components for the Perassannur Watershed

4.15.4 Weekly Rainfall and Water Balance Components for the Painkanoor Sub-watershed

Fig. 4.104 shows the Pearson's correlation coefficient (r) between the weekly water balance components for the Painkanoor sub-watershed. It was observed that 'r' between rainfall and runoff was 0.67, rainfall and soil moisture was 0.54, rainfall and height of GW table was 0.60, and rainfall and evapotranspiration was -0.55. Pearson's correlation coefficient was also observed as 0.79 between runoff and soil moisture, 0.81 between runoff and height of GW table, and -0.63 between runoff and ET. The 'r' value between soil moisture and height of GW table was 0.83, and between soil moisture and ET was -0.82. Also, the 'r' value between height of GW table and ET was -0.77. This shows that evapotranspiration has a negative correlation with other water balance components. The values of 'r' between weekly rainfall and runoff, rainfall and soil moisture, rainfall and height of GW table, and rainfall and ET have values less than 0.7, which shows a weak correlation. Thus, it is not possible to develop an acceptable relationship between monthly rainfall and water balance components for the Painkanoor sub-watershed.
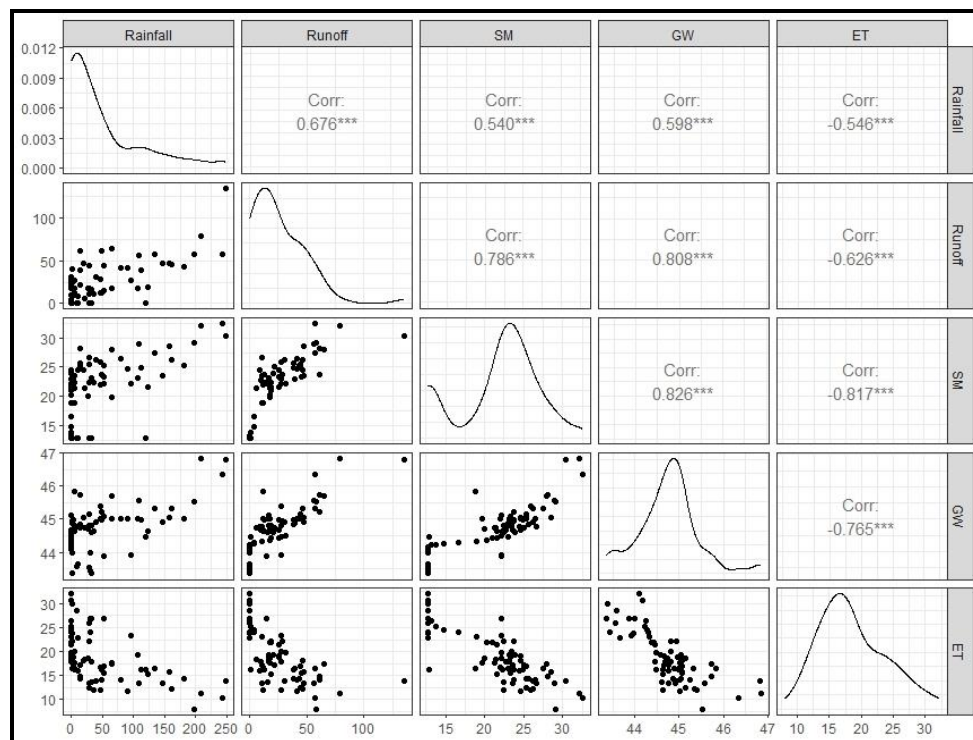
Fig. 4.104. Pearson's Correlation Coefficient for Weekly Water Balance Components for the Painkanoor Sub-watershed

4.16 SUGGESTIONS FOR SCIENTIFIC WATER MANAGEMENT PRACTICES

4.16.1 Salient Insights Obtained from the Study for Planning Scientific Water Conservation Practices

The results of this study have shown that the relief or elevation of the study area ranges from 5 to 161 m, with land slope ranging from 2 to 35%. The major slope classes of the area were identified as 3-6%, 6-9%, and 9-12%. About 62% of the total area was lying in the above-mentioned slope groups; areas with above 12% slope were about 25%, and areas below 3% slope were about 12%. The soil was lateritic with a high infiltration rate, and the soil depth in most places was above 2 m. The area's geology comprises stable, undivided Precambrian rock and Neogene sedimentary rock. Primary land uses of the watershed consist of coconut-based mono-crop and mixed crop, scrubs, forest and barren lands in the upland areas and paddy in the lowland areas. The mean depth of the water table in most of the upland area was more than 5 m deep.

Hydrological data of the watershed indicated that the monthly rainfall lies between 200-500 mm during the monsoon months from June to October, and the summer showers are marginal. ET during the monsoon months vary from 50 to 80 mm and 100 to 130 mm in summer months. The height of GW table was more than 8 m deep in the summer months, in about 45% of the total watershed area. It was more than 5 m deep in about 20% of the area. Further, results showed that the mean monthly soil moisture depletion rates during the post-monsoon season were 2.45, 1.83 and 1.39 mm day^{-1} for December, January, and February, respectively. The mean monthly GW depletion rates were 3.74, 2.84 and 5.5 mm day^{-1} for December, January and February, respectively. This shows tremendous scope for decreasing the height of GW table through appropriate water conservation measures. The mean monthly discharges through the watershed outlet were 8, 4, 2 and 1 m^{3}s^{-1} from November to February, respectively. From March to May, there is no flow in the stream, even at its outlet, which indicates that baseflow ceases by then.

4.16.2 Broad Scientific Water Conservation Measures

All possible measures should be undertaken for augmentation of the natural groundwater recharge, such as roof water harvesting and recharging below root zone depth from all residential and commercial buildings, constructing percolation pits to a depth below root zone depth and diverting concentrated surface runoff to it, construction of off-stream ponds on the bank of drain channels and redirect a part of streamflow to it, barren lands and boundary of private holdings need be planted with deep-rooted trees to facilitate deep percolation, stream discharge need to be reduced during the post-monsoon season so that GW storage will be lasting longer to cover the entire summer period.

The interventions could be such as the installation of a series of fixed sill level check dams in the streams for its first 15 m long; for the rest of the down reach, variable sill check dams can be constructed to allow seamless flow during monsoon and flow regulation during post-monsoon season. Any rise in the water level in the stream will lessen the baseflow discharge entering the stream. The baseflow is directly proportional to the hydraulic gradient. Hence, any rise in water level will decrease the hydraulic gradient of flow from the land area to the channel. The 1 m rise in water level in the stream would reduce the hydraulic gradient towards the mainstream by 0.001 for the study area as the lateral distance from the stream to the ridge is about 1 km. The rise of the water level in the stream will enhance the recharge into the neighbourhood aquifer storage.

About 20% of the watershed area is relatively low-lying paddy fields. In summer, most of the paddy fields remain as summer fallows. The watershed has ample scope for increasing summer paddy cultivation through water conservation and harvesting. For example, If cultivation is extended to about 25% of the summer fallow paddy fields, i.e. to 4 km^2 (400 ha), the water requirement would be about 400 x 10^4 x 0.5, which is 2 Mm^3 per crop season. Its water equivalent in-depth terms for the entire watershed would be 2.5 cm. The incremental rise required for the water table to meet this additional water requirement would be 25 cm, assuming a specific yield of 10% for the unconfined aquifer.

Both morphological and water balance information can be utilised to plan land treatment measures. SWAT model predicts considerable surface runoff, and hence, efforts should be made to check or reduce this runoff through infiltration enhancement measures. Between 3 to 9% slope area, there are about 46% land areas; bunding and trenching would be suggested in these areas. All the lands lying between the slope of 9 to 25% need slope modification, for which terraces with partial cutting and filling would be suggested.

4.16.3 Specific Water Harvesting Measures

4.16.3.1 Roof Water Harvesting

The results of the study show that if groundwater recharging is given in a distributed manner in the upland areas of the watershed, it can enhance groundwater storage and, in turn, it will improve the lean flow in the drainage channels. There is much surplus rainfall in the watershed after meeting the ET requirement, and hence, roof water harvesting can be successfully adopted. All areas above 15 m elevation can be suggested for roof water harvesting and groundwater recharge.

4.16.3.2 Water Conservation Measures for Drainage Channels

The longevity of baseflow is very short as it ceases about one month after the stop of the rainfall. The water depth in the channel can be increased by making small check dams right from the top region of the channel origin. The main channel has a length of about 14 km. Up to a reach of about 6 km, it can be given with pervious check dams so that groundwater recharge will increase. A water table rise of about 2 m from the existing scenario is feasible in all areas whose elevation is above 15 m. One metre rise of water level in the drain can also raise the water table by 1 m in the neighbouring places, enhancing groundwater storage at 1000 m^3ha^{-1} land area. Beyond the 6 km to 10 km reach of the main channel, cement concrete check dams of 1 m height can be constructed. Beyond the 10 km reach of the main channel to the outlet, Vented Cross Bars (VCBs) of 1.5 m to 2.0 m height can be planned.

The sites suitable for water harvesting structures in the study area were identified and shown in Fig. 4.105. A total of 21 sites were found to be ideal for permanent water conservation structures, which included three sites suitable for

VCBs, six for concrete check dams, and the remaining for pervious check dams in the entire study area. The water storage potential of these water conservation structures ranged from 0.01 to 0.14 Mm^3, as shown in Table 4.20. Also, 1407 sites were found suitable for soil/stone bunds, as shown in Fig. 4.105, which had a water storage potential of 0.93 Mm^3. The gross water storage achieved by all these drainge line treatment measures was about 2.27% of runoff.
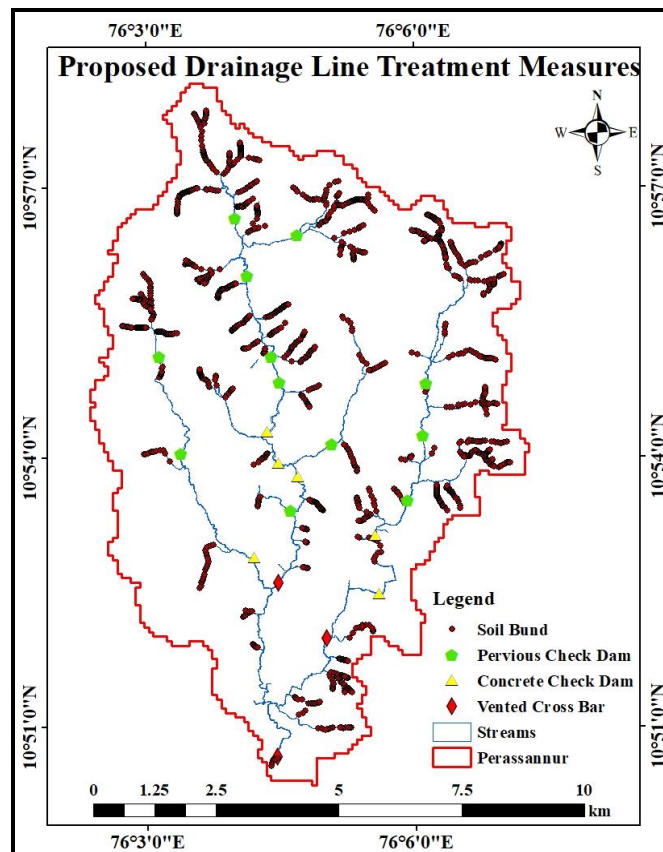
Fig. 4.105. Sites Suitable for Drainage Line Treatment Measures

In addition to check dams and VCBs, about 28 farm ponds were suggested near the lands having paddy, coconut and mixed vegetation. The cumulative storage volume of these farm ponds would come to 0.11 Mm^3, and the same can be utilised for irrigation. Also, 132 roof water harvesting structures were proposed for large institutional buildings having a roof area larger than 500 m^2. Most of these buildings were government offices, schools, colleges, etc., having ample space near their surroundings for making recharge structures. The sites suitable for these water harvesting measures are shown in Fig. 4.106.

Table 4.20: Volume of Water Stored by Water Conservation Structure

Sr. No.	Volume of Water Storage (m^3)	Volume of Water Storage ($M.m^3$)	Water Conservation Structure
1.	144023.62	0.14	Vented Cross Bar
2.	33973.05	0.03	
3.	33953.29	0.03	
4.	31655.69	0.03	Concrete Check Dam
5.	31541.09	0.03	
6.	30304.21	0.03	
7.	29798.04	0.03	
8.	28419.11	0.03	
9.	27361.40	0.03	
10.	25312.11	0.03	Pervious Check Dam
11.	22274.03	0.02	
12.	21948.09	0.02	
13.	19563.11	0.02	
14.	18644.58	0.02	
15.	15623.03	0.02	
16.	14602.24	0.01	
17.	14559.76	0.01	
18.	14488.02	0.01	
19.	14350.54	0.01	
20.	13017.44	0.01	
21.	12104.47	0.01	
Total	**597516.92**	**0.60**	

4.16.3.4 Specific Land Treatment Measures

As land treatment measures, graded contour bunds were suggested for an area of 2.66 km^2, where the land use was mixed cropping and coconut cultivation with a slope up to 9%. The staggered contour trenches were proposed for an area of 4.59 km^2, having pitches up to 9%, which are mainly comprised of mixed cropping, coconut, and rubber cultivation. The barren land and the land with scrubs in an area of 11.72 km^2, having a slope of 9 to 33%, were proposed to have terraces. The sites suitable for all these land treatment measures are shown in Fig. 4.107.
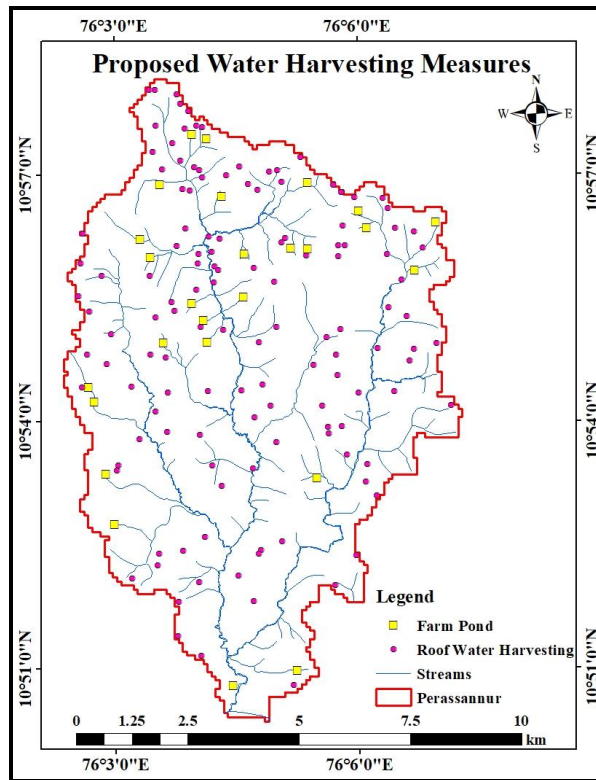
Fig. 4.106. Sites Suitable for Water Harvesting Measures
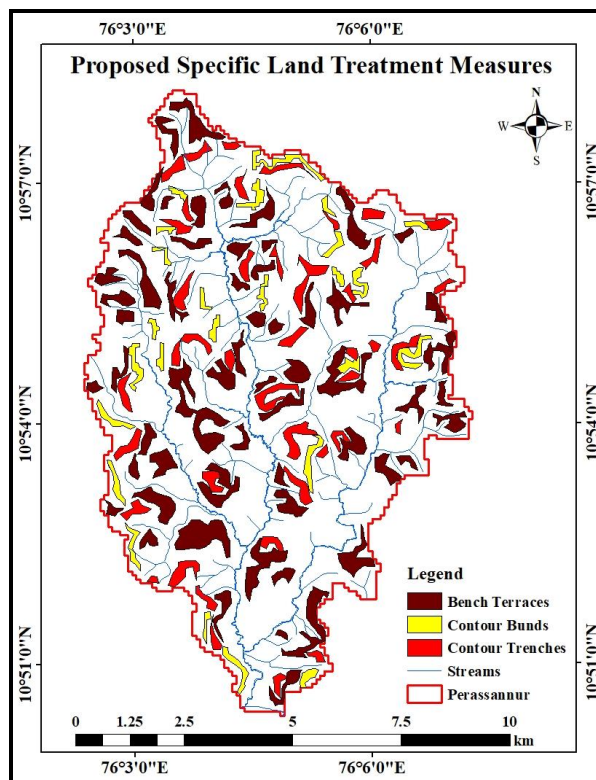
Fig. 4.107. Sites Suitable for Specific Land Treatment Measures

CHAPTER - V
SUMMARY AND CONCLUSIONS

This study entitled "Determination of water balance components of a micro watershed for improved water management practices" has been conducted with specific objectives of determination of water balance components, development of the relationship between monthly rainfall and water balance components, and suggestion of scientific water management practices for the watershed. The study's findings are summarised and concluded in the following sections of this Chapter.

5.1 SUMMARY

Water is the most essential natural resource for the survival of life on the earth. However, water scarcity is a severe issue requiring immediate attention from planners, the scientific community, and administrators. The incidents of water shortage are prevalent even in areas with high annual rainfall. The uneven distribution of rainfall, poor water conservation, and management are the primary reasons for this scarcity. The state of Kerala is a typical example of water scarcity in the midst of high annual rainfall. There are also places with water surpluses during the rainy season, and this issue also needs proper attention. Scientific water management practices (conservation, judicious utilisation, and safe disposal of the rest) are the only solution to mitigate the above-said water woes.

A water balance study with an appropriate temporal scale can reveal the ground realities of various inflow, outflow, and storage positions of a hydrologic unit, usually a watershed. This information can provide necessary inputs to scientific water management practices. A water balance study can provide valuable information such as rainfall input, runoff and evapotranspiration as output, soil moisture and groundwater storages within the watershed. The study focused on a watershed-level analysis to quantify the various components of the hydrologic processes related to the water balance.

The study was conducted in a sub-watershed of River Bharathapuzha, which has a geographical area of 79.66 km^2, encompassing the Valanchery municipal

town. The mainstream of the sub-watershed joins with the river Bharathapuzha at Perassannur in Kuttippuram block Panchayats, and hence, it was named the 'Perassannur watershed'. The length of the study watershed was 14.45 km, with a width of 9.06 km and a perimeter of 56.60 km. The maximum elevation difference was 161 m. The study was also replicated on another smaller watershed, 'Painkanoor sub-watershed', having an area of 35.36 km^2, length of 10.95 km, width of 6.19 km, and perimeter of 38.90 km, located between 5 to 151 m above mean sea level. The mean annual rainfall of the study area was 2582 mm, and the land use mainly comprised of paddy, mixed crop, and coconut plantation. The watershed comprises six soil series, predominantly the Irimbiliyam and Vettakode soil series.

Four tipping bucket rain gauges were established to measure the rainfall at the one minute interval and aggregated to get one hour rainfall. For runoff measurement, two gauging stations were established at the outlet of the Perassannur and Painkanoor sub-watersheds, and the discharge was determined using the area-velocity method. The rating curve was prepared to assess discharge from the continuously measured depth of flow data. The soil moisture was measured using capacitance-based and resistance-based automatic soil moisture meters. The height of the GW table was continuously monitored using a hydrostatic pressure-based automated water level recorder. The evapotranspiration was estimated using the PM method and also by the WB method.

The highest stream order was 4 for the Perassannur watershed, while for the Painkanoor sub-watershed, it was 3. For the Perassannur watershed, an area of 62.05% was covered in the elevation band of 15-70 m and an area of 61.20% was covered in the slope of 3-12%. For the Painkanoor sub-watershed, the area of 61.79% was covered in the elevation of 15-70 m, and the area of 62.73% was covered in the slope range of 3-12%. The geology of the study area consisted of undivided Precambrian rock and the Neogene sedimentary rock.

The mean annual rainfall, recorded by four rain gauges, was 2582 mm. The highest monthly rainfall was 529 mm, while the highest weekly rainfall was 250 mm. It was found that there were variations in rain catches between the rain gauge

stations, though they were placed in close geographical separation of about 3 km. However, the ANOVA test revealed that the observed variation was statistically insignificant.

The major component of water outflow from the watershed was runoff (with an average annual value of 125 mm). The percentage of runoff to annual rainfall was 68%, with the highest monthly runoff of 13.30 m^3s^{-1} at Perassannur and 9.95 m^3s^{-1} at the Painkanoor section, respectively. The maximum weekly runoff at section Perassannur went up to 18.52 m^3s^{-1}, reaching 7.88 m^3s^{-1} at section Painkanoor. The average soil moisture of root zone depth (1.5 m) varied from 17% to 31% on a volume basis. The variation of soil moisture between different depths showed that measurement at 0.5 m depth showed the lowest soil moisture content in all cases. The soil moisture depletion rate in summer months varied between 2.45 to 1.39 mm day^{-1}. The monthly height of the GW table from MSL ranged from 45.63 m to 43.48 m. The mean monthly GW depletion rates were 3.74, 2.84 and 5.5 mm day^{-1} from December to February, respectively. The ET was computed from climatological data using the PM method and had an average annual value of 87 mm, with the percentage of ET to yearly rainfall of 40%. The monthly ET ranged from 127.2 mm to 54.7 mm. The ET computed using climatological data and the water balance equation showed close similarity.

The SWAT model was also used to estimate the more detailed water balance components of the watershed. The land use map, soil map, and slope map were reclassified in the SWAT model and used as input for running the model. There were seven sub-watersheds and 439 HRUs defined for the study watershed. The predictive accuracy of the SWAT model for runoff was found to be very good with R^2 of 0.97, NSE 0.96, PBIAS 2.60, and RSR of 0.20 for the Perassannur watershed, while R^2 of 0.95, NSE 0.94, PBIAS 5.40, and RSR of 0.25 for the Painkanoor sub-watershed.

The water balance components given by the SWAT model for the Perassannur watershed showed that 32.96% of water outflow was surface runoff, 0.82% was lateral flow, and 29.14% was base flow. The ET was 30.16%, and deep

aquifer recharge was 6.94%. At the same time, the water outflow of the Painkanoor sub-watershed consisted of 39.26% as surface runoff, 0.83% as lateral flow, and 27.50% as base flow. The ET was 32.05%, and deep aquifer recharge was 0.36%.

The monthly relationship for the Perassannur watershed between rainfall and other water balance components was non-linear. The relationship between rainfall-runoff, rainfall-soil moisture, rainfall-height of GW, and rainfall-ET was polynomial having degree 4, 3, 5, and 3, respectively. The Painkanoor sub-watershed had a monthly relationship as a polynomial equation of degrees 4, 4, 4, and 2 for rainfall-runoff, rainfall-soil moisture, rainfall-height of GW table, and rainfall-ET, respectively. The relationship between rainfall-runoff, rainfall-soil moisture, and rainfall-height of the GW table gave satisfactory results. The weekly relationships gave unsatisfactory results for the Perassannur watershed and the Painkanoor sub-watershed.

The results of this study indicated that from March to May, there was no flow in the streams, which suggests that base flow ceased by then. It is found that there is tremendous scope for raising the GW table through appropriate water conservation measures. The rate of flow or velocity of flow in the channel needs to be slowed down, and also, the flow depth be increased to retard the groundwater discharge as baseflow. To address these requirements, groundwater recharge must be augmented through roof water harvesting and recharge, and land treatment measures. Pervious check dams, cement concrete check dams and vented cross bars are required in the drainage channels in the upper reaches, middle and lower reaches of the main drainage channel. About 21 sites have been identified for the permanent water conservation structures, and they can make a cumulative storage of 0.93 Mm^3, which would make about 2.27% of the total annual runoff. Sites for 28 off-stream farm ponds have also been identified with a cumulative storage of 0.11 Mm^3. Further, 132 sites for roof water harvesting were identified for institutional-type buildings.

5.2 CONCLUSIONS

The following conclusions can be drawn from the study:

- About 98% of rainfall received by the watershed is exited by runoff and ET, with a runoff share of 68%. The GW depletion rate is speedy, and the height of GW table is deep. All these show the need for more GW recharge wherever possible and reducing the discharge of streams through appropriate interventions.

- To provide a lean flow of 1 m^3s^{-1} during the three summer months (March to May), an additional groundwater storage of 8.01 Mm^3 is required. This can be achieved by another recharge corresponding to a depth of 10 cm of water throughout the basin area. The same result can be achieved by decreasing the runoff rate during October, November and December by about 1 m^3s^{-1}. If lean flow can be extended to the three months (March to May) of extreme summer, it can have immense social and environmental benefits.

- A channel discharge rate of 1 m^3s^{-1} for one month would need 2.67 Mm^3 of groundwater storage. This is equivalent to water released from a saturated aquifer thickness of 33 cm. A groundwater recharge of 3.3 cm depth of rainwater can facilitate a groundwater rise of 33 cm.

- An incremental rise of the GW table of 25 cm can provide about 2 Mm^3 of additional baseflow, using which about 400 ha of summer paddy fallow fields can be irrigated.

- The climatologically estimated ET and water balance based ET showed close comparison. Hence, ET can also be determined with reasonable accuracy from water balance components if accurate rainfall and runoff measurements are available.

5.3 FUTURE SCOPE

The future scope of the study is as follows:

- The study needs to be continued for at least five years so that sufficient primary data would be available and its analysis could lead to more reliable results and recommendations.

- Flow gauging, SM, and GW table measurements must be done at more places in the watershed to get more representative data on the water balance components.

- A study on the impact of land use and climate change on the water balance may be carried out.

- A detailed study of the soil, nutrient loss, and sedimentation can be taken up.

REFERENCES

Abbaspour, K.C., Rouholahnejad, E., Vaghefi, Srinivasan, R., Yang, H., and Kluve, B. 2015. A continental-scale hydrology and water quality model for Europe: Calibration and uncertainty of a high-resolution large-scale SWAT model. *J. Hydrol*. 524: 733-752.

Abbaspour, K.C., Vejdani, M., Haghighat, S., and Yang, J. 2007. *SWAT-CUP calibration and uncertainty programs for SWAT*. In MODSIM 2007 international congress on modelling and simulation, modelling and simulation society of Australia and New Zealand, Dubendorf, Switzerland: Swiss Federal Institute of Aquatic Science and Technology, pp. 1596-1602

Abdulla, F. and Al-Shurafat, A.W. 2020. Rainfall-Runoff modeling for Semi-arid and trans-boundary Yarmouk River Basin. *Proc. Manuf.*, 44: 180-188.

Abdulla, F., Eshtawi, T., and Assaf, H. 2009. Assessment of the impact of potential climate change on the water balance of a semi-arid watershed. *Water Resour. Manag*. 23: 2051-2068.

Alavinia, M., Saleh, F.N., and Asadi, H. 2019. Effects of rainfall patterns on runoff and rainfall-induced erosion. *Int. J. Sedim. Resour*. 34(3): 270-278.

Allen, R.G., Pereira, L.S., Raes, D., and Smith, M. 1998. *FAO Irrigation and Drainage Paper No. 56 Crop Evapotranspiration* (Guidelines for Computing Crop Water Requirements), FAO - Food and Agriculture Organization of the United Nations, Rome.

Alvarez-Garreton, C., Ryu, D., Western, A.W., Crow, W.T., and Robertson, D.E. 2014. The impacts of assimilating satellite soil moisture into a rainfall–runoff model in a semi-arid catchment. *J. Hydrol.* 519: 2763-2774.

Al-Wagdany, A.S. 2020. Intensity-duration-frequency curve derivation from different rain gauge records. *J. King Saud Uni.-Sci*. 32(8): 3421-3431.

Arnold, J.G., Allen, P.M., and Bernhardt, G. 1993. A comprehensive surface-groundwater flow model. *J. Hydrol.* 142(1-4): 47-69.

Arnold, J.G. and Allen, P.M. 1996. Estimating hydrologic budgets for three Illinois watersheds. *J. Hydrol*. 176(1-4): 57-77.

Arnold, J.G., Kiniry, J.R., Srinivasan, R., Williams, J.R., Haney, E.B., and Neitsch, S.L. 2012. *Soil and water assessment tool input/output documentation version 2012*. Texas water resources institute, 7.

Arnold, J.G., Srinivasan, R., Muttiah, R.S., and Williams, J.R. 1998. Large area hydrologic modeling and assessment part I: model development 1. *Amer. Water Res. Assoc.* 34(1): 73-89.

Awan, U.K. and Ismaeel, A. 2014. A new technique to map groundwater recharge in irrigated areas using a SWAT model under changing climate. *J. Hydrol.* 519: 1368-1382.

Ayivi, F. and Jha, M.K. 2018. Estimation of water balance and water yield in the Reedy Fork-Buffalo Creek Watershed in North Carolina using SWAT. *Int. Soil Water Conserv. Res*. 6(3): 203-213.

Bonuma, N.B., Rossi, C.G., and Arnold, J.G. 2013. Hydrology evaluation of the Soil and Water Assessment Tool considering measurement uncertainty for a small watershed in Southern Brazil. *Appl. Eng. Agric*. 29(2): 189-200.

Briak, H., Moussadek, R., Aboumaria, K., and Mrabet, R. 2016. Assessing sediment yield in Kalaya gauged watershed (Northern Morocco) using GIS and SWAT model. *Int. Soil Water Conserv. Res.* 4(3): 177-185.

Calamita, G., Brocca, L., Perrone, A., Piscitelli, S., Lapenna, V., Melone, F., and Moramarco, T. 2012. Electrical resistivity and TDR methods for soil moisture estimation in central Italy test-sites. *J. Hydrol.* 454: 101-112.

Campos, I., González-Piqueras, J., Carrara, A., Villodre, J., and Calera, A. 2016. Estimation of total available water in the soil layer by integrating actual evapotranspiration data in a remote sensing-driven soil water balance. *J. Hydrol.* 534: 427-439.

Carlesso, R., Spohr, R.B., Eltz, F.L.F., and Flores, C.H. 2011. Runoff estimation in southern Brazil based on Smith's modified model and the Curve Number method. *Agric. Water Manag*. 98(6): 1020-1026.

Chang, C.M., Yeh, H.D., and Chuang, M.H. 2019. Spectral analysis of temporal variability of nonlinear and nonstationary rainfall-runoff processes. *J. Hydrol.* 575: 1301-1307.

Chauhan, A., Kumari, S., Deva, M.U., and Shankar, V. 2020. *Impact of Land Use and Climate Change on Surface Runoff Using GIS and SWAT Model: A Case Study*. Roorkee Water Conclave, Indian Institute of Technology Roorkee and National Institute of Hydrology, Roorkee, pp.1-10.

Chen, Y., Faramarzi, M., Gan, T.Y., and She, Y. 2023. Evaluation and uncertainty assessment of weather data and model calibration on daily streamflow simulation in a large-scale regulated and snow-dominated river basin. *J. Hydrol.*, 617.

Chiphang, N., Bandyopadhyay, A., and Bhadra, A. 2022. Response assessment of hydrological processes to climate change using ArcSWAT in Mago basin of Eastern Himalaya. *J. Earth Syst. Sci*. 131(4): 252.

Cullum, R.F., Knight, S.S., Cooper, C.M., and Smith, S. 2006. Combined effects of best management practices on water quality in oxbow lakes from agricultural watersheds. *Soil Tillage Res*. 90(1-2): 212-221.

Dakhlalla, A.O. and Parajuli, P.B. 2019. Assessing model parameters sensitivity and uncertainty of streamflow, sediment, and nutrient transport using SWAT. *Inf. Process. Agric.* 6(1): 61-72.

De-Almeida, W.S., Seitz, S., de Oliveira, L.F.C., and de Carvalho, D.F. 2021. Duration and intensity of rainfall events with the same erosivity change sediment yield and runoff rates. *Int. Soil Water Conser. Res*. 9(1): 69-75.

De Jong, R. and Zentner, R.P. 1985. Assessment of the SPAW model for semi-arid growing conditions with minimal local calibration. *Agric. Water Manag*. 10(1): 31-46.

Deng, X., Gu, H., Yang, L., Lyu, H., Cheng, Y., Pan, L., Fu, Z., Cui, L., and Zhang, L. 2020. A method of electrical conductivity compensation in a low-cost soil moisture sensing measurement based on capacitance. *Measure.* 150.

Desai, S., Singh, D.K., Islam, A., and Sarangi, A. 2021. Multi-site calibration of hydrological model and assessment of water balance in a semi-arid river basin of India. *Quaternary Int.* 571: 136-149.

Dos-Santos, F.M., de Oliveira, R.P., and Mauad, F.F. 2020. Evaluating a parsimonious watershed model versus SWAT to estimate streamflow, soil loss and river contamination in two case studies in Tiete river basin, Sao Paulo, Brazil. *J. Hydrol.: Reg. Stud.* 29.

Eini, M.R., Javadi, S., Delavar, M., Gassman, P.W., and Jarihani, B. 2020. Development of alternative SWAT-based models for simulating water budget components and streamflow for a karstic-influenced watershed. *Catena.* 195.

Falalakis, G. and Gemitzi, A. 2020. A simple method for water balance estimation based on the empirical method and remotely sensed evapotranspiration estimates. *J. Hydroinform.* 22(2): 440-451.

FAO, 2017. *Water for sustainable food and agriculture a report produced for the G20 presidency of Germany*. Rome.

Favero, L.P., Belfiore, P., and de Freitas Souza, R. 2023. *Data science, analytics and machine learning with R*. Academic Press.

Ferreira, Q.D.C.G., Bacellar, L.D.A.P., and Viana, J.H.M. 2021. Evaluation of soil moisture by electrical resistivity in Oxisols of the central Brazilian savanna. *Geoderma Reg.* 26.

Flerchinger, G.N. and Cooley, K.R. 2000. A ten-year water balance of a mountainous semi-arid watershed. *J. Hydrol.* 237(1-2): 86-99.

Fousiya and Varughese, A. 2020. Modelling stream flow using swat model: A case study of Thuthapuzha river Basin, Kerala. *Int. J. Farm Sci.* 10(2): 86-95.

Fowler, A. 2002. Assessment of the validity of using mean potential evaporation in computations of the long-term soil water balance. *J. Hydrol.* 256(3-4): 248-263.

Fu, J., Wang, W., Shao, Q., Xing, W., Cao, M., Wei, J., Chen, Z., and Nie, W. 2022. Improved global evapotranspiration estimates using proportionality hypothesis-based water balance constraints. *Remote Sensing Environ.* 279.

Gassman, P.W., Reyes, M.R., Green, C.H., and Arnold, J.G. 2007. The soil and water assessment tool: historical development, applications, and future research directions. *Trans. of the ASABE*, 50(4): 1211-1250.

Garna, R.K., Fuka, D.R., Faulkner, J.W., Collick, A.S., and Easton, Z.M. 2023. Watershed model parameter estimation in low data environments. *J. Hydrol.: Reg. Stud.* 45.

Gebru, T.A. and Tesfahunegn, G.B. 2020. GIS based water balance components estimation in northern Ethiopia catchment. *Soil Tillage Res.*, 197.

Ghandhari, A. and Moghaddam, S.A. 2011. Water balance principles: a review of studies on five watersheds in Iran. *J. Environ. Sci. Technol.* 4(5): 465-479.

Gholami, F., Nemati, A., Li, Y., and Zhang, J. 2022. Calculation of runoff computation cost and sensitivity analysis of topological attributes. *Remote Sens. Appl.: Soc. Environ.* 26.

Girden E.R. 1992. *ANOVA: Repeated measures*. Sage.

Glendenning, C.J., Van Ogtrop, F.F., Mishra, A.K., and Vervoort, R.W. 2012. Balancing watershed and local scale impacts of rain water harvesting in India-A review. *Agric. Water Manag.* 107: 1-13.

Gophen, M. 2020. Climate and water balance changes in the Kinneret watershed: A review. *Open J. Mod. Hydrol.* 10(2): 21-29.

Gorelick, N., Hancher, M., Dixon, M., Ilyushchenko, S., Thau, D., and Moore, R. 2017. Google Earth Engine: Planetary-scale geospatial analysis for everyone. *Remote Sensing Environ.* 202: 18-27.

Green, W.H. and Ampt, G.A. 1911. Studies on Soil Physics. *The Journal of Agricultural Science*. 4(1): 1-24.

Gupta, S.C. and Kapoor, V.K. 2020. *Fundamentals of mathematical statistics*. Sultan Chand & Sons.

Ha, L.T., Bastiaanssen, W.G., van-Griensven, A., van-Dijk, A.I., and Senay, G.B. 2017. SWAT-CUP for calibration of spatially distributed hydrological processes and ecosystem services in a Vietnamese river basin using remote sensing. *Hydrol. Earth Sys. Sci. Disc.*, pp.1-35.

Hargreaves, G.H. and Samani, Z.A. 1985. Reference crop evapotranspiration from temperature. *Appl. Eng. Agric*. 1(2): 96-99.

Harmel, R.D. and Smith, P.K. 2007. Consideration of measurement uncertainty in the evaluation of goodness-of-fit in hydrologic and water quality modeling. *J. Hydrol*. 337(3-4): 326-336.

Heerspink, B.P., Kendall, A.D., Coe, M.T., and Hyndman, D.W. 2020. Trends in streamflow, evapotranspiration, and groundwater storage across the Amazon Basin linked to changing precipitation and land cover. *J. Hydrol.: Reg. Stud*. 32.

Hilhorst, M.A. 2000. A Pore Water Conductivity Sensor. *Soil Sci. Soc. Am. J.* 64(6): 1922-1925.

Hosseini, S.H. and Khaleghi, M.R. 2020. Application of SWAT model and SWAT-CUP software in simulation and analysis of sediment uncertainty in arid and semi-arid watersheds (case study: The Zoshk–Abardeh watershed). *Model. Earth Sys. Environ.* 6(4): 2003-2013.

Huang, Q., Wang, J., and Li, Y. 2017. Do water saving technologies save water? Empirical evidence from North China. *J. Environ. Econ. Manag.* 82: 1-16.

Hwang, S.H., Kim, K.B., and Han, D. 2020. Comparison of methods to estimate areal means of short duration rainfalls in small catchments, using rain gauge and radar data. *J. Hydrol*. 588.

IMD [India Meteorological Department]. 2021. *Standard Operating Procedure Hydrometeorological Services in India*. Ministry of Earth Sciences, Government of India.

IMSD [Integrated Mission for Sustainable Development], 1995. *Integrated mission for sustainable development technical guidelines*. National Remote Sensing Agency, Department of Space, Govt. of India.

IWMI [International Water Management Institute]. 2007. *Helping the World Adapt to Water Scarcity*. Annual Report: 2007-2008.

Jahn, R., Blume, H.P., Asio, V.B., Spaargaren, O. and Schad, P., 2006. *Guidelines for soil description*. FAO.

Juma, L.A., Nkongolo, N.V., Raude, J.M. and Kiai, C., 2022. Assessment of hydrological water balance in Lower Nzoia Sub-catchment using SWAT-model: towards improved water governace in Kenya. *Heliyon*. 8(7).

Kaletova, T. and Nemetova, Z. 2017. Determination of surface runoff from the modelled area. *Environ. Earth Ecol*. 1(1).

Kavvas, M.L., Chen, Z.Q., Anderson, M.L., Ohara, N., Yoon, J.Y., and Xiang, F., 2011. A study of water balances over the Tigris–Euphrates watershed. *Phys. Chem. Earth, Parts A/B/C*. 36(5-6): 197-203.

Khalid, K., Ali, M.F., Abd Rahman, N.F., Mispan, M.R., Haron, S.H., Othman, Z., and Bachok, M.F. 2016. Sensitivity analysis in watershed model using SUFI-2 algorithm. *Procedia Eng*. 162: 441-447.

Krause, P., Boyle, D.P., and Base, F. 2005. Comparison of different efficiency criteria for hydrological model assessment. *Adva. Geosci*. 5: 89-97.

Krishnan G., Kumar K.S., and Rejani R. 2018. Application of SWAT model for estimating runoff of Nethravathi river basin using sequential uncertainty fitting technique. *Int. J. Sci. Res*. 9(3): 893-902.

Kumar, A., Kanga, S., Taloor, A.K., Singh, S.K., and Durin, B. 2021. Surface runoff estimation of Sind river basin using integrated SCS-CN and GIS techniques. *Hydro. Res*. 4: 61-74.

Kumar, C.P. 2018. Water resources issues and management in India. *J. Sci. Eng. Res.* 5(9): 137-147.

Kumar, G. and Srinivasan, D. 2016. Climatic water balance study and drought assessment in Kallar watershed, Tamil Nadu, India. *Int. J. Earth Sci. and Eng*. 9(3): 958-962.

Kundu, S., Khare, D., and Mondal, A. 2017. Individual and combined impacts of future climate and land use changes on the water balance. *Ecol. Eng*. 105: 42-57.

Kuriakose, S.L., Devkota, S., Rossiter, D.G., and Jetten, V.G. 2009. Prediction of soil depth using environmental variables in an anthropogenic landscape, a case study in the Western Ghats of Kerala, India. *Catena*. 79(1): 27-38.

Ladekarl, U.L. 1998. Estimation of the components of soil water balance in a Danish oak stand from measurements of soil moisture using TDR. *For. Ecol. Manag*. 104(1-3): 227-238.

Lalanne, C. and Mesbah, M. 2016. *Biostatistics and Computer-based Analysis of Health Data Using R*. Elsevier.

Le-Coz, J., Camenen, B., Peyrard, X., and Dramais, G. 2012. Uncertainty in open-channel discharges measured with the velocity–area method. *Flow Meas. Instrum.* 26: 18-29.

Lee, J., Abbas, A., McCarty, G.W., Zhang, X., Lee, S., and Cho, K.H. 2023. Estimation of base and surface flow using deep neural networks and a hydrologic model in two watersheds of the Chesapeake Bay. *J. Hydrol.*, 617.

Lee, O., Kim, H.S., and Kim, S. 2020. Hydrological simple water balance modeling for increasing geographically isolated Doline wetland functions and its application to climate change. *Ecol. Eng*. 149.

Leta, M.K., Ebsa, D.G., and Regasa, M.S. 2022. Parameter uncertainty analysis for streamflow simulation using SWAT model in Nashe watershed, Blue Nile River basin, Ethiopia. *Appl. Environ. Soil Sci*. 2022.

Leta, O.T., El-Kadi, A.I., Dulai, H., and Ghazal, K.A. 2016. Assessment of climate change impacts on water balance components of Heeia watershed in Hawaii. *J. Hydrol.: Reg. Stud.* 8: 182-197.

Li, M., Di, Z., and Duan, Q. 2021. Effect of sensitivity analysis on parameter optimization: Case study based on streamflow simulations using the SWAT model in China. *J. Hydrol.* 603.

Li, Q., Luo, Z., Zhong, B., and Zhou, H. 2018. An improved approach for evapotranspiration estimation using water balance equation: case study of Yangtze River Basin. *Water.* 10(6): 812.

Liang, Y., Cai, Y., Sun, L., Wang, X., Li, C., and Liu, Q. 2021. Sensitivity and uncertainty analysis for streamflow prediction based on multiple optimization algorithms in Yalong River Basin of southwestern China. *J. Hydrol.* 601.

Lillesand, T.M. and Kiefer, R.W. 2000. *Remote sensing and image interpretation.* 4th edn.(John Wiley & Sons: New York).

Liu, D., Zhang, Y., Zhang, J., Xiong, L., Liu, P., Chen, H., and Yin, J. 2021. Rainfall estimation using measurement report data from time-division long term evolution networks. *J. Hydrol.*, 600.

Liu, Y.R., Li, Y.P., Huang, G.H., Zhang, J.L., and Fan, Y.R. 2017. A Bayesian-based multilevel factorial analysis method for analyzing parameter uncertainty of hydrological model. *J. Hydrol.* 553: 750-762.

Liu, Z., Yao, Z., Wang, R., and Yu, G. 2020. Estimation of the Qinghai-Tibetan Plateau runoff and its contribution to large Asian rivers. *Sci. Total Environ.* 749.

Lu, Z., Wei, Y., Xiao, H., Zou, S., Ren, J., and Lyle, C. 2015. Trade-offs between midstream agricultural production and downstream ecological sustainability in the Heihe River basin in the past half century. *Agric. Water Manag.* 152: 233-242.

Lv, M., Ma, Z., Yuan, X., Lv, M., Li, M., and Zheng, Z. 2017. Water budget closure based on GRACE measurements and reconstructed evapotranspiration using GLDAS and water use data for two large densely-populated mid-latitude basins. *J. Hydrol.* 547: 585-599.

Maliva, R. and Missimer, T. 2012. Arid lands water evaluation and management. *Springer Sci. Business Media*.

Meeravali K., Gopikrishna A., Rasool S.N., and Eliyas S.A. 2020. Tipping Bucket Raingauge with GPRS Data Logger DL-2016: Specifications, Installation and Analysis. *Materials Today: Proc*. 27(2): 1394-1400.

Melaku, N.D., Renschler, C.S., Flagler, J., Bayu, W., and Klik, A. 2018a. Integrated impact assessment of soil and water conservation structures on runoff and sediment yield through measurements and modeling in the Northern Ethiopian highlands. *Catena*. 169: 140-150.

Melaku, N.D., Renschler, C.S., Holzmann, H., Strohmeier, S., Bayu, W., Zucca, C., Ziadat, F., and Klik, A. 2018b. Prediction of soil and water conservation structure impacts on runoff and erosion processes using SWAT model in the northern Ethiopian highlands. *J. Soils Sedim*. 18: 1743-1755.

Mengistu, A.G., van Rensburg, L.D., and Woyessa, Y.E. 2019. Techniques for calibration and validation of SWAT model in data scarce arid and semi-arid catchments in South Africa. *J. Hydrol.: Reg. Stud*. 25.

Menzel, L., Koch, J., Onigkeit, J., and Schaldach, R. 2009. Modelling the effects of land-use and land-cover change on water availability in the Jordan River region. *Adv. Geosci*. 21: 73-80.

Mestry, A., Narwade, R., and Nagarajan, K. 2020. Estimation of water balance components of watersheds in the Manjira River Basin using SWAT model and GIS. *Int. J. Eng. Adv. Technol*. 9(3): 3898-3907.

Moazenzadeh, R. and Izady, A. 2022. A hybrid calibration method for improving hydrological systems using ground-based and remotely-sensed observations. *J. Hydrol*. 615.

Mohammadi, Z., Salimi, M., and Faghih, A. 2014. Assessment of groundwater recharge in a semi-arid groundwater system using water balance equation, southern Iran. *J. Afr. Earth Sci.*, 95: 1-8.

Molenat, J., Dages, C., Bouteffeha, M., and Mekki, I. 2021. Can small reservoirs be used to gauge stream runoff? *J. Hydrol.* 603.

Monteith, J.L., 1965. *Evaporation and environment. In Symposia of the society for experimental biology* (Vol. 19, pp. 205-234). Cambridge University Press (CUP) Cambridge.

Moriasi, D.N., Arnold, J.G., Van-Liew, M.W., Bingner, R.L., Harmel, R.D., and Veith, T.L. 2007. Model evaluation guidelines for systematic quantification of accuracy in watershed simulations. *Trans. ASABE*, 50(3): 885-900.

Muttiah, R.S. and Wurbs, R.A. 2002. Scale-dependent soil and climate variability effects on watershed water balance of the SWAT model. *J. Hydrol.* 256(3-4): 264-285.

Nagarajan, R., Roy, P.D., Jonathan, M.P., Lozano, R., Kessler, F.L., and Prasanna, M.V. 2014. Geochemistry of Neogene sedimentary rocks from Borneo Basin, East Malaysia: Paleo-weathering, provenance and tectonic setting. *Geochemistry.* 74(1): 139-146.

Nandakumaran, P. and Balakrishnan, K. 2020. Groundwater quality variations in Precambrian hard rock aquifers: a case study from Kerala, India. *Appl. Water Sci.* 10(1).

Nandgude, S., Kambale, A., Shinde, S., Mahale, D., and Shinde, V. 2014. Soil erodibility estimation for soil conservation in Dapoli region of Maharashtra. *Trends Biosci.* 7(6): 486-490.

Nash, J.E. and Sutcliffe, J.V., 1970. River flow forecasting through conceptual models part I-A discussion of principles. *J. Hydrol.* 10(3): 282-290.

Nasiri, S., Ansari, H., and Ziaei, A.N., 2020. Simulation of water balance equation components using SWAT model in Samalqan Watershed (Iran). *Arabian J. Geosci.*, 13: 1-15.

Neitsch, S.L., Arnold, J.G., Kiniry, J.R., Williams, J.R., and King, K.W. 2005. *Soil and water assessment tool theoretical documentation version 2005*. Grassland. Soil and Water Research Laboratory, Agricultural Research Service, Blackland Research Center, Texas Agricultural Experiment Station, Texas, 1, 494.

Neitsch, S.L., Arnold, J.G., Kiniry, J.R., and Williams, J.R. 2011. *Soil and water assessment tool theoretical documentation version 2009*. Texas Water Resources Institute.

Nour, A.M., Vallet-Coulomb, C., Gonçalves, J., Sylvestre, F., and Deschamps, P. 2021. Rainfall-discharge relationship and water balance over the past 60 years within the Chari-Logone sub-basins, Lake Chad basin. *J. Hydrol.: Reg. Stud.* 35.

Noviadi, S.C., Sukarno, S., Setiawan, E., and Wardani, K. 2019. Water Balance Analysis in Bera Watershed Sumbawa River Basin. *Satia Cahya Noviadi J. Eng. Res. Appl.* 9(7): 33-39.

Nyatuame, M., Amekudzi, L.K., and Agodzo, S.K. 2020. Assessing the land use/land cover and climate change impact on water balance on Tordzie watershed. *Remote Sens. Appl.: Soc. Environ.* 20.

NWP [National Water Policy]. 2012. *Ministry of Water Resources. (Government of India)*, pp. 1-13.

Oroud, I.M. 2015. Water budget assessment within a typical semiarid watershed in the eastern Mediterranean. *Environ. Proc.* 2(2): 395-409.

Ouallali, A., Briak, H., Aassoumi, H., Beroho, M., Bouhsane, N., and Moukhchane, M. 2020. Hydrological foretelling uncertainty evaluation of water balance components and sediments yield using a multi-variable optimization approach in an external Rif's catchment, Morocco. *Alexandria Eng. J.* 59(2): 775-789.

Paciolla, N., Corbari, C., Hu, G., Zheng, C., Menenti, M., Jia, L., and Mancini, M. 2021. Evapotranspiration estimates from an energy-water-balance model calibrated on satellite land surface temperature over the Heihe basin. *J. Arid Environ*. 188.

Pasha, M.M. 2022. Characterisation of Hydrologic Responses of Micro Watersheds using Geospatial Techniques. *Ph.D. (Agril. Engg.) Thesis, Kerala Agricultural University*.

Pravalie, R., Piticar, A., Roșca, B., Sfica, L., Bandoc, G., Tiscovschi, A., and Patriche, C. 2019. Spatio-temporal changes of the climatic water balance in Romania as a response to precipitation and reference evapotranspiration trends during 1961–2013. *Catena*. 172: 295-312.

Priestley, C.H.B. and Taylor, R.J. 1972. *On the assessment of surface heat flux and evaporation using large-scale parameters*. Monthly weather review, 100(2): 81-92.

Qi, J., Wang, Q., and Zhang, X. 2019. On the use of NLDAS2 weather data for hydrologic modeling in the Upper Mississippi River Basin. *Water*, 11(5): 960.

Rao, A.S. and Saxton, K.E. 1995. Analysis of soil water and water stress for pearl millet in an Indian arid region using the SPAW Model. *J. Arid Environ*. 29(2): 155-167.

Rohtash, L.N.T., Thakural, L.N., Choudhary, M.K., and Tiwari, D. 2018. Rainfall runoff modeling using SWAT model for Chaliyr basin Kerala India. *J. Int. Sci. Res*. 8.

Safari, M.J.S., Arashloo, S.R., and Mehr, A.D. 2020. Rainfall-runoff modeling through regression in the reproducing kernel Hilbert space algorithm. *J. Hydrol.*, 587.

Saha, D. and Ray, R.K., 2019. *Groundwater resources of India: potential, challenges and management*. Groundwater development and management: Issues and challenges in South Asia, pp.19-42.

Sajikumar, N. and Remya, R.S. 2015. Impact of land cover and land use change on runoff characteristics. *J. Environ. Manag*. 161: 460-468.

Sanchez-Gomez, A., Martinez-Perez, S., Perez-Chavero, F.M., and Molina-Navarro, E. 2022. Optimization of a SWAT model by incorporating geological information through calibration strategies. *Optim. Eng*. 23(4): 2203-2233.

Sandra, G. and Sathian, K.K. 2016. Assessment of water balance of a watershed using SWAT model for water resources management. *Int. J. Eng. Sci. Res. Technol.* 5(4): 177-184.

Santhi, C., Arnold, J.G., Williams, J.R., Dugas, W.A., Srinivasan, R., and Hauck, L.M. 2001. Validation of the swat model on a large river basin with point and nonpoint sources 1. *J. Amer. Water Res. Assoc*. 37(5): 1169-1188.

Sao, D., Kato, T., Tu, L.H., Thouk, P., Fitriyah, A., and Oeurng, C. 2020. Evaluation of different objective functions used in the SUFI-2 calibration process of SWAT-CUP on water balance analysis: A case study of the Pursat river basin, Cambodia. *Water.* 12(10): 2901.

Saxton, K.E. and Willey, P.H. 2006. *The SPAW model for agricultural field and pond hydrologic simulation*. Watershed models, pp.401-435.

Serur, A.B. and Adi, K.A. 2022. Multi-site calibration of hydrological model and the response of water balance components to land use land cover change in a rift valley Lake Basin in Ethiopia. *Sci. African*. 15.

Shaw, S.K., Sharma, A., Khatua, K.K., and Oliveto, G. 2023. An Integrated Approach to Evaluating Crop Water Requirements and Irrigation Schedule for Optimizing Furrow Irrigation Design Parameters in Kurnool District, India. *Water*. 15(10).

Shedlock, C.J. and Stumpo, K.A. 2022. Data parsing in mass spectrometry imaging using R Studio and Cardinal: A tutorial. *J. Mass Spectrometry Advanc. Clinical Lab.* 23: 58-70.

Shivhare, N., Dikshit, P.K.S., and Dwivedi, S.B. 2018. A comparison of SWAT model calibration techniques for hydrological modeling in the Ganga river watershed. *Eng.* 4(5): 643-652.

Singh, A. and Jha, S.K. 2021. Identification of sensitive parameters in daily and monthly hydrological simulations in small to large catchments in Central India. *J. Hydrol.* 601.

Singh, J., Knapp, H.V., Arnold, J.G., and Demissie, M. 2005. Hydrological modeling of the Iroquois river watershed using HSPF and SWAT 1. *J. Amer. Water Res. Assoc.* 41(2): 343-360.

Singh, L. and Saravanan, S. 2020. Simulation of monthly streamflow using the SWAT model of the Ib River watershed, India. *HydroRes.* 3: 95-105.

Singh, V. and Goyal, M.K. 2017. Curve number modifications and parameterization sensitivity analysis for reducing model uncertainty in simulated and projected streamflows in a Himalayan catchment. *Ecol. Eng*. 108: 17-29.

Sinha, J., Jha, S., and Goyal, M.K. 2019. Influences of watershed characteristics on long-term annual and intra-annual water balances over India. *J. Hydrol.* 577.

Sith, R., Watanabe, A., Nakamura, T., Yamamoto, T., and Nadaoka, K. 2019. Assessment of water quality and evaluation of best management practices in a small agricultural watershed adjacent to Coral Reef area in Japan. *Agric. Water Manag.* 213: 659-673.

Skierucha, W., Wilczek, A., and Alokhina, O. 2008. Calibration of a TDR probe for low soil water content measurements. *Sensors Actuators A: Phys.*, 147(2): 544-552.

Smith, M. 1992. *CROPWAT: A computer program for irrigation planning and management (No. 46)*. Food & Agric. Org.

Song, S., Brocca, L., Wang, W., and Cui, W. 2020. Testing the potential of soil moisture observations to estimate rainfall in a soil tank experiment. *J. Hydrol.* 581.

Song, Y., Han, D., and Rico-Ramirez, M.A. 2016. High temporal resolution rainfall information retrieval from tipping-bucket rain gauge measurements. *Proc. Eng*. 154: 1193-1200.

Spruill, C.A., Workman, S.R., and Taraba, J.L. 2000. Simulation of daily and monthly stream discharge from small watersheds using the SWAT model. *Trans. ASAE*. 43(6): 1431-1439.

Sreenath, G. 2013. *Ground water information booklet of Malappuram District.* Technical Report, Government of Kerala, pp. 1-4.

Stancalie G., Marica A., and Toulios L. 2010. Using Earth Observation Data and CROPWAT Model to Estimate the Actual Crop Evapotranspiration. *Phys. Chem. Earth*. 35: 25-30.

Tamiminia, H., Salehi, B., Mahdianpari, M., Quackenbush, L., Adeli, S., and Brisco, B. 2020. Google Earth Engine for geo-big data applications: A meta-analysis and systematic review. *ISPRS J. Photogrammetry Remote Sensing*. 164: 152-170.

Tan, M. and Zheng, L. 2019. Increase in economic efficiency of water use caused by crop structure adjustment in arid areas. *J. Environ. Manag.* 230: 386-391.

Tang, F.F., Xu, H.S., and Xu, Z.X. 2012. Model calibration and uncertainty analysis for runoff in the Chao River Basin using sequential uncertainty fitting. *Procedia Environ. Sci.* 13: 1760-1770.

Tejaswini, V. and Sathian, K.K. 2018. Assessment of hydrological processes in a small watershed using SWAT. *Int. J. Agric. Eng*. 11(1): 41-48.

Teklay, A., Dile, Y.T., Setegn, S.G., Demissie, S.S., and Asfaw, D.H. 2019. Evaluation of static and dynamic land use data for watershed hydrologic process simulation: A case study in Gummara watershed, Ethiopia. *Catena.* 172: 65-75.

Thavhana, M.P., Savage, M.J., and Moeletsi, M.E. 2018. SWAT model uncertainty analysis, calibration and validation for runoff simulation in the Luvuvhu River catchment, South Africa. *Phys. Chem. Earth, Parts A/B/C*. 105: 115-124.

Topp G.C., Davis J.L., and Annan A.P. 1980. Electromagnetic Determination of Soil Water Content: Measurements in Coaxial Transmission Lines. *Water Resources Res.* 16(3): 574-582.

Touhami, I., Chirino, E., Andreu, J.M., Sanchez, J.R., Moutahir, H., and Bellot, J. 2015. Assessment of climate change impacts on soil water balance and aquifer recharge in a semiarid region in south east Spain. *J. Hydrol.* 527: 619-629.

Tripathi, M.P., Raghuwanshi, N.S., and Rao, G.P. 2006. Effect of watershed subdivision on simulation of water balance components. *Hydrol. Process.: Int. J.* 20(5): 1137-1156.

Tuset, J., Vericat, D., and Batalla, R.J. 2016. Rainfall, runoff and sediment transport in a Mediterranean mountainous catchment. *Sci. Total Environ.* 540: 114-132.

Uniyal, B., Jha, M.K., Verma, A.K., and Anebagilu, P.K. 2020. Identification of critical areas and evaluation of best management practices using SWAT for sustainable watershed management. *Sci. Total Environ.* 744.

Upton, G.J.G. and Rahimi, A.R. 2003. On-line detection of errors in tipping-bucket raingauges. *J. Hydrol.* 278(1-4): 197-212.

USDA, S., 1972. *National engineering handbook, section 4: Hydrology*. Washington, DC.

Van Liew, M.W., Arnold, J.G., and Garbrecht, J.D. 2003. Hydrologic simulation on agricultural watersheds: Choosing between two models. *Trans. ASAE*, 46(6): 1539-1551.

Varma, A. 2017. *Groundwater resource and governance in Kerala: Status, issues and prospects*. Forum for Policy Dialogue on Water Conflicts in India.

Varughese, A. and Hajilal, M.S. 2020. Impact of climate change on the hydrology of Bharathappuzha river in Kerala, India. *Climate Change Environ. Sustainability*. 8(2): 181-190.

Varughese, A. and Hajilal, M.S. 2022. Trends in Streamflow in Relation to Water Retention Structures: A Case Study in Bharathpuzha River Basin, India. *Int. J. Environ. Clim. Change.* 12(5): 84-96.

Villoro, A., Latorre, B., Tormo, J., Jiménez, J.J., Lopez, M.V., Nicolau, J.M., Vicente, J., Gracia, R., and Moret-Fernández, D. 2021. A TDR wireless device for volumetric water content sensing. *Comp. Electron. Agric.* 181.

Walker, J.P., Willgoose, G.R., and Kalma, J.D. 2004. In situ measurement of soil moisture: a comparison of techniques. *J. Hydrol.* 293(1-4): 85-99.

Wang, Q., Wang, X., Liu, Y., and Li, R. 2021. Urbanization and water consumption at national-and subnational-scale: The roles of structural changes in economy, population, and resources. *Sustain. Cities Soc.* 75.

Wang, Z., He, Y., Li, W., Chen, X., Yang, P., and Bai, X. 2023. A generalized reservoir module for SWAT applications in watersheds regulated by reservoirs. *J. Hydrol.* 616.

Watson D.F. and Philip G.M. 1985. A Refinement of Inverse Distance Weighted Interpolation. *J. of Geo-Processing*. 2: 315-327.

Wolka, K., Sterk, G., Biazin, B., and Negash, M. 2018. Benefits, limitations and sustainability of soil and water conservation structures in Omo-Gibe basin, Southwest Ethiopia. *Land Use Policy*. 73: 1-10.

Wyatt, B.M., Ochsner, T.E., Krueger, E.S., and Jones, E.T. 2020. In-situ soil moisture data improve seasonal streamflow forecast accuracy in rainfall-dominated watersheds. *J. Hydrol.* 590.

Xiang, X., Ao, T., Xiao, Q., Li, X., Zhou, L., Chen, Y., Bi, Y., and Guo, J. 2022. Parameter Sensitivity Analysis of SWAT Modeling in the Upper Heihe River Basin Using Four Typical Approaches. *Appl. Sci.* 12(19).

Xu, C.Y. and Singh, V.P. 1998. A review on monthly water balance models for water resources investigations. *Water Res. Manag*. 12: 20-50.

Xueman, Y., Wenxi, L., Yongkai, A., and Weihong, D. 2020. Assessment of parameter uncertainty for non-point source pollution mechanism modeling: A Bayesian-based approach. *Environ. Pollution*. 263.

Yang, L., Driscol, J., Sarigai, S., Wu, Q., Chen, H., and Lippitt, C.D. 2022. Google Earth Engine and artificial intelligence (AI): a comprehensive review. *Remote Sensing*. 14(14).

Yetukuri, B.N., Yetukuri, N.V., and Fischer, G.W. 1996. SPAW: a design tool for planning a manufacturing process in a concurrent engineering environment. *Comp. in Industry*. 32(1): 79-93.

Zanetti, S.S., Cecílio, R.A., Silva, V.H., and Alves, E.G. 2015. General calibration of TDR to assess the moisture of tropical soils using artificial neural networks. *J. Hydrol.* 530: 657-666.

Zhang, A., Zheng, C., Wang, S., and Yao, Y. 2015. Analysis of streamflow variations in the Heihe River Basin, northwest China: Trends, abrupt changes, driving factors and ecological influences. *J. of Hydrol.: Reg. Stud.* 3: 106-124.

Zhang, Y., He, B., Guo, L., Liu, J., and Xie, X. 2019. The relative contributions of precipitation, evapotranspiration, and runoff to terrestrial water storage changes across 168 river basins. *J. Hydrol.* 579.

Zheng, H., Nie, X., Liu, Z., Mo, M., and Song, Y. 2021. Identifying optimal ridge practices under different rainfall types on runoff and soil loss from sloping farmland in a humid subtropical region of Southern China. *Agric. Water Manag.* 255.

APPENDICES

APPENDIX - A
Goggle Earth Engine Program for LULC

```
var start= '2022-10-01',
    end= '2022-12-31';
/*-------------------------------------Satellite Data----------------------------------*/
var TrainingImage= ee.ImageCollection("COPERNICUS/S2_SR")
        .filterDate(start, end)
        .filterBounds(Watershed)
        .filterMetadata('CLOUDY_PIXEL_PERCENTAGE','less_than',10)
        .map(masks2)
        .median()
        .select(['B2','B3','B4','B5','B6','B7','B8'])
// .clip(Perassannur)
Map.addLayer(TrainingImage.clip(Watershed), VisParam,'Sentinel2',false);
print('Sentinel2',TrainingImage)
// /*-------------------------------------Classification----------------------------------*/
// Set a new property class
        // var Paddy= Paddy.set('Class',0);
        // var MixedCropping= MixedCropping.set('Class',1);
        // var Coconut= Coconut.set('Class',2);
        // var LandwithScrub= LandwithScrub.set('Class',3);
        // var Urban= Urban.set('Class',4);
        // var Forest= Forest.set('Class',5);
        // var Rubber= Rubber.set('Class',6);
        // var WaterBodies= WaterBodies.set('Class',7);
        // var Barren= Barren.set('Class',8)
// add a random column
        var Paddy = Paddy.randomColumn("random");
        var MixedCropping = MixedCroppingColumn("random");
        var Coconut = Coconut.randomColumn("random")
```

```
        var LandwithScrub = LandwithScrub.randomColumn("random")

        var Urban = Urban.randomColumn("random")

        var Forest = Forest.randomColumn("random")

        var Rubber = Rubber.randomColumn("random")

        var WaterBodies = WaterBodies.randomColumn("random")

        var Barren = Barren.randomColumn("random")
// create a training sample
        var Paddy _Train = Paddy.filter(ee.Filter.lt("random",0.7));

        var MixedCropping _Train =
MixedCropping.filter(ee.Filter.lt("random",0.7));

        var Coconut_Train = Coconut.filter(ee.Filter.lt("random",0.7));

        var LandwithScrub_Train = LandwithScrub.filter(ee.Filter.lt("random",0.7));

        var Urban_Train = Urban.filter(ee.Filter.lt("random",0.7));

        var Forest_Train = Forest.filter(ee.Filter.lt("random",0.7));

        var Rubber_Train = Rubber.filter(ee.Filter.lt("random",0.7));

        var WaterBodies_Train = WaterBodies.filter(ee.Filter.lt("random",0.7));

        var Barren_Train = Barren.filter(ee.Filter.lt("random",0.7));
// // create a validation sample
        var Paddy _Val = Paddy.filter(ee.Filter.gt("random",0.7));

        var MixedCropping _Val = MixedCropping (ee.Filter.gt("random",0.7));

        var Coconut_Val = Coconut.filter(ee.Filter.gt("random",0.7));

        var LandwithScrub_Val = LandwithScrub.filter(ee.Filter.gt("random",0.7));

        var Urban_Val = Urban.filter(ee.Filter.gt("random",0.7));

        var Forest_Val = Forest.filter(ee.Filter.gt("random",0.7));

        var Rubber_Val = Rubber.filter(ee.Filter.gt("random",0.7));

        var WaterBodies_Val = WaterBodies(ee.Filter.gt("random",0.7));

        var Barren_Val = Barren.filter(ee.Filter.gt("random",0.7));
// // Combine the data into a training and validation dataset
// // combine training data
var TrainingSample = Paddy _Train
        .merge(MixedCropping_Train)
```

```
        .merge(Coconut_Train)

        .merge(LandwithScrub _Train)

        .merge(Urban_Train)

        .merge(Forest_Train)

        .merge(Rubber_Train)

        .merge(WaterBodies_Train)

        .merge(Barren_Train)
// // combine validation data
var validationSample = Paddy_Val

        .merge(MixedCropping_Val)

        .merge(Coconut_Val)

        .merge(LandwithScrub_Val)

        .merge(Urban_Val)

        .merge(Forest_Val)

        .merge(Rubber_Val)

        .merge(WaterBodies _Val)

        .merge(Barren_Val)
// Train the random forest classifier and print the variable importance
// sample the image
    var trainingSample = TrainingImage.sampleRegions({
    collection:TrainingSample,
    properties:["Class"],
    scale:10,
    tileScale: 16 });
// create a list with bandNames
    var bandNames = TrainingImage.bandNames();
// train the random forest classifier
    var classifier = ee.Classifier.smileRandomForest(6)
    .train({features:trainingSample,classProperty:"Class",inputProperties:bandName
s });
// get the classified image
```

```
    var classification = TrainingImage.select(bandNames).classify(classifier);
 // get info from classifier
    var dict = classifier.explain();
// get the variable importance from dict
    var variable_importance = ee.Feature(null,
ee.Dictionary(dict).get('importance'));
    print('variable_importance',variable_importance)
// plot the variable importance
    var chart =
        ui.Chart.feature.byProperty(variable_importance)
        .setChartType('ColumnChart')
        .setOptions({
        title: 'Random Forest Variable Importance',
        legend: {position: 'none'},
        hAxis: {title: 'Bands'},
        vAxis: {title: 'Importance'} });
 print(chart);
// add layer to map
Map.addLayer(classification.clip(Watershed), {min: 2, max: 6,
    palette: ['#90ee90' //1,
    '#ffff00' //2,
    '#ffa5000' //3,
    '#add8e6' //4,
    '#808080' //5,
    '#013220' //6,
    '#ffc0cb' //7,
    '#00008b' //8,
     '#964b00']}, //9
    'classified');
// Print the statistics of Classifier:  // get the confustion matrix
var confMatrix = classifier.confusionMatrix();
```

```
        var OA = confMatrix.accuracy();

        var CA = confMatrix.consumersAccuracy().toList();

        var Kappa = confMatrix.kappa();

        var Order = confMatrix.order();

        var PA = confMatrix.producersAccuracy();
print(confMatrix,'Confusion Matrix');
print(OA,'Overall Accuracy');
print(CA,'Consumers Accuracy');
print(Kappa,'Kappa');
print(Order,'Order');
print(PA,'Producers Accuracy')
```

APPENDIX - B
R Studio Program

```
library(readxl)
pera_m <- read_excel("C:/Users/Adwait/Desktop/Perassannur.xlsx")
View(Perassannur)
    library(tidyverse)
    View(Perassannur)
    library(Hmisc)
    lapply(Perassannur,Hmisc::describe)
    library(GGally)
    library(ggthemes)
    library(ggplot2)
ggpairs(Perassannur,columns=2:6) +   theme_bw()

pic1<-ggplot(Perassannur)+aes(x=Rainfall ,y=Runoff)+geom_point()
pic1+ggtitle("Relationship between Rainfall and Runoff")
pic1+geom_smooth(method="gam",formula = y~poly(x,4),se=TRUE,col="blue")+
    ylab(bquote('Runoff  '("mm")))+
    xlab(bquote('Rainfall ' (mm))) +
    theme(plot.title = element_text(hjust = 0.5)) +
    theme_bw(base_size = 12) +
    theme(text=element_text(family="Times New Roman", face="bold", size=12))

pic2<-ggplot(Perassannur)+aes(x=Rainfall ,y=SM)+geom_point()
pic2+ggtitle("Relationship between Rainfall and Soil Moisture")
pic2+geom_smooth(method="gam",formula =
y~poly(x,3),se=TRUE,col="orange")+
    ylab(bquote('Soil Moisture  '("%")))+
    xlab(bquote('Rainfall ' (mm))) +
    theme(plot.title = element_text(hjust = 0.5)) +
    theme_bw(base_size = 12) +
    theme(text=element_text(family="Times New Roman", face="bold", size=12))
```

```
pic3<-ggplot(Perassannur)+aes(x=Rainfall ,y=GW)+geom_point()
pic3+ggtitle("Relationship between Rainfall and Groundwater Table")
pic3+geom_smooth(method="gam",formula = y~poly(x,5),se=TRUE,col="red")+
    ylab(bquote('Depth to GW Table from MSL  '(m)))+
    xlab(bquote('Rainfall ' (mm))) +
    theme(plot.title = element_text(hjust = 0.5)) +
    theme_bw(base_size = 12) +
    theme(text=element_text(family="Times New Roman", face="bold", size=12))

pic4<-ggplot(Perassannur)+aes(x=Rainfall ,y=GW)+geom_point()
pic4+ggtitle("Relationship between Rainfall and Evapotranspiration")
pic4+geom_smooth(method="gam",formula =
y~poly(x,3),se=TRUE,col="darkgreen")+
    ylab(bquote('Evapotranspiration  '("mm")))+
    xlab(bquote('Rainfall ' (mm))) +
    theme(plot.title = element_text(hjust = 0.5)) +
    theme_bw(base_size = 12) +
    theme(text=element_text(family="Times New Roman", face="bold", size=12))

model1=lm(Runoff~poly(Rainfall,4),data= Perassannur)
summary(model1)
model2=lm(SM~poly(Rainfall,3),data= Perassannur)
summary(model2)
model3=lm(GW~poly(Rainfall,5),data= Perassannur)
summary(model3)
model4=lm(ET~poly(Rainfall,3),data= Perassannur)
summary(model4)

plot(residuals(model1)); plot(model1,1); plot(model1,2)
plot(residuals(model2)); plot(model2,1); plot(model2,2)
plot(residuals(model3)); plot(model3,1); plot(model3,2)
plot(residuals(model4)); plot(model4,1); plot(model4,2)
```

DETERMINATION OF WATER BALANCE COMPONENTS OF A MICRO WATERSHED FOR IMPROVED WATER MANAGEMENT PRACTICES

by

BOWLEKAR ADWAIT PRAKASH

2019-28-002

ABSTRACT OF THESIS

Submitted in the partial fulfilment of the
requirements for the degree of

DOCTOR OF PHILOSOPHY

IN

AGRICULTURAL ENGINEERING
(Soil and Water Conservation Engineering)

Faculty of Agricultural Engineering and Technology
Kerala Agricultural University

DEPARTMENT OF SOIL AND WATER CONSERVATION ENGINEERING

**KELAPPAJI COLLEGE OF AGRICULTURAL ENGINEERING
AND TECHNOLOGY, TAVANUR - 679 573**

KERALA, INDIA
2023

ABSTRACT

The incidents of water shortage are prevalent even in areas with high annual rainfall and are a serious issue requiring immediate attention. The uneven temporal distribution of rainfall, poor water conservation, and management are the primary reasons for this scarcity. A water balance study on a watershed basis can provide objective solutions to water scarcity and other water management issues. Hence, such a study on a sub-watershed of river Bharathapuzha, having a catchment area in and around Valanchery municipal town in Malappuram district, has been carried out in this research work. Major objectives of the study included the determination of monthly water balances of the watershed, developing relationships between them, and suggesting scientific water management practices for the watershed.

Four automatic tipping bucket rain gauges were installed in the study area to record the rainfall. The stream runoff was determined by the area-velocity method, using automatic water level sensors, data loggers, and cup-type current meters. The soil moisture was measured using both capacitance and resistance-based soil moisture sensors, and a water level sensor recorded the groundwater level. The evapotranspiration (ET) was estimated using the FAO Penman-Monteith (PM) method and the water balance method. The sub-components of water balance were also assessed using the Soil and Water Assessment Tool (SWAT). The SWAT-CUP (Calibration and Uncertainty Programme) was used for sensitivity analysis and calibration of the model. The monthly and weekly relationships were found between the rainfall and other water balance components using R software. The soil and water conservation measures were suggested for the study based on the morphometric and water balance information.

The average annual rainfall of the study area was found to be 2582 mm. Runoff measurement showed that 58 per cent of rainfall was transformed to runoff, while ET of the basin was 40 per cent. Soil moisture depletion rate in summer months varied between 2.45 to 1.39 mm day^{-1}, while the mean monthly GW depletion rates were 3.74, 2.84, and 5.5 mm day^{-1} from December to February,

respectively. The ET estimated by the PM and water balance methods showed a close comparison. The SWAT model showed that its predictive ability for runoff was good with the R^2 value of 0.97, NSE 0.96, PBIAS 2.60, and RSR 0.20. The monthly relationships between rainfall and other elements of water balances were non-linear, with polynomial equations of degrees 3 to 5.

There was no flow even at the outlet of the mainstream of the watershed during the summer months from March to May. If the flow rate in the channel could be reduced during the later part of the monsoon and post-monsoon months (October to December), a lean flow of 1 m^3s^{-1} in the stream can be ensured. Groundwater recharge in the upper reaches of the catchment can further improve the lean flow. Roof water harvesting, recharging, bunding, trenching, terracing, and other vegetative measures have been suggested for the upper catchment. Pervious check dams, cement concrete check dams and vented cross bars were suggested for the main drainage channels.

Keywords: Evapotranspiration, groundwater, rainfall, runoff, water.